

## ABSTRACT

PARK, SEONGHYUN. Simple Strategy for Production of Single-Component and Tunable Cellulose-Based Hydrogels and Their Potential Applications. (Under the direction of Dr. Sunkyu Park and Dr. Stephen S. Kelley)

As global concern for environmental issues continues to rise, there is a growing demand for sustainable materials. This has led to an increase in research on naturally occurring polymers, which offer a range of benefits including low carbon footprint, biocompatibility, and biodegradability. Among these polymers, cellulose has gained significant attention due to its availability and ease of access. One area of research that shows promise involves the development of hydrogels derived from cellulose. Hydrogels are versatile materials that have found applications in various fields such as cosmetics, hygiene products, drug delivery, and biomedical research. While both natural and synthetic polymers can be used to create hydrogels, natural polymers offer several advantages. However, the production of natural polymer-based hydrogels presents technical challenges that hinder their industrial-scale usage, leading to a greater reliance on synthetic polymer-based hydrogels. To increase the use of natural polymer-based hydrogels, it is necessary to develop simpler and more efficient techniques for their production. This study aims to address this need by proposing a simple strategy for the production of hydrogels based on cellulose and exploring their potential applications.

Chapter 1 lays the foundation for subsequent chapters (Chapters 1-3) investigating single-component hydrogels based on cellulose. These hydrogels can be formed by utilizing the self-assembly properties of amphiphilic copolymers in water. Amphiphilic cellulose derivatives, specifically, cellulose acetate sulfate (CAS), which can form hydrogels when the balance between sulfate and acetyl moieties is optimal. Single-component hydrogels based on CAS can be formed by adding only deionized water, without crosslinking agents or other polymers. In the following

chapters, the potential applications of CAS hydrogels are explored. Chapter 1 assesses the feasibility of CAS hydrogels as drug release matrices. Hydrophilic drugs were integrated into CAS hydrogel matrices, and the release of the drugs was controlled by the balance between sulfate and acetyl moieties in the hydrogels. Chapter 2 investigates the use of CAS hydrogels as adsorbents for treating aqueous contaminants. The negatively charged functional groups in CAS hydrogels, such as hydroxyl and sulfate moieties, allow them to interact with cationic contaminants and remove them effectively. Chapter 3 studies the application of CAS hydrogels as films and coatings for food packaging. The physicochemical properties of CAS films depend on the balance between sulfate and acetyl moieties, but regardless of the balance, all CAS coatings are effective in prolonging the shelf life of bananas.

The production of cellulose acetate (CA), a widely used cellulose derivative, has been challenged by the formation of insoluble gel particles (IGP) that deteriorate the quality of the product and hinder the production process. These IGPs are mainly composed of xylan acetate (XA) and CA, but their formation mechanism is not yet fully understood despite extensive research. Therefore, Chapter 4 and 5 are devoted to exploring IGP formation during CA production. Chapter 4 delves into the formation of IGP during CA production by studying the impact of XA and process conditions through simulation of industrial CA production. It is unveiled that the formation of IGP during the production of CA is linked to intermolecular interactions between CA and XA induced by the precipitation process. Furthermore, the essential characteristics of XA that lead to IGP formation have been investigated. In Chapter 5, a newly discovered impurity in dissolving pulps, sulfuric acid insoluble substances (SIS), which have an adverse impact on the quality of cellulose acetate, is investigated. To comprehend the origin and impact of SIS, fiber fractionation and hydrolysis techniques are utilized. The formation of

insoluble gel particles (IGP) during industrial cellulose acetate production is explored by simulating the CA synthesis and precipitation processes, investigating the roles of SIS.

© Copyright 2023 by Seonghyun Park

All Rights Reserved

Simple Strategy for Production of Single-Component and Tunable Cellulose Acetate Sulfate  
Hydrogels and Their Potential Applications.

by  
Seonghyun Park

A dissertation or thesis submitted to the Graduate Faculty of  
North Carolina State University  
in partial fulfillment of the  
requirements for the degree of  
Doctor of Philosophy

Forest Biomaterials

Raleigh, North Carolina  
2023

APPROVED BY:

---

Dr. Sunkyu Park  
Committee Co-Chair

---

Dr. Stephen S. Kelley  
Committee Co-Chair

---

Dr. Melissa A. Pasquinelli

---

Dr. Rohan A. Shirwaiker

---

Dr. Trevor Treasure

## **DEDICATION**

Finally, I am proud to say that I have made it

## **BIOGRAPHY**

Seonghyun Park was born January 16<sup>th</sup>, 1991 in Cheongju, Republic of Korea. He graduated from Seoul National University in February 2016 with a B.S. degree in Environmental Material Science. From January 2016, he started his career in Optical Material Division at LG Chem in Cheongju, South Korea as a process engineer. While working at LG Chem, he was mainly in charge of managing and operating a pilot production line for polarizing films. Inspired by the scientific principles behind the production of polarizing films, he decided to pursue an advanced degree. From August 2018, he started his Ph.D. program at the Department of Forest Biomaterials under the advice of Dr. Sunkyu Park and Dr. Stephen S. Kelley. He participated in several projects funded by Eastman Chemical Company. During the Ph.D. program, he interned at Eastman Chemical Company in Kingsport, Tennessee from January 2022 to May 2022.

## ACKNOWLEDGMENTS

I am sincerely grateful for the unwavering and productive guidance provided by my advisors, Dr. Hasan Jameel, Dr. Stephen Kelley, and Dr. Sunkyu Park. Their mentorship has been invaluable in providing me with the knowledge, tools, and support needed to overcome various challenges. I am grateful for their patience, encouragement, and expertise, which have helped me grow both as a researcher and as a person. I am extremely grateful for the opportunity to collaborate with distinguished experts within the institution, which has not only expanded my research perspective but also provided me with valuable insights and guidance. Specifically, I would like to express my appreciation for Dr. Rohan Shirwaiker's exceptional support and expertise, which proved to be particularly helpful in an area of research that was previously unfamiliar to me. Additionally, I am deeply grateful for Dr. Mellissa Pasquinelli's generous assistance and invaluable insights regarding molecular dynamic simulations. Furthermore, I would like to extend my heartfelt gratitude to Dr. Trevor Treasure, who served as my project advisor, mentor, and manager. His exceptional insights and guidance have been instrumental in my academic success and have helped me navigate the various challenges encountered during my research.

## TABLE OF CONTENTS

LIST OF TABLES .....	viii
LIST OF FIGURES .....	ix
<b>Chapter 1: Simple Strategy for Production of Tunable and Single-Component Cellulose Acetate Sulfate Hydrogels for Drug Release .....</b>	
<b>Acetate Sulfate Hydrogels for Drug Release .....</b>	<b>1</b>
Abstract .....	1
Introduction.....	2
Materials and Methods.....	5
Results and Discussions.....	11
Conclusion .....	31
References.....	32
<b>Chapter 2: Production of Single-Component Cellulose-Based Hydrogel and Its Utilization as Adsorbent for Aqueous Contaminants.....</b>	
<b>as Adsorbent for Aqueous Contaminants.....</b>	<b>40</b>
Abstract .....	40
Introduction.....	41
Materials and Methods.....	44
Results and Discussions.....	50
Conclusion .....	67
References.....	69
<b>Chapter 3: Development and Characterization of Cellulose Acetate Sulfate Films for Food Packaging Applications .....</b>	
<b>Packaging Applications .....</b>	<b>77</b>

Abstract.....	77
Introduction.....	78
Materials and Methods.....	81
Results and Discussions.....	88
Conclusion.....	103
References.....	105

#### **Chapter 4: Understanding the Formation of Insoluble Gel Particles during Cellulose**

<b>Acetylation.....</b>	<b>113</b>
Abstract.....	113
Introduction.....	113
Materials and Methods.....	117
Results and Discussions.....	126
Conclusion.....	144
References.....	147

#### **Chapter 5: Predicting the Quality of Cellulose Acetate for Impurity Analysis of the Cotton**

<b>Lintar Pulp.....</b>	<b>152</b>
Abstract.....	152
Introduction.....	153
Materials and Methods.....	154
Results and Discussions.....	160

Conclusion .....	172
References.....	174
<b>Appendices</b> .....	178
<b>Appendix A</b> (Supporting Information for Chapter 1) .....	179
<b>Appendix B</b> (Supporting Information for Chapter 2) .....	189
<b>Appendix C</b> (Supporting Information for Chapter 3) .....	190
<b>Appendix D</b> (Supporting Information for Chapter 4) .....	191
<b>Appendix E</b> (Supporting Information for Chapter 5) .....	196

## LIST OF TABLES

Table 1.1	Molecular weight of CA samples .....	5
Table 2.1	Molecular weight and polydispersity index of CA and the resulting CAS .....	44
Table 2.2	MB adsorption kinetics parameters .....	65
Table 2.3	MB adsorption isotherm parameters .....	65
Table 3.1	DS <sub>sulfate</sub> , DS <sub>acetyl</sub> , and molecular weight of the reference CA and CAS .....	81
Table 3.2	Properties of CAS Films.....	94
Table 3.3	Water dissolution time and oil permeability of CAS films .....	95
Table 3.4	Mechanical properties of CAS films .....	98
Table 4.1	Recovery efficiency of xylan and XA from commercially relevant solvents at room temperature (25 °C).....	126
Table 4.2	Carbohydrate composition of insoluble residues .....	133
Table 4.3	Carbohydrate composition of insoluble residues .....	138
Table 4.4	Carbohydrate composition of insoluble residues precipitated from acetic acid, and dried. ....	141
Table 5.1	Length weight mean length and weight fraction of each fractionated cotton linters pulp.....	161
Table 5.2	Carbohydrate composition of fractionated cotton linter fibers .....	163
Table 5.3	Degree of substitution (DS) and the turbidity of synthesized cellulose acetates in acetone.....	164
Table 5.4	The amount of SIS in two-step hydrolysate and turbidity of the solutions.....	170

## LIST OF FIGURES

Figure 1.1	A sequential procedure for the synthesis of CAS and preparation of CAS hydrogels .....	11
Figure 1.2	Photographs of CA and the resulting CAS that are able to form single-component solutions/hydrogels: (a) CA $DS_{acetyl}$ of 1.8, (b) CAS $DS_{sulfate}/DS_{acetyl}$ ratio of 0.2, (c) CAS $DS_{sulfate}/DS_{acetyl}$ ratio of 0.3, (d) CAS $DS_{sulfate}/DS_{acetyl}$ ratio of 0.4, (e) CAS $DS_{sulfate}/DS_{acetyl}$ ratio of 0.6, and (f) IR spectra of CA $DS_{acetyl}$ of 1.8 and each CAS .....	14
Figure 1.3	Behaviors of CAS with varying $DS_{acetyl}$ and $DS_{sulfate}$ in deionized water: (a) Behaviors of CAS synthesized from commercially available CAS ( $DS_{acetyl}$ 1.8, 2.5, and 2.8) and (b) Photographs of CAS synthesized from CA having $DS_{acetyl}$ of 1.8.....	15
Figure 1.4	Front and side view of molded CAS solutions/hydrogels with varying $DS_{sulfate}/DS_{acetyl}$ ratios and solid contents .....	18
Figure 1.5	Estimation of critical gelation solid content: (a) CAS $DS_{sulfate}/DS_{acetyl}$ ratio of 0.2, (b) CAS $DS_{sulfate}/DS_{acetyl}$ ratio of 0.4, and (c) $DS_{sulfate}/DS_{acetyl}$ ratio of 0.6 .....	19
Figure 1.6	Rheological characterizations of CAS solutions/hydrogels with varying the $DS_{sulfate}/DS_{acetyl}$ ratios and solid contents: (a) Frequency sweep tests of CAS solutions/hydrogels with varying the $DS_{sulfate}/DS_{acetyl}$ ratios at the fixed solid content (3 wt. %), Frequency sweep tests of (b) CAS $DS_{sulfate}/DS_{acetyl}$ ratio 0.2 with varying solid contents 2 – 5 wt. %, (c) CAS $DS_{sulfate}/DS_{acetyl}$ ratio 0.4 with varying solid contents 2 – 5 wt. %, and (d) CAS $DS_{sulfate}/DS_{acetyl}$ ratio 0.6 with varying solid contents 2 – 6 wt. % .....	21
Figure 1.7	Demonstration of thermal reversibility of CAS solutions/hydrogels with varying the ratios of $DS_{sulfate}/DS_{acetyl}$ (0.2, 0.4, and 0.6) .....	23
Figure 1.8	Illustration of CAS hydrogels formation mechanism.....	25
Figure 1.9	XRD spectra of CAS hydrogel films with varying the ratios of $DS_{sulfate}/DS_{acetyl}$ (0.2, 0.4, and 0.6).....	26
Figure 1.10	(a) Preparation procedure for CAS hydrogel disks incorporated with sodium salicylate (SAL), (b) CAS hydrogel disks incorporated with SAL, (c) Fluorescence microscopic images of NIH3T3 cells cultured on the surface of CAS hydrogels ( $DS_{sulfate}/DS_{acetyl}$ ratios of 0.2, 0.3, and 0.4) after 1, 4, and 7 days of incubation in complete media at 37 °C using live (green) and dead (red) cell staining assay, scale bars are 300 $\mu$ m, and (d) Cell viability of CAS hydrogels ( $DS_{sulfate}/DS_{acetyl}$ ratios of 0.2, 0.3, and 0.4) after 1, 4, and	

7 days of incubation (n = 3).....	28
Figure 1.11 (a) Schematic representation of SAL release mechanism via CAS hydrogel matrices and (b) SAL release profile in aqueous media via CAS hydrogel matrices. ....	29
Figure 2.1 CAS hydrogel formation procedure and its thermal reversibility (Solid content: 4.5 wt. %).....	50
Figure 2.2 Rheological behaviors of CAS solutions/hydrogels with varying the DS <sub>sulfate</sub> and DS <sub>acetyl</sub> ratios and solid contents .....	52
Figure 2.3 (a) Behaviors of molded CAS hydrogels (DS <sub>sulfate</sub> /DS <sub>acetyl</sub> ratio of 0.4 and solid content of 4.5 wt. %) with and without ionic crosslinking in deionized water and (b) The changes in the solid content of CAS hydrogels (DS <sub>sulfate</sub> /DS <sub>acetyl</sub> ratio of 0.4 and solid content of 4.5 wt. %) with and without ionic crosslinking in deionized water.....	53
Figure 2.4 (a) Fabrication scheme of double-crosslinked CAS hydrogels, (b) Behaviors of molded CAS hydrogels (DS <sub>sulfate</sub> /DS <sub>acetyl</sub> ratio of 0.4 and solid content of 4.5 wt. %) with and without ionic crosslinking in deionized water, and (c) The changes in the solid content of CAS hydrogels (DS <sub>sulfate</sub> /DS <sub>acetyl</sub> ratio of 0.4 and solid content of 4.5 wt. %) with and without ionic crosslinking in deionized water.....	55
Figure 2.5 Procedure for the preparation of CAS hydrogel 3D structures (DS <sub>sulfate</sub> /DS <sub>acetyl</sub> ratio of 0.4 and the solid content of all employed CAS hydrogels was held constant at 4.5 wt. %) .....	57
Figure 2.6 (a) Influence of adsorbent mass and DS <sub>sulfate</sub> /DS <sub>acetyl</sub> ratios on adsorption capacity (C <sub>0</sub> = 100 mg/L, 7 days of contact time at 23 °C), (b) Influences of pH on adsorption capacity (DS <sub>sulfate</sub> /DS <sub>acetyl</sub> ratio of 0.4, C <sub>0</sub> = 100 mg/L, 7 days of contact time at 23 °C ), (c) ATR-FTIR spectra of MB, and double crosslinked CAS hydrogel adsorbent (DS <sub>sulfate</sub> /DS <sub>acetyl</sub> ratio of 0.4) before and after the adsorption experiment, and (d) Influences of initial pH on the zeta potential of CAS hydrogel having DS <sub>sulfate</sub> /DS <sub>acetyl</sub> ratio of 0.4 before and after the ionic crosslinking with Ca <sup>2+</sup> .....	58
Figure 2.7 MB removal behaviors of the CAS hydrogel adsorbent: (a) kinetics (C <sub>0</sub> = 100 mg/L and pH =7 at 23 °C), (b) Intra-particle diffusion model (C <sub>0</sub> = 100 mg/L and pH =7 at 23 °C), (c) Isotherm (pH = 7, exposal time = 24 h at 23 °C) of MB, and (d) Influences of initial MB concentrations on the adsorption capacity (pH = 7, exposal time = 24 h at 23 °C). ....	62
Figure 2.8 Photos of the desorption process of MB from a CAS hydrogel adsorbent in 0.1 M HCl, and (b) MB removal ratio of regenerated CAS hydrogel adsorbents	

measured at each cycle: $DS_{\text{sulfate}}/DS_{\text{acetyl}}$ ratio = 0.4, $C_0 = 100 \text{ mg/L}$ , $\text{pH} = 7$ , and $t = 48 \text{ hours}$ at $23 \text{ }^\circ\text{C}$ .....	66
Figure 3.1 FT-IR spectra of the synthesized CAS .....	89
Figure 3.2 The procedure for preparing CAS film solutions.....	90
Figure 3.3 Viscosity of the CAS film solutions.....	91
Figure 3.4 (a) A CAS film prepared from a CAS film solution with the $DS_{\text{sulfate}}/DS_{\text{acetyl}}$ balance of 0.7/1.8 and (b) Three strips of CAS films made from different film solutions with varying the $DS_{\text{sulfate}}/DS_{\text{acetyl}}$ balances (0.4/1.8, 0.7/1.8, and 1.0/1.8) .....	92
Figure 3.5 SEM surface images of (a) $DS_{\text{sulfate}}/DS_{\text{acetyl}}$ 0.4/1.8, (b) $DS_{\text{sulfate}}/DS_{\text{acetyl}}$ 0.7/1.8, and (c) $DS_{\text{sulfate}}/DS_{\text{acetyl}}$ 1.0/1.8 CAS films; SEM cross section images of (d) $DS_{\text{sulfate}}/DS_{\text{acetyl}}$ 0.4/1.8, (e) $DS_{\text{sulfate}}/DS_{\text{acetyl}}$ 0.7/1.8, and (f) $DS_{\text{sulfate}}/DS_{\text{acetyl}}$ 1.0/1.8 CAS films .....	93
Figure 3.6 Photographs of (a) $DS_{\text{sulfate}}/DS_{\text{acetyl}}$ 0.4/1.8, (b) $DS_{\text{sulfate}}/DS_{\text{acetyl}}$ 0.7/1.8, (c) $DS_{\text{sulfate}}/DS_{\text{acetyl}}$ 1.0/1.8 film, (d) $DS_{\text{sulfate}}/DS_{\text{acetyl}}$ 0.4/1.8 film, and (e) $DS_{\text{sulfate}}/DS_{\text{acetyl}}$ 0.7/1.8 film upon immersion in deionized water for 1 hour .....	96
Figure 3.7 The contact angle and WVP of CAS films with varying the $DS_{\text{sulfate}}/DS_{\text{acetyl}}$ 0.4/1.8, 0.7/1.8, and 1.0/1.8 balances .....	97
Figure 3.8 Comparative study of CAS coating using $DS_{\text{sulfate}}/DS_{\text{acetyl}}$ 0.4/1.8, 0.7/1.8, and 1.0/1.8 film forming solutions.....	101
Figure 4.1 (a) Cellulose acetate production process and (b) centrifugation was used to isolate IGP contained in a commercial CA with a DS of 2.45 also commonly referred to as cellulose diacetate (CDA) .....	115
Figure 4.2 Behaviors of beechwood xylan ( $DS = 0$ ) and XA ( $DS = 1.0$ and $2.0$ ) in the relevant solvent.....	127
Figure 4.3 (a) Collected insoluble fraction after centrifugation and (b) Polymer-polymer interaction energy of beechwood xylan and XA in the relevant solvents .....	128
Figure 4.4 Photo of (a) precipitated IGP-free CDA/beechwood xylan aggregates before drying and (b) Vacuum dried IGP-free CDA/beechwood xylan aggregates.....	130
Figure 4.5 Demonstration of Type B IGP-formation in acetone and acetic acid .....	132
Figure 4.6 Photos of insoluble residue (a) collected after the demonstration of Type B IGP formation, (b) collected after acetylation and hydrolysis process,	

	(c) collected from an experiment for investigating influences of the precipitation process, and (d) collected from an experiment for investigating influences of the drying process .....	133
Figure 4.7	(a) The examination of roles of beechwood xylan, as well as its behavior in a solvent in the formation of Type B IGP and (b) Influences of DS of XA on the turbidity of IGP-free CDA/beechwood xylan or XA (DS = 1.0 and 2.0) aggregates acetone solution.....	137
Figure 4.8	FTIR spectra collected from insoluble residues produced from (a) CA with DS of 1.85/XA with varying DS (0, 1.0, and 2.0), (b) CA with DS of 2.45/XA with varying DS (0, 1.0, and 2.0), and (c) CA with DS of 2.85/XA with varying DS (0, 1.0, and 2.0).....	142
Figure 4.9	(a) PCA loading plot and showing the FTIR vibrations that differentiate the CA, XA, and insoluble residues and (b) Results of PLS analysis of the IR spectra predicting the glucose content of all the insoluble residues.....	143
Figure 5.1	Schematic drawing of Bauer-McNett fiber classifier.....	155
Figure 5.2	Two-step hydrolysate solutions produced from long fibers (left) and short fibers (right).....	162
Figure 5.3	Cellulose acetate acetone solutions .....	164
Figure 5.4	FT-IR spectra obtained from original SIS and IGP made from SIS .....	167
Figure 5.5	Size distribution of IGP measured by DLS .....	169
Figure 5.6	Correlation between (a) amount of SIS and turbidity and (b) Sum of wt. % of xylan and turbidity and amount of IGP .....	171

## CHAPTER 1

### Simple Strategy for Production of Tunable and Single-Component Cellulose Acetate Sulfate Hydrogels for Drug Release

#### Abstract

Cellulose-based hydrogels have potential biomedical applications due to their biocompatibility, hydrophilicity, and biodegradability. However, their technical complexity in the formulation of cellulose-based hydrogels has limited their use. In this study, we propose a simple strategy for producing cellulose-based hydrogels by one-pot sulfation of commercially available cellulose acetate. The resulting cellulose acetate sulfate (CAS) forms single-component hydrogels in deionized water within a specific range of degree of sulfation ( $DS_{\text{sulfate}}$ ) and degree of acetylation ( $DS_{\text{acetyl}}$ ), without the need for crosslinking agents or supplementary polymers. The rheological properties of CAS hydrogels can be tuned by adjusting the balance between sulfate and acetyl moieties, solid content, and temperature, making them versatile for processing into various shapes. We evaluated the drug release profiles of CAS hydrogel matrices loaded with sodium salicylate (SAL) by varying the balance between sulfate and acetyl moieties. Our results demonstrate the feasibility of CAS hydrogels as drug release matrices. Our approach offers a novel and simplified method for producing cellulose-based hydrogels, with potential applications in various fields.

## 1. Introduction

Some hydrophilic polymers possess a unique ability to construct complex 3D polymer networks in water via physical and chemical bonding. Unlike traditional hydrophilic polymers that typically dissolve in water, these 3D polymer networks can hold a significant amount of water molecules within the networks while retaining their characteristic structures. These distinctive polymer complexes have been named hydrogels [1, 2]. Due to their versatility and unique properties, hydrogels have been considered a promising material for a wide range of applications, including cosmetics, personal hygiene products, wound dressing and drug delivery [3-5]. Drug delivery is one of the emerging fields in which hydrogels have been extensively researched [6, 7]. Hydrogels have been shown to function as drug reservoirs, and it is possible to achieve controlled drug release by modifying the properties of the hydrogel matrices [8, 9]. Hydrogels have been formulated from two different sources: synthetic and natural polymers. Natural polymers, including cellulose, hemicellulose, alginates, chitosan, and hyaluronic acid have been recognized as desirable materials for preparing hydrogels for drug delivery applications due to their biodegradability, biocompatibility, and non-toxicity compared to synthetic polymers [10].

Cellulose, among these natural polymers, has gained considerable attention for hydrogel production due to its abundance and the presence of hydrophilic moieties in its backbone [11]. Cellulose consists of  $\beta$ -D-glucose units linked by  $\beta$ -1,4-glycosidic bonds. Cellulose has distinctive semi-crystalline structures due to the presence of three free hydroxyl moieties in each glucose unit that enable the formation of inter- and intramolecular hydrogen bonds [12]. However, the hydrogen-bonded structures of cellulose result in the insolubility in water or conventional organic solvents, hindering the preparation of cellulose-based hydrogels [10, 13, 14]. Numerous approaches for formulating cellulose-based hydrogels have been developed; however, many of

them commonly utilize complicated techniques and supplementary components [15, 16]. For example, cellulose is typically subjected to intricate chemical modifications to introduce moieties that enable the formation of covalently crosslinked polymer networks via the usage of crosslinkers or UV [17, 18]. Moreover, despite the commercial availability of cellulose derivatives for the preparation of cellulose-based hydrogels, complex formulation techniques such as freeze-thaw [19], grinding and homogenization [20], and radiation [21], along with the addition of supplementary components, are still necessary to formulate cellulose-based hydrogels. The technical challenges related to the formulation of cellulose-based hydrogels may eventually lead to the waning of cellulose-based hydrogels usage [22]. Thus, the development of a simple strategy for preparing cellulose-based hydrogels would significantly help promote the utilization of cellulose-based hydrogels.

Certain amphiphilic block and random copolymers exhibit the ability to spontaneously self-assemble into distinct supramolecular structures through non-covalent intermolecular interactions, including hydrophobic association, hydrogen bonding, electrostatic interactions, and host-guest complexation, and others [6, 23]. Advanced synthesis techniques have enabled the preparation of amphiphilic cellulose derivatives, and their self-assembly behaviors have been the subject of extensive investigation [3, 24]. Moreover, by controlling the balance between hydrophobic and hydrophilic segments, the unique self-assembly behavior of amphiphilic copolymers can lead to the formation of "single-component" hydrogels, not only self-assembled microgels or nanogels [25]. Amphiphilic cellulose derivatives have shown the potential to form single-component hydrogels. It has been demonstrated that the rheological properties of water-soluble cellulose derivative solutions can be modulated by the introduction of hydrophobic moieties which induce the formation of supramolecular structures via additional hydrophobic

associations [26, 27]. Nonetheless, the research conducted on preparation of single-component cellulose-based hydrogels utilizing amphiphilic cellulose derivatives remains limited.

Herein, a simple and facile approach to produce "single-component and tunable" cellulose-based hydrogels inspired by the unique behavior of amphiphilic copolymers is proposed. This involved the synthesis of amphiphilic cellulose derivatives (cellulose acetate sulfate, CAS) by introducing hydrophilic sulfate moieties to hydrophobically modified cellulose (cellulose acetate, CA), instead of utilizing the previously reported strategy of introducing hydrophobic moieties to water-soluble cellulose derivatives. The behavior of the resulting CAS with varying balances between sulfate and acetyl moieties in deionized water was examined, and the formulation of single-component CAS hydrogel was demonstrated using CAS synthesized from CA with a  $DS_{\text{acetyl}}$  of 1.8. Compared to other methods for preparing cellulose-based hydrogels, the simplicity of this scheme is a significant advantage. In a specific range of the balance between hydrophilic sulfate moieties and hydrophobic acetyl moieties, the chemical compound known as CAS can form hydrogels with ease by introducing deionized water, without the need for supplementary components such as crosslinking agents or additional polymers. The rheological properties of CAS solutions/hydrogels with different balances between sulfate and acetyl moieties were investigated using a rheometer. It was hypothesized that differences in the number of sulfate moieties in CAS hydrogels could lead to changes in the interaction with drug molecules in the matrices, thereby resulting in changes in the drug release rate. To test this, CAS hydrogel was incorporated with a hydrophilic drug (sodium salicylate, SAL), and drug release profiles of each CAS matrix were studied while varying the balance between sulfate and acetyl moieties.

## 2. Materials and Methods

### 2.1. Materials

Commercially available CA samples ( $DS_{\text{acetyl}}$  of 1.8, 2.5, and 2.8) were kindly provided by Eastman Chemical Company. (Kingsport, TN). *N, N*-dimethylformamide (DMF), sulfamic acid, sodium acetate, ethanol, sodium salicylate, sodium hydroxide, Dulbecco's modified Eagle's medium (DMEM), Fetal bovine serum (FBS), phosphate-buffered saline (PBS), and antibiotic and antimycotic were purchased from Fisher-Scientific (Hampton, NH) and utilized as received. Cookie dough press cutters were purchased from a local grocery.

Table 1. Molecular weight of CA samples

	$M_w$	PDI ( $M_w/M_n$ )
CA $DS_{\text{acetyl}}$ of 2.8	323,000	2.9
CA $DS_{\text{acetyl}}$ of 2.5	205,000	2.6
CA $DS_{\text{acetyl}}$ of 1.8	111,000	2.2
* Molecular weight ( $M_w$ ) and polydispersity index (PDI) were measured by GPC employing polystyrene as a standard		

### 2.2. Synthesis of Cellulose Acetate Sulfate

CAS synthesis was conducted as described elsewhere [28]. Briefly, oven-dried CA flakes (15 g) were dissolved in 100 ml of anhydrous DMF at 80 °C. In the meantime, a predetermined amount of sulfamic acid was dissolved in 70 ml of anhydrous DMF to prepare a sulfating agent. Once the dissolution of CA flakes in DMF was achieved, the prepared sulfating agent was slowly introduced and stirred at 80 °C for 2 hours. The resulting CAS was recovered by the precipitation with ethanol containing 3 wt. % of sodium acetate, rinsed several times with an excess amount of ethanol to remove residual DMF and sodium salt, and air-dried at room temperature in a fume hood. The synthesis of CAS was examined by attenuated total reflection

Fourier transform infrared spectroscopy (Spectrum 3 spectrometer, PerkinElmer, Waltham, MA). Air-dried CAS powders were scanned 16 times from 650 to 4000  $\text{cm}^{-1}$  at a resolution of 2  $\text{cm}^{-1}$ .

### **2.3. Behavior of CAS in Deionized Water**

To investigate the behaviors of synthesized CAS, air-dried CAS powder with varying  $\text{DS}_{\text{sulfate}}/\text{DS}_{\text{acetyl}}$  ratios (0.2, 0.4, and 0.6) was subjected to washing with deionized water several times. Then, a predetermined amount of deionized water was introduced to adjust the solid content to 4 wt. %. Swelling and homogenization were conducted in a water bath (HBR 4 control, IKA, Wilmington, NC) at an elevated temperature (70 °C). The resulting samples were centrifuged to remove bubbles created during the homogenization and kept in a refrigerator to cool them down to room temperature.

### **2.4. Behavior of CAS Solutions and Hydrogels**

CAS powders with different  $\text{DS}_{\text{sulfate}}/\text{DS}_{\text{acetyl}}$  ratios of 0.2, 0.4, and 0.6 were selected to examine the behaviors of CAS solutions/hydrogels. The solid content of CAS hydrogels was computed by gravimetrically comparing the weight before and after oven-drying at 105 °C for 24 h, and details are provided in supporting information. To investigate the thermal reversibility of CAS hydrogels, each CAS hydrogel (5 g and solid content of 4 wt. %) was transferred to each 20 ml vial. The temperature of CAS hydrogels was controlled in a water bath (HBR 4 control, IKA, Wilmington, NC). The temperature gradually increased from 23 to 63 °C and was held at 37 °C, 50 °C, and 63 °C for 30 min to equilibrate the CAS solutions/hydrogels at each temperature. Lastly, the CAS solutions/hydrogels were cooled down to room temperature (23 °C) to examine the behaviors compared to the original state.

CAS powders with the  $DS_{\text{sulfate}}/DS_{\text{acetyl}}$  ratios of 0.2, 0.4, and 0.6 were utilized to produce each CAS solution/hydrogel. The solid contents of CAS solutions/hydrogels were controlled from 2 to 5 wt. % (in the case of CAS with  $DS_{\text{sulfate}}/DS_{\text{acetyl}}$  ratios of 0.2 and 0.4) and from 2 to 6 wt. % (in the case of CAS with  $DS_{\text{sulfate}}/DS_{\text{acetyl}}$  ratio of 0.6) by adding predetermined amounts of deionized water. The behaviors of CAS solutions/hydrogels were investigated by pouring CAS hydrogels in cookie dough press cutters having various shapes. After treating CAS solutions/hydrogels in the water bath at 70 °C to make them flow easily, they were poured into the cookie dough press cutters. Molded CAS solutions/hydrogels were kept in a refrigerator for 30 min. To equilibrate the samples at room temperature (23 °C), the molded samples were placed on a plastic plate for an hour. Afterward, mold frames were carefully removed, and pictures of molded solutions/hydrogels were taken to compare behaviors and shape fidelities qualitatively.

## **2.5. Rheological Measurement**

CAS solutions/hydrogels with varying  $DS_{\text{sulfate}}/DS_{\text{acetyl}}$  ratios (0.2, 0.4, and 0.6) and solid contents (2 to 5 wt. % in the case of  $DS_{\text{sulfate}}/DS_{\text{acetyl}}$  ratios of 0.2 and 0.4 and 2 to 6 wt. % in the case of  $DS_{\text{sulfate}}/DS_{\text{acetyl}}$  ratio of 0.6) were prepared to investigate rheological properties with a dynamic rotational rheometer (MCR 72, Anton Parr, Ashland, VA) equipped with a parallel plate (PP25) with fixed gap size at 1 mm. The changes in the storage modulus ( $G'$ ) and loss modulus ( $G''$ ) were recorded with angular frequency sweep mode ( $10^{-1}$  to  $10^2$  rad/s). All measurements were carried out at room temperature (23 °C) with a pre-equilibration time of 1 min.

## 2.6. X-ray Diffraction

CAS hydrogels with varying  $DS_{\text{sulfate}}/DS_{\text{acetyl}}$  ratios (0.2, 0.4, and 0.6) were prepared. By decreasing the solid content of each hydrogel down to 1.5 wt. %, CAS film-forming solutions were obtained. CAS films were casted by pouring the solutions over Teflon evaporating dishes (diameter 100 mm). The amount of CAS in an evaporating dish was fixed at 0.004 g/cm<sup>2</sup>. X-ray diffraction patterns of CAS hydrogel films were collected by using a SmartLab X-ray diffractometer (Rigaku, Woodlands, TX). The operating voltage and current were 40 kV and 44 mA. A Cu K $\alpha$  X-ray tube was used to generate X-rays at a wavelength of 0.1541 nm. A graphite monochromator and K $\beta$  filter were used for the collection of the diffracted beams. CAS hydrogel films were placed on a quartz-supported sample holder. Then, the sample holder was placed inside the x-ray chamber. Measurement of  $2\theta$  angle range was set from 4 degrees to 55 degrees. Each step was 0.025 degree, and the X-ray detector remained constant for 2.5 seconds at each step to collect the diffracted X-rays. Background subtraction and signal smoothing were done with HighScore Plus 3.0 software (PANalytical, Westborough, MA).

## 2.7. Cell Viability

CAS hydrogels with varying  $DS_{\text{sulfate}}/DS_{\text{acetyl}}$  ratios (0.2, 0.3, and 0.4) were prepared and heated in a water bath at 60 °C to process them into substrates for cell viability test by pouring CAS solutions into 6-well plates. All CAS hydrogels were crosslinked with 3 wt. % of a CaCl<sub>2</sub> aqueous solution overnight and rinsed with fresh phosphate-buffered saline (PBS) several times to remove remaining Ca<sup>2+</sup> ions. Then, all CAS hydrogels were sterilized under UV light for 2 hours, immersed into filter sterilized cell culture media prepared with 89% Dulbecco's Modified Eagle Medium (DMEM, Gibco<sup>TM</sup>), 10 % fetal bovine serum (FBS, Gibco<sup>TM</sup>) and 1% antibiotic and

antimycotic (Gibco™), and incubated at 37 °C under 5 % CO<sub>2</sub> for 24 h. After this period, the pH was measured to ensure a suitable cell growth environment. The NIH3T3 murine embryonic fibroblasts (CRL-1658, ATCC, Manassas, VA) cells were employed to examine the cell viability of CAS hydrogels. The cells were seeded ( $3 \times 10^5$  per well) on the top of each hydrogel substrate on the 6-well plates and cultured in the incubator at 37 °C and 5 % CO<sub>2</sub> in 3 mL cell culture media prepared as mentioned above. The media was replaced with fresh media every 24 hours. Cell viability of CAS hydrogels was investigated with a LIVE/DEAD™ Viability/Cytotoxicity Kit, for mammalian cells (Invitrogen) on days 1, 4, and 7. For the live/dead assay, media was removed from each well, washed three times with PBS, and incubated with 2 mL of Live/Dead reagent at 37 °C for 30 minutes. The Live/Dead assay reagent was prepared as per the instruction provided in the protocol. Briefly, 1 μL of 4mM Calcein AM and 4 μL of 2mM ethidium homodimer (EthD) were added per 2 mL of PBS. After the incubation, all the samples were washed three times with PBS. The treated cells were examined with a fluorescence microscopy (SP8, Leica Microsystems) and analysis of obtained images was conducted employing ImageJ [29, 30].

## **2.8. Drug Release Test**

CAS powders with the DS<sub>sulfate</sub>/DS<sub>acetyl</sub> ratios of 0.2, 0.3, and 0.4 was prepared to produce hydrogel matrices for the drug release test. The drug was incorporated in CAS hydrogels (solid content 4 wt. %) during the formulation. For this, 5 wt. % of sodium salicylate based on the oven-dried mass of each CAS powder was dissolved in deionized water prior to introducing deionized water to CAS powders. Afterward, all CAS hydrogels were treated in the water bath at 70 °C and molded into hydrogel disks incorporated with the drug by pouring CAS hydrogels into

a 40 well-plate (1 cm in diameter and 2 cm in height for each well). The hydrogels were kept in a refrigerator overnight and carefully detached before use.

A calibration curve of sodium salicylate in the range of 0.005 – 0.1 mg/ml for a back-calculation of the drug concentration in a drug-releasing medium was plotted by utilizing a linear correlation between absorption at 296 nm and drug concentration. To prepare a drug-releasing medium, NaCl (0.5 w/v %) was dissolved in Milli-Q water and the pH of the medium was adjusted to 7 with NaOH. Each hydrogel disk (known mass) was introduced into a glass Erlenmeyer flask filled with the drug-releasing medium (known volume). Aliquots of the medium were obtained at predetermined times for absorbance measurements. The drug release experiments were conducted in a constant temperature chamber at 25 °C and all the drug release tests were triplicated.

## **2.9. Statistical Analysis**

Statistical analysis was conducted using one-way ANOVA (for studies corresponding to results shown in Figure 1.9 d) at a significance level of  $\alpha = 0.05$  with Tukey HSD post hoc tests. The sample size was fixed constant at  $n = 3$  for the studies.

### 3. Results and Discussions

#### 3.1. Synthesis of CAS and Formation of Single-Component CAS Hydrogels

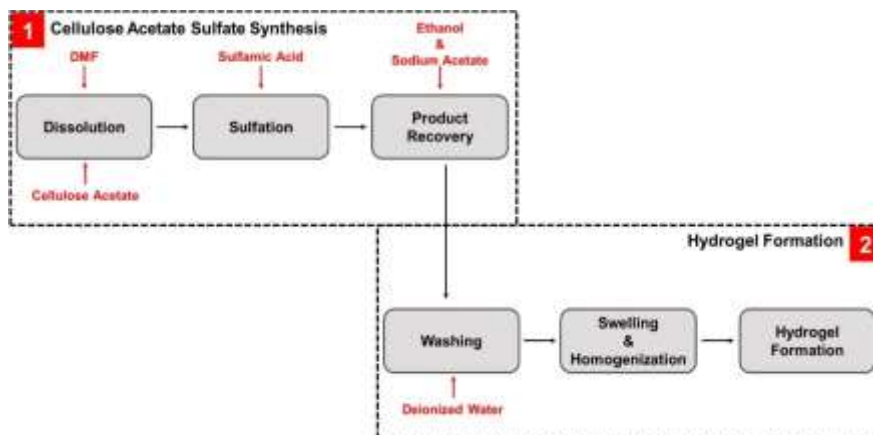


**Figure 1.1.** A sequential procedure for the synthesis of CAS and preparation of CAS hydrogels.

Several strategies have been developed to formulate hydrogels based on CA. Generally, the production of CA-based hydrogels requires the introduction of crosslinking agents, supplementary polymers, or combinations of these additional components [31-33]. These production schemes for CA-based hydrogels suggest that hydroxyl and acetyl moieties alone are insufficient to establish strong intermolecular interactions necessary for the formulation of a ‘single-component’ hydrogel composed of only water molecules and CA chains. It has been known that the formation of single component hydrogels using amphiphilic copolymers is attributed to the interplay of intermolecular interactions. These forces can cause self-assembly behaviors, resulting in the formation of polymer networks that are suitable for hydrogels without the need for external additives such as crosslinking agents or supplementary polymers [23, 34]. The behavior of amphiphilic copolymers has inspired a new and simple approach to the formation of ‘single-component’ cellulose-based hydrogels. This strategy involves the introduction of hydrophilic sulfate moieties ( $-\text{OSO}_3^-$ ) into hydrophobic CA, instead of employing additional components.

These sulfate moieties can theoretically induce more vigorous intermolecular interactions, such as hydrogen bonding and ionic interaction, which are essential in establishing polymer networks suitable for the formulating hydrogels [27, 34, 35]. Figure 1.1 demonstrates the sequential procedure for synthesizing CAS and preparing single-component CAS hydrogels. For the synthesis, commercially available CA were dissolved in DMF, and the sulfation of CA was initiated by introducing the sulfating agent, sulfamic acid. CAS with varying  $DS_{\text{sulfate}}$  were prepared by varying the amount of the sulfating agent used. The synthesis was quenched by introducing ethanol containing 3 wt. % of sodium acetate, which stabilized the newly substituted sulfate moieties in CAS. Changes in the affinity of CAS toward the solvent mixture induced the precipitation of the resulting CAS [28].

The synthesis of CAS can be evaluated both qualitatively and quantitatively. The original color of the starting material, CA, was white. However, during the synthesis of CAS, the color of the product gradually changed from white to yellowish as the  $DS_{\text{sulfate}}$  increased (Figure 1.2a-e). The ATR-FTIR spectra of the synthesized CAS provide qualitative information on the presence of moieties in CAS (Figure 1.2f). In the synthesis of CAS, acetyl moieties in CA serve as a protecting group [14, 28]. Peaks observed near  $1730\text{ cm}^{-1}$  in the ATR-FTIR spectra confirmed the presence of acetyl moieties in the CAS, as they are associated with the C=O stretching vibrations in acetyl groups. [36]. The acetyl content of the CAS samples was also analyzed qualitatively, and no significant changes were observed during the synthesis, consistent with previous research (Table S1) [14, 28]. The IR spectrum obtained from the pristine CA did not exhibit a peak near  $820\text{ cm}^{-1}$ , indicating the absence of sulfate moieties [37, 38]. Whereas other IR spectra obtained from CAS showed a new peak assigned to sulfate moieties near  $820\text{ cm}^{-1}$ , providing evidence for the partial substitution of hydroxyl moieties with sulfate moieties.  $DS_{\text{sulfate}}$

of the CAS was also experimentally determined based on the content of sulfur [39]. It was demonstrated that the  $DS_{\text{sulfate}}$  could be effectively controlled by varying the amount of the sulfating agent used in the synthesis. Additionally, a broad peak at around  $3440\text{ cm}^{-1}$  was observed, indicating the presence of unsubstituted hydroxyl moieties. [40]. The effects of synthesis conditions on the molecular weight ( $M_w$ ) of CAS was investigated. Polystyrene standards were used to determine the  $M_w$  of synthesized CAS samples [41], and  $M_w$  of the resulting CAS are presented in Table S1. The  $M_w$  of CAS samples synthesized from CA with a DS of 2.8 remained unchanged, while the  $M_w$  of CAS samples synthesized from CA with a DS values of 2.5 decreased as  $DS_{\text{sulfate}}$  increased. In the case of CAS synthesized from CA with a DS of 1.8, a decrease in the  $M_w$  of the CAS was observed, however, the  $M_w$  of CAS remained constant at the decreased level, regardless of  $DS_{\text{sulfate}}$ .

The formulation of CAS hydrogels was successfully demonstrated using amphiphilic CAS samples synthesized from CA with a DS of 1.8. The simplicity of CAS hydrogel formation is an outstanding advantage over other cellulose-based hydrogel formation methods. At a certain range of the balance between hydrophilic sulfate moieties and hydrophobic acetyl moieties, the formation of ‘single-component’ CAS hydrogels was simply achieved by introducing deionized water. Neither additional components, such as crosslinking agents and other supplementary polymers, nor complicated formulation techniques are necessary to produce CAS hydrogels. It suggests that additional intermolecular interactions resulting from substituted sulfate moieties induce structural changes in polymer networks, making them suitable for CAS hydrogel formation. Full details of the CAS hydrogel formation are described in Figure S1.1.

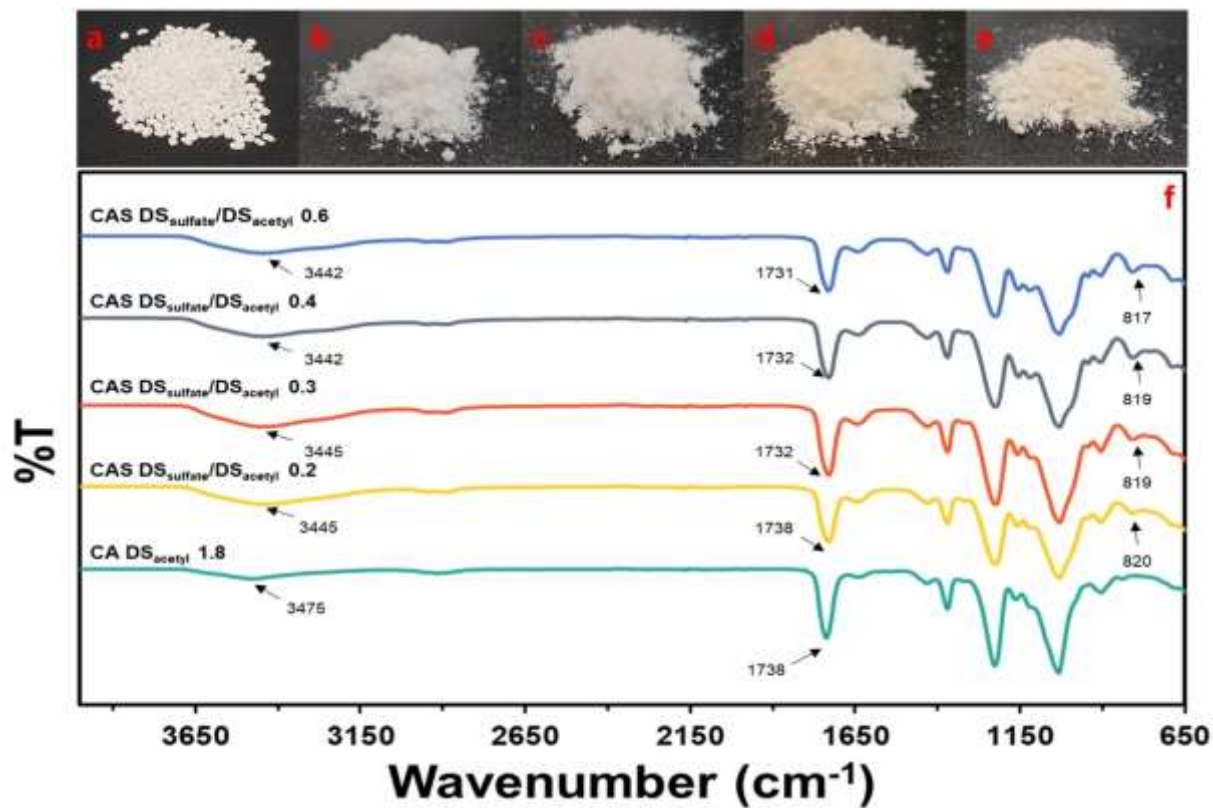


**Figure 1.2.** Photographs of CA and the resulting CAS that are able to form single-component solutions/hydrogels: (a) CA  $DS_{acetyl}$  of 1.8, (b) CAS  $DS_{sulfate}/DS_{acetyl}$  ratio of 0.2, (c) CAS  $DS_{sulfate}/DS_{acetyl}$  ratio of 0.3, (d) CAS  $DS_{sulfate}/DS_{acetyl}$  ratio of 0.4, (e) CAS  $DS_{sulfate}/DS_{acetyl}$  ratio of 0.6, and (f) IR spectra of CA  $DS_{acetyl}$  of 1.8 and each CAS.

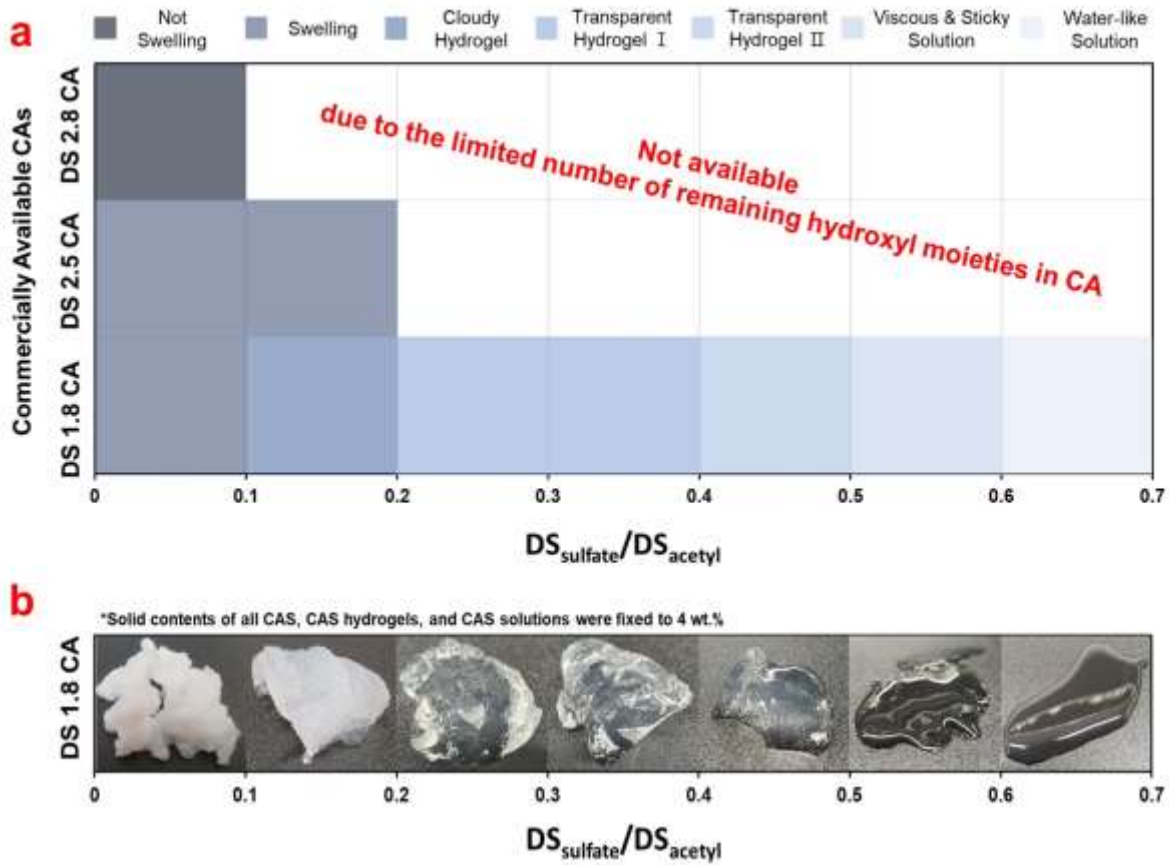


**Figure 1.3.** Behaviors of CAS with varying  $DS_{acetyl}$  and  $DS_{sulfate}$  in deionized water: (a) Behaviors of CAS synthesized from commercially available CAs ( $DS_{acetyl}$  1.8, 2.5, and 2.8) and (b) Photographs of CAS synthesized from CA having  $DS_{acetyl}$  of 1.8.

\*All  $DS_{sulfate}/DS_{acetyl}$  ratios are calculated by dividing  $DS_{sulfate}$  by  $DS_{acetyl}$ .

### 3.2. Behaviors of CAS in Deionized Water

The hydrophobicity of CA is endowed by substituted acetyl moieties and its hydrophobicity depends strongly on the  $DS_{\text{acetyl}}$  [40, 42]. In aqueous media, hydrophobic associations induced by acetyl moieties occur to minimize interactions with water molecules, resulting in the insolubility of CA in water [43, 44]. As for the formation of CA-based hydrogels, crosslinking agents and additional polymers participate in the establishment of new polymer networks capable of absorbing and holding water molecules within the networks [31, 33]. Therefore, to achieve the formation of single-component hydrogels without using additional components, the hydrophobic associations need to be transformed to some extent by other intermolecular interactions to induce structural changes in polymer networks. For CAS with relatively higher  $DS_{\text{acetyl}}$  values of 2.5 and 2.8, although the substitution of hydroxyl moieties in CAs with sulfate moieties was performed to the maximum extent, they could not be transformed into hydrogels in deionized water under experimental conditions. The observation that cellulose acetate sulfate (CAS) with higher  $DS_{\text{acetyl}}$  values of 2.5 and 2.8 fails to form hydrogels in deionized water, despite maximal substitution of hydroxyl moieties with sulfate moieties, suggests that weak intermolecular interactions induced by the sulfate moieties are insufficient to transform the hydrophobic associations. If the influence of the sulfate moieties can be further increased, it may be possible to form CAS hydrogels. However, since the number of unsubstituted hydroxyl moieties in the CAs is limited, it is not possible to achieve the optimum balance required for hydrogel formation.

Interesting observations were made on the behavior of CAS in deionized water, particularly on CAS synthesized from CA with a relatively low  $DS_{\text{acetyl}}$  of 1.8. At a low  $DS_{\text{sulfate}}$ , CAS synthesized from CA with  $DS_{\text{acetyl}}$  of 1.8 showed similar behavior to those synthesized from

CA with higher  $DS_{\text{acetyl}}$ . At this range of  $DS_{\text{sulfate}}$ , newly established intermolecular interactions by sulfate moieties might not be strong enough to change hydrophobic associations. As a result, CAS merely swelled in deionized water (Figure 1.3b). Nonetheless, as the influences of sulfate moieties gradually increased, the formation of CAS hydrogels began to occur. CAS with a  $DS_{\text{sulfate}}/DS_{\text{acetyl}}$  ratio within the range of 0.1-0.2 formed an intermediate form of hydrogel, a cloudy one (Figure 1.3b). As the  $DS_{\text{sulfate}}$  increased, the formation of CAS hydrogels started to occur from the  $DS_{\text{sulfate}}/DS_{\text{acetyl}}$  ratio range of 0.2-0.4. At this  $DS_{\text{sulfate}}/DS_{\text{acetyl}}$  ratio range, competitions among intermolecular interactions (e.g., hydrophobic associations, hydrogen bonding formation, ionic interactions, etc.) might attain an optimum point for the formation of CAS hydrogels. CAS hydrogels with  $DS_{\text{sulfate}}/DS_{\text{acetyl}}$  ratios within 0.2-0.4 accommodated water molecules within their polymer networks while maintaining their shape well. As the influence of sulfate moieties increased even further, within the  $DS_{\text{sulfate}}/DS_{\text{acetyl}}$  ratio range of 0.4-0.5, interesting changes were observed in the behavior of CAS hydrogels. While still maintaining their initial structure at the beginning, the hydrogels began to slowly exhibit lateral spreading over time. This phenomenon is likely due to the increase in the influence of intermolecular interactions induced by sulfate moieties over the hydrophobic associations. As a result, the original shape of the hydrogels was gradually altered over time [45]. When the amount of sulfate moieties in CAS exceeds a certain threshold, their influence overcomes that of the hydrophobic associations, leading to a loss of the original structural integrity. Instead, the CAS becomes a viscous solution. This occurs particularly in CAS with a  $DS_{\text{sulfate}}/DS_{\text{acetyl}}$  ratio above 0.5. Overall, at a fixed solid content, the behavior of the CAS in deionized water is primarily determined by the balance between sulfate and acetyl moieties.

### 3.3. Behaviors of CAS Solutions/Hydrogels

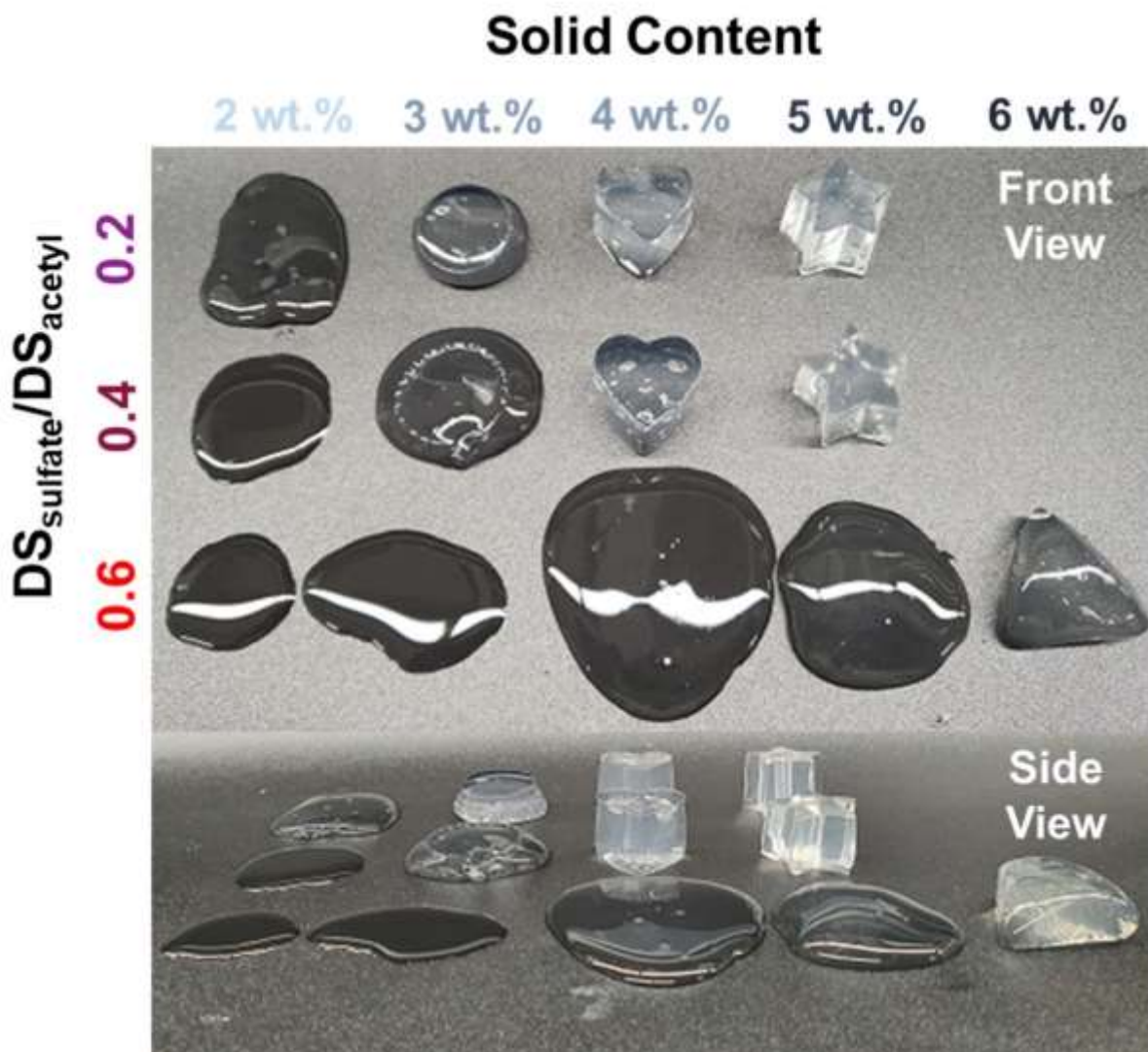


**Figure 1.4.** Front and side view of molded CAS solutions/hydrogels with varying  $DS_{\text{sulfate}}/DS_{\text{acetyl}}$  ratios and solid contents.

When CAS hydrogels are formulated, neither crosslinking agents nor additional polymers that could be engaged in the formation of covalent bonding are introduced. Instead, the development of a 3D network structure is driven primarily by intermolecular interactions, including hydrophobic associations, ionic interactions, hydrogen bonding, etc. As a result, single-

component CAS hydrogels can be categorized as physically crosslinked hydrogels [4]. The properties of physically crosslinked hydrogels are known to be affected by both characteristics of 3D polymer networks and external stimuli [46, 47]. We found that internal features of CAS polymer networks (e.g., the balance between sulfate and acetyl moieties and solid content) influenced the rheological properties of CAS solutions/hydrogels and their effects on the rheological properties were examined with CAS synthesized from CA having  $DS_{acetyl}$  of 1.8 by systematically tuning both characteristics.

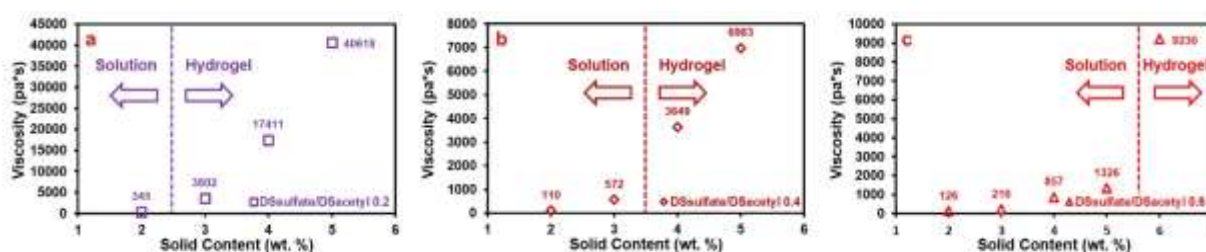


**Figure 1.5.** Estimation of critical gelation solid content: (a) CAS  $DS_{sulfate}/DS_{acetyl}$  ratio of 0.2, (b) CAS  $DS_{sulfate}/DS_{acetyl}$  ratio of 0.4, and (c)  $DS_{sulfate}/DS_{acetyl}$  ratio of 0.6.

Determining the critical gelation solid content (CGS) is an essential factor for physically crosslinked hydrogels, as it indicates the threshold solid content at which a solution undergoes a transition to a hydrogel. In our study, rheological characterizations were performed to determine the CGS for CAS with varying  $DS_{sulfate}/DS_{acetyl}$  ratios (0.2, 0.4, and 0.6). The viscosity of CAS with a  $DS_{sulfate}/DS_{acetyl}$  ratio of 0.2 increased by an order of magnitude when the solid content was increased from 2 wt. % to 3 wt. %. This suggests that the CGS of CAS with this ratio is between 2-3 wt. %. Figure 1.4 provides support for this finding. After being molded, the CAS sample with a  $DS_{sulfate}/DS_{acetyl}$  ratio of 0.2 and solid content of 2 wt. % lost its original shape and spread laterally over time, while the sample with a solid content of 3 wt. % maintained its shape

well, indicating a transition from a CAS solution to a CAS hydrogel. Furthermore, the CGS was dependent on the  $DS_{\text{sulfate}}/DS_{\text{acetyl}}$  ratio of CAS. Specifically, a reverse correlation was established between the CGS and the  $DS_{\text{sulfate}}/DS_{\text{acetyl}}$  ratio, with higher ratios resulting in a lower CGS. At low  $DS_{\text{sulfate}}/DS_{\text{acetyl}}$  ratios, where the influence of acetyl moieties is greater, hydrophobic associations may compete with intermolecular interactions induced by sulfate moieties, even at low solid content. However, as the  $DS_{\text{sulfate}}/DS_{\text{acetyl}}$  ratio increases, intermolecular interactions induced by sulfate moieties become more dominant, gradually altering the structure of the CAS polymer networks (Figure 1.9). Consequently, to offset the influence of sulfate moieties, a higher concentration of CAS chains is required, as this can increase the physical crosslinking density [48].

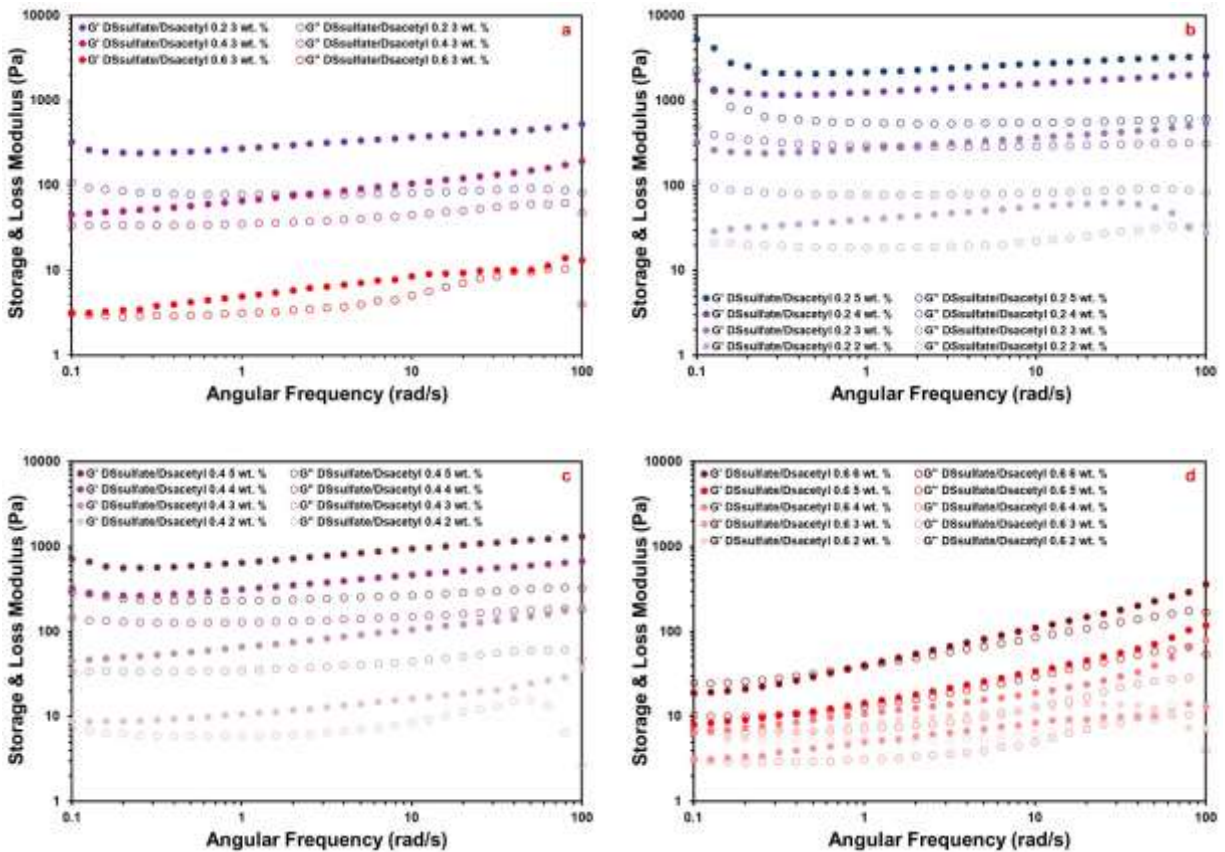


**Figure 1.6.** Rheological characterizations of CAS solutions/hydrogels with varying the  $DS_{\text{sulfate}}/DS_{\text{acetyl}}$  ratios and solid contents: (a) Frequency sweep tests of CAS solutions/hydrogels with varying the  $DS_{\text{sulfate}}/DS_{\text{acetyl}}$  ratios at the fixed solid content (3 wt. %), Frequency sweep tests of (b) CAS  $DS_{\text{sulfate}}/DS_{\text{acetyl}}$  ratio 0.2 with varying solid contents 2 – 5 wt. %, (c) CAS  $DS_{\text{sulfate}}/DS_{\text{acetyl}}$  ratio 0.4 with varying solid contents 2 – 5 wt. %, and (d) CAS  $DS_{\text{sulfate}}/DS_{\text{acetyl}}$  ratio 0.6 with varying solid contents 2 – 6 wt. %.

This study investigates the impact of the  $DS_{\text{sulfate}}/DS_{\text{acetyl}}$  ratio and solid content on the structure of CAS solutions and hydrogels. Figure 1.4 depicts the structural evolution of hydrogels with varying  $DS_{\text{sulfate}}/DS_{\text{acetyl}}$  ratios at a fixed solid content of 3 wt. %. The hydrogel with a ratio of 0.6 lost its molded shape immediately upon removal of the mold, while hydrogels with lower ratios maintained their shape and integrity. Rheological characterization was performed to further examine the influence of the  $DS_{\text{sulfate}}/DS_{\text{acetyl}}$  ratio and solid content on the hydrogel structure. The results reveal an inverse relationship between the  $DS_{\text{sulfate}}/DS_{\text{acetyl}}$  ratio and the storage modulus ( $G'$ ), indicating that a higher number of sulfate moieties leads to a weaker network structure (Figure 1.6a). Specifically, the CAS solution with a  $DS_{\text{sulfate}}/DS_{\text{acetyl}}$  ratio of 0.6 exhibited the lowest  $G'$  value, while the  $G'$  value increased by an order of magnitude as the ratio decreased. These results support the qualitative observations of the transition from CAS solutions to hydrogels with decreasing  $DS_{\text{sulfate}}/DS_{\text{acetyl}}$  ratio (Figure 1.4). The effect of solid content on  $G'$  was also examined for samples with the same  $DS_{\text{sulfate}}/DS_{\text{acetyl}}$  ratio. The data demonstrate an increasing trend in  $G'$  values with increasing solid content, consistent with the transition from CAS solutions to hydrogels (Figures 1.6b-d).

### 3.4. Formation Mechanism of CAS hydrogels

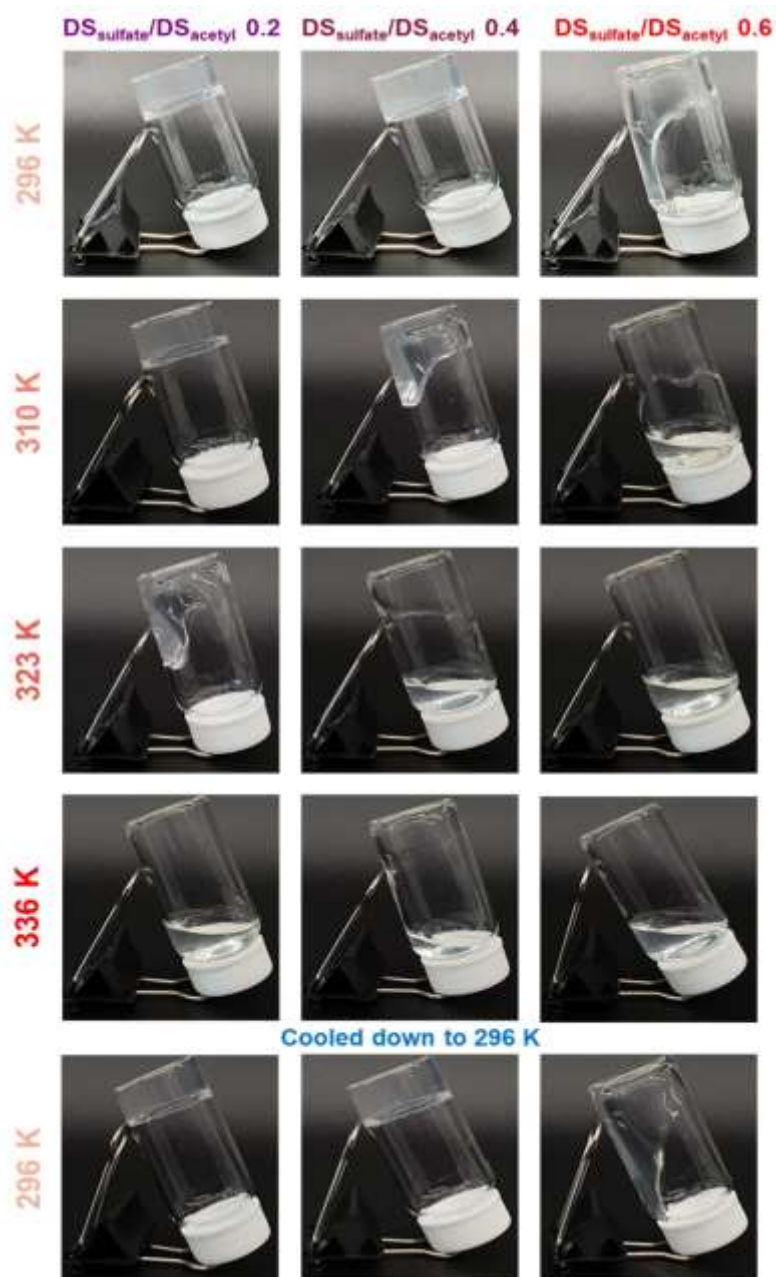


**Figure 1.7.** Demonstration of thermal reversibility of CAS solutions/hydrogels with varying the ratios of DS<sub>sulfate</sub>/DS<sub>acetyl</sub> (0.2, 0.4, and 0.6). The solid content of all the CAS hydrogels in Figure 1.7 was fixed at 4 wt. %.

CAS hydrogels belong to a class of physically crosslinked hydrogels that are affected not only by internal variations of polymer networks, but also by external stimuli [49]. Temperature is a significant external stimulus that has a substantial impact on the rheological properties of CAS hydrogels. Figure 1.7 illustrates the thermal reversibility of CAS hydrogels, which is dependent on the  $DS_{\text{sulfate}}/DS_{\text{acetyl}}$  ratio. At room temperature (23 °C), only the CAS hydrogel with the highest  $DS_{\text{sulfate}}/DS_{\text{acetyl}}$  ratio (0.6) exhibited flow, while other CAS hydrogels maintained their shape well (Figure 1.7). At an elevated temperature of 37 °C, the CAS hydrogel with a  $DS_{\text{sulfate}}/DS_{\text{acetyl}}$  ratio of 0.4 started to flow under its weight, while the hydrogel with the lowest amount of sulfate moieties ( $DS_{\text{sulfate}}/DS_{\text{acetyl}}$  ratio of 0.2) still retained its shape. Eventually, the CAS hydrogel with a  $DS_{\text{sulfate}}/DS_{\text{acetyl}}$  ratio of 0.2 started to flow at a higher temperature of 50 °C. All samples were subjected to an elevated temperature of 63 °C to investigate thermal reversibility, and as depicted in Figure 1.7, all CAS hydrogels showed similar flowing behaviors compared to their original forms. The presence of sulfate moieties in the CAS polymer network results in additional intermolecular interactions, which occur at the expense of hydrophobic associations. Consequently, CAS hydrogels with higher  $DS_{\text{sulfate}}/DS_{\text{acetyl}}$  ratios require less thermal energy to dissociate, resulting in the flow of the hydrogel at lower temperatures.

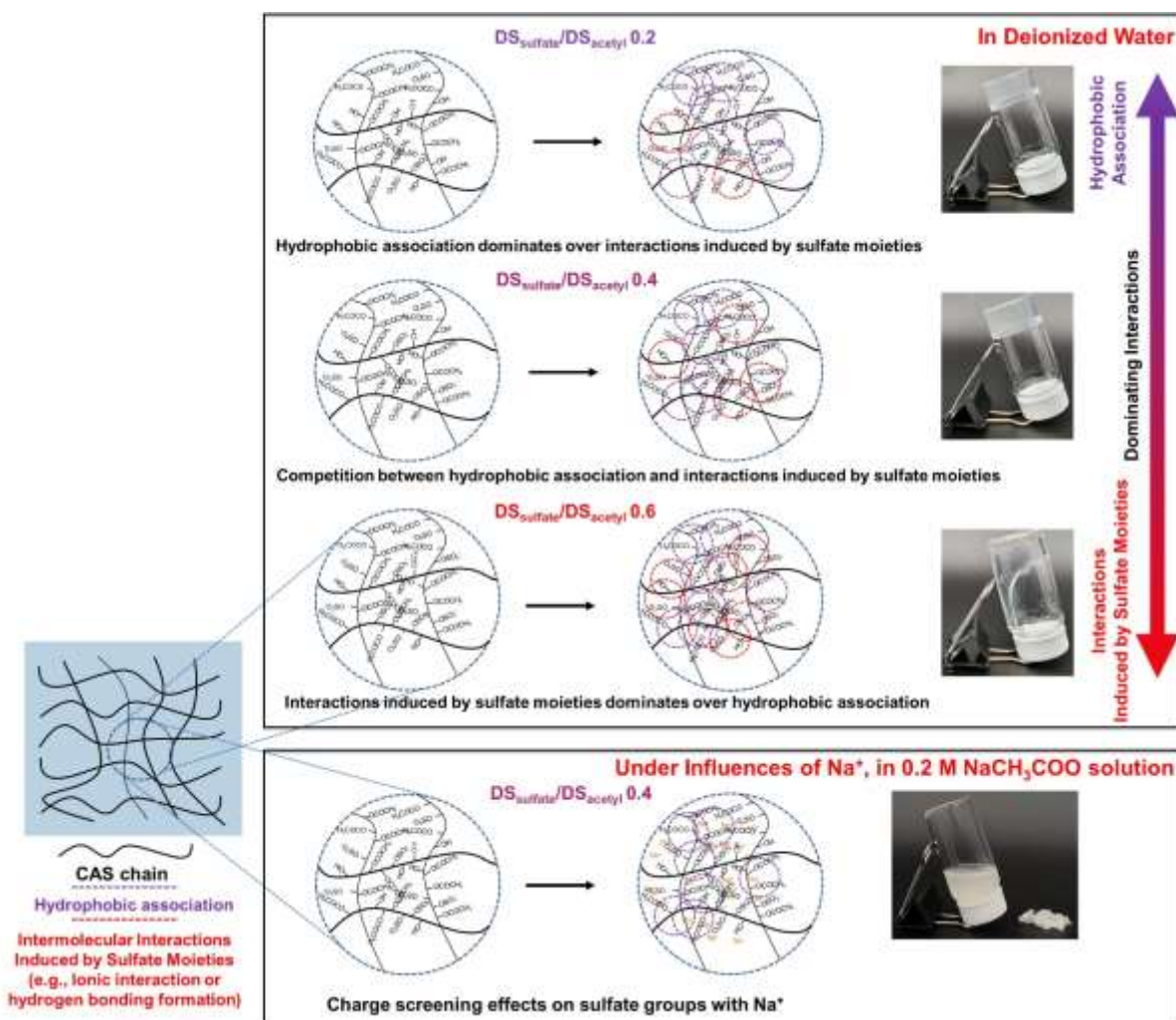


**Figure 1.8.** Illustration of CAS hydrogels formation mechanism

The presence of sulfate moieties is a crucial factor that enables the formation of CAS hydrogels by facilitating additional intermolecular interactions such as hydrogen bonding and ionic interactions. Sulfate moieties contain additional oxygen atoms and charges that enhance intermolecular interactions, as compared to hydroxyl moieties (-OH) present in CAs [35]. To investigate the role of sulfate moieties in CAS hydrogel formation, an aqueous solution containing cations was used instead of deionized water. However, the addition of cations inhibits the

intermolecular interactions facilitated by sulfate moieties due to charge screening effects and hindrance of ionic interactions [50-53]. An increase in the ionic strength of a solvent can also destabilize intramolecular hydrogen bonding [54]. Thus, using a 0.2 M sodium acetate aqueous solution for hydrogel formation resulted in CAS swelling in the solution rather than forming a hydrogel (Figure 1.8). The failure of CAS hydrogel formation in the presence of cations is also observed in already formulated CAS hydrogels, which absorb water and eventually lose their original shape when immersed in deionized water. However, storing CAS hydrogels in an aqueous solution containing sodium cations significantly hinders swelling, allowing them to maintain their original shape over time (Figure S1.2).

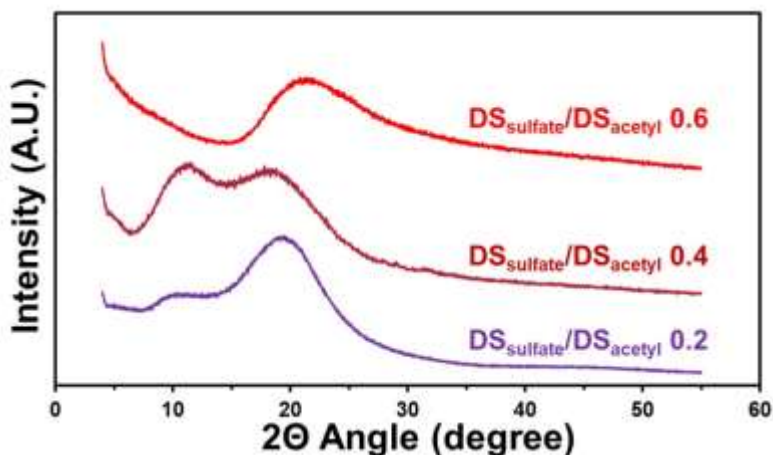


**Figure 1.9.** XRD spectra of CAS hydrogel films with varying the ratios of DS<sub>sulfate</sub>/DS<sub>acetyl</sub> (0.2, 0.4, and 0.6).

The formation of CAS hydrogels is dependent on the balance between hydrophobic associations and additional intermolecular interactions induced by newly introduced sulfate moieties. As the number of sulfate moieties increases, the CAS chain arrangement gradually changes, resulting in the formation of 3D network structures suitable for hydrogel formation. However, if the influence of sulfate moieties surpasses a certain range and overcomes the

hydrophobic associations, the polymer chain arrangement is further altered, leading to a transition from a hydrogel to a solution. The optimal  $DS_{\text{sulfate}}/DS_{\text{acetyl}}$  ratio range is crucial for the formation of CAS hydrogels, as insufficient or excessive sulfate moieties will hinder the formation of a hydrogel. To investigate the structural changes of CAS hydrogels with respect to the amount of sulfate moieties, XRD was used. Results showed that CAS hydrogels with  $DS_{\text{sulfate}}/DS_{\text{acetyl}}$  ratios of 0.2 and 0.4 had stereotypical XRD patterns of CA, with (002) reflection recorded at approximately 20 degrees of  $2\Theta$  angle and (101) reflection observed around 10 degrees [55]. However, in a CAS hydrogel with a  $DS_{\text{sulfate}}/DS_{\text{acetyl}}$  ratio of 0.6, the (101) reflection disappeared, and the (002) reflection was shifted to a higher range of  $2\Theta$  angle, indicating changes in the structure of CAS hydrogels. Therefore, the substitution of sulfate moieties can modify the polymer network structure in CAS hydrogels, resulting in different rheological behaviors.

### 3.5. Cell Viability and Controlled Release of Hydrophilic Sodium Salicylate via CAS Hydrogel Matrices

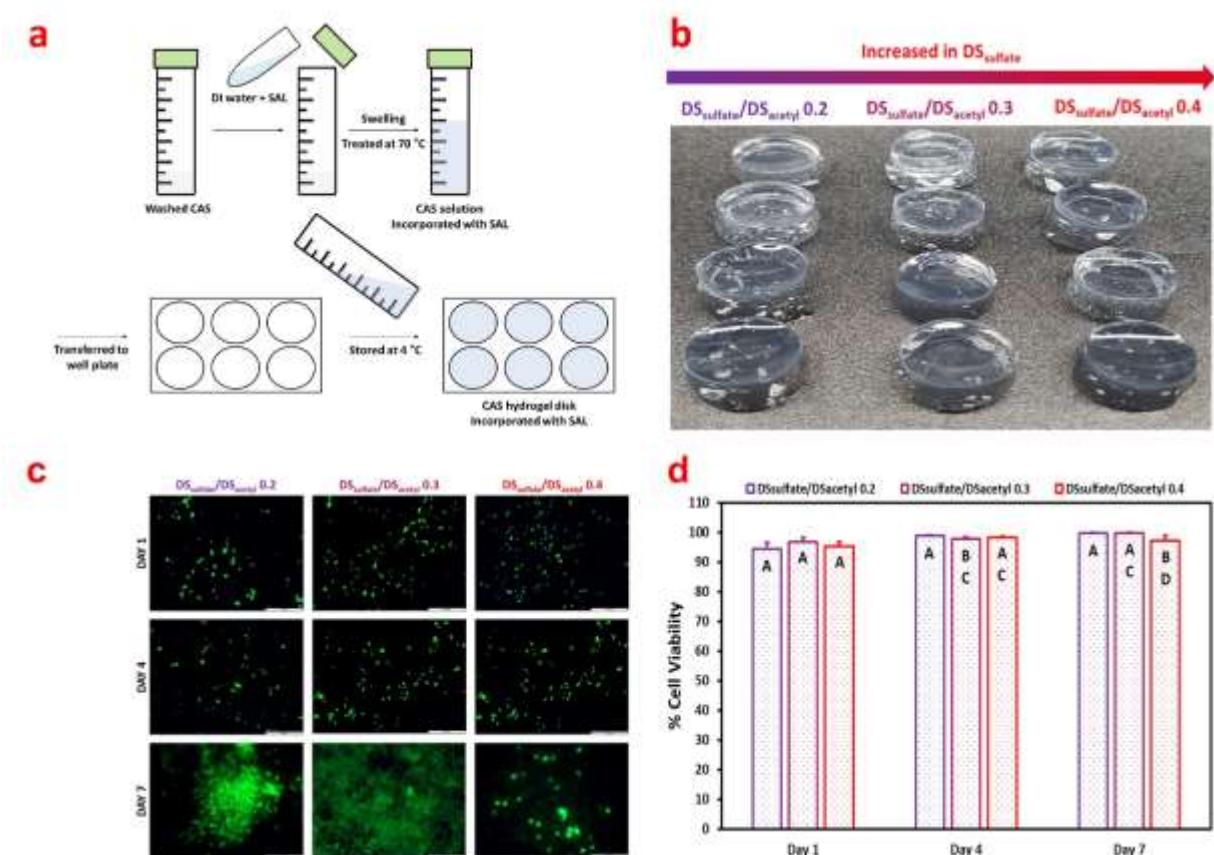


**Figure 1.10.** (a) Preparation procedure for CAS hydrogel disks incorporated with sodium salicylate (SAL), (b) CAS hydrogel disks incorporated with SAL, (c) Fluorescence microscopic images of NIH3T3 cells cultured on the surface of CAS hydrogels (DS<sub>sulfate</sub>/DS<sub>acetyl</sub> ratios of 0.2, 0.3, and 0.4) after 1, 4, and 7 days of incubation in complete media at 37 °C using live (green) and dead (red) cell staining assay, scale bars are 300 μm, and (d) Cell viability of CAS hydrogels (DS<sub>sulfate</sub>/DS<sub>acetyl</sub> ratios of 0.2, 0.3, and 0.4) after 1, 4, and 7 days of incubation (n = 3). \*Letters in the same group in Figure 1.10d represent a statistically significant difference (p < 0.05) based on Tukey Post-hoc HSD.

The biocompatibility should be guaranteed for a material to be employed as a drug release matrix [56]. Therefore, the cell viability test of CAS hydrogels with varying  $DS_{\text{sulfate}}/DS_{\text{acetyl}}$  ratios (0.2, 0.3, and 0.4) was performed to assess the biocompatibility of CAS hydrogels. To maintain CAS hydrogels' structural integrities under the influences of cell culture conditions, crosslinking with  $Ca^{2+}$  was carried out prior to seeding fibroblast NIH3T3 cells on the top of CAS hydrogels. The cell viability of CAS hydrogels was qualitatively assessed by imaging living and dead cells after predetermined incubation times (1, 4, and 7 days). As illustrated in Figures 1.10c and 1.10d, all CAS hydrogels can provide suitable conditions for NIH3T3 cells. The pH was found within the range between 7.4 – 7.8, which is suitable for mammalian cell growth [57, 58]. Even though CAS hydrogels with  $DS_{\text{sulfate}}/DS_{\text{acetyl}}$  ratio of 0.4 exhibited slightly lower % cell viability (97 %) compared to other CAS hydrogels, most of the cells cultured on the CAS hydrogels survived after 7 days of incubation. These results confirmed that all CAS hydrogels are biocompatible and showed the feasibility of CAS hydrogels as drug release matrices.

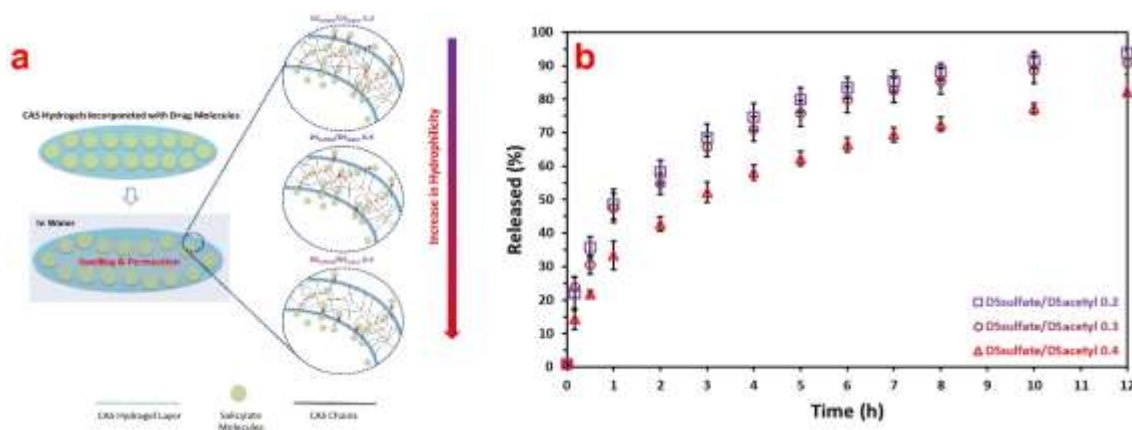


**Figure 1.11.** (a) Schematic representation of SAL release mechanism via CAS hydrogel matrices and (b) SAL release profile in aqueous media via CAS hydrogel matrices.

CAS hydrogel matrices not only provide protection but also modulate the interactions of entrapped molecules with surrounding media, owing to the different affinity toward hydrophilic molecules originating from the varied amount of sulfate moieties in CAS hydrogels. To investigate the impact of sulfate moieties on drug release, three different CAS hydrogel matrices with varying  $DS_{\text{sulfate}}/DS_{\text{acetyl}}$  ratios were prepared and tested using hydrophilic sodium salicylate (SAL) as a model drug. The drug release profiles showed similar shapes but different release rates, depending on the  $DS_{\text{sulfate}}/DS_{\text{acetyl}}$  ratio (Figure 1.11b). The matrix with the lowest amount of sulfate moieties released SAL molecules the fastest, while the matrix with the highest amount of sulfate moieties released SAL molecules the slowest (Figure 1.11b). The variations in hydrophilicity of the matrices, resulting from the differences in the number of sulfate moieties, influenced the rate of SAL molecule diffusion through the CAS hydrogel matrices. SAL molecules could interact more readily with matrices that had higher hydrophilicity, leading to a decrease in the drug release rate (Figure 1.11a). To study the drug release mechanism via CAS hydrogel matrices, the Korsmeyer-Peppas model, which describes drug release through a polymer system, was employed [59]. The exponent  $n$  values were calculated for all cases and found to be less than or equal to 0.45, indicating that the drug release mechanism followed a quasi-Fickian diffusion (Table S2) [60]. Values of exponent  $n$  close to 0.89 suggest that drug release is governed by matrix swelling, whereas values close to 0.45 indicate that drug release primarily occurs via diffusion [61]. These results are consistent with the observation that, regardless of the  $DS_{\text{sulfate}}/DS_{\text{acetyl}}$  ratio, CAS hydrogels exhibit limited swelling under the influence of  $\text{Na}^+$  (Figure S1.3). Thus, drug release is mainly driven by diffusion via well-established CAS hydrogel matrices, resulting in exponent  $n$  values less than or close to 0.45.

#### **4. Conclusion**

This study introduces a simple method for producing single-component cellulose-based hydrogels, inspired by the self-assembly behavior of amphiphilic copolymers. The method involves synthesizing amphiphilic cellulose acetate sulfate (CAS) from hydrophobic cellulose acetate (CA), and investigating their behavior in deionized water. The successful formation of CAS hydrogels is demonstrated using CAS synthesized from CA with a DS of 1.8, offering the advantage of simplicity in the formulation process, as there is no need for crosslinking agents or additional polymers. Formation of CAS hydrogels is based on intermolecular interactions among CAS polymer chains, which are influenced by the balance between sulfate and acetyl moieties. Therefore, identifying the optimal balance between these two moieties is crucial for the successful formation of CAS hydrogels. The physical crosslinking nature of CAS hydrogels allows for the easy adjustment of their rheological properties by modifying internal characteristics, such as the balance between sulfate and acetyl moieties and solid content, as well as external stimuli such as temperature. Moreover, CAS hydrogels show promise as drug-release matrices, as they are biocompatible and demonstrate modulated drug release profiles that can be controlled by adjusting the number of sulfate moieties. Overall, this study provides a simple and versatile approach for producing single-component cellulose-based hydrogels, which could also be applied to the production of other natural polymer-based hydrogels. Additionally, the potential use of CAS hydrogels as drug-release systems further expands their application in biomedical and pharmaceutical fields.

## REFERENCES

- [1] H. Saito, A. Sakurai, M. Sakakibara, H. Saga, Preparation and properties of transparent cellulose hydrogels, *Journal of applied polymer science* 90(11) (2003) 3020-3025.
- [2] R. Narain, *Polymer science and nanotechnology: fundamentals and applications*, Elsevier 2020.
- [3] E.M. Ahmed, Hydrogel: Preparation, characterization, and applications: A review, *Journal of advanced research* 6(2) (2015) 105-121.
- [4] S. Sharma, S. Tiwari, A review on biomacromolecular hydrogel classification and its applications, *International Journal of Biological Macromolecules* 162 (2020) 737-747.
- [5] S. Cascone, G. Lamberti, Hydrogel-based commercial products for biomedical applications: A review, *International journal of pharmaceutics* 573 (2020) 118803.
- [6] X. Jiang, X. Yang, B. Yang, L. Zhang, A. Lu, Highly self-healable and injectable cellulose hydrogels via rapid hydrazone linkage for drug delivery and 3D cell culture, *Carbohydrate polymers* 273 (2021) 118547.
- [7] O. Wichterle, D. Lim, Hydrophilic gels for biological use, *Nature* 185(4706) (1960) 117-118.
- [8] J. Li, D.J. Mooney, Designing hydrogels for controlled drug delivery, *Nature Reviews Materials* 1(12) (2016) 1-17.
- [9] C.A. Dreiss, Hydrogel design strategies for drug delivery, *Current opinion in colloid & interface science* 48 (2020) 1-17.
- [10] J. Liao, B. Hou, H. Huang, Preparation, properties and drug controlled release of chitin-based hydrogels: An updated review, *Carbohydrate polymers* (2022) 119177.

- [11] Y. Yao, D. Zhou, Y. Shen, H. Wu, H. Wang, Morphology-controllable amphiphilic cellulose microgels made from self-assembly of hydrophobic long-chain bromide-alkylated-cellulose/gelatin copolymer, *Carbohydrate polymers* 269 (2021) 118265.
- [12] S. Park, J.O. Baker, M.E. Himmel, P.A. Parilla, D.K. Johnson, Cellulose crystallinity index: measurement techniques and their impact on interpreting cellulase performance, *Biotechnology for biofuels* 3 (2010) 1-10.
- [13] T. Kondo, Hydrogen bonds in cellulose and cellulose derivatives, *Polysaccharides: Structural diversity and functional versatility* (2005) 69-98.
- [14] T. Heinze, O.A. El Seoud, A. Koschella, *Cellulose derivatives: synthesis, structure, and properties*, Springer 2018.
- [15] S.H. Zainal, N.H. Mohd, N. Suhaili, F.H. Anuar, A.M. Lazim, R. Othaman, Preparation of cellulose-based hydrogel: A review, *Journal of Materials Research and Technology* 10 (2021) 935-952.
- [16] C. Chang, L. Zhang, Cellulose-based hydrogels: Present status and application prospects, *Carbohydrate polymers* 84(1) (2011) 40-53.
- [17] G.F. El Fawal, M.M. Abu-Serie, M.A. Hassan, M.S. Elnouby, Hydroxyethyl cellulose hydrogel for wound dressing: Fabrication, characterization and in vitro evaluation, *International Journal of Biological Macromolecules* 111 (2018) 649-659.
- [18] Y. Zhang, Y. Huang, Rational design of smart hydrogels for biomedical applications, *Frontiers in Chemistry* 8 (2021) 615665.
- [19] H. Dai, S. Ou, Z. Liu, H. Huang, Pineapple peel carboxymethyl cellulose/polyvinyl alcohol/mesoporous silica SBA-15 hydrogel composites for papain immobilization, *Carbohydrate polymers* 169 (2017) 504-514.

- [20] M.T. Islam, M.M. Alam, A. Patrucco, A. Montarsolo, M. Zoccola, Preparation of nanocellulose: A review, *AATCC Journal of Research* 1(5) (2014) 17-23.
- [21] A.M. Elbarbary, H.A. Abd El-Rehim, N.M. El-Sawy, E.-S.A. Hegazy, E.-S.A. Soliman, Radiation induced crosslinking of polyacrylamide incorporated low molecular weights natural polymers for possible use in the agricultural applications, *Carbohydrate polymers* 176 (2017) 19-28.
- [22] I.B. Bwatanglang, Y. Musa, N.A. Yusof, Market analysis and commercially available cellulose and hydrogel-based composites for sustainability, clean environment, and human health, *Sustainable Nanocellulose and Nanohydrogels from Natural Sources*, Elsevier2020, pp. 65-79.
- [23] T. Terashima, Controlled self-assembly of amphiphilic random copolymers into folded micelles and nanostructure materials, *Journal of oleo science* (2020) ess20089.
- [24] Y. Song, L. Zhang, W. Gan, J. Zhou, L. Zhang, Self-assembled micelles based on hydrophobically modified quaternized cellulose for drug delivery, *Colloids and Surfaces B: Biointerfaces* 83(2) (2011) 313-320.
- [25] S.K. Kozawa, K. Matsumoto, A. Suzuki, M. Sawamoto, T. Terashima, Self-assembly of amphiphilic ABA random triblock copolymers in water, *Journal of Polymer Science Part A: Polymer Chemistry* 57(3) (2019) 313-321.
- [26] D. Charpentier, G. Mocanu, A. Carpov, S. Chapelle, L. Merle, G. Müller, New hydrophobically modified carboxymethylcellulose derivatives, *Carbohydrate polymers* 33(2-3) (1997) 177-186.
- [27] G. Chauvelon, J.-L. Doublier, A. Buléon, J.-F. Thibault, L. Saulnier, Rheological properties of sulfoacetate derivatives of cellulose, *Carbohydrate research* 338(8) (2003) 751-759.

- [28] D. Klemm, B. Philipp, T. Heinze, U. Hewinze, W. Wagenknecht, *Comprehensive cellulose chemistry. Volume 2: Functionalization of cellulose*, Wiley-VCH Verlag GmbH 1998.
- [29] J. Schindelin, I. Arganda-Carreras, E. Frise, V. Kaynig, M. Longair, T. Pietzsch, S. Preibisch, C. Rueden, S. Saalfeld, B. Schmid, Fiji: an open-source platform for biological-image analysis, *Nature methods* 9(7) (2012) 676-682.
- [30] P. Chansoria, S. Asif, N. Gupta, J. Piedrahita, R.A. Shirwaiker, Multiscale Anisotropic Tissue Biofabrication via Bulk Acoustic Patterning of Cells and Functional Additives in Hybrid Bioinks, *Advanced Healthcare Materials* (2022) 2102351.
- [31] A.M. Senna, V.R. Botaro, Biodegradable hydrogel derived from cellulose acetate and EDTA as a reduction substrate of leaching NPK compound fertilizer and water retention in soil, *Journal of Controlled Release* 260 (2017) 194-201.
- [32] A.M. Senna, K.M. Novack, V.R. Botaro, Synthesis and characterization of hydrogels from cellulose acetate by esterification crosslinking with EDTA dianhydride, *Carbohydrate polymers* 114 (2014) 260-268.
- [33] A. El-Mohdy, Radiation synthesis of nanosilver/poly vinyl alcohol/cellulose acetate/gelatin hydrogels for wound dressing, *Journal of Polymer Research* 20(6) (2013) 1-12.
- [34] P. Von Tiedemann, J. Yan, R.D. Barent, R.J. Spontak, G. Floudas, H. Frey, R.A. Register, Tapered multiblock star copolymers: synthesis, selective hydrogenation, and properties, *Macromolecules* 53(11) (2020) 4422-4434.
- [35] Z. Yang, S. Lu, L. Lan, X. Liu, S. Zhao, S. Sun, Z. Zhang, X. Chen, Z. Yang, X. Jia, Twelve-coordinated sulfate hydrogen bonding interactions in water-containing Fe (II) system, *Molecular Crystals and Liquid Crystals* 680(1) (2019) 96-104.

- [36] S. Nunes, F. Ramacciotti, A. Neves, E.M. Angelin, A.M. Ramos, É. Roldão, N. Wallaszkovits, A.A. Armijo, M.J. Melo, A diagnostic tool for assessing the conservation condition of cellulose nitrate and acetate in heritage collections: Quantifying the degree of substitution by infrared spectroscopy, *Heritage Science* 8(1) (2020) 1-14.
- [37] D. Grant, W.F. Long, C.F. Moffat, F.B. Williamson, INFRARED-SPECTROSCOPY OF HEPARINS SUGGESTS THAT THE REGION 750-950 CM-1 IS SENSITIVE TO CHANGES IN IDURONATE RESIDUE RING CONFORMATION, *Biochem. J.* 275 (1991) 193-197.
- [38] J. Rohowsky, K. Heise, S. Fischer, K. Hettrich, Synthesis and characterization of novel cellulose ether sulfates, *Carbohydrate polymers* 142 (2016) 56-62.
- [39] N. Bhatt, P. Gupta, S. Naithani, Preparation of cellulose sulfate from  $\alpha$ -cellulose isolated from *Lantana camara* by the direct esterification method, *Journal of applied polymer science* 108(5) (2008) 2895-2901.
- [40] J. Brandrup, E.H. Immergut, E.A. Grulke, A. Abe, D.R. Bloch, *Polymer handbook*, Wiley New York 1999.
- [41] T. Hashizume, Y. Okamoto, K. Nagai, S. Shimamoto, Mechanism of sodium-hypochlorite-induced degradation of cellulose acetate and the enhancement of its degradation resistance by chemical modification, *Textile Research Journal* 92(13-14) (2022) 2487-2500.
- [42] B. Caballero, L.C. Trugo, P.M. Finglas, *Encyclopedia of food sciences and nutrition*, Academic 2003.
- [43] D. Chandler, Interfaces and the driving force of hydrophobic assembly, *Nature* 437(7059) (2005) 640-647.

- [44] J. Chen, J. Li, B. Li, Identification of molecular driving forces involved in the gelation of konjac glucomannan: Effect of degree of deacetylation on hydrophobic association, *Carbohydrate polymers* 86(2) (2011) 865-871.
- [45] B. Solo-de-Zaldívar, C. Tovar, A. Borderías, B. Herranz, Effect of deacetylation on the glucomannan gelation process for making restructured seafood products, *Food Hydrocolloids* 35 (2014) 59-68.
- [46] M. Bustamante-Torres, D. Romero-Fierro, B. Arcentales-Vera, K. Palomino, H. Magaña, E. Bucio, Hydrogels classification according to the physical or chemical interactions and as stimuli-sensitive materials, *Gels* 7(4) (2021) 182.
- [47] F. Ullah, M.B.H. Othman, F. Javed, Z. Ahmad, H.M. Akil, Classification, processing and application of hydrogels: A review, *Materials Science and Engineering: C* 57 (2015) 414-433.
- [48] C. Qiao, X. Cao, F. Wang, Swelling behavior study of physically crosslinked gelatin hydrogels, *Polymers and Polymer Composites* 20(1-2) (2012) 53-58.
- [49] S.K. Gulrez, S. Al-Assaf, G.O. Phillips, Hydrogels: methods of preparation, characterisation and applications, *Progress in molecular and environmental bioengineering-from analysis and modeling to technology applications* 117150 (2011).
- [50] A. Rastogi, A.K. Ghosh, S. Suresh, Hydrogen bond interactions between water molecules in bulk liquid, near electrode surfaces and around ions, *Thermodynamics-Physical chemistry of aqueous systems* (2011) 351-364.
- [51] Z. Kříž, J. Klusák, Z. Křištofiková, J. Koča, How ionic strength affects the conformational behavior of human and rat beta amyloids—a computational study, *PloS one* 8(5) (2013) e62914.

- [52] R. Perez-Jimenez, R. Godoy-Ruiz, B. Ibarra-Molero, J.M. Sanchez-Ruiz, The efficiency of different salts to screen charge interactions in proteins: a Hofmeister effect?, *Biophysical journal* 86(4) (2004) 2414-2429.
- [53] D.J. Lockhart, P.S. Kim, Electrostatic screening of charge and dipole interactions with the helix backbone, *Science* 260(5105) (1993) 198-202.
- [54] A. Chandra, Effects of ion atmosphere on hydrogen-bond dynamics in aqueous electrolyte solutions, *Physical Review Letters* 85(4) (2000) 768.
- [55] H.S. Barud, A.M. de Araújo Júnior, D.B. Santos, R.M. de Assunção, C.S. Meireles, D.A. Cerqueira, G. Rodrigues Filho, C.A. Ribeiro, Y. Messaddeq, S.J. Ribeiro, Thermal behavior of cellulose acetate produced from homogeneous acetylation of bacterial cellulose, *Thermochimica acta* 471(1-2) (2008) 61-69.
- [56] K.J. Rambhia, P.X. Ma, Controlled drug release for tissue engineering, *Journal of Controlled Release* 219 (2015) 119-128.
- [57] L.F. Mellor, R.C. Nordberg, P. Huebner, M. Mohiti-Asli, M.A. Taylor, W. Efirid, J.T. Oxford, J.T. Spang, R.A. Shirwaiker, E.G. Lobo, Investigation of multiphasic 3D-bioploted scaffolds for site-specific chondrogenic and osteogenic differentiation of human adipose-derived stem cells for osteochondral tissue engineering applications, *Journal of Biomedical Materials Research Part B: Applied Biomaterials* 108(5) (2020) 2017-2030.
- [58] P.J. Price, Best practices for media selection for mammalian cells, *In Vitro Cellular & Developmental Biology-Animal* 53(8) (2017) 673-681.
- [59] D. Caccavo, An overview on the mathematical modeling of hydrogels' behavior for drug delivery systems, *International journal of pharmaceutics* 560 (2019) 175-190.

[60] M. Vigata, C. Meinert, D.W. Hutmacher, N. Bock, Hydrogels as drug delivery systems: A review of current characterization and evaluation techniques, *Pharmaceutics* 12(12) (2020) 1188.

[61] C.-C. Lin, A.T. Metters, Hydrogels in controlled release formulations: network design and mathematical modeling, *Advanced drug delivery reviews* 58(12-13) (2006) 1379-1408.

## CHAPTER 2

### **Production of Single-Component Cellulose-Based Hydrogel and Its Utilization as Adsorbent for Aqueous Contaminants**

#### **Abstract**

The growing concern for the environment has resulted in renewed interest in bio-based resources. This study aims to produce a hydrogel adsorbent from cellulose and examine its adsorption performance. In pursuit of this goal, we report a simple one-pot synthesis of cellulose acetate sulfate (CAS), followed by the formation of CAS hydrogels and their subsequent adsorption performances. CAS contains both hydrophilic and hydrophobic functional groups that enable the formation of a single-component hydrogel through intermolecular interactions in deionized water. The thermal reversibility of CAS hydrogels make them easily processable into various shapes. The addition of divalent cations (e.g.,  $\text{Ca}^{2+}$ ) can enhance the durability of the CAS hydrogel adsorbents by creating ionically crosslinked hydrogels. The ionically a crosslinked CAS hydrogel adsorbent shows a maximum adsorption capacity of 245 mg/g towards methylene blue (MB) at a pH of 7 and 23 °C. The adsorption behavior of MB onto the CAS hydrogel is consistent with both a pseudo-second-order model and a Langmuir adsorption isotherm model. Furthermore, the CAS hydrogel adsorbent maintains a 70% removal ratio after five cycles. The simplicity of synthesis and hydrogel formation opens up new possibilities for producing and utilizing cellulose-based hydrogels as adsorbents for aqueous contaminants.

## 1. Introduction

Human activities have led to continuous increases in the inadvertent release of countless aqueous contaminants into the environment [1]. In response, environmental regulations have increased, and extensive efforts have been devoted to the recovery or reduction of these contaminants [2, 3]. One common class of aqueous contaminants is synthetic dyes, which are widely used in the production of textiles, food, plastics, and paper. Although synthetic dyes are versatile and useful, they require careful attention to prevent or limit their release into municipal wastewater systems [4, 5]. Some synthetic dyes are considered to possess cytotoxicity to mammalian cells [6, 7]. Moreover, due to the stable nature of synthetic dyes originating from aromatic structures, most of the synthetic dyes have resistance to biodegradation [8]. Thus, once discharged without proper treatments, synthetic dyes cause significant increases in oxygen demands, eventually damaging the photosynthetic activities of water bodies [9]. For these reasons, if synthetic dyes are released into the aquatic system, they are not only difficult to remove but also can have a persistent negative impact on the environment [10, 11].

Over the past few decades, global warming has emerged as an impending international issue. To address this challenge, numerous attempts have been made to reduce fossil fuel-derived materials, while promoting the development and use of sustainable, bio-based alternatives in various fields [12-14]. One specific area of interest is bio-based materials in wastewater treatment [15]. Naturally occurring polymers such as cellulose, collagen, alginate, hyaluronic acid, chitosan, and their derivatives are promising candidates for the removal of pollutants from wastewater owing to the presence of natural or introduced moieties (-OH,  $-\text{SO}_3^{2-}$ ,  $-\text{OSO}_3^-$ ,  $-\text{COOH}$ ,  $-\text{NH}_2$ , etc.), which create specific interactions between the polymers and many contaminants [16, 17]. Cellulose is one of the most attractive natural polymers for a wide range of applications due to its abundance

and commercial availability [18]. Cellulose is a linear polysaccharide consisting of  $\beta$ -D-glucose units, which are linked by  $\beta$ -1,4-glycosidic bonds, and can form inter- and intra-molecular hydrogen bonds via the three hydroxyl groups of each glucose unit. This results in a semi-crystalline structure, making cellulose insoluble in both water and organic solvents [19]. Given these unique properties, various forms of cellulose, such as sheets, foams, and nanocellulose materials, have been investigated as adsorbents for the removal of synthetic dyes from aqueous solutions [20]. Although cellulose is an effective adsorbent due to the presence of hydroxyl moieties, its functionality can be further improved by introducing more polar moieties [19]. One example of a cellulose derivative that has shown promise as an adsorbent is carboxymethyl cellulose (CMC) [21]. CMC contains anionic moieties ( $-\text{COOH}$  or  $\text{COO-R}^+$ ) that can bind to cationic contaminants via electrostatic interactions. As a result, CMC-based adsorbents have demonstrated enhanced adsorption capabilities toward cationic synthetic dyes like methylene blue (MB) compared to native cellulose [22].

Although several alternative processes have been developed to replace conventional wastewater treatment for removing dyes (such as physical, chemical, and biological processes), adsorption processes remain one of the most commonly used methods [23, 24]. While activated carbon is a widely employed adsorbent, its high operating costs and need for post-use regeneration have led to a strong interest in developing cost-effective and environmentally friendly alternatives [25, 26]. Activated carbon from alternative sources [27], and different materials such as graphene oxide [28], nanocellulose [29], and hydrogels [30] have all been evaluated as adsorbents. Among these alternatives, hydrogels have shown potential as adsorbents for dye removal due to their high adsorption capacity, effective separation, and ease of reuse [31]. Cellulose-based hydrogels possess inherent individual advantages, which make them a promising option as a bio-based

adsorbent for wastewater treatment. However, their widespread deployment has been hindered due to the challenges in formulating and processing them into commercially viable structures and modules [32, 33]. The formulation of cellulose-based hydrogels typically requires complex techniques and the addition of supplementary components such as crosslinking agents, additional polymers, and minerals. These components increase the cost and complexity of the process, making it less accessible for widespread use [34]. Therefore, in order to make cellulose-based hydrogels a more effective adsorbent, it is essential to develop a simpler and readily accessible approach for their formulation

This study introduces a novel approach for the formulation of cellulose-based hydrogels. The approach involves the synthesis of amphiphilic cellulose acetate sulfate (CAS) from commercially available cellulose acetate (CA). Unlike traditional methods, this approach does not require the use of supplementary components to form a hydrogel, as CAS can form a hydrogel via intermolecular interactions. The hydrogels can be engineered by adjusting the balance between the hydrophilic sulfate moieties ( $DS_{\text{sulfate}}$ ) and hydrophobic acetyl moieties ( $DS_{\text{acetyl}}$ ), which govern the critical gelation solids content, swelling ratio, and water retention ratio. The CAS hydrogel adsorbents are subjected to a double-crosslinking strategy prior to adsorption to enhance its durability. To evaluate the adsorption performance of the hydrogels, cationic methylene blue (MB) is used as a model dye. Several kinetics and isotherm models are employed to study the adsorption behavior of MB onto the CAS hydrogel adsorbent.

## 2. Materials and Methods

### 2.1. Materials

Cellulose acetate having  $DS_{\text{acetyl}}$  of 1.8 was kindly provided by Eastman Chemical Company (Kingsport, TN). *N, N*-dimethylformamide (DMF), sulfamic acid, ethanol, sodium acetate, sodium hydroxide, hydrochloric acid, calcium hydroxide, calcium chloride, and methylene blue (MB) were purchased from Fisher-Scientific (Hampton, NH) and used as received.

**Table 2.1.** Molecular weight and polydispersity index of CA and the resulting CAS

Sample	$M_w$ (g/mol)	PDI
CA $DS_{\text{acetyl}}$ 1.8	111,000	2.2
CAS $DS_{\text{sulfate}}/DS_{\text{acetyl}}$ ratio of 0.2	102,000	2.1
CAS $DS_{\text{sulfate}}/DS_{\text{acetyl}}$ ratio of 0.3	98,000	1.9
CAS $DS_{\text{sulfate}}/DS_{\text{acetyl}}$ ratio of 0.4	100,000	2.0
* The molecular weight ( $M_w$ ) and polydispersity index (PDI) were determined by using polystyrene as a standard		

### 2.2. Cellulose Acetate Sulfate (CAS) Synthesis and Preparation of CAS Hydrogels for Dye Removal

CAS was synthesized as described elsewhere [19]. Briefly, oven-dried CA (15 g) was dissolved in 100 ml of DMF at 80 °C. The sulfating agents were prepared by dissolving a predetermined amount of sulfamic acid in 70 ml of DMF. After the complete dissolution of CA, the sulfating agent was carefully added to the CA solution and held for 2 h at 80 °C. The resulting CAS was precipitated with an excess of ethanol with 3 wt. % sodium acetate. Residual DMF and reaction by-products were removed by repeated washing of the precipitated CAS with pure ethanol and then air-drying overnight.

To initiate the formation of CAS hydrogels, air-dried CAS powder was added to a predetermined amount of deionized water to create a moderately viscous homogeneous solution

using a water bath (HBR 4 control, IKA, Wilmington, NC) held at 70 °C. The resulting samples were centrifuged to remove bubbles and equilibrated to room temperature (23 °C). To fabricate the continuous CAS hydrogel fibers (solids content of 4.5 wt. %) used for the MB dye removal studies, the CAS hydrogels were warmed to 70 °C in the water bath to lower their viscosity, which facilitated their transfer to a 3 ml syringe. The CAS hydrogels were equilibrated at room temperature (23 °C) for 15 min and manually extruded to create single fibers and 3D structures.

### **2.3. Gel Permeation Chromatography**

To determine the molecular weight ( $M_w$ ) and polydispersity index (PDI) of the reference CA and the resulting CAS, a 1260 Infinity GPC/SEC system equipped with a PLgel MIXED-B column (Agilent, Santa Clara, CA) was utilized with a method previously described, but with minor modifications [35]. The eluent employed for the measurement was composed of LiBr/N-methylpyrrolidone (0.1 mol/L), which flowed at a rate of 0.25 mL/min through the column oven set at 60°C. Polystyrene was employed as an internal standard to calibrate the system, and both CA and the resulting CAS samples were prepared at a concentration of 0.5 wt.%. An injection volume of 50  $\mu$ L was used for the samples.

### **2.4. Critical Gelation Solid Content, Swelling Ratio, and Water Retention Ratio**

The critical gelation solids content was investigated for CAS having  $DS_{\text{sulfate}}/DS_{\text{acetyl}}$  ratios of 0.2, 0.3, and 0.4 at 23 °C. The solid contents of CAS solutions/hydrogels were systematically controlled by adding a predetermined amount of deionized water and the critical gelation solid content was determined by tube inversion test [36]. The swelling ratio of CAS

hydrogels at each critical gelation solid content was gravimetrically calculated based on the weight difference before and after oven-drying at 105 °C overnight.

$$SR = \frac{W_e - W_d}{W_d} \times 100\% \quad (1)$$

Where,  $W_e$  and  $W_d$  mean the weight of swollen hydrogels having the critical gelation solid content and the weight of the oven-dried CAS hydrogels, respectively.

The water retention ratio was measured at 23 °C. CAS hydrogels ( $DS_{\text{sulfate}}/DS_{\text{acetyl}}$  ratios of 0.2, 0.3, and 0.4 and solid content of 4.5 wt. %) were kept at relative humidity  $\approx 40\%$ . The weight of CAS hydrogels was measured at predetermined time intervals (1-8 h) and the water retention ratio was calculated using the following equation [37].

$$WRR = \frac{W_t - W_d}{W_s - W_d} \times 100\% \quad (2)$$

Where,  $W_t$  is the weight of the CAS hydrogels at time t and  $W_s$  represents the weight of swollen CAS hydrogels.

## 2.5. Zeta potential measurement

The zeta potential of the CAS hydrogels before and after ionic crosslinking with  $Ca^{2+}$  was measured as a function of pH with Zetasizer Nano ZS (Malvern Panalytical, UK). The pH of the deionized water was controlled by 0.1 M of HCl and 0.1 M of NaOH aqueous solution.

## 2.6. Dye Adsorption Experiments

To enhance the durability of the CAS hydrogels, they were first ionically crosslinked with  $Ca^{2+}$  overnight before performing the dye adsorption experiments. The concentrations of MB in the solutions before and after adsorption were determined using a UV-VIS spectrophotometer

(GENESYS Spectrophotometer, Thermo Scientific, Waltham, MA) at wavelengths ranging from 400 to 800 nm, with MB dye exhibiting maximum absorbance at  $\lambda=664$  nm. A calibration curve of MB in the concentration range of 0.008 mg/ml – 0.08 mg/ml was used to establish a linear correlation between absorption at 664 nm and MB concentration, which allowed us to back-calculate the MB remaining in the aqueous solutions. The removal ratio (R%) and the adsorption capacity ( $q_e$ ) were determined utilizing equations (3) and (4).

$$R\% = \frac{C_i - C_e}{C_i} \times 100\% \quad (3)$$

Where,  $C_i$  and  $C_e$  are the initial and equilibrium (final) concentrations of dye ( $\text{mg L}^{-1}$ ), respectively.

$$q_e = \frac{(C_i - C_e) \times V}{m} \quad (4)$$

Where,  $V$  (L) is the volume of MB solution and  $m$  (g) is the oven-dried weight of CAS hydrogel adsorbents.

### 2.6.1. Dye Adsorption Condition Optimization

To determine the optimal conditions for MB adsorption, the influence of adsorbent dosage and sulfate moieties was first evaluated. Adsorbents were created using CAS hydrogels with  $DS_{\text{sulfate}}/DS_{\text{acetyl}}$  ratios of 0.2, 0.3, and 0.4, and varying amounts of CAS hydrogel (0.5 g, 1 g, 1.5 g, and 2.0 g) were introduced into 50 mL of MB solution ( $100 \text{ mg L}^{-1}$ ) at room temperature ( $23 \text{ }^\circ\text{C}$ ) and a pH of 7. The equilibrium MB concentrations of the solutions were measured after 7 days of exposal time. The CAS hydrogel with a  $DS_{\text{sulfate}}/DS_{\text{acetyl}}$  ratio of 0.4 was selected for further evaluation due to the highest MB uptake under the experimental conditions. A constant CAS hydrogel adsorbent mass of 1 g was used throughout all subsequent dye adsorption experiments. Lastly, the effect of the initial MB solutions' pH on MB adsorption was investigated by adding

CAS hydrogels to 50 mL of MB solution (100 mg L<sup>-1</sup>) with varying pH at 23 °C. The equilibrium concentration of MB solution was measured after 7 days of contact time.

### 2.6.2. Dye Adsorption Kinetics

To study the adsorption kinetics, CAS hydrogel adsorbents were introduced to 50 ml of pH 7 MB solution (100 mg L<sup>-1</sup>) at 23 °C. The concentrations of MB solution were measured at predetermined time intervals (0, 15, 30, 45, 60, 120, 240, 360, 480, 600, and 720 min). Pseudo-first-order (eq. 5), pseudo-second-order (eq. 6), and intra-particle diffusion (eq. 7) models are employed to interpret the time-dependent adsorption behaviors of MB.

$$q_t = q_{e1}(1 - e^{-k_1t}) \quad (5)$$

$$q_t = \frac{k_2q_{e2}^2t}{1 + k_2q_{e2}t} \quad (6)$$

$$q_t = k_it^{1/2} + C \quad (7)$$

Where,  $q_t$  is the adsorption capacity at time  $t$ .  $q_{e1}$  and  $q_{e2}$  are the adsorption capacity derived from the non-linear fitting of each pseudo-first-order kinetics model and pseudo-second-order kinetics model, respectively.  $k_1$  (min<sup>-1</sup>) and  $k_2$  (g mg<sup>-1</sup>min<sup>-1</sup>) are the rate constant for pseudo-first-order and pseudo-second-order model, respectively,  $k_i$  (mg g<sup>-1</sup>min<sup>-1/2</sup>) is the intra-particle diffusion rate constant, and  $C$  (mg g<sup>-1</sup>) is related to the thickness of the boundary layer.

### 2.6.3. Dye Adsorption Isotherm

To examine the adsorption isotherm, CAS hydrogel adsorbents were introduced to MB solutions with varying MB concentrations (50, 100, 150, 200, 250, 300, 350, and 400 mg L<sup>-1</sup>) at a pH of 7 and 23 °C. Langmuir and Freundlich isotherm models were employed to explain the adsorption behaviors of MB into CAS hydrogel adsorbents. The Langmuir and Freundlich

isotherm models are shown by Eq. 8 and Eq. 10, respectively. The favorability of an adsorption process can be determined by the following equation (9) in the case of the Langmuir isotherm model.

$$q_e = \frac{q_m K_L C_e}{1 + K_L C_e} \quad (8)$$

$$R_L = \frac{1}{1 + K_L C_i} \quad (9)$$

$$q_e = K_F C_e^{1/n} \quad (10)$$

Where,  $q_e$  ( $\text{mg g}^{-1}$ ) is the adsorption capacity at equilibrium,  $q_m$  ( $\text{mg g}^{-1}$ ) is the maximum adsorption capacity derived from Langmuir isotherm model,  $C_e$  ( $\text{mg L}^{-1}$ ) is the equilibrium concentration of a MB solution,  $K_L$  ( $\text{L mg}^{-1}$ ) is the Langmuir adsorption constant  $R_L$  (dimensionless) is the separation factor,  $C_i$  ( $\text{mg L}^{-1}$ ) is the initial concentration of a MB solution,  $K_F$  ( $(\text{mg g}^{-1})/(\text{mg L}^{-1})^{1/n}$ ) is the Freundlich isotherm constant, and  $n$  is the heterogeneity factor of Freundlich model.

## 2.7. ATR-FTIR Spectral Analysis

MB dye and CAS hydrogel adsorbent (before and after the adsorption experiments) were examined by employing attenuated total reflection Fourier transform infrared spectrometer (Spectrum 3 spectrometer, PerkinElmer, Waltham, MA). All samples were scanned 16 times ranging from 650 to 4000  $\text{cm}^{-1}$  at the resolution of 2  $\text{cm}^{-1}$ .

## 2.8. Recyclability of CAS Hydrogel Adsorbent

As indicated above, 1 g of the CAS hydrogel adsorbent was introduced into 50 ml of a pH 7 MB solution ( $100 \text{ mg L}^{-1}$ ) and held until it reached equilibrium adsorption (48 h). To regenerate the CAS hydrogel adsorbents, desorption experiments were conducted using 0.1 M of

aqueous HCl solution (50 ml) and soaking the adsorbents for 6 hours. The regenerated CAS adsorbents were recovered, washed with deionized water several times, and utilized for another set of MB adsorption experiments using the same conditions. The MB removal ratio was calculated by equation (3) after each adsorption cycle.

### 3. Results and Discussions

#### 3.1. Synthesis of CAS and Preparation of CAS hydrogels



**Figure 2.1.** CAS hydrogel formation procedure and its thermal reversibility (Solid content: 4.5 wt. %)

Amphiphilic block- or random-copolymers can exhibit self-assembly behavior in a solvent by establishing interactions among segments and polymer chains via hydrogen bonding, hydrophobic associations, and ionic interactions, etc. [38]. The specific characteristics of the amphiphilic copolymers (e.g., type of interaction, blocky character, and pH or ionic properties of the solution) enable the formation of various structures, which can possibly lead to the formation of single-component hydrogels or organogels with complex structures [39]. Acetyl moieties introduced in cellulose provide it with hydrophobic characteristics, but CA still exhibits hydrophilicity due to the remaining hydroxyl moieties. To our knowledge, single-component CA hydrogels have not been reported, despite the amphiphilic nature of CA. Previous research has

relied on crosslinking agents and supplementary polymers to create CA-based hydrogels, suggesting that the intermolecular interactions within CA may not be strong enough to produce single-component hydrogels [40, 41]. Hence, partial substitution of hydroxyl moieties in CA with sulfate moieties was carried out to enhance the strength of intermolecular interactions, facilitating the establishments of hydrogen bonding and ionic interactions [42, 43]. The presence of hydrophilic sulfate moieties has potential to enhance intermolecular interactions within the CAS, potentially leading to phase separation and the formation of “single-component” hydrogels.

To simplify the synthesis, sulfate moieties were added to commercially available CA ( $DS_{\text{acetyl}}$  of 1.8), employing sulfamic acid as a sulfating agent. The resulting CAS was examined with ATR-FTIR. New peaks representing substituted sulfate moieties appeared in all CAS around  $820\text{ cm}^{-1}$ , which were not shown in the original CA (Figure S2.1) [44]. The results presented in Table S1 are consistent with previous studies suggesting that the sulfating agent preferentially reacts with the free hydroxyl groups in CA, without inducing hydrolysis of the original acetyl groups, as observed under the current synthesis conditions [19]. Thus, in all IR spectra, regardless of  $DS_{\text{sulfate}}$ , signature peaks assigned to C=O of acetyl moieties were observed around  $1730\text{ cm}^{-1}$ . The broad band around  $3400\text{ cm}^{-1}$ , which was assigned to hydroxyl moieties, proved the presence of unreacted hydroxyl moieties in CAS after the synthesis (Figure S2.1) [45]. The beauty of this CAS hydrogel production method lies in its simplicity. At certain  $DS_{\text{sulfate}}/DS_{\text{acetyl}}$  ratios, and solid content, CAS spontaneously swelled in deionized water and transformed itself into single-component CAS hydrogels without supplementary components such as crosslinking agents or other polymers.

### 3.2. Critical Gelation Solid Content, Swelling, and Water Retention Ratio of CAS Hydrogels

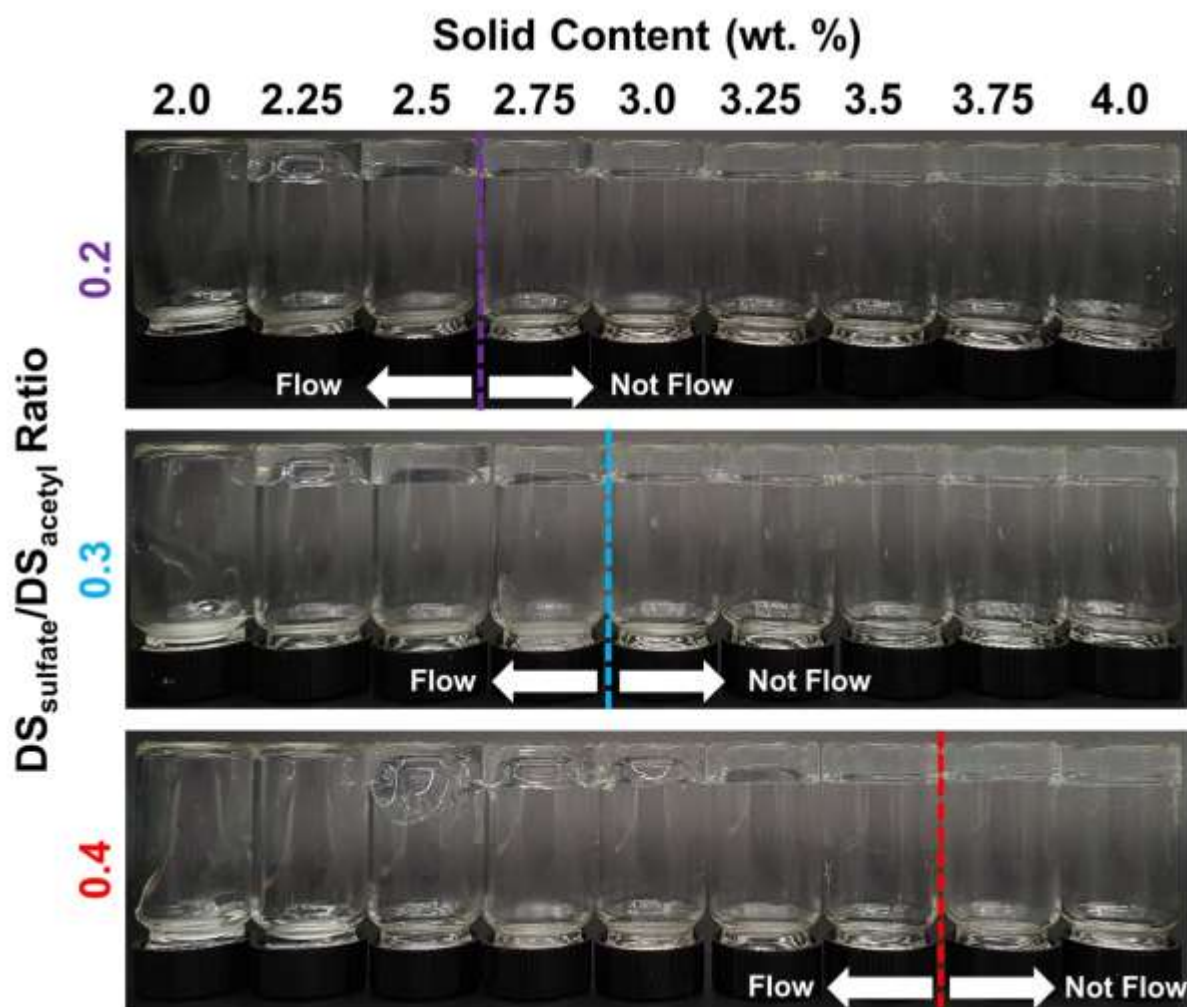


**Figure 2.2.** Rheological behaviors of CAS solutions/hydrogels with varying the  $DS_{\text{sulfate}}$  and  $DS_{\text{acetyl}}$  ratios and solid contents

Hydrogels are generally categorized into two types: physically crosslinked hydrogels and chemically crosslinked hydrogels [46]. Physical hydrogels are formed through weak and reversible intermolecular interactions, such as electrostatic interactions, hydrophobic associations, hydrogen bonding, etc. [47]. The CAS hydrogels can be classified as physically crosslinked hydrogels since their preparation does not require any supplementary components, and the hydrogels are solely

formulated through intermolecular interactions. For physically crosslinked hydrogels, it is important to determine the critical gelation solid content (CGS) where a solution undergoes a transition from liquid to gel. Experimentally, the CGS of a physically crosslinked hydrogel was examined by tube inversion test and determined at the lowest solid content where a solution no longer flowed under its own weight [36].

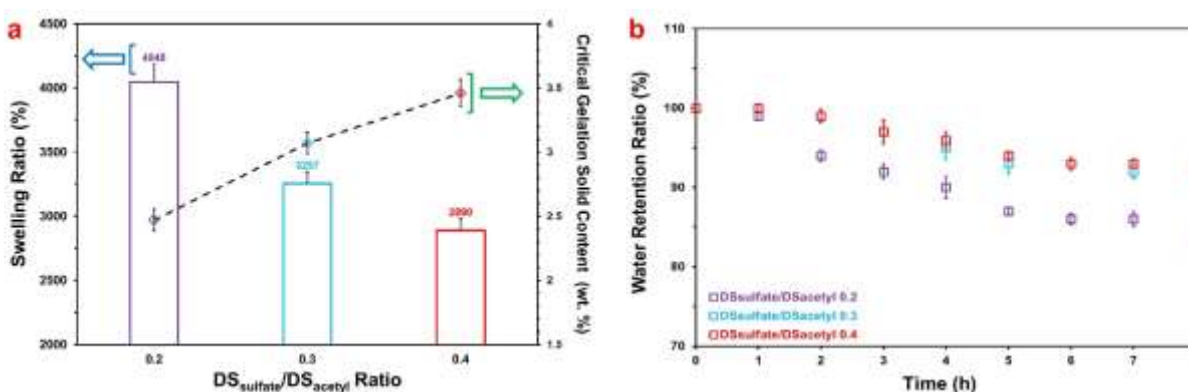


**Figure 2.3.** (a) Behaviors of molded CAS hydrogels ( $DS_{\text{sulfate}}/DS_{\text{acetyl}}$  ratio of 0.4 and solid content of 4.5 wt. %) with and without ionic crosslinking in deionized water and (b) The changes in the solid content of CAS hydrogels ( $DS_{\text{sulfate}}/DS_{\text{acetyl}}$  ratio of 0.4 and solid content of 4.5 wt. %) with and without ionic crosslinking in deionized water

After exceeding the CGS, a CAS solution made a transition into a CAS hydrogel (Figure 2.2). It was found that an intrinsic feature of polymer networks (balance between sulfate and acetyl moieties) affects the CGS. As shown in Figure 2.2, an inverse correlation between the  $DS_{\text{sulfate}}/DS_{\text{acetyl}}$  ratio and CGS was observed, suggesting that a low  $DS_{\text{sulfate}}/DS_{\text{acetyl}}$  ratio of CAS hydrogels results in exhibiting enhanced resistance to flow under its own weight, while concurrently a higher water storage capacity within its polymer network. The results suggest that

the structural properties of CAS hydrogels are predominantly governed by influences of acetyl moieties, while sulfate moieties contribute to the retention of water molecules within the polymer networks. A hydrogel with a lower  $DS_{\text{sulfate}}/DS_{\text{acetyl}}$  ratio is more susceptible to the evaporation of water molecules. The presence of a greater number of sulfate moieties increase chances to establish additional intermolecular interactions with water molecules, leading to a slower rate of water molecule loss.

### 3.3. Fabrication of Double-Crosslinked CAS Hydrogel Adsorbents and Their Feasibility

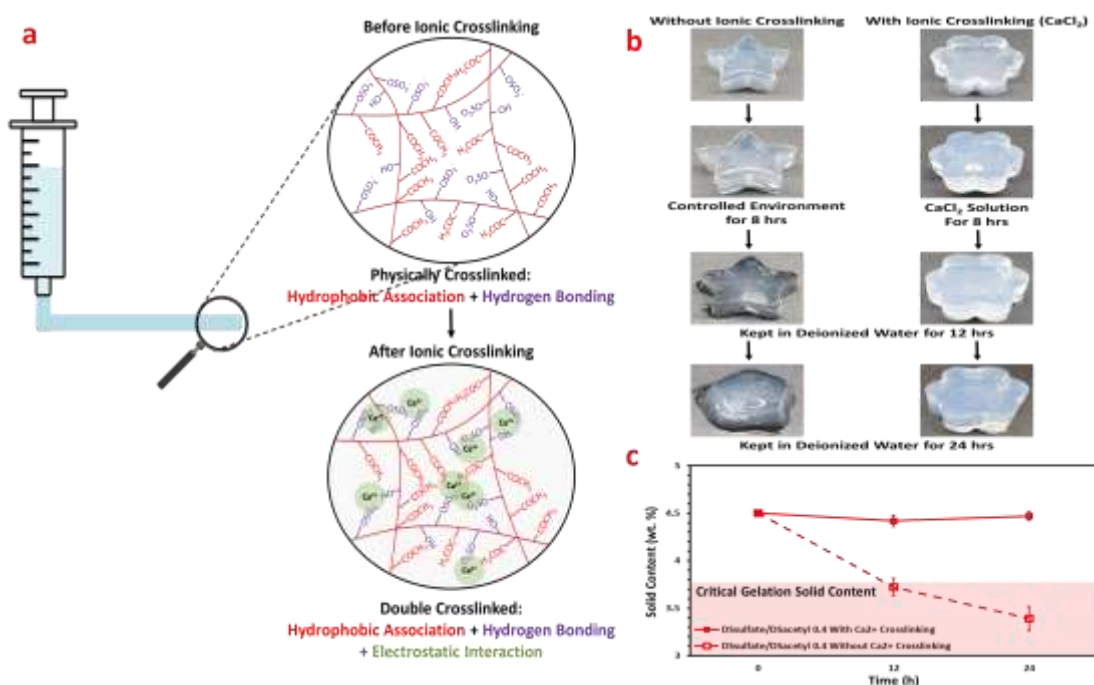


**Figure 2.4.** (a) Fabrication scheme of double-crosslinked CAS hydrogels, (b) Behaviors of molded CAS hydrogels ( $DS_{sulfate}/DS_{acetyl}$  ratio of 0.4 and solid content of 4.5 wt. %) with and without ionic crosslinking in deionized water, and (c) The changes in the solid content of CAS hydrogels ( $DS_{sulfate}/DS_{acetyl}$  ratio of 0.4 and solid content of 4.5 wt. %) with and without ionic crosslinking in deionized water

As shown in Figure 2.1, one of the external stimuli affecting the rheological properties of CAS hydrogels is temperature. CAS hydrogels display a fluidic behavior at elevated temperatures and subsequently recover their gel-like state upon cooling. The thermal reversibility helps process CAS hydrogels into various structures via molding or extrusion (Figure 2.5). If physically crosslinked CAS hydrogels are kept in deionized water, the hydrophilic CAS hydrogels continue to absorb water. As the solids content of the physically crosslinked hydrogels decreases and approaches the CGS, the physically crosslinked CAS hydrogels gradually lose their structural

integrity (Figures 2.4b and c). Therefore, to make the physically crosslinked CAS hydrogels useful in commercial applications, a method to enhance the durability of the CAS hydrogels during the adsorption process must be invented. In other work using hydrogels from alginate, ionic crosslinking (e.g.,  $\text{Ca}^{2+}$ ,  $\text{Sr}^{2+}$ ,  $\text{Ba}^{2+}$ , etc.) has been widely applied to create more durable hydrogels [48]. Inspired by this prior work, ionic crosslinking with  $\text{Ca}^{2+}$  was employed to produce double-crosslinked CAS hydrogels (physical and ionic crosslinking). After ionic crosslinking with  $\text{Ca}^{2+}$ , water absorption into polymeric networks of the CAS hydrogel was more limited but the overall durability of the hydrogel was significantly improved. The solid content of the double-crosslinked CAS hydrogel remained almost constant and maintained its original molded structures in deionized water (Figures 2.4b and c). Ionic crosslinking of the CAS hydrogels with  $\text{Ca}^{2+}$  was found to be effective to enhance the durability of CAS hydrogels in deionized water.

In the following section, all the results refer to works conducted with double-crosslinked CAS hydrogels. To prevent lateral spreading after the fabrication, the solid content of these employed CAS hydrogels was held constant at 4.5 wt. %. As described in Figure 2.5, 3D scaffold-like structures were prepared with the CAS hydrogels and then crosslinked with  $\text{Ca}^{2+}$ . After conducting ionic crosslinking, the 3D CAS hydrogel structures were introduced into an MB solution to examine the feasibility of CAS hydrogels as an adsorbent for MB dye. The double-crosslinked CAS hydrogel 3D structures did not lose their structure during the MB adsorption process (Figure 2.5). Compared to the molded CAS hydrogel adsorbent, which had a color gradient consistent with an MB concentration gradient, the 3D CAS hydrogel structures showed a uniform color distribution throughout the structure. This is likely due to the CAS hydrogel fiber structures having a higher surface-to-volume ratio than the molded sample, allowing them to reach

equilibrium more quickly. Therefore, for further adsorption experiments, 3D structures of the double-crosslinked CAS hydrogel adsorbents were employed for the subsequent work.

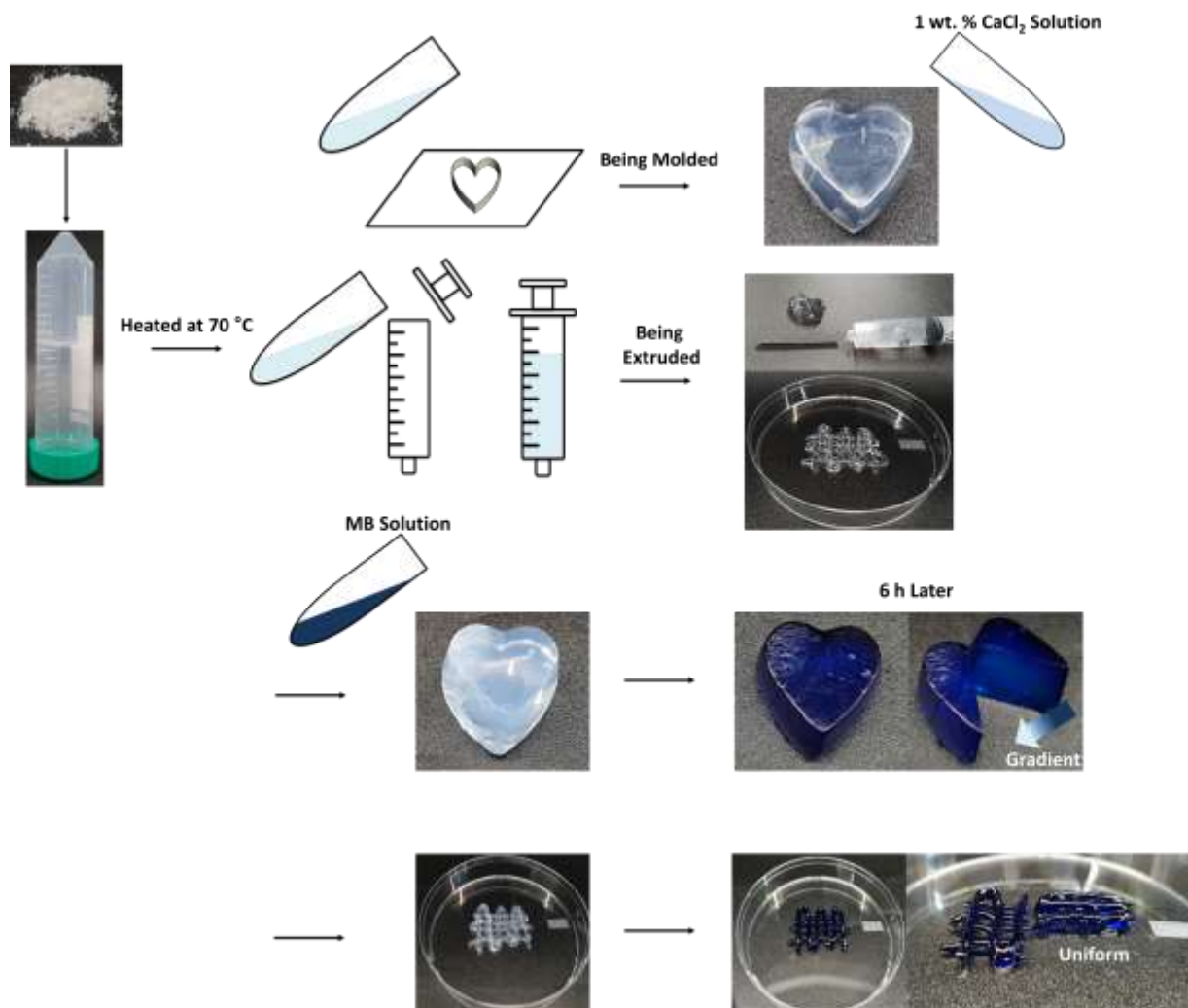


**Figure 2.5.** Procedure for the preparation of CAS hydrogel 3D structures ( $DS_{\text{sulfate}}/DS_{\text{acetyl}}$  ratio of 0.4 and the solid content of all employed CAS hydrogels was held constant at 4.5 wt. %)

### 3.4. Dye Removal Performance

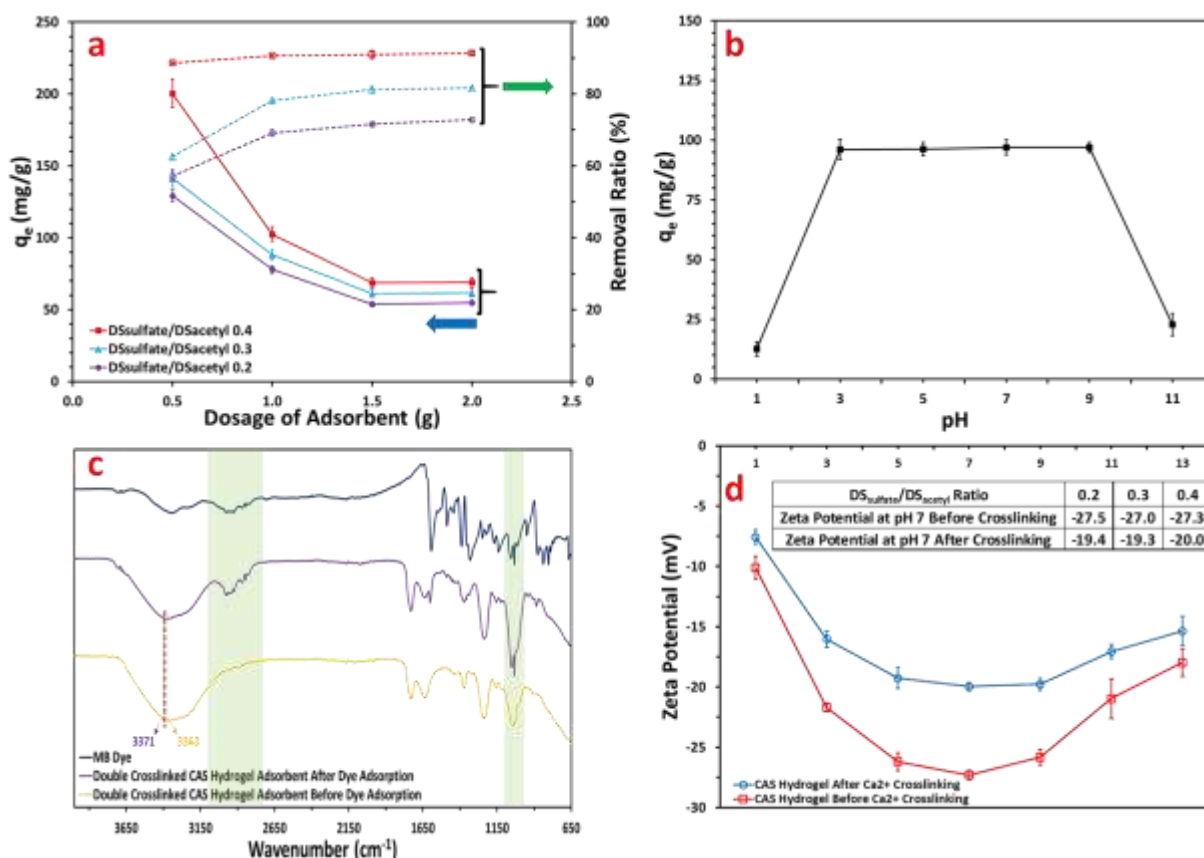


**Figure 2.6.** (a) Influence of adsorbent mass and DS<sub>sulfate</sub>/DS<sub>acetyl</sub> ratios on adsorption capacity ( $C_0 = 100$  mg/L, 7 days of contact time at 23 °C), (b) Influences of pH on adsorption capacity (DS<sub>sulfate</sub>/DS<sub>acetyl</sub> ratio of 0.4,  $C_0 = 100$  mg/L, 7 days of contact time at 23 °C), (c) ATR-FTIR spectra of MB, and double crosslinked CAS hydrogel adsorbent (DS<sub>sulfate</sub>/DS<sub>acetyl</sub> ratio of 0.4) before and after the adsorption experiment, and (d) Influences of initial pH on the zeta potential of CAS hydrogel having DS<sub>sulfate</sub>/DS<sub>acetyl</sub> ratio of 0.4 before and after the ionic crosslinking with Ca<sup>2+</sup>.

### 3.4.1. Dye Adsorption Process Optimization

In order to achieve an efficient and cost-effective commercial dye removal process, it is crucial to determine the optimal point at which the adsorbent dosage and removal efficiency can be optimized. Hence, a series of experiments were designed to investigate the correlation between adsorption capacity, removal ratio, and adsorbent dosage. The results revealed an inverse relationship between adsorption capacity and adsorbent dosage for all CAS hydrogel adsorbents, regardless of their  $DS_{\text{sulfate}}/DS_{\text{acetyl}}$  ratios. At higher adsorbent dosages, the available adsorption sites were not fully saturated with MB, leading to a decrease in the adsorption capacity [49]. In the case of removal ratio, an increase in adsorbent dosage resulted in an increase in the removal ratio regardless of the  $DS_{\text{sulfate}}/DS_{\text{acetyl}}$  ratios, and the removal ratio was found to reach a plateau at the adsorbent dosage of 1 g (Figure 2.6a). Additionally, it was observed that the increase in adsorption capacity was contributed by sulfate moieties. The highest adsorption capacity (102.5 mg/g) and removal ratio (90.7%) were achieved using a CAS hydrogel adsorbent with a  $DS_{\text{sulfate}}/DS_{\text{acetyl}}$  ratio of 0.4 and an adsorbent dosage of 1 g. Based on these results, an adsorbent dosage of 1 g and a CAS hydrogel having a  $DS_{\text{sulfate}}/DS_{\text{acetyl}}$  ratio of 0.4 were selected for further adsorption experiments.

### 3.4.2. Effect of pH

The pH of a system with ionic interactions is a critical factor affecting the adsorption behavior because changes in pH lead to changes in the zeta potential of adsorbents. Especially for ionic dyes, the zeta potential of an adsorbent has a significant impact on adsorption behaviors [50]. The investigation of changes in the zeta potential of a CAS hydrogel adsorbent with a

$DS_{\text{sulfate}}/DS_{\text{acetyl}}$  ratio of 0.4 in response to changes in solution pH was carried out before and after the ionic crosslinking process with  $\text{Ca}^{2+}$ . After the ionic crosslinking, the absolute value of the CAS hydrogel adsorbent's zeta potential increased across the pH range (Figure 2.6d). The absolute value of the zeta potential of the CAS hydrogel showed a maximum at pH 7 (-20.0 mV) and gradually decreased as the solutions became more acidic or basic (pH 1 and pH 13). Therefore, the adsorption of cationic MB dye onto the CAS hydrogels via electrostatic interactions was expected to be favorable because the CAS hydrogels exhibited a negatively charged surface over the entire practical pH range. To further examine the influences of electrostatic interactions on the CAS adsorption behavior for MB, MB solutions having different pH (1, 3, 5, 7, 9, and 11) were prepared. At extreme pH ranges such as pH 1 and 11, the influences of electrostatic interactions can be seen. Under the extremely acidic condition, the sulfate groups in the CAS hydrogel would be protonated, resulting in a decrease in the zeta potential of the CAS hydrogel (Figure 2.6d) [51]. For cationic dyes like MB, this condition was not favored to establish electrostatic interaction. As a result, a significant decrease in the adsorption capacity at pH 1 was observed (12.6 mg/g, Figure 2.6b). Under the extremely basic condition, due to the charge screening effect originating from excess  $\text{Na}^+$  ions, electrostatic interactions between sulfate groups and MB would be hindered, also resulting in the low adsorption capacity [52]. In the range of pH 3-9 at 23 °C, the adsorption capacity of the CAS hydrogel appeared to be constant around 96 mg/g (Figure 2.6b). In this pH range, other factors besides the electrostatic interactions dominate the adsorption behavior of the CAS hydrogel for MB. Even though the zeta potential of CAS hydrogel adsorbents that had different  $DS_{\text{sulfate}}/DS_{\text{acetyl}}$  ratios (0.2, 0.3, and 0.4) showed the similar value (Figure 2.6d), noticeable differences in the adsorption capacities among the CAS hydrogels were observed (Figure 2.6a). Based on the ATR-FTIR spectra shown in Figure 2.6c, the adsorption of MB into

the CAS hydrogel adsorbent can be readily observed. New peaks originating from MB (around 1000 and 2900  $\text{cm}^{-1}$ ) appeared after the adsorption. The formation of hydrogen bonding between the CAS hydrogel and MB can be checked by peak shift in ATR-FTIR spectra [53, 54]. The ATR-FTIR spectra of the CAS hydrogel-MB complex and CAS hydrogel looked similar, however, there were slight shifts in hydroxyl peaks, which may be caused by the formation of the hydrogen bonds between the CAS hydrogel and MB (Figure 2.6c). Based on these results, the adsorption behavior of MB into the CAS hydrogel adsorbent can be explained by the synergetic effects of electrostatic interactions and the formation of hydrogen bonding between CAS hydrogel and MB.

### **3.4.3. Dye Adsorption Kinetics**

Adsorption kinetics models are useful to estimate the rate of adsorption behaviors and also to give an insight into the adsorption mechanisms [55]. The adsorption kinetics of MB were studied by employing three different kinetics models, 1) non-linear pseudo-first-order model, 2) non-linear pseudo-first-order model, and 3) the Weber-Morris intra-particle diffusion model. Figure 2.7a depicts the adsorption of MB on the CAS hydrogel adsorbent as a function of exposure time.

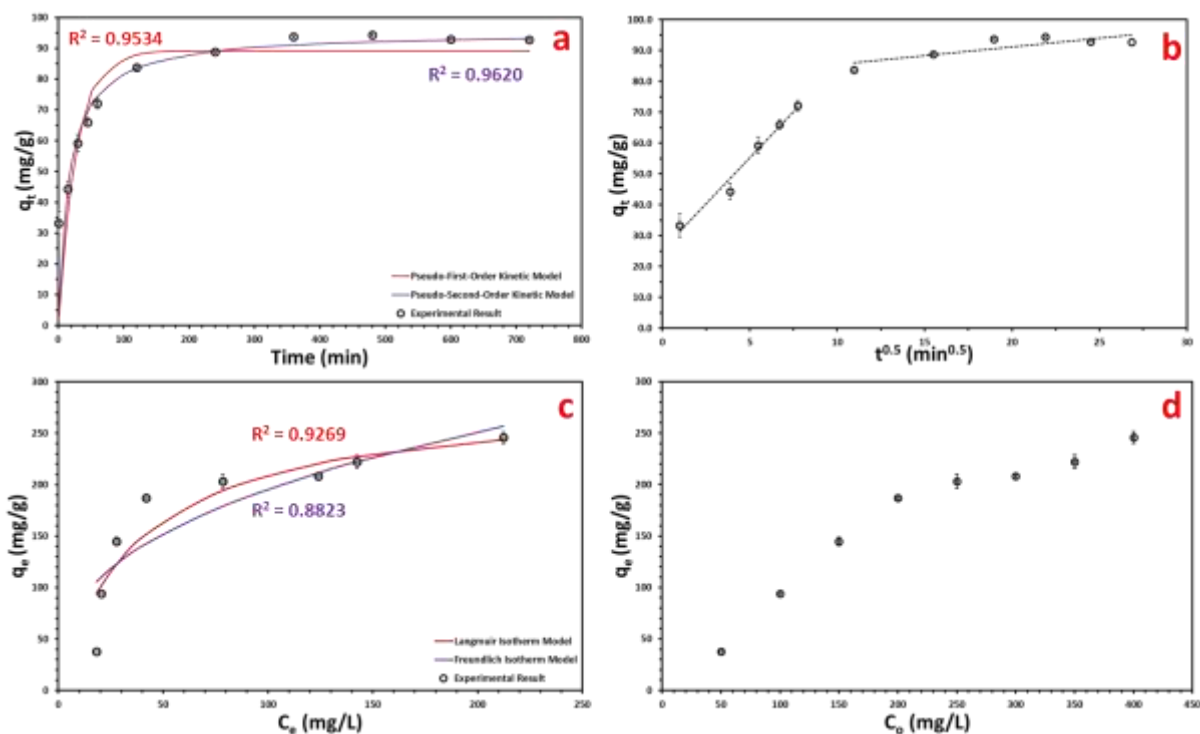


**Figure 2.7.** MB removal behaviors of the CAS hydrogel adsorbent: (a) kinetics ( $C_0 = 100$  mg/L and pH = 7 at 23 °C), (b) Intra-particle diffusion model ( $C_0 = 100$  mg/L and pH = 7 at 23 °C), (c) Isotherm (pH = 7, exposal time = 24 h at 23 °C) of MB, and (d) Influences of initial MB concentrations on the adsorption capacity (pH = 7, exposal time = 24 h at 23 °C).

MB adsorption increased steeply in the early stage, and the equilibrium of MB adsorption was attained within 6 hours (93.7 mg/g). According to the Weber-Morris intra-particle diffusion model, if a straight line is produced from a plot ( $q_t$  versus  $t^{1/2}$ ), it represents the adsorption process is solely governed by intra-particle diffusion. Whereas, if a plot shows two or more linear sections, then the adsorption behavior consists of at least two individual steps [56]. In the case of the CAS hydrogel adsorbent, the plot ( $q_t$  versus  $t^{1/2}$ ) exhibited two individual linear lines (Figure 2.7b), which means that the MB adsorption has at least two distinct phases. The first linear section that had a steeper slope represented a rapid surface, or near surface, adsorption stage. This is

consistent with the diffusion of MB from a bulk solution onto external surfaces of a CAS hydrogel adsorbent [57]. The second section has a lower slope, which represents the slow diffusion of MB into the interior of a CAS hydrogel adsorbent [57]. Weber-Morris intra-particle model also gives a clue into the mechanism. It suggests that after the initial rapid surface adsorption (about 2 h), the MB started to diffuse into the interior of a CAS hydrogel adsorbent at a slow rate (Figure 2.7b). To study the adsorption mechanism of MB further, the pseudo-first-order model and pseudo-second-order model were considered. Based on the correlation coefficients derived from each model, the pseudo-second-order kinetics model is a better fit for the adsorption behavior of MB onto a CAS hydrogel adsorbent. Therefore, in the case of CAS hydrogel adsorbents, chemisorption is a better option to explain the adsorption behavior of MB [58, 59]. These results were consistent with the previous results shown in Figure 2.6, which represented that electrostatic interactions and hydrogen bonding formation were key factors in capturing MB.

#### **3.4.4. Dye Adsorption Isotherm**

Isotherm models can provide additional insights into the adsorption process [60]. In this work, non-linear Langmuir and non-linear Freundlich isotherm models were considered to explain the adsorption behavior of MB. At 23 °C, the adsorption capacity ( $q_e$ ) gradually increased up to 245 mg/g with an increase in the initial MB concentration ( $C_0$ ) (Figure 2.7d). The low  $q_e$  at the low initial MB concentration could be attributed to the low extent of saturation of the adsorption sites. As the initial MB concentration increased, the adsorption sites in the CAS hydrogel were gradually occupied with MB and eventually reaching an equilibrium state. The strength of the interactions for the adsorption process can be estimated by the separation factor ( $R_L$ ). If the value of  $R_L$  falls into the range of 0-1, it indicates that this adsorption process is

favorable [59]. In the case of the CAS hydrogel adsorbent, all MB concentrations utilized for the adsorption isotherm experiments lay within the  $R_L$  range of 0-1. Therefore, MB adsorption onto the CAS hydrogel adsorbent is favorable under these experimental conditions. Considering the correlation coefficient of each model, the Langmuir isotherm model is a more suitable model to describe the adsorption behaviors of MB (Table 3). The interactions between the CAS sulfate groups and the MB dominate the adsorption behavior creating a good agreement with the Langmuir model, which represents that monolayer adsorption dominates the adsorption process [59].

**Table 2.2.** MB adsorption kinetics parameters

Adsorbent	Dye	Pseudo-First-Order			Pseudo-Second-Order		
		$q_e$ (mg g <sup>-1</sup> )	$k_1$ (min <sup>-1</sup> )	$R^2$	$q_e$ (mg g <sup>-1</sup> )	$k_2 * 10^{-3}$ (g mg <sup>-1</sup> min <sup>-1</sup> )	$R^2$
Double-Crosslinked CAS Hydrogel Adsorbent DS <sub>sulfate</sub> /DS <sub>acetyl</sub> 0.4	MB	89.1	0.0375	0.9534	95.3	$6.23 \times 10^{-7}$	0.9620

**Table 2.3.** MB adsorption isotherm parameters

Adsorbent	Dye	Model	Parameter	Value
CAS Hydrogel DS <sub>sulfate</sub> /DS <sub>acetyl</sub> 0.4	MB	Langmuir	$q_m$ (mg g <sup>-1</sup> )	286
			$K_L$ (L mg <sup>-1</sup> )	0.027
			$R^2$	0.9269
		Freundlich	$1/n$	0.36
			$K_F$ ((mg g <sup>-1</sup> )/(mg L <sup>-1</sup> ) <sup>1/n</sup> )	36.83
			$R^2$	0.8823

### 3.5. Recycling CAS Hydrogel Adsorbent

The potential to regenerate and reuse the CAS hydrogel adsorbent is important for commercial processes and the overall sustainability of the system. The potential for recycling of the CAS was examined by conducting 5 cycles of MB adsorption-desorption process. Taking advantage of unfavorable MB adsorption in extremely acidic conditions (12.6 mg/g at pH =1), adsorbed MB can be desorbed from the CAS hydrogel. Release of the MB from CAS hydrogel adsorbents was successfully achieved in 0.1 M of aqueous HCl solution and qualitatively shown in Figure 2.8a.

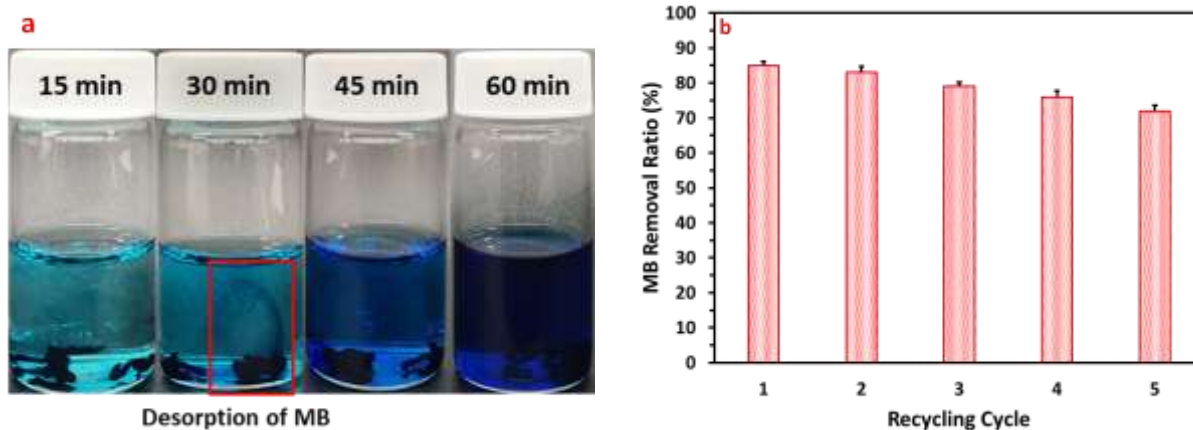


**Figure 2.8.** Photos of the desorption process of MB from a CAS hydrogel adsorbent in 0.1 M HCl, and (b) MB removal ratio of regenerated CAS hydrogel adsorbents measured at each cycle:  $DS_{\text{sulfate}}/DS_{\text{acetyl}}$  ratio = 0.4,  $C_0 = 100$  mg/L, pH = 7, and  $t = 48$  hours at 23 °C.

Figure 2.8b shows the overall MB removal ratio of each recycling cycle. In the first recycling cycle, the MB removal ratio of the regenerated CAS hydrogel adsorbents reached 85 %. After the fifth recycling cycle, the MB removal ratio of CAS hydrogel adsorbents dropped to 72 %. The decrease in the removal ratio could be attributed to several processes. The desorption process is time-dependent and the 6 hours of desorption time could be extended to improve the

overall extent of MB desorption. Also, as shown in Figure 2.6b, even in the extremely acidic condition (pH 1), CAS hydrogel adsorbent can retain a certain amount of MB (12.6 mg/g). Therefore, a small amount of MB could remain in the adsorbent after the desorption process, decreasing the removal ratio in subsequent cycles. An additional explanation for the drops in the removal ratio might be due to a loss of the CAS itself during the recovery process after the desorption. However, since the overall structural integrity of CAS hydrogel adsorbents was well-maintained during the recycles, the loss of CAS is modest. These results showed that the double-crosslinked CAS hydrogel could be a potential candidate for a sustainable and recyclable natural polymer-based adsorbent.

#### **4. Conclusion**

The study demonstrated the formulation of single-component CAS hydrogels within a specific  $DS_{\text{sulfate}}/DS_{\text{acetyl}}$  ratio range of 0.2-0.4 and solid contents. The presence of sulfate moieties facilitated additional intermolecular interactions, resulting in the formation of physically crosslinked hydrogels. Upon exceeding the critical gelation solid content (CGS), the transition from a solution to a hydrogel was observed. The CAS hydrogels exhibited the thermal rheological responses, making them suitable for facile processing into various shapes via molding or extrusion. For CAS hydrogels with a solid content exceeding their CGS, excellent shape fidelity was observed upon molding or extrusion. However, when immersed in deionized water, a gradual water absorption occurred, leading to a reduction in the solid content of the hydrogel below the CGS and eventual loss of structural integrity.

To enhance the durability of CAS hydrogels during the adsorption process, ionic crosslinking with  $\text{Ca}^{2+}$  was conducted. The CAS hydrogels were first extruded into 3D scaffold-

like structures, which were then strengthened by ionic crosslinks. The adsorption performance of the resulting double-crosslinked (physically and ionically crosslinked) CAS hydrogel adsorbents was evaluated using MB as a model dye. The adsorption capacity of the double-crosslinked CAS hydrogel adsorbents was found to depend on  $DS_{\text{sulfate}}$ . At the CAS  $DS_{\text{sulfate}}/DS_{\text{acetyl}}$  ratio of 0.4, the double-crosslinked CAS hydrogel adsorbent showed the maximum adsorption capacity of 245 mg/g. The adsorption behavior of MB on the CAS hydrogel adsorbents was well-described by the pseudo-second-order kinetics and Langmuir isotherm models. The pseudo-second-order kinetics model suggested that the adsorption of MB was due to the combined effects of hydrogen bonding and electrostatic interactions between the negatively charged CAS and positively charged MB. The Langmuir isotherm model indicated that monolayer adsorption was the dominant MB adsorption mechanism on the CAS hydrogel adsorbent. The recyclability of the double-crosslinked CAS hydrogel adsorbent was evaluated using five adsorption-desorption cycles, and the adsorbent maintained a removal ratio of 70% even after five cycles. This study demonstrated a simple approach for producing hydrogels from cellulose and examined the feasibility of using CAS hydrogels as an adsorbent, which could offer a more sustainable solution for wastewater treatment.

## REFERENCES

- [1] J.S. Shapiro, Pollution trends and US environmental policy: Lessons from the past half century, *Review of Environmental Economics and Policy* 16(1) (2022) 42-61.
- [2] F.S. Chapin III, S.R. Carpenter, G.P. Kofinas, C. Folke, N. Abel, W.C. Clark, P. Olsson, D.M.S. Smith, B. Walker, O.R. Young, Ecosystem stewardship: sustainability strategies for a rapidly changing planet, *Trends in ecology & evolution* 25(4) (2010) 241-249.
- [3] B. Chen, M. Wang, M. Duan, X. Ma, J. Hong, F. Xie, R. Zhang, X. Li, In search of key: protecting human health and the ecosystem from water pollution in China, *Journal of Cleaner Production* 228 (2019) 101-111.
- [4] Z. Carmen, S. Daniela, Textile organic dyes-characteristics, polluting effects and separation/elimination procedures from industrial effluents-a critical overview, *IntechOpen Rijeka*2012.
- [5] Q. Husain, Peroxidase mediated decolorization and remediation of wastewater containing industrial dyes: a review, *Reviews in Environmental Science and Bio/Technology* 9(2) (2010) 117-140.
- [6] N.A. Littlefield, B.-N. Blackwell, C.C. Hewitt, D.W. Gaylor, Chronic toxicity and carcinogenicity studies of gentian violet in mice, *Toxicological Sciences* 5(5) (1985) 902-912.
- [7] W. Au, S. Pathak, C.J. Collie, T. Hsu, Cytogenetic toxicity of gentian violet and crystal violet on mammalian cells in vitro, *Mutation Research/Genetic Toxicology* 58(2-3) (1978) 269-276.
- [8] K.A. Wani, N.K. Jangid, A.R. Bhat, *Impact of Textile Dyes on Public health and the Environment*, IGI Global2019.

- [9] B. Lellis, C.Z. Fávaro-Polonio, J.A. Pamphile, J.C. Polonio, Effects of textile dyes on health and the environment and bioremediation potential of living organisms, *Biotechnology Research and Innovation* 3(2) (2019) 275-290.
- [10] D. Yaseen, M. Scholz, Textile dye wastewater characteristics and constituents of synthetic effluents: a critical review, *International journal of environmental science and technology* 16(2) (2019) 1193-1226.
- [11] G. de Aragao Umbuzeiro, H.S. Freeman, S.H. Warren, D.P. De Oliveira, Y. Terao, T. Watanabe, L.D. Claxton, The contribution of azo dyes to the mutagenic activity of the Cristais River, *Chemosphere* 60(1) (2005) 55-64.
- [12] M. Manzanera, *Alternative fuel, BoD–Books on Demand* 2011.
- [13] C.-M. Liu, S.-Y. Wu, From biomass waste to biofuels and biomaterial building blocks, *Renewable Energy* 96 (2016) 1056-1062.
- [14] H.Y. Leong, C.-K. Chang, K.S. Khoo, K.W. Chew, S.R. Chia, J.W. Lim, J.-S. Chang, P.L. Show, Waste biorefinery towards a sustainable circular bioeconomy: a solution to global issues, *Biotechnology for Biofuels* 14(1) (2021) 1-15.
- [15] A. Saravanan, P. Thamarai, P.S. Kumar, G. Rangasamy, Recent advances in polymer composite, extraction, and their application for wastewater treatment: A review, *Chemosphere* (2022) 136368.
- [16] B. Balakrishnan, R. Banerjee, Biopolymer-based hydrogels for cartilage tissue engineering, *Chemical reviews* 111(8) (2011) 4453-4474.
- [17] S. Van Vlierberghe, P. Dubruel, E. Schacht, Biopolymer-based hydrogels as scaffolds for tissue engineering applications: a review, *Biomacromolecules* 12(5) (2011) 1387-1408.

- [18] C. Brigham, *Biopolymers: Biodegradable alternatives to traditional plastics*, Green Chemistry, Elsevier 2018, pp. 753-770.
- [19] T. Heinze, O.A. El Seoud, A. Koschella, *Cellulose derivatives: synthesis, structure, and properties*, Springer 2018.
- [20] M. Ma, Y. Chen, X. Zhao, F. Tan, Y. Wang, Y. Cao, W. Cai, Effective removal of cation dyes from aqueous solution using robust cellulose sponge, *Journal of Saudi Chemical Society* 24(12) (2020) 915-924.
- [21] S.H. Zainal, N.H. Mohd, N. Suhaili, F.H. Anuar, A.M. Lazim, R. Othaman, Preparation of cellulose-based hydrogel: A review, *Journal of Materials Research and Technology* 10 (2021) 935-952.
- [22] M. Rahman, M. Hasan, A.S. Nitai, S. Nam, A.K. Karmakar, M. Ahsan, M.J. Shiddiky, M.B. Ahmed, Recent developments of carboxymethyl cellulose, *Polymers* 13(8) (2021) 1345.
- [23] M.T. Yagub, T.K. Sen, S. Afroze, H.M. Ang, Dye and its removal from aqueous solution by adsorption: a review, *Advances in colloid and interface science* 209 (2014) 172-184.
- [24] G. Crini, P.-M. Badot, Application of chitosan, a natural aminopolysaccharide, for dye removal from aqueous solutions by adsorption processes using batch studies: A review of recent literature, *Progress in polymer science* 33(4) (2008) 399-447.
- [25] J.R. Perrich, *Activated carbon adsorption for wastewater treatment*, CRC press 2018.
- [26] S. Wong, N. Ngadi, I.M. Inuwa, O. Hassan, Recent advances in applications of activated carbon from biowaste for wastewater treatment: a short review, *Journal of Cleaner Production* 175 (2018) 361-375.
- [27] P. Malik, Dye removal from wastewater using activated carbon developed from sawdust: adsorption equilibrium and kinetics, *Journal of Hazardous Materials* 113(1-3) (2004) 81-88.

- [28] K. Soleimani, A.D. Tehrani, M. Adeli, Bioconjugated graphene oxide hydrogel as an effective adsorbent for cationic dyes removal, *Ecotoxicology and environmental safety* 147 (2018) 34-42.
- [29] M. Tavakolian, H. Wiebe, M.A. Sadeghi, T.G. van de Ven, Dye removal using hairy nanocellulose: experimental and theoretical investigations, *ACS applied materials & interfaces* 12(4) (2019) 5040-5049.
- [30] V. Sinha, S. Chakma, Advances in the preparation of hydrogel for wastewater treatment: A concise review, *Journal of Environmental Chemical Engineering* 7(5) (2019) 103295.
- [31] I. Ayouch, I. Kassem, Z. Kassab, I. Barrak, A. Barhoun, J. Jacquemin, K. Draoui, M. El Achaby, Crosslinked carboxymethyl cellulose-hydroxyethyl cellulose hydrogel films for adsorption of cadmium and methylene blue from aqueous solutions, *Surfaces and Interfaces* 24 (2021) 101124.
- [32] H. Zhang, F. Zhang, R. Yuan, Applications of natural polymer-based hydrogels in the food industry, *Hydrogels based on natural polymers*, Elsevier2020, pp. 357-410.
- [33] E.M. Ahmed, Hydrogel: Preparation, characterization, and applications: A review, *Journal of advanced research* 6(2) (2015) 105-121.
- [34] S. Kabir, P.P. Sikdar, B. Haque, M. Bhuiyan, A. Ali, M. Islam, Cellulose-based hydrogel materials: Chemistry, properties and their prospective applications, *Progress in biomaterials* 7(3) (2018) 153-174.
- [35] T. Hashizume, Y. Okamoto, K. Nagai, S. Shimamoto, Mechanism of sodium-hypochlorite-induced degradation of cellulose acetate and the enhancement of its degradation resistance by chemical modification, *Textile Research Journal* 92(13-14) (2022) 2487-2500.
- [36] C.B. Oliveira, S.R. Veloso, E.M. Castanheira, P.R. Figueiredo, A.T. Carvalho, L. Hilliou, R.B. Pereira, D.M. Pereira, J.A. Martins, P.M. Ferreira, An injectable, naproxen-conjugated,

supramolecular hydrogel with ultra-low critical gelation concentration—prepared from a known folate receptor ligand, *Soft Matter* 18(20) (2022) 3955-3966.

[37] W. Tanan, J. Panichpakdee, S. Saengsuwan, Novel biodegradable hydrogel based on natural polymers: Synthesis, characterization, swelling/reswelling and biodegradability, *European Polymer Journal* 112 (2019) 678-687.

[38] R.J. Spontak, J.J. Ryan, Polymer blend compatibilization by the addition of block copolymers, *Compatibilization of Polymer Blends*, Elsevier 2020, pp. 57-102.

[39] Y. Hirai, T. Terashima, M. Takenaka, M. Sawamoto, Precision self-assembly of amphiphilic random copolymers into uniform and self-sorting nanocompartments in water, *Macromolecules* 49(14) (2016) 5084-5091.

[40] A.M. Senna, K.M. Novack, V.R. Botaro, Synthesis and characterization of hydrogels from cellulose acetate by esterification crosslinking with EDTA dianhydride, *Carbohydrate polymers* 114 (2014) 260-268.

[41] M.M. Senna, A.E.-K.B. Mostafa, S.R. Mahdy, A.W.M. El-Naggar, Characterization of blend hydrogels based on plasticized starch/cellulose acetate/carboxymethyl cellulose synthesized by electron beam irradiation, *Nuclear Instruments and Methods in Physics Research Section B: Beam Interactions with Materials and Atoms* 386 (2016) 22-29.

[42] G. Chauvelon, J.-L. Doublier, A. Buléon, J.-F. Thibault, L. Saulnier, Rheological properties of sulfoacetate derivatives of cellulose, *Carbohydrate research* 338(8) (2003) 751-759.

[43] O. Guvench, E.K. Whitmore, Sulfation and calcium favor compact conformations of chondroitin in aqueous solutions, *ACS omega* 6(20) (2021) 13204-13217.

- [44] W. Li, Y. Xue, M. He, J. Yan, L.A. Lucia, J. Chen, J. Yu, G. Yang, Facile Preparation and Characteristic Analysis of Sulfated Cellulose Nanofibril via the Pretreatment of Sulfamic Acid-Glycerol Based Deep Eutectic Solvents, *Nanomaterials* 11(11) (2021) 2778.
- [45] I. Skorniyakov, V. Komar, IR spectra and the structure of plasticized cellulose acetate films, *Journal of applied spectroscopy* 65(6) (1998) 911-918.
- [46] P. Sikdar, M.M. Uddin, T.M. Dip, S. Islam, M.S. Hoque, A.K. Dhar, S. Wu, Recent advances in the synthesis of smart hydrogels, *Materials Advances* (2021).
- [47] M. Bustamante-Torres, D. Romero-Fierro, B. Arcentales-Vera, K. Palomino, H. Magaña, E. Bucio, Hydrogels classification according to the physical or chemical interactions and as stimuli-sensitive materials, *Gels* 7(4) (2021) 182.
- [48] A. Dodero, L. Pianella, S. Vicini, M. Alloisio, M. Ottonelli, M. Castellano, Alginate-based hydrogels prepared via ionic gelation: An experimental design approach to predict the crosslinking degree, *European Polymer Journal* 118 (2019) 586-594.
- [49] D.G. Njuguna, H. Schönherr, Xanthan gum hydrogels as high-capacity adsorbents for dye removal, *ACS Applied Polymer Materials* 3(6) (2021) 3142-3152.
- [50] H. Li, X. Cao, C. Zhang, Q. Yu, Z. Zhao, X. Niu, X. Sun, Y. Liu, L. Ma, Z. Li, Enhanced adsorptive removal of anionic and cationic dyes from single or mixed dye solutions using MOF PCN-222, *RSC advances* 7(27) (2017) 16273-16281.
- [51] A. Barth, J.E. Corrie, Characterization of a new caged proton capable of inducing large pH jumps, *Biophysical journal* 83(5) (2002) 2864-2871.
- [52] K. Sharma, B. Kaith, V. Kumar, S. Kalia, V. Kumar, H. Swart, Water retention and dye adsorption behavior of Gg-cl-poly (acrylic acid-aniline) based conductive hydrogels, *Geoderma* 232 (2014) 45-55.

- [53] T. Fornaro, D. Burini, M. Biczysko, V. Barone, Hydrogen-bonding effects on infrared spectra from anharmonic computations: uracil–water complexes and uracil dimers, *The Journal of physical chemistry A* 119(18) (2015) 4224-4236.
- [54] B. Athokpam, S.G. Ramesh, R.H. McKenzie, Effect of hydrogen bonding on the infrared absorption intensity of OH stretch vibrations, *Chemical Physics* 488 (2017) 43-54.
- [55] X. Song, J. An, C. He, J. Zhou, Y. Xu, H. Ji, L. Yang, J. Yin, W. Zhao, C. Zhao, A bioinspired strategy towards super-adsorbent hydrogel spheres via self-sacrificing micro-reactors for robust wastewater remediation, *Journal of Materials Chemistry A* 7(37) (2019) 21386-21403.
- [56] K.M. Doke, E.M. Khan, Equilibrium, kinetic and diffusion mechanism of Cr (VI) adsorption onto activated carbon derived from wood apple shell, *Arabian journal of chemistry* 10 (2017) S252-S260.
- [57] B. Salunkhe, T.P. Schuman, Super-Adsorbent Hydrogels for Removal of Methylene Blue from Aqueous Solution: Dye Adsorption Isotherms, Kinetics, and Thermodynamic Properties, *Macromol* 1(4) (2021) 256-275.
- [58] P. Hadi, M.-H. To, C.-W. Hui, C.S.K. Lin, G. McKay, Aqueous mercury adsorption by activated carbons, *Water Research* 73 (2015) 37-55.
- [59] V. Manirethan, K. Raval, R. Rajan, H. Thaira, R.M. Balakrishnan, Kinetic and thermodynamic studies on the adsorption of heavy metals from aqueous solution by melanin nanopigment obtained from marine source: *Pseudomonas stutzeri*, *Journal of environmental management* 214 (2018) 315-324.
- [60] H.M. Jang, S. Yoo, Y.-K. Choi, S. Park, E. Kan, Adsorption isotherm, kinetic modeling and mechanism of tetracycline on *Pinus taeda*-derived activated biochar, *Bioresource Technology* 259 (2018) 24-31.



## CHAPTER 3

### Development and Characterization of Cellulose Acetate Sulfate Films for Food Packaging

#### Applications

#### Abstract

The demand for sustainable and biodegradable packaging materials has significantly increased in recent years. This study introduces a simple method for producing cellulose-based films, which represent a promising option for environmentally friendly packaging solutions. To achieve this, amphiphilic cellulose derivatives (cellulose acetate sulfate, CAS) was synthesized and CAS films with varying  $DS_{\text{sulfate}}/DS_{\text{acetyl}}$  balances (0.4/1.8, 0.7/1.8, and 1.0/1.8) were prepared. The resulting CAS films exhibited transparency, flexibility, homogeneity, and excellent resistance to oils. The  $DS_{\text{sulfate}}/DS_{\text{acetyl}}$  balance strongly influenced the physicochemical and mechanical properties of the CAS films. CAS films with  $DS_{\text{sulfate}}/DS_{\text{acetyl}}$  ratios of 0.4/1.8 and 0.7/1.8 showed hydrogel behavior upon re-exposure to water, while those with a ratio of 1.0/1.8 dissolved. Furthermore, the wettability and water vapor permeability (WVP) of the CAS films increased with an increase in  $DS_{\text{sulfate}}$ . The CAS films with a  $DS_{\text{sulfate}}/DS_{\text{acetyl}}$  ratio of 0.4/1.8 exhibited the highest tensile strength (TS) and elastic modulus (E) among the three conditions tested. The potential for CAS films to be used in food packaging was demonstrated by coating bananas with CAS solutions. Regardless of the  $DS_{\text{sulfate}}$  used, all coated bananas exhibited prolonged shelf life compared to uncoated bananas.

## 1. Introduction

Over the past few years, there has been a surge in global awareness and concern for environmental issues, leading to an increased demand for eco-friendly and sustainable materials [1, 2]. The growing demand for sustainable materials has driven research into naturally occurring polymers, which are known for their advantageous properties such as low carbon footprint, biocompatibility, and biodegradability [3, 4]. An area of active research involves the development of edible films derived from sustainable resources [5, 6]. Edible films serve a critical function in enhancing the quality and extending the shelf-life of food products by providing essential protection against physical, chemical, and biological degradation as a surface coating [7]. Among natural polymers, proteins, polysaccharides, and lipids are recognized as particularly promising candidates for the development of edible films with desirable properties [8-10].

Cellulose, a polysaccharide composed of  $\beta$ -D-glucopyranose units linked through glycosidic bonds, can be sourced from various materials, including plants, bacteria, algae, and others [11]. Owing to its abundance and ease of access, cellulose has been extensively studied for its diverse range of applications [12]. The semi-crystalline structures formed by the hydrogen bonding between the three free hydroxyl groups on each glucose monomer contribute to the exceptional stability of cellulose in both water and conventional organic solvents [13]. However, this stability also presents a challenge for the chemical modification of cellulose, as the semi-crystalline structure restricts the access of chemical reagents to the reactive sites on the glucose units [14]. Despite this limitation, the advancements in synthesis techniques have enabled the

development of strategies to modify cellulose chemically, making it a versatile platform for imparting desired properties suitable for specific applications [13, 15].

Cellulose ethers are highly versatile derivatives of cellulose that can be obtained through chemical reactions with various etherifying agents [16]. Some of the most commonly used cellulose ethers include hydroxypropyl methylcellulose (HPMC), methylcellulose (MC), and carboxymethylcellulose (CMC). Cellulose ethers have emerged as promising candidates for the fabrication of edible films, owing to their unique properties, including non-toxicity, tastelessness, and water solubility [17]. Cellulose ether-based films and edible coatings have shown moderate resistance to water, oils, greases, and non-polar organic solvents, making them suitable for use in food packaging to control the migration of moisture and gases in and out of foods [18]. Moreover, incorporating mineral and essential oils can endow these films and coatings with additional functionality, such as nutrient delivery and antimicrobial properties, enhancing their potential applications in food packaging and preservation [19, 20].

Cellulose sulfate (CS) is a derivative of cellulose that is synthesized by introducing sulfate groups to some or all of the hydroxyl groups in cellulose [21]. Due to its unique properties such as biocompatibility, biodegradability, microbicidal and anticoagulant activity, CS has attracted considerable interest and has been extensively studied in various fields over the past decade [22]. Furthermore, the water solubility and film-forming properties of CS make it a promising alternative for developing edible films or coatings for food packaging applications [23]. Films and edible coatings based on CS have demonstrated acceptable mechanical and barrier properties, making them useful for food protection and extending the shelf life of foods [23]. Similar to cellulose ether-based films or coatings, the functionality of CS-based films or coatings can be modified by blending them with essential oils or oleic acid [24, 25].

Cellulose acetate sulfate (CAS) is a cellulose derivative that possesses both hydrophilic (-OH and  $\text{OSO}_3^-$ ) and hydrophobic (-COCH<sub>3</sub>) functional groups. It can be synthesized by simultaneous employment of sulfating and acetylating agents [13]. CAS is known for its biocompatibility and microbicidal activity, and has been studied for its potential application in drug delivery [26, 27]. Moreover, CAS exhibits water solubility within a specific range of hydrophilic sulfate and hydrophobic acetyl groups, allowing it to form a solution capable of producing a film upon casting [28]. Although a potential has been displayed by CAS as films or edible coatings for foods, to the best of our knowledge, the characteristics of films or edible coatings based on CAS have never been explored. Therefore, the objective of this study is to prepare films and edible coatings based on CAS with varying balances of sulfate and acetyl groups. The CAS used to prepare CAS solutions is synthesized from commercially available cellulose acetate (CA). The fundamental properties of CAS films are investigated, and how the balance of sulfate and acetyl groups influences their mechanical and barrier properties is analyzed. Bananas are well-known for their short shelf life, making them a suitable choice for evaluating the effectiveness of a coating in extending their shelf life. To evaluate efficacy of CAS coating, CAS solutions with different balances of sulfate and acetyl groups are applied to the surface of bananas. This study will expand the range of raw materials available for producing films or edible coatings for food packaging.

## 2. Materials and Methods

### 2.1. Materials

CA ( $DS_{\text{acetyl}}$  1.8) was kindly provided by Eastman Chemical Company (Kingsport, TN). *N,N*-dimethylformamide (DMF), sulfamic acid ( $\text{NH}_2\text{SO}_3\text{H}$ ), ethanol, sodium acetate, sodium hydroxide, hydrochloric acid, barium chloride, silicone oil and 1.5  $\mu\text{m}$  nylon syringe filters were purchased from Fisher-Scientific (Hampton, NH). Bananas and a bottle of canola oil were purchased from a grocery store

**Table 3.1.**  $DS_{\text{sulfate}}$ ,  $DS_{\text{acetyl}}$ , and molecular weight of the reference CA and the resulting CAS

Samples	$DS_{\text{sulfate}}$	$DS_{\text{acetyl}}$	$M_w$ (g/mol)	PDI ( $M_w/M_n$ )
Reference CA	-	1.82	111,000	2.2
CAS $DS_{\text{sulfate}}/DS_{\text{acetyl}}$ 0.4/1.8	0.41	1.79	98,000	2.1
CAS $DS_{\text{sulfate}}/DS_{\text{acetyl}}$ 0.7/1.8	0.72	1.81	101,000	1.9
CAS $DS_{\text{sulfate}}/DS_{\text{acetyl}}$ 1.0/1.8	1.03	1.80	96,000	2.0

Molecular weight ( $M_w$ ) and polydispersity index (PDI) were measured by GPC employing polystyrene as a standard.

### 2.2. Synthesis of CAS

The CAS synthesis was conducted by following a method suggested elsewhere [13, 15]. Firstly, the sulfation of commercially available CA was carried out in anhydrous DMF. After oven-drying at 105 °C overnight, the CA (15 g) was transferred to 100 ml of anhydrous DMF at 80 °C. To initiate the CAS synthesis, a sulfating agent (sulfamic acid) was introduced, and the  $DS_{\text{sulfate}}$  of CAS was modulated by varying the amount of the sulfating agent. After the synthesis, the resulting CAS was recovered by precipitation with a mixture of sodium acetate and ethanol (3 wt.%), and it was washed with pure ethanol several times to remove residual DMF and sodium acetate salt. Finally, it was air-dried at room temperature overnight.

### **2.3. Gel Permeation Chromatography**

The molecular weight ( $M_w$ ) and polydispersity index (PDI) of both the reference CA and the resulting CAS were determined using a PLgel MIXED-B column on a 1260 Infinity GPC/SEC system (Agilent, Santa Clara, CA). The method was similar to a previously described protocol with minor modifications [29]. The eluent, which flowed at a rate of 0.25 mL/min through the column oven set at 60°C, was composed of LiBr/N-methylpyrrolidone (0.1 mol/L). The system was calibrated with polystyrene as an internal standard, and both CA and the resulting CAS samples were prepared at a concentration of 0.5 wt.%. An injection volume of 50  $\mu$ L was used for the samples.

### **2.4. Fourier Transform Infrared Spectroscopy**

Synthesized CAS were examined using a Spectrum 3 spectrometer (PerkinElmer, Waltham, MA). The CAS samples were scanned 16 times from 650  $\text{cm}^{-1}$  to 4000  $\text{cm}^{-1}$  at the resolution of 2  $\text{cm}^{-1}$ .

### **2.5. Preparation of CAS Films**

#### **2.5.1. Preparation of CAS Film Solutions**

To prepare the CAS film solutions, three samples with varying  $DS_{\text{sulfate}}/DS_{\text{acetyl}}$  ratios (0.4/1.8, 0.7/1.8, and 1.0/1.8) were used. The method for preparing the CAS hydrogels has been described elsewhere. In summary, 3 g of air-dried CAS powder was placed in a 50 ml centrifuge tube and washed with deionized water. Next, a predetermined amount of water (CAS solid

content: 6 wt.% based on oven-dried weight) was added to prepare the CAS hydrogels. The mixture was then swelled and homogenized in a water bath (HBR 4 control, IKA, Wilmington, NC) at 70 °C until a visually homogeneous and viscous solution was formed. The CAS hydrogel was obtained by allowing the sample to cool to 4 °C for 30 min. Once the CAS hydrogel was obtained, the solid content was reduced to 2 wt.% by adding a predetermined amount of deionized water and further treating the sample at 70 °C for 30 min. The solid content of both the CAS hydrogels and film solutions was determined by weighing before and after overnight oven drying at 105 °C.

### **2.5.2. Viscosity Measurement**

The viscosity of CAS film solutions with varying the  $DS_{\text{sulfate}}/DS_{\text{acetyl}}$  (0.4/1.8, 0.7/1.8, and 1.0/1.8) were recorded using a dynamic rotational rheometer (MCR 72, Anton Parr, Ashland, VA) equipped with a parallel plate (PP25) having a fixed gap size of 1 mm. The changes in the viscosity were recorded with angular frequency sweep mode ( $10^{-1}$  to  $10^2$  rad/s). All the measurements were conducted at room temperature (23 °C) with a pre-equilibration time of 1 min.

### **2.5.3. Casting of CAS Films**

To remove impurities, the solutions were filtered using a 1.5  $\mu\text{m}$  syringe filter and degassed with a vacuum chamber. The treated solutions were collected again by centrifugation. For film preparation, circular Teflon evaporating dishes with a diameter of 100 mm were gently filled with the CAS solutions. The amount of CAS was standardized to 0.004  $\text{g}/\text{cm}^2$ , resulting in

a total oven-dried weight of 0.31 g for each film. The evaporating dishes were placed on a level surface in a fume hood at room temperature (23 °C) for 24 hours. Once formed, the CAS films were carefully detached from the dishes and stored in a controlled environment (23 °C and 50% relative humidity) for further evaluation

## **2.6. Morphology of CAS Films**

The microstructure of the cast CAS films was analyzed using a field emission scanning electron microscope (FEI Verios 460L, Thermo Fisher Scientific, Waltham, MA). The films were first kept in a desiccator until a constant weight was achieved. For surface imaging, the films were attached to sample holders with double-sided carbon tape, while for cross-sections, the films were cut with a razor blade. The images were captured without any further modifications, and the accelerating voltage was adjusted based on the samples, starting at 5 kV.

## **2.7. Film Thickness**

After allowing for equilibration, the thickness of the CAS films was measured using a 49-56 micrometer (Messmer Büchel, Netherlands) at 10 mm intervals for a total of 10 measurements.

## **2.8. Transparency Measurement**

The light transmittance (%T) of the CAS films was determined using a UV-VIS spectrophotometer (GENESYS Spectrophotometer, Thermo Fisher Scientific, Waltham, MA) at 560 nm. Rectangular films (1 cm × 4.5 cm) were prepared and attached to the wall of the test cell

using tape. The thickness of each CAS film with varying the  $DS_{\text{sulfate}}/DS_{\text{acetyl}}$  ratios was listed in Table 3.2 and the %T of the empty test cell (air) was used as a reference.

## **2.9. Integrity, Flexibility, and Water Solubility of CAS Films**

The integrity and folding endurance of the CAS films were evaluated according to established protocols [23, 25]. Specifically, the films were inspected for any visible defects, such as cracks or flaws, upon detachment from the evaporating dishes. A film was deemed to possess good integrity if it exhibited no such imperfections.

The flexibility of the CAS films was determined by repetitively folding the films at the same point until they fractured, after conditioning the films at 23 °C and 50% RH for 24 hours. The number of folding cycles that each sample endured before breaking was used as a measure of film flexibility, as described in previous studies [25]. The flexibility of the films was categorized as poor (folding cycles < 20), middle ( $20 \leq$  folding cycles < 50), good ( $50 \leq$  folding cycles < 100), and excellent (folding cycles  $\geq$  100).

To conduct the water solubility test, 600 mg of each CAS film was placed in 100 ml of deionized water at room temperature and left undisturbed. The films were considered completely soluble in deionized water when no visible residues remained.

## **2.10. Mechanical Properties**

The mechanical properties of CAS hydrogel films, such as tensile strength (TS), elongation at break (EAB, %), and elastic modulus (E), were measured using the ASTM standard method [30]. The tests were performed with a Universal Testing Machine (Instron 4400 series,

Norwood, MA). The CAS films were equilibrated at a constant temperature and humidity room (23 °C and 50% RH) for 24 hours before the measurements. Rectangular-shaped films (10 cm × 2.5 cm) were used for the tests, and both sides of the films were fixed by the grips of the instrument with a 50 mm gap between them. The films were pulled apart at a crosshead speed of 5 mm/min and a preload of 2 N to measure their mechanical properties.

## **2.11. Barrier Properties**

### **2.11.1. Contact Angle**

The CAS films were subjected to contact angle measurements using a Phoenix 300 touch automatic contact angle analyzer (Surface Electro Optics, South Korea). A rectangular-shaped sample (1 cm × 9 cm) was affixed to a sample holder using tape, after which a drop of Milli-Q water was dispensed onto the surface of each film using a 3 ml syringe. The contact angle of each film was then determined by analyzing images of a sessile drop that was captured immediately after water dispersion and after 60 seconds. The contact angle was calculated using FTA 32 software.

### **2.11.2. Water Vapor Permeability**

The water vapor permeability (WVP) of CAS films was measured in a room with a constant temperature and humidity of 23 °C and 50% RH, using the water method described in E96/E96M [31]. WVP testing cups were filled with water up to 20 mm from the CAS hydrogel films, and the exposed area of the films had a diameter of 63 mm. Rubber bands were used to tightly seal the films and prevent water evaporation from the edges. The weight of the testing

cups was periodically measured for 48 hours to calculate the water vapor transmission rate (WVTR) and WVP, according to equations 3 and 4.

$$\text{WVTR (g m}^{-2}\text{s}^{-1}) = \Delta w / (\Delta t * A)$$

Equation 3

Where,  $\Delta w / \Delta t$  = transfer rate ( $\text{g/s}^{-1}$ ), which represents the amount of moisture loss per sec and A = area of films exposed to moisture transfer ( $\text{m}^2$ ).

$$\text{WVP (g m}^{-1}\text{s}^{-1}\text{Pa}^{-1}) = (\text{WVTR} * L) / \Delta p$$

Equation 4

Where, L = the thickness of the films (m) and  $\Delta p$  is the difference in partial water vapor pressure across the two side of the films (1412 Pa, 23 °C).

### **2.11.3. Oil Barrier Properties**

The oil barrier properties of CAS hydrogel films were examined using silicone oil and canola oil, following a previously described method [23]. A glass tube (inner and outer diameter: 25 mm and 27 mm, respectively) was filled with 3 g of each oil, and CAS films were placed at the open end of the tube and sealed. The tubes were then inverted and placed on filter paper to ensure that the open end of the tubes was in contact with the filter paper. The barrier properties of the CAS hydrogel films were evaluated by examining the filter paper for three consecutive days. The test samples were maintained at 23 °C and 50% RH with 10 replicates for each CAS film.

## **2.12. Banana Coating Test**

The whole surface of bananas was coated with CAS solutions with varying the  $DS_{\text{sulfate}}/DS_{\text{acetyl}}$  ratios (0.4/1.8, 0.7/1.8, and 1.0/1.8) using a silicone brush at room temperature. The bananas were then dried in a fume hood at room temperature to form CAS films on their surfaces. All bananas, including a control, were kept in the fume hood at room temperature, and changes in their appearance were monitored over time. Photos of the bananas were taken at the beginning and after 5, 10, 15, and 20 days.

## **2.13. Statistical Analysis**

The experimental data were presented as the mean  $\pm$  standard deviations obtained from at least triplicated experiments. The data was processed using a one-way analysis of variance (ANOVA) followed by Tukey tests to figure out differences among mean values. The mean values were considered statistically significant if p-values  $< 0.05$

# **3. Results and Discussions**

## **3.1. Synthesis of CAS**

In previous studies, it was observed that unique behavior in deionized water was exhibited only by CAS synthesized from CA with a  $DS_{\text{acetyl}}$  of 1.8. Therefore, for the production of CAS films in this study, CA with a  $DS_{\text{acetyl}}$  of 1.8 was selected for the preparation of CAS. The synthesis of CAS was examined in both qualitative and quantitative ways. The free hydroxyl groups in CA were primarily reacted with the sulfating agent during the synthesis, while the acetyl groups remained protected [13].

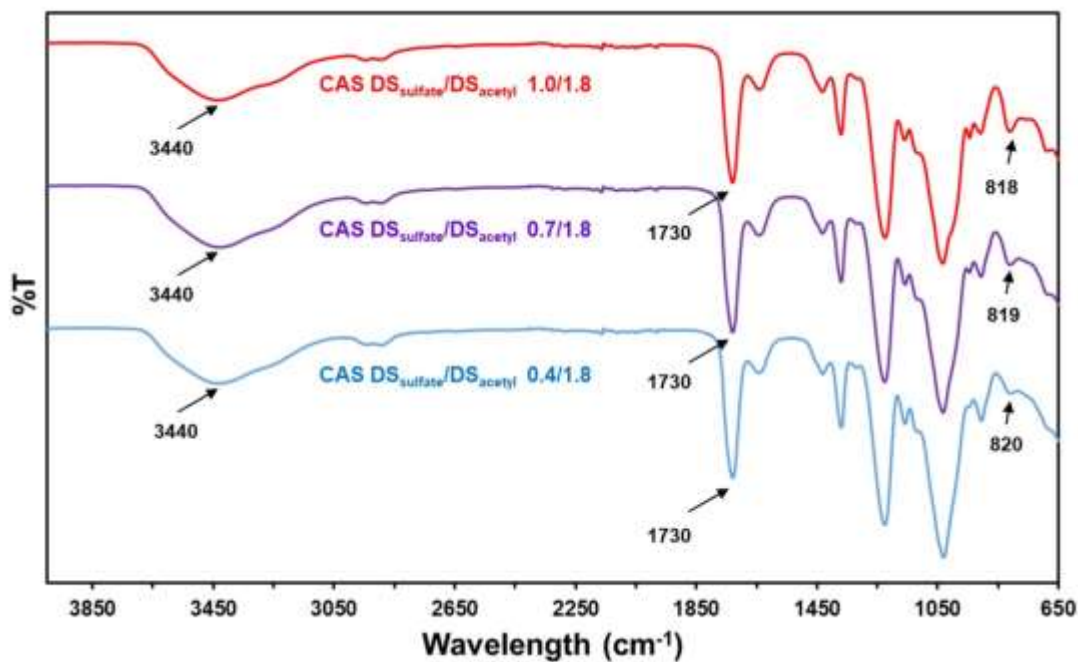


**Figure 3.1.** FT-IR spectra of the synthesized CAS

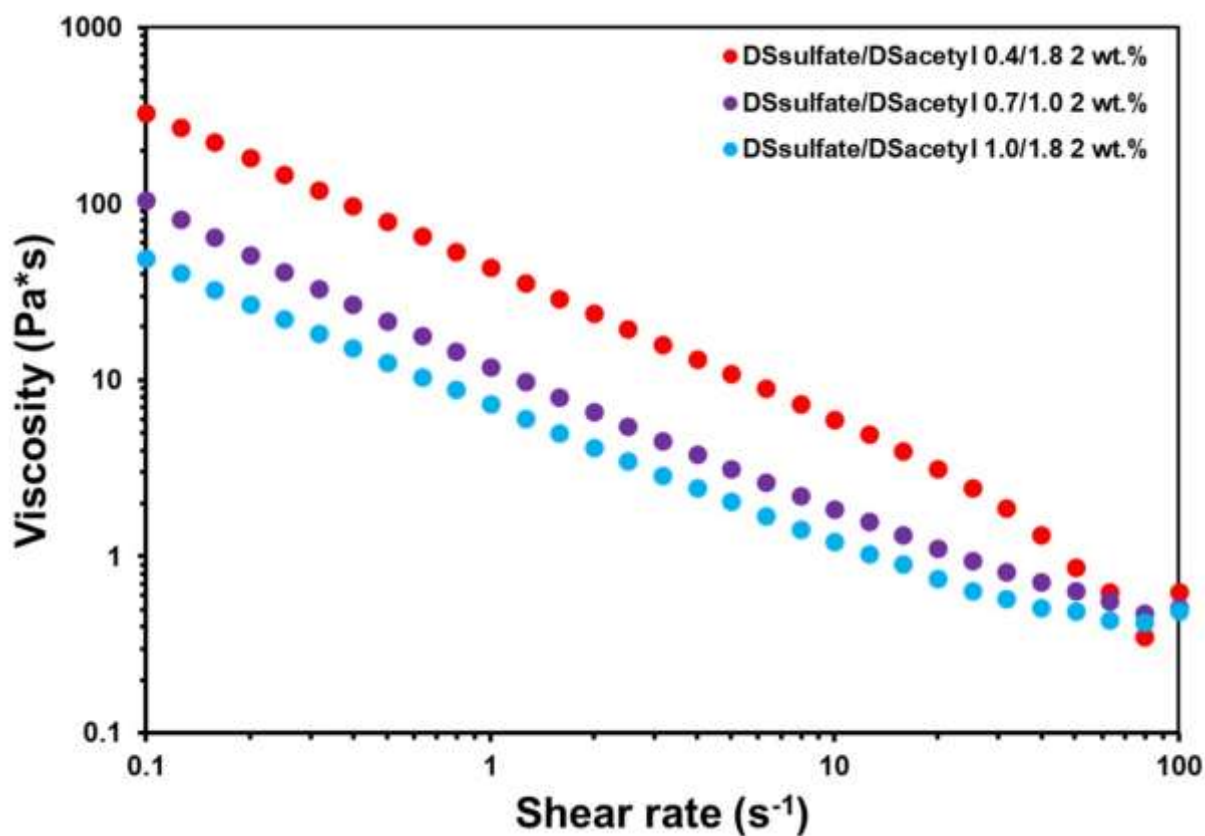
At  $1730\text{ cm}^{-1}$ , a characteristic C=O peak from the acetyl groups was detected in the IR spectra of all CAS samples [32]. The results in Table 3.1 demonstrate that the acetyl groups in the initial CA were not affected by the synthesis process, which is consistent with previous studies [13]. Based on the peaks observed around  $820\text{ cm}^{-1}$  which corresponded to 6-O-sulfate in CAS, the presence of substituted sulfate groups can be examined [33, 34]. Additionally, Table 3.1 presents the quantitatively measured  $DS_{\text{sulfate}}$  of each CAS, demonstrating how the  $DS_{\text{sulfate}}$  changed with the amount of the sulfating agent used. The broad bands observed at approximately  $3400\text{ cm}^{-1}$  indicate the presence of unreacted hydroxyl groups in the CAS synthesized [32]. The spectral data confirms the presence of both hydrophobic and hydrophilic functional groups. The  $M_w$  of the resulting CAS is determined and listed in Table 3.1. While the  $M_w$  of the CAS samples decreased compared to the reference CA, their  $M_w$  were similar to each other, despite being at a lower level overall.

### 3.2. Preparation of CAS Film Solutions and Film Casting



**Figure 3.2.** The procedure for preparing CAS film solutions

As previously reported, CAS is capable of forming single-component, physically crosslinked hydrogels within a specific range of  $DS_{\text{sulfate}}/DS_{\text{acetyl}}$  balance and solid content. To prepare film solutions based on CAS, hydrogels were first prepared, and their solid content was reduced below the critical gelation solid content, allowing them to transform into film-forming solutions. The solid content of all CAS film solutions was fixed at 2 wt. %, which was below the critical gelation solid content for each CAS.



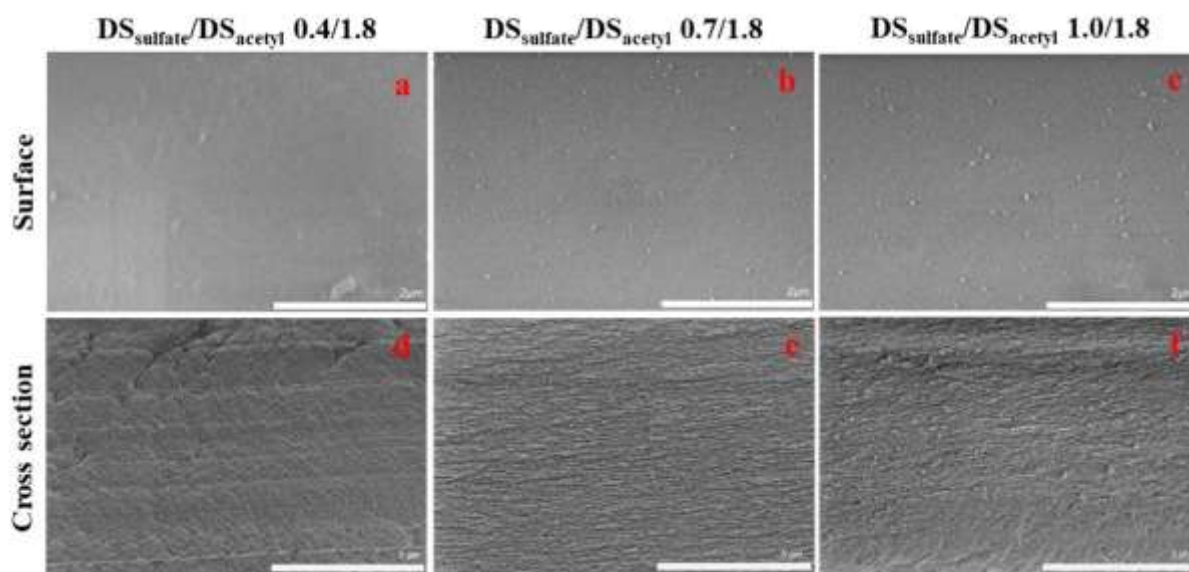
**Figure 3.3.** Viscosity of the CAS film solutions

Figure 3.3 illustrates the viscosity of CAS solutions with varying the  $DS_{\text{sulfate}}/DS_{\text{acetyl}}$  balances. Since the  $M_w$  of the resulting CAS remained constant across the all levels of  $DS_{\text{sulfate}}$ , the viscosity of the CAS solutions was primarily influenced by the  $DS_{\text{sulfate}}/DS_{\text{acetyl}}$  balance [35, 36]. Regardless of  $DS_{\text{sulfate}}/DS_{\text{acetyl}}$  balance, all solutions displayed shear-thinning behavior. The relative influence of acetyl groups was found to be a key determinant of the viscosity of the film solutions. With increasing  $DS_{\text{sulfate}}$ , which indicates a decreased influence of acetyl groups, the viscosity of the film solutions decreased accordingly. The film-forming ability of all CAS solutions was confirmed by the production of transparent, uncolored, self-supporting, and flexible films, which were easily detached from the Teflon evaporating dish, as depicted in Figures 3.4a and 3.4b.



**Figure 3.4.** (a) A CAS film prepared from a CAS film solution with the  $DS_{\text{sulfate}}/DS_{\text{acetyl}}$  balance of 0.7/1.8 and (b) Three strips of CAS films made from different film solutions with varying the  $DS_{\text{sulfate}}/DS_{\text{acetyl}}$  balances (0.4/1.8, 0.7/1.8, and 1.0/1.8)

### 3.3. Microstructure of CAS Films



**Figure 3.5.** SEM surface images of (a)  $DS_{\text{sulfate}}/DS_{\text{acetyl}} = 0.4/1.8$ , (b)  $DS_{\text{sulfate}}/DS_{\text{acetyl}} = 0.7/1.8$ , and (c)  $DS_{\text{sulfate}}/DS_{\text{acetyl}} = 1.0/1.8$  CAS films; SEM cross section images of (d)  $DS_{\text{sulfate}}/DS_{\text{acetyl}} = 0.4/1.8$ , (e)  $DS_{\text{sulfate}}/DS_{\text{acetyl}} = 0.7/1.8$ , and (f)  $DS_{\text{sulfate}}/DS_{\text{acetyl}} = 1.0/1.8$  CAS films

The microstructures of CAS films with varying  $DS_{\text{sulfate}}/DS_{\text{acetyl}}$  balances were examined qualitatively using SEM. In film formation, the presence of supplementary components that are not well-miscible can lead to uneven and even phase-separated films [37-39]. However, the use of a single-component film-forming solution like CAS enables the production of highly uniform and defect-free microstructures [40, 41]. Regardless of the  $DS_{\text{sulfate}}/DS_{\text{acetyl}}$  balance, all CAS solutions produced films with continuous and dense structures, free from visible defects on both the surface and cross-section. This is attributed to the absence of supplementary components, which ensures the homogeneity of the solution and minimizes the

risk of phase separation during film formation, leading to the formation of a uniform and homogeneous film.

### 3.4. Properties of CAS Films

**Table 3.2.** Properties of CAS Films

Sample	Thickness ( $\mu\text{m}$ )	Integrity	Flexibility	Transparency (%)
DS <sub>sulfate</sub> /DS <sub>acetyl</sub> 0.4/1.8	31.0 $\pm$ 1.8	Complete	Excellent	92.6 $\pm$ 0.2
DS <sub>sulfate</sub> /DS <sub>acetyl</sub> 0.7/1.8	29.7 $\pm$ 1.9	Complete	Excellent	92.5 $\pm$ 0.3
DS <sub>sulfate</sub> /DS <sub>acetyl</sub> 1.0/1.8	31.9 $\pm$ 0.4	Complete	Excellent	92.4 $\pm$ 0.2

Tables 3.2 and 3.3 present several properties of CAS films, including thickness, integrity, folding flexibility, water solubility, barrier for oils, and transparency. The visually homogeneous and highly transparent CAS films were easily peeled from Teflon evaporating dishes without any visible cracks, demonstrating the complete integrity of the CAS films. The folding flexibility tests confirmed the excellent flexibility of the CAS films, with no visible cracks or flaws observed. Compared to CS-based films, which are readily soluble in water, only CAS films with a DS<sub>sulfate</sub>/DS<sub>acetyl</sub> balance of 1.0/1.8 were found to be water-soluble [23].

Nevertheless, it is important to note that these films took significantly longer to dissolve completely in water at room temperature than CS films, possibly due to the presence of hydrophobic acetyl groups in the CAS structure. Previous studies have shown that the critical gelation solid content (CGS) of CAS is dependent on the balance between DS<sub>sulfate</sub> and DS<sub>acetyl</sub>, with a higher proportion of sulfate groups leading to an increase in CGS. For CAS films with a DS<sub>sulfate</sub>/DS<sub>acetyl</sub> balance of 1.0/1.8, the overall solid content began to decrease upon immersion in

water, and the CGS was achieved within 30 min. Consequently, the film became soluble in water. In contrast, CAS films with  $DS_{\text{sulfate}}/DS_{\text{acetyl}}$  balances of 0.4/1.8 and 0.7/1.8 take longer to reach their CGS, resulting in their transformation into hydrogels rather than dissolving in water within the experimental time frame.

**Table 3.3.** Water dissolution time and oil permeability of CAS films

Sample	Water Dissolution Time (min)	Oil Permeability (%)	
		Canola	Silicone
$DS_{\text{sulfate}}/DS_{\text{acetyl}}$ 0.4/1.8	N/A	0	0
$DS_{\text{sulfate}}/DS_{\text{acetyl}}$ 0.7/1.8	N/A	0	0
$DS_{\text{sulfate}}/DS_{\text{acetyl}}$ 1.0/1.8	27 min	0	0
* N/A: Films did not dissolve in water but instead formed hydrogels			

Great importance is placed on the barrier properties of food packaging films against oils to maintain food quality and safety. In addition to preventing the penetration of oily contaminants, such films should also prevent hydrophobic components of food from leaking out [42, 43]. It was demonstrated that CAS films exhibit excellent barrier properties against oils, as evidenced by the absence of any permeation of silicone or canola oils through CAS films, regardless of the  $DS_{\text{sulfate}}$ . Despite having a high affinity for oils, CAS films exhibited a remarkable resistance to oil permeation. [44, 45].



**Figure 3.6.** Photographs of (a)  $DS_{\text{sulfate}}/DS_{\text{acetyl}} \ 0.4/1.8$ , (b)  $DS_{\text{sulfate}}/DS_{\text{acetyl}} \ 0.7/1.8$ , (c)  $DS_{\text{sulfate}}/DS_{\text{acetyl}} \ 1.0/1.8$  film, (d)  $DS_{\text{sulfate}}/DS_{\text{acetyl}} \ 0.4/1.8$  film, and (e)  $DS_{\text{sulfate}}/DS_{\text{acetyl}} \ 0.7/1.8$  film upon immersion in deionized water for 1 hour

### 3.5. Wettability and Water Vapor Permeability of CAS Films

Wettability is a crucial characteristic of food packaging films as it plays a significant role in determining their potential applications [42]. To evaluate the wettability of CAS films, the surface contact angle was measured. If a film has a contact angle greater than  $90^\circ$ , it is deemed hydrophobic, and vice versa [46]. Despite the hydrophobic acetyl groups present in the CAS films, they exhibited a fundamentally hydrophilic nature, owing to the presence of added sulfate groups

and residual hydroxyl groups. The study revealed that the wettability of CAS films can be regulated by adjusting the balance between sulfate and acetyl groups.

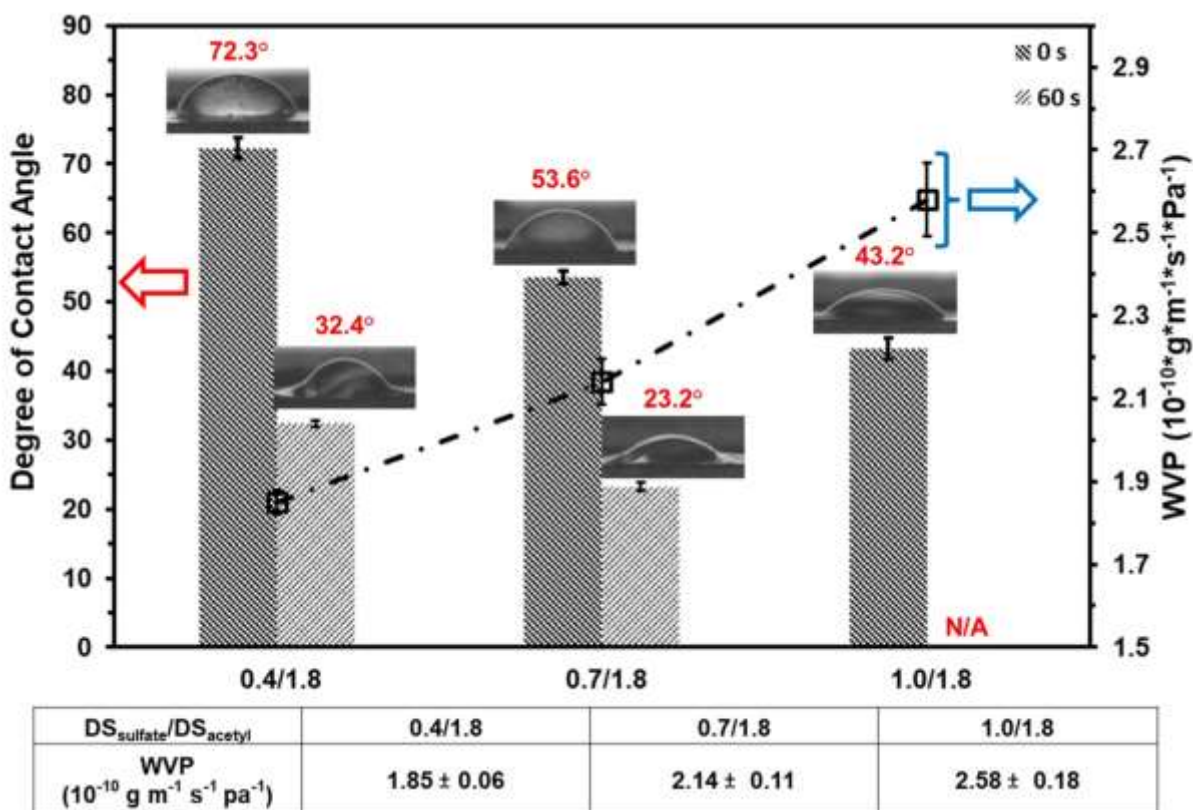


**Figure 3.7.** The contact angle and WVP of CAS films with varying the DS<sub>sulfate</sub>/DS<sub>acetyl</sub> 0.4/1.8, 0.7/1.8, and 1.0/1.8 balances.

\* Photographs were taken 0 s and 60 s after dispensing a single drop of water.

\* N/A: Water droplet was completely absorbed by the film

The study revealed that the wettability of CAS films can be regulated by adjusting the balance between sulfate and acetyl groups. As anticipated, the contact angle of CAS films decreased as the influences of sulfate groups increased, which was in line with dissolution times recorded in Table 3.3. Moisture is a crucial factor affecting the deterioration of food in

packaging, making WVP a significant consideration in food packaging films [43]. Figure 3.7 illustrates the impact of the influences of sulfate groups in CAS films on WVP. The influence of sulfate groups on the WVP of CAS films was as predicted, with an increase in  $DS_{\text{sulfate}}$  causing a significant increase in WVP. The number of sulfate groups in CAS films affects the WVP due to changes in hydrophilicity [47]. This alteration can modify water-film interactions, leading to an increased water diffusion rate through the films [48].

### 3.6. Mechanical Properties of CAS Films

**Table 3.4.** Mechanical properties of CAS films

	E (Mpa)	EAB (%)	TS (Mpa)
$DS_{\text{sulfate}}/DS_{\text{acetyl}}$ 0.4/1.8	$2131.6 \pm 156.7^a$	$5.0 \pm 1.4^a$	$36.7 \pm 4.0^a$
$DS_{\text{sulfate}}/DS_{\text{acetyl}}$ 0.7/1.8	$1760.7 \pm 122.6^b$	$4.0 \pm 0.9^a$	$29.6 \pm 2.7^b$
$DS_{\text{sulfate}}/DS_{\text{acetyl}}$ 1.0/1.8	$1689.1 \pm 171.6^b$	$3.9 \pm 1.5^a$	$27.9 \pm 3.6^b$
Mean values with different letter within a column indicate that there are significant differences ( $p < 0.05$ )			

Table 3.4 presents the mechanical properties of CAS films with varying  $DS_{\text{sulfate}}/DS_{\text{acetyl}}$  balances, including elastic modulus (E), elongation at break (EAB), and tensile strength (TS). The effect of the equilibrium moisture content on the mechanical properties of polymer films has been widely recognized in previous studies [49, 50]. Therefore, the equilibrium moisture contents of the CAS films were determined and listed in Table S1. It was noted that the highest equilibrium moisture content was exhibited by CAS films with a  $DS_{\text{sulfate}}/DS_{\text{acetyl}}$  balance of 1.0/1.8. However, no significant differences in the equilibrium moisture content were observed among the CAS films based on the statistical analysis. As a result, it can be concluded that the equilibrium moisture content did not have a noticeable effect on the mechanical properties of the

CAS films. The E of the CAS films exhibited a decrease with increasing influence of sulfate groups. The highest E was observed for CAS films with a  $DS_{\text{sulfate}}/DS_{\text{acetyl}}$  balance of 0.4/1.8, reaching a maximum value of 2131.6 MPa. The incorporation of hydrophobic groups into hydrophilic cellulose derivatives can lead to changes in the rheological properties of their solutions through the formation of supramolecular structures facilitated by hydrophobic associations [51, 52]. In the case of CAS, the acetyl and sulfate groups may compete with each other, potentially leading to a trade-off in their contributions. Previous studies have shown that the storage modulus of CAS solutions or hydrogels decreases as the number of sulfate groups increases, while maintaining constant solid content. This increase in sulfate groups may cause changes in the molecular structure of CAS films, leading to a reduction in E. When examining the p value of the E for CAS films with  $DS_{\text{sulfate}}/DS_{\text{acetyl}}$  balances of 0.7/1.8 and 1.0/1.8, two films did not exhibit a significant difference in their E. This phenomenon may be attributed to the size of sulfate groups and the competition between electrostatic repulsion and the hydrogen bonding induced by sulfate groups [53, 54]. The introduction of sulfate groups into CAS films can possibly lead to a more loosely packed molecular structure due to the bulkier size of sulfate groups compared to hydroxyl groups [54, 55]. Furthermore, the negatively charged sulfate groups can induce electrostatic repulsion [53]. However, the formation of hydrogen bonding facilitated by the sulfate groups can offset this effect [56-58]. As the number of sulfate groups increases, more hydrogen bonding sites become available, possibly enhancing the formation of hydrogen bonds and strengthening the overall structure of the CAS films. Hence, CAS films with  $DS_{\text{sulfate}}/DS_{\text{acetyl}}$  balances of 0.7/1.8 and 1.0/1.8 did not exhibit a substantial difference in E, which may be due to the equilibrium between the size effect of sulfate groups, electrostatic repulsion, and hydrogen bonding. A similar trend was observed in the TS, with a decreasing trend established as the influences of sulfate groups

increased. The CAS films with a  $DS_{\text{sulfate}}/DS_{\text{acetyl}}$  balance of 0.4/1.8 exhibited the highest TS among all the samples, with a maximum value of 36.7 MPa. While the TS of CAS films with a  $DS_{\text{sulfate}}/DS_{\text{acetyl}}$  balance of 0.7/1.8 was higher than that of CAS films with a  $DS_{\text{sulfate}}/DS_{\text{acetyl}}$  balance of 1.0/1.8, the difference was not statistically significant based on their p values. This phenomenon can be attributed to the same reasons as those explained earlier for the E, as all the CAS films exhibited similar EAB values.

### **3.7. CAS Coatings on Bananas**

To test the effectiveness of the CAS films as an edible coating, bananas were selected due to their relatively short shelf life. Bananas are known to ripen rapidly and develop brown spots, which can affect consumer perception and purchasing decisions [59]. The CAS film forming solutions ( $DS_{\text{sulfate}}/DS_{\text{acetyl}}$  0.4/1.8, 0.7/1.8, and 1.0/1.8) were used to coat the surface of the bananas, while one banana was left uncoated as a reference. Photos were taken at the beginning, as well as after 5, 10, 15, and 20 days to observe the changes in the appearance of the bananas over time (as shown in Figure 3.8).



**Figure 3.8.** Comparative study of CAS coating using  $DS_{\text{sulfate}}/DS_{\text{acetyl}}$  0.4/1.8, 0.7/1.8, and 1.0/1.8 film forming solutions.

Throughout the observation period, changes in the appearance of both the coated and uncoated bananas were observed. After 5 days, new brown spots started to appear in the control banana and the one coated with CAS  $DS_{\text{sulfate}}/DS_{\text{acetyl}}$  1.0/1.8 solution, in addition to the existing brown spots. The control banana had brown spots all over, while the coated banana had new spots in different areas. After 10 days, the uncoated banana had dried out and wrinkled, while the coated bananas still had some green parts. The brown spots on the banana coated with CAS  $DS_{\text{sulfate}}/DS_{\text{acetyl}}$  1.0/1.8 solution had become larger, but the overall surface did not appear dried out. By day 15, only the banana coated with  $DS_{\text{sulfate}}/DS_{\text{acetyl}}$  0.4/1.8 solution retained any green areas, while the other coated bananas had become brownish and the banana coated with  $DS_{\text{sulfate}}/DS_{\text{acetyl}}$  1.0/1.8 solution had started to dry out and wrinkle. Finally, by day 20, the surface of the control banana became darker compared to the coated ones, and there were differences in color observed among the coated bananas.

The changes observed in the coated bananas were in line with the variations in the WVP of the CAS films. The CAS films with a  $DS_{\text{sulfate}}/DS_{\text{acetyl}}$  balance of 0.4/1.8 had the least WVP, suggesting that applying this coating to the banana's surface would reduce moisture loss, slow the ripening process, and increase the banana's shelf life. It is also worth noting that the green area on the banana coated with the  $DS_{\text{sulfate}}/DS_{\text{acetyl}}$  0.4/1.8 solution lasted the longest. Overall, the CAS coatings were found to be effective in extending the shelf life of bananas when compared to uncoated bananas, regardless of the  $DS_{\text{sulfate}}/DS_{\text{acetyl}}$  balances.

#### 4. Conclusion

The method for casting single-component CAS films was described. To prepare CAS solutions capable of forming films, CA with a  $DS_{\text{acetyl}}$  of 1.8 was used as the starting material, and the  $DS_{\text{sulfate}}$  was varied during the synthesis process. Three CAS solutions with different  $DS_{\text{sulfate}}/DS_{\text{acetyl}}$  balances (0.4/1.8, 0.7/1.8, and 1.0/1.8) were prepared, and the resulting CAS films exhibited homogeneity, flexibility, and transparency, and could be easily fabricated through casting. To investigate the potential of CAS films as an edible coating material, various properties, including microstructure, barrier properties, mechanical properties, and other basic characteristics, were evaluated. It was demonstrated that the physicochemical properties of the CAS films can be engineered by adjusting the  $DS_{\text{sulfate}}/DS_{\text{acetyl}}$  balance. The increase in  $DS_{\text{sulfate}}$  resulted in an increase in WVP. The mechanical properties of CAS films, such as E and TS, exhibited a decreasing trend with an increase in  $DS_{\text{sulfate}}$ . Specifically, the maximum values of E and TS were observed in CAS films with a  $DS_{\text{sulfate}}/DS_{\text{acetyl}}$  balance of 0.4/1.8, while there were no significant differences in E and TS for CAS films with  $DS_{\text{sulfate}}/DS_{\text{acetyl}}$  balances of 0.7/1.8 and 1.0/1.8. These observations could be attributed to the intermolecular interactions induced by sulfate and acetyl groups that may be competing with each other. Bananas were coated with CAS solutions to demonstrate their potential for edible coating. The application of CAS coating on bananas resulted in a slower ripening process compared to uncoated bananas. Additionally, The rate of ripening could be regulated by adjusting the  $DS_{\text{sulfate}}/DS_{\text{acetyl}}$  balance of the CAS solutions. Given that CAS films have demonstrated their effectiveness as an edible coating, and their properties can be adjusted by varying the  $DS_{\text{sulfate}}/DS_{\text{acetyl}}$  balance, they hold great potential for various food packaging applications. This makes them a promising material for a wide range

of food packaging applications, and could expand the options available for food packaging materials

## REFERENCES

- [1] N. Asim, M. Badiei, M. Mohammad, Recent advances in cellulose-based hydrophobic food packaging, *Emergent Materials* (2021) 1-16.
- [2] K. Huang, Y. Wang, Recent applications of regenerated cellulose films and hydrogels in food packaging, *Current Opinion in Food Science* 43 (2022) 7-17.
- [3] B. Malhotra, A. Keshwani, H. Kharkwal, Natural polymer based cling films for food packaging, *Int. J. Pharm. Pharm. Sci* 7(4) (2015) 10-18.
- [4] Y. Liu, S. Ahmed, D.E. Sameen, Y. Wang, R. Lu, J. Dai, S. Li, W. Qin, A review of cellulose and its derivatives in biopolymer-based for food packaging application, *Trends in Food Science & Technology* 112 (2021) 532-546.
- [5] D. Das, P.S. Panesar, C.S. Saini, J.F. Kennedy, Improvement in properties of edible film through non-thermal treatments and nanocomposite materials: A review, *Food Packaging and Shelf Life* 32 (2022) 100843.
- [6] J.H. Han, Edible films and coatings: a review, *Innovations in food packaging* (2014) 213-255.
- [7] A.M. Ribeiro, B.N. Estevinho, F. Rocha, Preparation and incorporation of functional ingredients in edible films and coatings, *Food and Bioprocess Technology* 14 (2021) 209-231.
- [8] S. Galus, Functional properties of soy protein isolate edible films as affected by rapeseed oil concentration, *Food Hydrocolloids* 85 (2018) 233-241.
- [9] A. Hambleton, A. Voilley, F. Debeaufort, Transport parameters for aroma compounds through i-carrageenan and sodium alginate-based edible films, *Food Hydrocolloids* 25(5) (2011) 1128-1133.

- [10] D. Kowalczyk, B. Baraniak, Effect of candelilla wax on functional properties of biopolymer emulsion films—a comparative study, *Food Hydrocolloids* 41 (2014) 195-209.
- [11] V. Ganapathy, G. Muthukumaran, P.E. Sudhagar, A. Rashedi, M.N.F. Norraahim, R.A. Ilyas, K.L. Goh, M. Jawaid, J. Naveen, Mechanical properties of cellulose-based multiscale composites: A review, *Polymer Composites* 44(2) (2023) 734-756.
- [12] H. Seddiqi, E. Oliaei, H. Honarkar, J. Jin, L.C. Geonzon, R.G. Bacabac, J. Klein-Nulend, Cellulose and its derivatives: Towards biomedical applications, *Cellulose* 28(4) (2021) 1893-1931.
- [13] T. Heinze, O.A. El Seoud, A. Koschella, *Cellulose derivatives: synthesis, structure, and properties*, Springer 2018.
- [14] S. Park, J.O. Baker, M.E. Himmel, P.A. Parilla, D.K. Johnson, Cellulose crystallinity index: measurement techniques and their impact on interpreting cellulase performance, *Biotechnology for biofuels* 3 (2010) 1-10.
- [15] D. Klemm, B. Philipp, T. Heinze, U. Hewinze, W. Wagenknecht, *Comprehensive cellulose chemistry. Volume 2: Functionalization of cellulose*, Wiley-VCH Verlag GmbH 1998.
- [16] H.C. Arca, L.I. Mosquera-Giraldo, V. Bi, D. Xu, L.S. Taylor, K.J. Edgar, Pharmaceutical applications of cellulose ethers and cellulose ether esters, *Biomacromolecules* 19(7) (2018) 2351-2376.
- [17] J. Zhang, Q. Yingping, S. Yongfeng, L. Hua, Research Progress on Chemical Modification and Application of Cellulose: A Review, *Materials Science* 28(1) (2022) 60-67.
- [18] M. Yildirim-Yalcin, F. Tornuk, O.S. Toker, Recent advances in the improvement of carboxymethyl cellulose-based edible films, *Trends in Food Science & Technology* (2022).

- [19] A. Boчек, N. Zabivalova, V. Yudin, I. Gofman, V. Lavrent'ev, B. Volчек, E. Vlasova, I. Abalov, N. Brusilovskaya, I. Osovskaya, Properties of carboxymethyl cellulose aqueous solutions with nanoparticle additives and the related composite films, *Polymer Science Series A* 53(12) (2011) 1167-1174.
- [20] N. Sanla-Ead, A. Jangchud, V. Chonhenchob, P. Suppakul, Antimicrobial Activity of cinnamaldehyde and eugenol and their activity after incorporation into cellulose-based packaging films, *Packaging Technology and Science* 25(1) (2012) 7-17.
- [21] P. Thivya, S. Akalya, V. Sinija, A comprehensive review on cellulose-based hydrogel and its potential application in the food industry, *Applied Food Research* (2022) 100161.
- [22] Q.-X. Wu, Y.-X. Guan, S.-J. Yao, Sodium cellulose sulfate: A promising biomaterial used for microcarriers' designing, *Frontiers of Chemical Science and Engineering* 13 (2019) 46-58.
- [23] G. Chen, B. Zhang, J. Zhao, H. Chen, Development and characterization of food packaging film from cellulose sulfate, *Food Hydrocolloids* 35 (2014) 476-483.
- [24] G. Chen, B. Zhang, J. Zhao, Dispersion process and effect of oleic acid on properties of cellulose sulfate-oleic acid composite film, *Materials* 8(5) (2015) 2346-2360.
- [25] G. Chen, B. Liu, Cellulose sulfate based film with slow-release antimicrobial properties prepared by incorporation of mustard essential oil and  $\beta$ -cyclodextrin, *Food Hydrocolloids* 55 (2016) 100-107.
- [26] H.K. Agarwal, A. Kumar, G.F. Doncel, K. Parang, Synthesis, antiviral and contraceptive activities of nucleoside–sodium cellulose sulfate acetate and succinate conjugates, *Bioorganic & Medicinal Chemistry Letters* 20(23) (2010) 6993-6997.

- [27] T. Savitskaya, E. Shakhno, D. Grinshpan, O. Ivashkevich, Soluble Polymer Complexes of Ceftriaxone and Cefotaxime with Cellulose Sulfate Acetate Salt Forms and Their Adsorption on Carbon Sorbents, *Polymer Science, Series A* 61 (2019) 274-286.
- [28] D. Grinshpan, T. Savitskaya, N. Tsygankova, S. Makarevich, S. Tretsiakova, T. Nevar, Cellulose acetate sulfate as a lyotropic liquid crystalline polyelectrolyte: synthesis, properties, and application, *International Journal of Polymer Science* 2010 (2010).
- [29] T. Hashizume, Y. Okamoto, K. Nagai, S. Shimamoto, Mechanism of sodium-hypochlorite-induced degradation of cellulose acetate and the enhancement of its degradation resistance by chemical modification, *Textile Research Journal* 92(13-14) (2022) 2487-2500.
- [30] ASTM, ASTM D882-12, Standard test method for tensile properties of thin plastic sheeting, ASTM International 2012.
- [31] ASTM, E96/E96M-16. Standard test methods for water vapor transmission of materials, *Annual Book of ASTM Standards*; American Society for Testing and Materials: West Conshohocken, PA, USA (2016) 719-725.
- [32] J. Brandrup, E.H. Immergut, E.A. Grulke, A. Abe, D.R. Bloch, *Polymer handbook*, Wiley New York 1999.
- [33] A. De Nino, M.A. Tallarida, V. Algieri, F. Olivito, P. Costanzo, G. De Filpo, L. Maiuolo, Sulfonated cellulose-based magnetic composite as useful media for water remediation from amine pollutants, *Applied Sciences* 10(22) (2020) 8155.
- [34] D. Grant, W.F. Long, C.F. Moffat, F.B. Williamson, INFRARED-SPECTROSCOPY OF HEPARINS SUGGESTS THAT THE REGION 750-950 CM-1 IS SENSITIVE TO CHANGES IN IDURONATE RESIDUE RING CONFORMATION, *Biochem. J.* 275 (1991) 193-197.

- [35] P. Snetkov, K. Zakharova, S. Morozkina, R. Olekhnovich, M. Uspenskaya, Hyaluronic acid: The influence of molecular weight on structural, physical, physico-chemical, and degradable properties of biopolymer, *Polymers* 12(8) (2020) 1800.
- [36] F.K. Mwiiri, R. Daniels, Influence of PVA molecular weight and concentration on electrospinnability of birch bark extract-loaded nanofibrous scaffolds intended for enhanced wound healing, *Molecules* 25(20) (2020) 4799.
- [37] R.K. Arya, Phase separation in multicomponent polymer-solvent-nonsolvent coatings, *South African Journal of Chemical Engineering* 18(1) (2013) 30-40.
- [38] I.C. Hoeger, I. Filpponen, R. Martin-Sampedro, L.-S. Johansson, M. Osterberg, J. Laine, S. Kelley, O.J. Rojas, Bicomponent lignocellulose thin films to study the role of surface lignin in cellulolytic reactions, *Biomacromolecules* 13(10) (2012) 3228-3240.
- [39] T. Kietzke, D. Neher, K. Landfester, R. Montenegro, R. Güntner, U. Scherf, Novel approaches to polymer blends based on polymer nanoparticles, *Nature materials* 2(6) (2003) 408-412.
- [40] D.P. The, F. Debeaufort, A. Voilley, D. Luu, Biopolymer interactions affect the functional properties of edible films based on agar, cassava starch and arabinoxylan blends, *Journal of food Engineering* 90(4) (2009) 548-558.
- [41] S. Galus, A. Lenart, Development and characterization of composite edible films based on sodium alginate and pectin, *Journal of food Engineering* 115(4) (2013) 459-465.
- [42] M. Jawaid, S.K. Swain, *Bionanocomposites for packaging applications*, Springer 2018.
- [43] S.A. Mohamed, M. El-Sakhawy, M.A.-M. El-Sakhawy, Polysaccharides, protein and lipid-based natural edible films in food packaging: A review, *Carbohydrate Polymers* 238 (2020) 116178.

- [44] W. Chen, Y. Su, L. Zheng, L. Wang, Z. Jiang, The improved oil/water separation performance of cellulose acetate-graft-polyacrylonitrile membranes, *Journal of Membrane Science* 337(1-2) (2009) 98-105.
- [45] X. Zhang, B. Wang, B. Wang, Y. Feng, W. Han, C. Liu, C. Shen, Superhydrophobic cellulose acetate/multiwalled carbon nanotube monolith with fiber cluster network for selective oil/water separation, *Carbohydrate Polymers* 259 (2021) 117750.
- [46] K.-Y. Law, Definitions for hydrophilicity, hydrophobicity, and superhydrophobicity: getting the basics right, ACS Publications, 2014, pp. 686-688.
- [47] S.J. Metz, W. Van de Ven, J. Potreck, M. Mulder, M. Wessling, Transport of water vapor and inert gas mixtures through highly selective and highly permeable polymer membranes, *Journal of Membrane Science* 251(1-2) (2005) 29-41.
- [48] T. Bui, Y. Wong, K. Thu, S. Oh, M. Kum Ja, K.C. Ng, I. Raisul, K. Chua, Effect of hygroscopic materials on water vapor permeation and dehumidification performance of poly (vinyl alcohol) membranes, *Journal of Applied Polymer Science* 134(17) (2017).
- [49] R.Y. Aguirre-Loredo, A.I. Rodríguez-Hernández, E. Morales-Sánchez, C.A. Gómez-Aldapa, G. Velazquez, Effect of equilibrium moisture content on barrier, mechanical and thermal properties of chitosan films, *Food Chemistry* 196 (2016) 560-566.
- [50] S. Zhang, N. Kim, W. Yokoyama, Y. Kim, Effects of moisture content on mechanical properties, transparency, and thermal stability of yuba film, *Food Chemistry* 243 (2018) 202-207.
- [51] G. Chauvelon, J.-L. Doublier, A. Buléon, J.-F. Thibault, L. Saulnier, Rheological properties of sulfoacetate derivatives of cellulose, *Carbohydrate research* 338(8) (2003) 751-759.

- [52] R. Tanaka, J. Meadows, G. Phillips, P. Williams, Viscometric and spectroscopic studies on the solution behaviour of hydrophobically modified cellulosic polymers, *Carbohydrate Polymers* 12(4) (1990) 443-459.
- [53] C. Faure, J.-F. Tranchant, E.J. Dufourc, Comparative effects of cholesterol and cholesterol sulfate on hydration and ordering of dimyristoylphosphatidylcholine membranes, *Biophysical journal* 70(3) (1996) 1380-1390.
- [54] T. Guan, Y. Miao, L. Xu, S. Yang, J. Wang, H. He, X. Tang, C. Cai, H. Xu, Injectable nimodipine-loaded nanoliposomes: preparation, lyophilization and characteristics, *International journal of pharmaceutics* 410(1-2) (2011) 180-187.
- [55] A.M. Forgiarini, C. Scorzza, J. Velásquez, F. Vejar, E. Zambrano, J.-L. Salager, Influence of the mixed propoxy/ethoxy spacer arrangement order and of the ionic head group nature on the adsorption and aggregation of extended surfactants, *Journal of surfactants and detergents* 13 (2010) 451-458.
- [56] H. Luecke, F.A. Quioco, High specificity of a phosphate transport protein determined by hydrogen bonds, *Nature* 347(6291) (1990) 402-406.
- [57] A. Sauza-de la Vega, H. Salazar-Lozas, W.E.V. Narváez, M. Hernández-Rodríguez, T. Rocha-Rinza, Water clusters as bifunctional catalysts in organic chemistry: the hydrolysis of oxirane and its methyl derivatives, *Organic & Biomolecular Chemistry* 19(31) (2021) 6776-6780.
- [58] L. Zhou, X. Liu, S. Jiang, X. Wang, Z. Meng, X. Li, G. Chen, S. Wang, Y. Jiang, In-situ microstructure regulation towards feasible production of self-reinforced lignocellulose nanopaper with multifunctionality, *Industrial Crops and Products* 193 (2023) 116229.

[59] F. Kittur, N. Saroja, R. Tharanathan, Polysaccharide-based composite coating formulations for shelf-life extension of fresh banana and mango, *European food research and technology* 213(4) (2001) 306-311.

## CHAPTER 4

### Understanding the Formation of Insoluble Gel Particles during Cellulose Acetylation

#### Abstract

The formation of insoluble colloidal materials, also known as insoluble gel particles (IGP), during cellulose acetylation poses a longstanding commercial challenge, as it can impede both the intermediate processing of cellulose acetate (CA) production and the final products. While IGP formation has been attributed to several mechanisms, including incomplete cellulose acetylation and the presence of hemicellulose acetates, its root cause remains controversial. This study investigates the role of xylan acetate (XA), which is insoluble in solvents commonly used for processing CA, in IGP formation. A series of experiments were conducted to examine the behavior of xylan and XA in CA processing solvents, complemented by molecular dynamics (MD) simulations. In addition, this study explores the impact of CA production processes on IGP formation, analyzing the composition of XA and CA in IGP produced under varying processes condition using high-performance liquid chromatography (HPLC), and Fourier-transform infrared (FT-IR) spectroscopy coupled with multivariate analysis.

#### 1. Introduction

Cellulose consists of D-anhydroglucopyranose units (AGU) linked by  $\beta$ -1, 4 glycosidic bonds. The three hydroxyls in native cellulose create strong hydrogen-bonded networks that support the formation of crystalline domains imparting native cellulose many of its unique properties [1]. These hydroxyl groups also play a critical and complicated role during cellulose

derivatization processes, where they can react to create an array of ester and ether derivatives with great commercial value [2]. Cellulose acetates (CA) are common cellulose ester derivatives that have been commercially produced for more than 80 years, and are used in a wide variety of fibers, films and molded products [3]. With increasing interest in sustainable bio-based plastics, CA has attracted renewed interest. At the same time, many of the traditional application of CA continues to demand higher quality and performance.

While there are a multitude of methods that can be used in the laboratory for preparation of cellulose derivatives, only a very few methods have been successfully applied for commercial production [4]. Currently, the acetic acid/acetic anhydride production method is the dominant method used for manufacturing CAs [3]. The common commercial CA products have a degree of substitution (DS) between 1.85 and 2.85. Within this final DS range, these CA have very different solubility, thermal stability, and mechanical properties. Nonetheless, they share the same ‘front end’ system that involves activation and complete acetylation (to essentially DS of 3.0) followed by a variety of hydrolysis processes that remove acetyl groups until the final target DS is reached (Figure 4.1a) [5, 6]. The activation process is designed to enhance the diffusion of chemical reagents to facilitate acetylation [7]. After activation, the cellulose gradually reacts with acetic anhydride, while acetic acid acts as a solvent and sulfuric acid as a catalyst [8]. This acetylation process is intended to produce homogeneous cellulose triacetate that can then be back-hydrolyzed to produce a uniformly substituted CA with varying DS. Then, CA is filtered and precipitated from the acetic acid/water hydrolysis mixture, washed to recover acetic acid, and dried for commercial use [8].

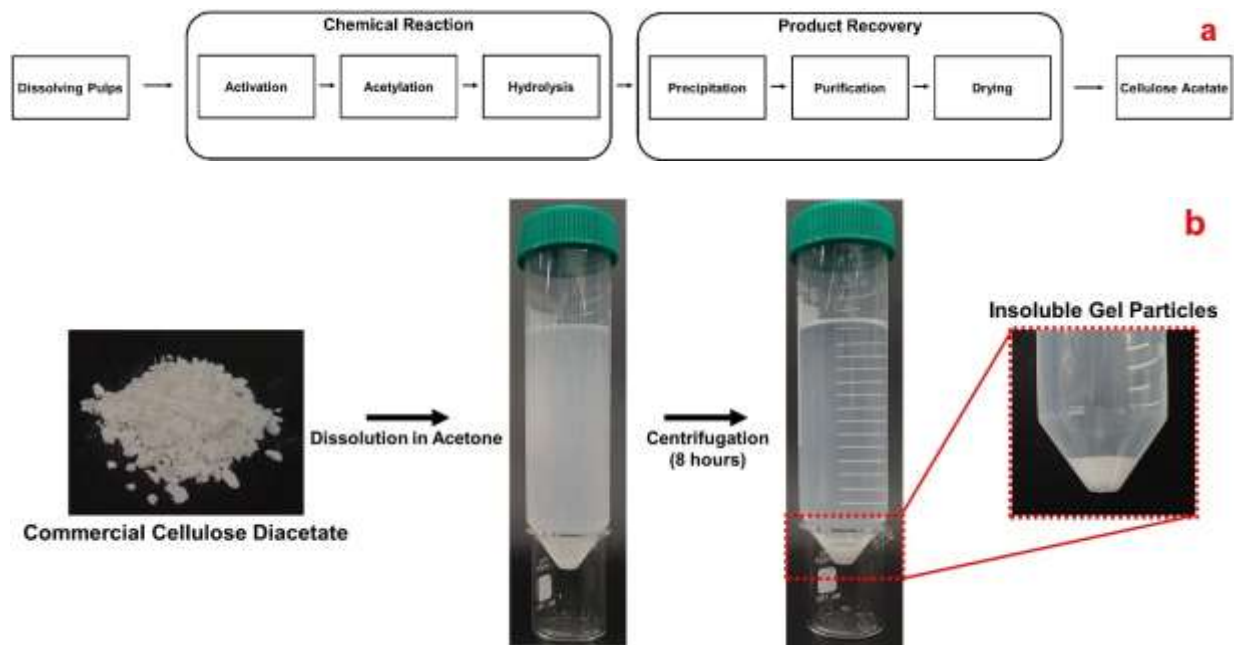


**Figure 4.1.** (a) Cellulose acetate production process and (b) centrifugation was used to isolate IGP contained in a commercial CA with a DS of 2.45 also commonly referred to as cellulose diacetate (CDA)

As shown in Figure 4.1b, a critical quality control challenge in the CA production process is the formation of inhomogeneous colloids, which are often referred to as insoluble gel particles (IGP) [6, 9]. These IGP have a negative impact on both the quality of the final products and their intermediate processability [6]. For instance, when CA films are used as optical polarizers, the entire film must have uniform optical properties. However, IGP in the CA causes haze which lowers the quality of the optical polarizer [10]. During the spinning of CDA fibers, the IGP do not dissolve in acetone and can clog the holes in the spinneret, resulting in an interruption of the continuous spinning process. Until now, the formation of IGP has been mainly attributed to incomplete activation and acetylation, or the presence of hemicelluloses in dissolving pulp feedstocks. As previously mentioned, the activation process enhances the accessibility of hydroxyl

groups in cellulose for chemical reagents, leading to a more homogeneous reaction. The impact of the activation process on cellulose acetylation is widely recognized, as producing CA with a DS beyond 2.0 is challenging without activation [6, 11]. Moreover, studies have shown that activated pulps can achieve a higher DS than non-activated ones under the same acetylation conditions [12]. These findings indicate that improper activation can result in underreacted CA production, leading to the generation of IGP. In addition, the poor solubility of hemicellulose acetates in solvents employed during the acetylation and post-CA processing (e.g., water, acetic acid, and acetone) suggests that hemicellulose acetates may be an additional source of IGP [6, 9, 13, 14]. It was found that a dissolving pulp containing more hemicelluloses produced CDA with a higher amount of IGP [15]. The carbohydrate composition analysis revealed that among hemicelluloses, XA was a dominant component consisting of IGP [16].

The formation of insoluble gel particles (IGPs) can result from incomplete acetylation and the presence of hemicelluloses, both of which are influenced by the quality of the original dissolving pulps and the precise management of chemical reaction processes. However, the respective roles of CA production processes and hemicellulose acetates in the formation of IGP have not been clarified. Thus, the purpose of this study is to explore the contributions of hemicelluloses and individual CA production process variables to the formation of IGP. For clarity, two classes of IGP are defined, Type A IGP and Type B IGP. Type A IGP refers to IGP generated due to the poor initial activation and incomplete reaction between acetic anhydride and the commercial dissolving pulp [15, 16]. Type B IGP is the second source and arises from the limited solubility of XA in solvents such as acetone and acetic acid that are commonly used for processing of CDA. This low solubility can result in the formation of aggregates, composed of CA and XA, during precipitation. Firstly, the solubility of beechwood xylan and its derivatives (XA) are

explored in relevant solvents. In addition, MD simulations were used to provide insights to explain the behavior of the beechwood xylan and XA in the relevant solvents. An array of experiments simulating the industrial manufacturing process of CA are performed at a lab scale, examining the impact of each CA production process on the formation of Type B IGP. The insoluble residues generated from the experiments are analyzed using HPLC and FT-IR. Multivariate analysis (MVA) techniques are employed to process the FT-IR spectra, enabling the establishment of a prediction model for the carbohydrate composition of the insoluble residues. In total, these findings provide insights into the formation of IGP during the commercial production of CA.

## **2. Materials and Methods**

### **2.1. Materials**

CA (DS 1.85, 2.45, and 2.85) were kindly provided by Eastman Chemical Company (Kingsport, TN). Beechwood xylan was purchased from Megazyme (Chicago, IL). Other chemicals such as dimethyl sulfoxide (DMSO), acetic acid, sulfuric acid, acetone, acetic anhydride, and 1, 5-diazabicyclo [4.3.0] non-5-ene (DBN) were purchased from Fisher Scientific (Pittsburgh, PA).

### **2.2. General sample preparation procedure**

#### **2.2.1. CDA with IGP removed**

Commercially available CDA flakes (900 mg) were introduced into 29.1g of acetone (3 wt. %). The mixture was placed on a shaker until CDA flakes were fully dissolved. The Type A IGP were collected by centrifugation at 4,400 rpm for 6 hours. The collected Type A IGP were

discarded, and an excess amount of deionized water was slowly poured into the supernatant to obtain the Type A IGP-free CDA. The collected IGP-free CDA was vacuum at 50 °C dried for 24 hours.

### **2.2.2. Acetylation of beechwood Xylan in [DBNH][OAc] ionic liquid system**

The acetylation of beechwood xylan in the [DBNH][OAc] ionic liquid system is described elsewhere [17]. Briefly, the ionic liquid was prepared by mixing 3.75 g of DBN and 2.25 g of acetic acid. Then, 300 mg of beechwood xylan was introduced to the ionic liquid, and the mixture was treated at 85 °C for 2 hours to achieve complete dissolution of beechwood xylan. Next, 938 mg of additional DBN was added after the beechwood xylan was fully dissolved in ionic liquid. The solution was then cooled to 50 °C, and acetic anhydride was added to initiate the acetylation reaction for 1 hour. The DS of the beechwood XA was controlled by varying the mole ratio of acetic anhydride to xylan hydroxyls. The XA was recovered by pouring the reaction solution into 17 g of 95 % ethanol. The precipitated XA was collected by centrifugation at 4,400 rpm for 5 min, and rinsed several times with 95 % ethanol, then vacuum-dried for 24 hours. To determine the acetyl DS of the XA, 20 mg of XA was dissolved in 1 ml of DMSO-d<sub>6</sub> or CDCl<sub>3</sub> for <sup>1</sup>H NMR analysis. <sup>1</sup>H NMR spectra was obtained by Bruker Avance NEO 500 MHz NMR. The DS of beechwood XA was computed by comparing the relative intensities of signals originating from acetyl groups at 2 ppm and signals of all carbohydrates (3.0-5.6 ppm) in <sup>1</sup>H NMR spectra [17]. Following equation 1 was employed.

$$DS = (Integral\ of\ acetyl\ protons/3)/(Integral\ of\ carbohydrate\ ring\ protons/6)$$

Eq. 1

## **2.3. Behaviors of Beechwood Xylan and XA in the Relevant Solvents**

### **2.3.1. Visual Observation & Recovery Efficiency**

To examine the behaviors of beechwood xylan (DS of 0) and XA (DS of 1.0 and 2.0) in the relevant solvents such as acetic acid, acetone, and DMSO/deionized water (9:1 w/w), 90 mg of vacuum-dried xylan or XA was introduced into 30 ml of the relevant solvent. The mixtures were placed on a shaker at 23 °C for 24 hrs, then centrifuged at 4,400 rpm for 8 hours to collect undissolved residues. The collected residues were rinsed with an excess of ethanol, air-dried and vacuum-dried at 50 °C for 24 hrs. The recovery efficiency of beechwood xylan and XA was calculated based on the weight differences between the original addition amount and collected residues.

### **2.3.2. Molecular Dynamic Simulations**

MD simulations were performed for two different systems, diluted and concentrated solutions, to gain insight into the behaviors of beechwood xylan (DS of 0) and XA (DS of 1.0 and 2.0) in acetic acid, acetone, and DMSO/water (9:1 w/w).

### **2.3.3. Construction of Molecular Models of Single Polymer Chains**

XA chains with DS of 0, 1.0 and 2.0 were generated using Scienomics MAPS Software Suite (MAPS version 4.2)[18]. In order to create the polymer solutions, one chain of each polymer with a degree of polymerization (DP) of 100 was inserted into the separate 3D-periodic simulation boxes ( $240 \times 240 \times 240 \text{ \AA}^3$ ). Then the box was filled with different solvent molecules (~10,000). The initial density for these systems is  $0.2 \text{ g/cm}^3$ . To create the concentrated polymer solutions, 20

chains (DP=100) of each polymer were inserted into the 3D-periodic simulation boxes with the initial density of 0.2 g/cm<sup>3</sup>. Finally, 1,000 molecules of each solvent were inserted into the 3D-periodic simulation boxes to create the final system with an initial density of 0.5 g/cm<sup>3</sup>.

#### **2.3.4. Perform MD Simulations**

In this study, the MD simulations were carried out with the Amber force field [19]. The parameters established and reported in the literature for acetic acid [20], acetone[21], and DMSO [22] were used in this work. For water molecules, the SPC/E model was employed [23]. Once the systems were prepared, the MD simulations were carried out using the LAMMPS software to thermally equilibrate the molecular model systems in three stages [24]. First, the geometries were optimized using the Conjugate Gradient (CG) method for all systems [25]. Then, the MD simulations with an NPT (constant number of atoms, N; constant pressure, P; constant temperature, T) ensemble were run at 300 K and 1 atm for 2 ns. Next, a series of heating/cooling cycles were applied to ensure the polymer chains were not trapped in local energy minima. For this purpose, the NPT-MD simulations were performed at 2,000 K and 1,000 atm for 1 ns. Then, the systems were cooled down to 300 K and atmospheric pressure at a rate of 1.7 K/ps and 1 atm/ps. Next, NPT MD simulations were run at 300 K and 1 atm for 2 ns. This cycle was repeated 5 times for all systems. In this work, all simulations used a time step of 1 fs, a cut-off distance of 1.2 nm for long-range interactions, and the particle–particle–particle–mesh (PPPM) method for electrostatic potential calculations [26]. Moreover, we used the Nosé-Hoover thermostat [27] and Parrinello and Rahman barostat [28] to control the temperature and pressure, respectively.

### 2.3.5. Flory–Huggins Interaction Parameter Calculation

In this work, the Flory-Huggins interaction parameter for single-chain polymer solutions ( $\chi_{ps}$ ) are calculated by employing the following equation [29].

$$\chi_{ps} = \left( \frac{\Delta E_{mix}}{RT} \right) V_m$$

Eq. 2

where,  $\Delta E_{mix}$  is the energy of mixing of the polymer chain and solvent molecules.  $R$  is the gas constant.  $T$  is temperature.  $V_m$  is the molar volume of the repeating unit of XA.

$\Delta E_{mix}$  can be calculated using the cohesive energy density ( $\frac{E_{coh}}{V}$ ) of each component in polymer solutions.

$$\Delta E_{mix} = \phi_p \left( \frac{E_{coh}}{V} \right)_p + \phi_s \left( \frac{E_{coh}}{V} \right)_s - \left( \frac{E_{coh}}{V} \right)_{ps}$$

Eq. 3

where, subscribes  $p$ ,  $s$  and  $ps$  represent polymer, solvent and polymer/solvent, respectively.  $\phi_p$  and  $\phi_s$  are the volume fraction of polymer and solvent, respectively.  $\frac{E_{coh}}{V}$  is the calculated cohesive energy density of each component, i.e. the bulk XA and the bulk solvents.

## **2.4. Demonstration of Type B IGP Formation**

IGP-free CDA (900 mg) was dissolved in 29.1 g of acetic acid (3 wt. %) using a shaker table until the IGP-free CDA was fully dissolved. Once a transparent solution was obtained, 90 mg of beechwood xylan was added to the solution. The IGP-free CDA-beechwood xylan mixture was then placed on the shaker and allowed to mix for 4 hrs. The well-mixed suspension was precipitated by the addition of an excess of deionized water. The precipitated solid was collected by vacuum filtration and repeatedly rinsed with distilled water until the water pH reached of 6, and then dried in a vacuum oven at 50 °C for 24 hrs. The dried aggregates were then redissolved in 29.1 g of acetone or acetic acid at room temperature for 6 hours on a shaker table. Insoluble residues (Type B IGP) were collected by centrifugation at 4,400 rpm for 6 hrs, and were subsequently rinsed first with the solvent used for re-dissolution, then with an excess amount of ethanol. The residues were air-dried, and vacuum-dried at 50 °C for 24 hrs. The supplementary information provides a detailed procedure for preparing IGP-free CDA and the experimental procedure is shown schematically in Figure S4.

## **2.5. Influences of Each CA Production Step on the Formation of Type B IGP**

### **2.5.1. Acetylation & Hydrolysis Process**

To emulate the common acetylation reaction, but eliminate questions about the effects of activation and residual cellulose crystallinity, a commercial CA with a DS of 1.85 and unsubstituted beechwood xylan were acetylated based on the procedure reported elsewhere [16]. An excess of acetic anhydride was used to completely acetylate both the CA and beechwood xylan and produce CA DS 3.0 and XA DS 2.0. The acetylation was carried out at 50 °C for 1 hr. To

quench the acetylation, a large excess of 88 wt.% of aqueous acetic acid (acetic acid/water, 88 wt.%/12 wt.%) was used. After 3 hrs of hydrolysis, the solution was transferred to a centrifuge tube to collect the insoluble residues by centrifugation at 4,400 rpm for 6 hrs. The collected residues were subsequently rinsed first with acetic acid, then with an excess amount of ethanol. After that, the residues were air-dried and then vacuum-dried to remove any residual solvents.

### **2.5.2. Precipitation Process**

Beechwood xylan (90 mg) was added to IGP-free CDA acetic acid solution (3 wt. %; 30 g) and shaken for 4 hrs. Residues were then collected by centrifugation, rinsed with excess ethanol, and dried in a fume hood for 4 hrs before being vacuum-dried for 20 hrs. The resulting residue was reintroduced into acetone (29.1 g) to examine the formation of Type B IGP. After 8 hrs of redissolution in acetone, the final insoluble residues were collected via centrifugation (4,400 rpm for 6 hrs), and were subsequently rinsed first with acetic acid, then with an excess amount of ethanol. The residues were air-dried and vacuum-dried.

### **2.5.3. Effect of the Drying Process**

Aggregates consisting of beechwood xylan and IGP-free CDA were prepared as described in Figure S4. One set of aggregates was subjected to vacuum-drying at 50 °C for 24 hrs. In contrast, the other set of aggregates was recovered with 2 hrs of vacuum filtration, but not subjected to vacuum-drying. The ‘filtration only’ IGP were intended to allow water to remain hydrogen bonded with either the beechwood xylan or CDA, or both. While the vacuum dried IGP were intended to be essentially free from water, and thus generate more hydrogen bonding or other

intermolecular interactions between the polymer chains. The recovered aggregates were introduced into 29.1 g of acetone to examine the formation of Type B IGP. Insoluble residues were collected via centrifugation at 4,400 rpm for 6 hrs, rinsed with an excess amount of acetone, air-dried and vacuum-dried.

## **2.6. Influences of Impurities on the Formation of Type B IGP**

### **2.6.1. Influence of Solvents on Type B IGP**

Aggregates consisting of beechwood xylan and CDA were prepared by following the procedure shown in Fig S4. The aggregates were introduced into acetone or DMSO/deionized water (9:1 w/w), to examine the formation and persistence of Type B IGP. Insoluble residues were collected via centrifugation at 4,400 rpm for 6 hrs, rinsed with an excess amount of ethanol, air-dried and vacuum-dried.

### **2.6.2. Influence of CA DS on Type B IGP**

Following the procedure shown in Figure S4 a series of Type B IGP were created with CA and XA with varying DS (CA: DS of 1.85, 2.45, and 2.85 and XA: DS 0, 1.0, and 2.0). After the formation and recovery of these aggregates, they were introduced into 29.1 g of acetic acid and placed on a shaker for 6 hrs. Insoluble residues were collected via centrifugation at 4,400 rpm for 6 hrs, rinsed first with acetic acid, then, an excess amount of ethanol. Afterward, the insoluble residues were air-dried and vacuum-dried.

## 2.7. Carbohydrate Composition Analysis

Carbohydrate composition analysis was conducted using a procedure detailed elsewhere [30]. Briefly, the vacuum dried insoluble residues were hydrolyzed with 72% H<sub>2</sub>SO<sub>4</sub> at 30 °C for 2 hours. The solutions were diluted by adding deionized water and secondary hydrolysis was carried out at 121 °C for 1 hour. The hydrolysate was neutralized to pH 7 and the monomeric sugars were measured with an Agilent 1200 HPLC equipped with a Shodex sugar SP0810 column. The carbohydrate composition analysis only focused on the characterization of glucose and xylose fraction because the experiments were conducted by utilizing IGP-free CDA and beechwood xylan without further modifications. The following equations are employed to compute the contents of glucose and xylose.

$$\text{Glucose (\%)} = \frac{\text{Integrated peak area of glucose}}{\text{Integrated peak area of glucose} + \text{Integrated peak area of xylose}} \times 100$$

Eq. 4

$$\text{xylose (\%)} = \frac{\text{Integrated peak area of xylose}}{\text{Integrated peak area of glucose} + \text{Integrated peak area of xylose}} \times 100$$

Eq. 5

## 2.8. FTIR and Multivariate Analysis.

The FTIR spectra were all collected with a Spectrum 3 spectrometer (PerkinElmer, Waltham, MA). IGP-free CA (DS 1.85, DS 2.45, and DS 2.85), beechwood XAs (DS 0, 1.0, and 2.0), and insoluble residues obtained from the precipitation experiments as described in Figure S4 were scanned 16 times from 650 cm<sup>-1</sup> to 4000 cm<sup>-1</sup> at the resolution of 2 cm<sup>-1</sup>. At least triplicated individual IR spectra were collected on each sample. IR spectra were processed using standard baseline correction and normalization approaches using Unscrambler software package

[31-34]. Both principal component analysis (PCA) and partial least squares (PLS) analysis were used to evaluate all the samples.

### 3. Results and Discussions

#### 3.1. Behaviors of Beechwood Xylan and XA in the Relevant Solvents

**Table 4.1.** Recovery efficiency of xylan and XA from commercially relevant solvents at room temperature (25 °C).

	DS	Acetone	Acetic Acid	DMSO/Deionized water (9:1 w/w)
Beechwood Xylan	0	85 ± 2 %	89 ± 1 %	0 %
XA	1.0	94 ± 1 %	96 ± 2 %	0 %
	2.0	97 ± 2 %	95 ± 3 %	93 ± 1 %

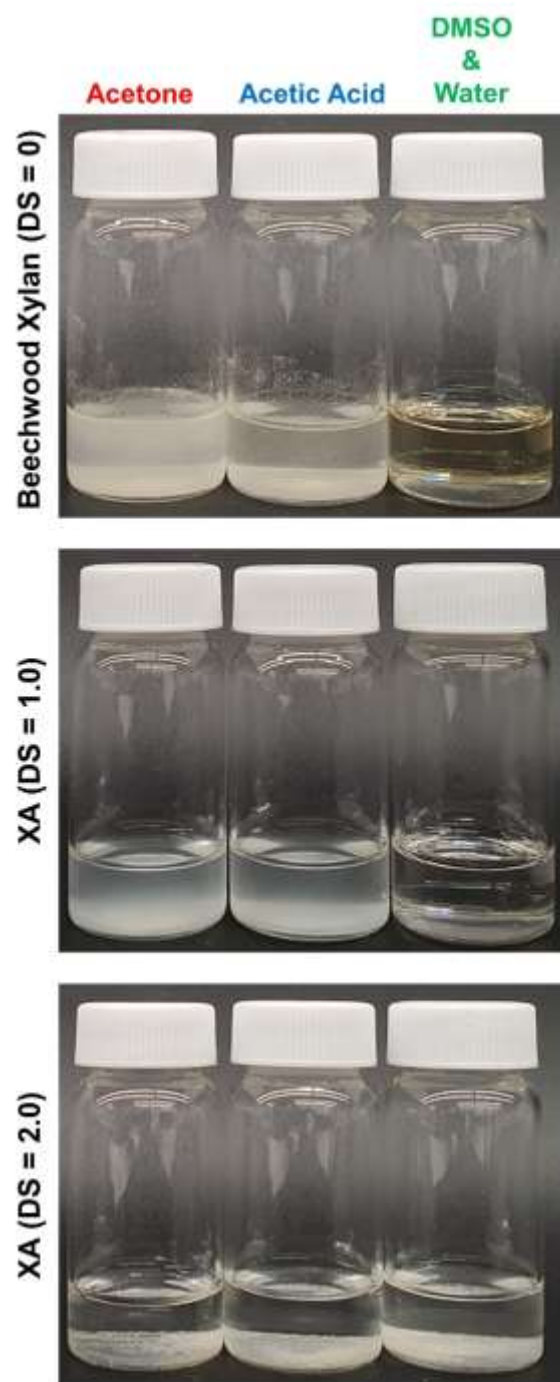


**Figure 4.2.** Behaviors of beechwood xylan (DS = 0) and XA (DS = 1.0 and 2.0) in the relevant solvent

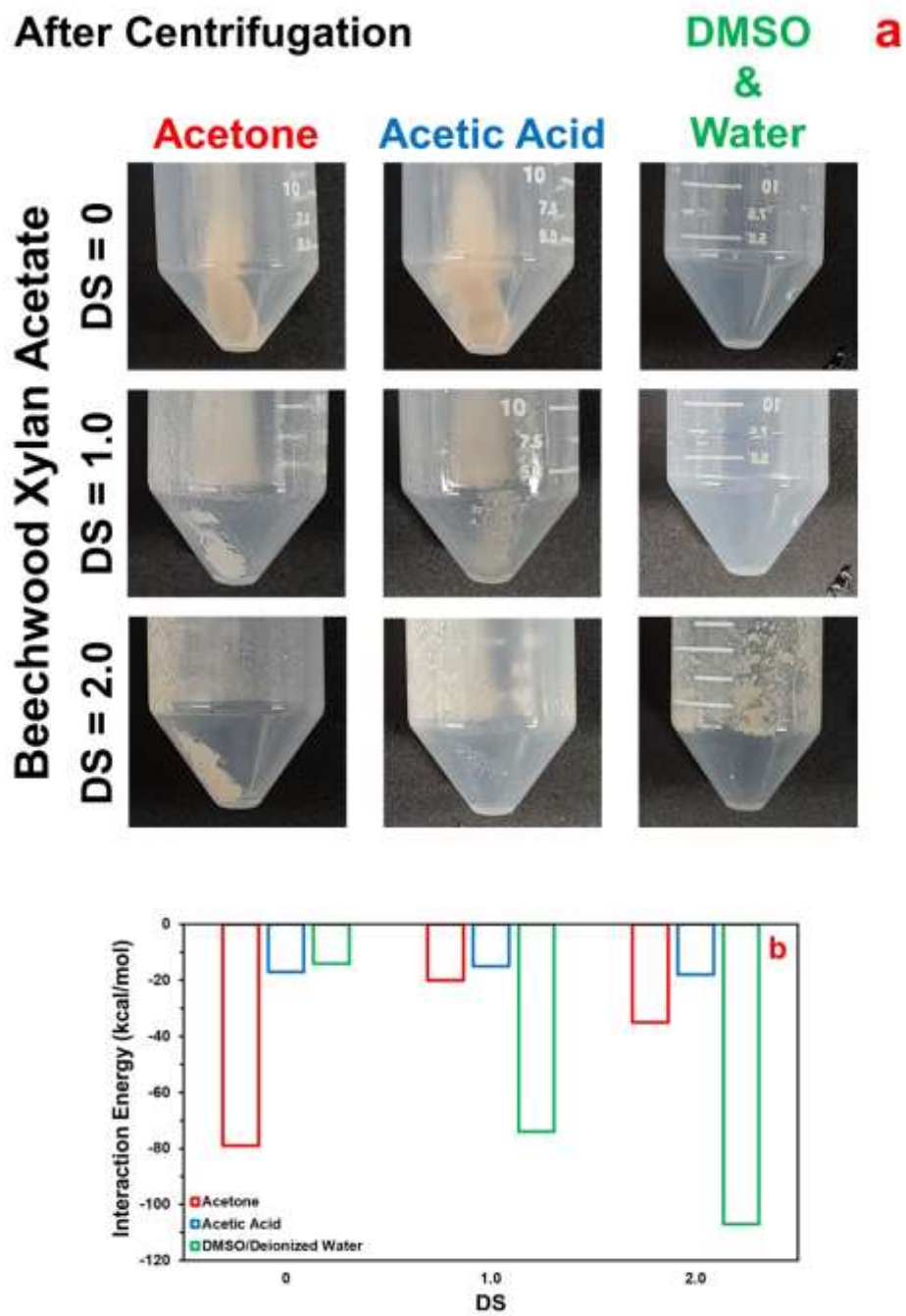


**Figure 4.3.** (a) Collected insoluble fraction after centrifugation and (b) Polymer-polymer interaction energy of beechwood xylan and XA in the relevant solvents

The behavior of beechwood xylan (DS = 0) and XA (DS = 1.0 and 2.0) in the solvents of interest is described in Figure 4.2 and Table 4.1. As expected, with acetone and acetic acid, the beechwood xylan was not soluble and formed a heterogeneous suspension. The recovery efficiency of the beechwood xylan after dispersion in acetone and acetic acid was 85 % and 89 %, respectively. The incomplete recovery was due to incomplete separation via centrifugation, which was similar to the situation described in Figure S7. In contrast, DMSO/water dissolved beechwood xylan or enabled the formation of a clear dispersion [35]. A clear solution was obtained, and no insoluble residues were recovered from the solution after centrifugation. XA with DS of 1.0 exhibited a similar trend to the beechwood xylan. In acetone and acetic acid, XA with DS of 1.0 formed a heterogeneous suspension and centrifugation provided high recovery efficiency. The XA with DS of 1.0 was soluble in DMSO/water and the recovery efficiency of XA with DS of 1.0 was 0 %. The fully acetylation xylan (DS=2.0) was insoluble in all three solvents and the recovery efficiency was above 93 %.

Molecular dynamics simulations were conducted to gain insight into the behavior of beechwood xylan and XA in different solvents. The results showed that in acetone, XA chains with an intermediate DS exhibited the lowest polymer-polymer interaction energy, while experimental observations indicated that XA with a DS of 1.0 formed a heterogeneous mixture in acetone, suggesting a preference for polymer-polymer interactions. In contrast, in acetic acid, predicted polymer-polymer interaction energy was similar regardless of DS. For DMSO/water, beechwood xylan exhibited the lowest polymer-polymer interaction energy, while XA with a higher DS showed increased polymer-polymer interaction energy. However, XA with a DS of 1.0 was still dissolved or formed a clear dispersion (as shown in Figure 4.2 and 4.3a). Furthermore,

complete acetylation resulted in the highest polymer-polymer interaction energy, which was consistent with the poor solubility of XA with a DS of 2.0 in DMSO/water.

### 3.2. Demonstration of Type B IGP Formation

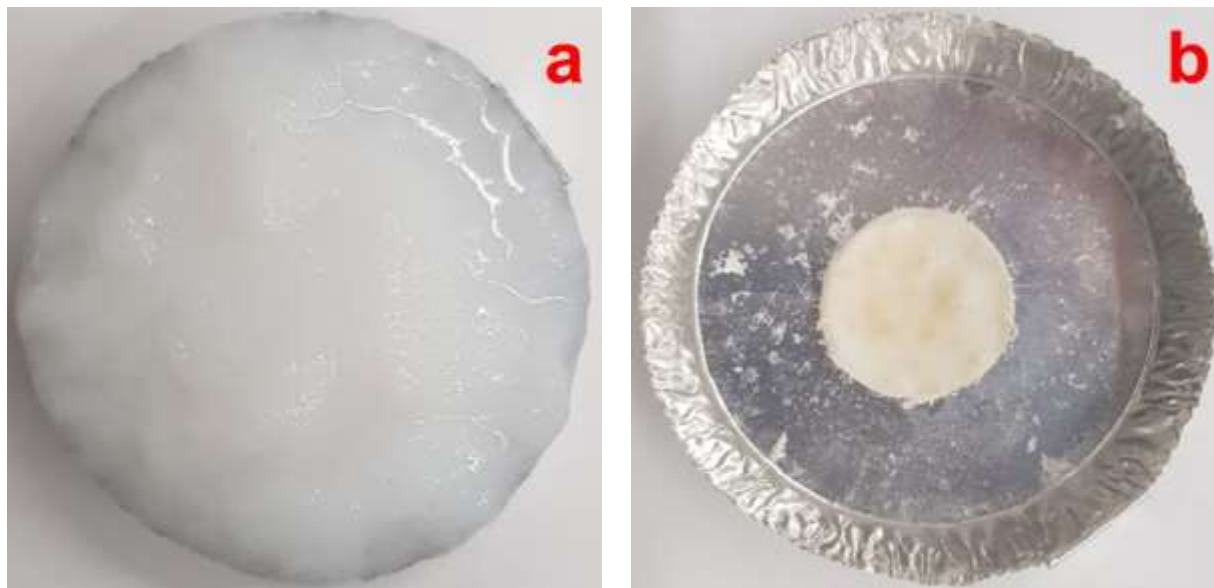


**Figure 4.4.** Photo of (a) precipitated IGP-free CDA/beechwood xylan aggregates before drying and (b) Vacuum dried IGP-free CDA/beechwood xylan aggregates

To date, the common hypothesis for the formation of IGPs are the lack of solubility originating from improperly activated/acetylated CAs, and other impurities such as hemicellulose acetates [6, 9, 13, 15, 16, 36]. In this work IGP originating from the improper activation and acetylation of cellulose are termed Type A IGP, and are not the focus of this current work. Type B IGP are defined as IGP derived from intermolecular interactions between XA and CA, and the poor solubility of XA in some solvents. The formation of aggregates consisting of CA and XA during the precipitation process initiates the intermolecular interactions that contribute to the

formation of Type B IGP. Our findings challenge the existing knowledge by demonstrating that IGP-free CDA, which represents uniformly acetylated CDA, can also contribute to the formation of IGP during precipitation, which has not been previously recognized.

To gain a deeper understanding of Type B IGP formation, acetic acid was used as the solvent and water as the precipitation medium to simulate industrial CA production processes. As shown in Figure 4.5, commercial CDA dissolved in acetone contains a small amount of IGP resulting in a turbid solution. These IGP were removed by centrifugation to produce a clear transparent solution (Figure 4.5). The starting CA for this experiment was obtained by precipitating IGP-free CDA from the supernatant. To simulate the process conditions immediately after the hydrolysis of CA, the IGP-free CDA was dissolved in acetic acid. Then, beechwood xylan was introduced to serve as a model impurity in the system. As expected, based on Figure 4.2, IGP-free CDA acetic acid solution and beechwood xylan formed a heterogeneous mixture. This heterogeneous CDA-xylan mixture was precipitated by introducing an excess amount of deionized water. Considering the observed color of aggregates (Figure 4.4a and 4.4b), it can be inferred that beechwood xylan was entrapped within the CDA precipitates.

In this work, the formation of Type B IGP was confirmed by both qualitative and quantitative studies of isolated insoluble residue. A visual verification method was developed based on a distinctive behavior of beechwood xylan in acetone and acetic acid. It was concluded that a complete separation of beechwood xylan from IGP-free CDA in either acetone or acetic acid was very difficult to achieve via centrifugation (Figure S7). If the poorly soluble beechwood xylan in aggregates are unable to inhibit the redissolution of adjacent CDA in acetone, the CDA fraction would completely dissolve, and the beechwood xylan would be released from the aggregates. As a result, beechwood xylan would be present in the supernatant after centrifugation, as shown in

Figure S7. Similarly, the isolated insoluble residues would exhibit a similar carbohydrate composition compared to that of the beechwood xylan.

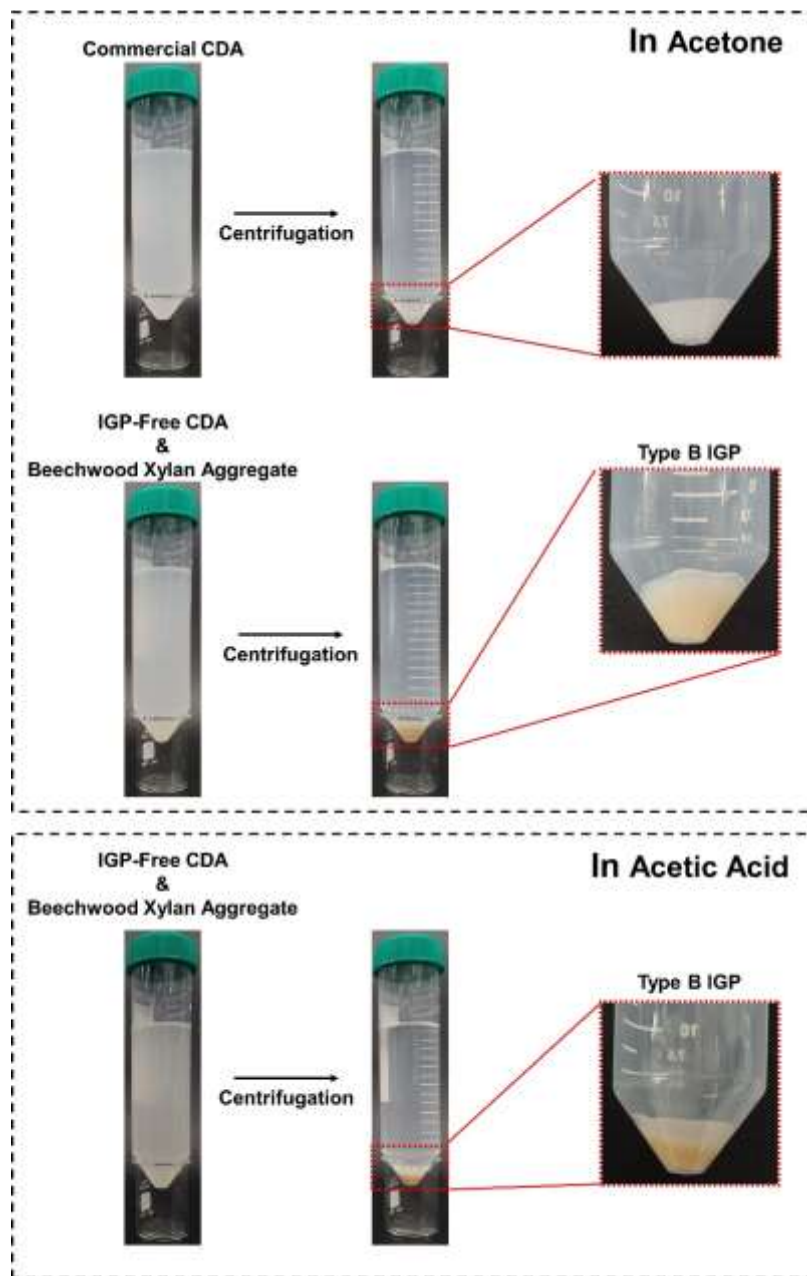


**Figure 4.5.** Demonstration of Type B IGP-formation in acetone and acetic acid

**Table 4.2.** Carbohydrate composition of insoluble residues

	Glucose (%)	Xylose (%)	Visible Residues in Supernatant
Non-acetylated Beechwood Xylan	5.9 ± 0.1 <sup>A</sup>	94.1 ± 0.1 <sup>A</sup>	N/A
Demonstration of Type B IGP Formation	21.3 ± 1.1 <sup>B</sup>	78.7 ± 1.1 <sup>B</sup>	X
Influences of Acetylation and Hydrolysis	6.5 ± 0.6 <sup>A</sup>	93.5 ± 0.6 <sup>A</sup>	X
Influences of Precipitation	6.9 ± 0.5 <sup>A</sup>	93.5 ± 0.5 <sup>A</sup>	O
Influences of Drying	9.2 ± 0.4 <sup>C</sup>	90.8 ± 0.4 <sup>C</sup>	X

\* In the Table 2, all the samples were prepared with IGP-free CDA and non-acetylated beechwood xylan.  
\* Statistical analysis: ANOVA with Tukey's comparisons test; mean values with different superscript letters (A-C) in the same column indicate that there are significant differences ( $p < 0.05$ )



**Figure 4.6.** Photos of insoluble residue (a) collected after the demonstration of Type B IGP formation, (b) collected after acetylation and hydrolysis process, (c) collected from an experiment for investigating influences of the precipitation process, and (d) collected from an experiment for investigating influences of the drying process.

To examine the formation of Type B IGP, vacuum-dried aggregates were introduced into acetone to allow redissolution of any CDA in aggregates, followed by centrifugation which produced a clear supernatant without any visible residues (Figure 4.5). The distinctive color difference between IGP-free CDA and beechwood xylan made it possible to visually confirm the formation of Type B IGP, which were produced using IGP-free CDA and beechwood xylan (Figure 4.5). Moreover, the insoluble residues exhibited a statistically significant difference in the carbohydrate composition compared to that of beechwood xylan (Table 4.2). The results obtained from both experiments provide evidence for the formation of Type B IGP. The incomplete dissolution of the CDA fraction within the Type B IGP suggests that strong intermolecular interactions and entanglements have formed between the two components, inhibiting the redissolution of highly soluble CDA.

### **3.3. Influences of Each Cellulose Acetate Production Process**

#### **3.3.1. Acetylation and Hydrolysis**

Since the industrialized cellulose acetylation process consists of various steps (Figure 4.1a), the formation of Type B IGP could occur at several different process operations. The influence of the acetylation and hydrolysis processes were investigated by simulating cellulose acetylation at a lab scale. Beechwood xylan was used as an impurity. However, to eliminate the well-known influences of improperly activated cellulose, IGP-free CA having a DS of 1.85 was employed as a starting material instead of cellulose. Following acetylation, hydrolysis, and subsequent centrifugation, the supernatant no longer displayed any visually detectable insoluble residues. However, the carbohydrate composition analysis of the collected insoluble residues revealed no

significant difference when compared to that of beechwood xylan (Table 4.2). The result suggests that the intermolecular interactions established between CA and XA during the acetylation and hydrolysis processes are not strong enough to retain extra CA on XA. Consequently, the acetylation and hydrolysis process does not significantly contribute to the formation of Type B IGP.

### **3.3.2. Precipitation**

As previously mentioned, upon precipitation, IGP-free CDA captures the beechwood xylan present in the solution, leading to the formation of aggregates. A hypothesis was made that the formation of aggregates during precipitation was necessary to establish strong intermolecular interactions that hinder the redissolution of IGP-free CDA in Type B IGP. However, It is possible to develop intermolecular interactions between dissolved IGP-free CDA and beechwood xylan that may hinder the redissolution of IGP-free CDA adjacent to beechwood xylan. To test the hypothesis, the addition of deionized water, which triggers the formation of aggregates, was omitted. Similar to the simple mixture made by introducing beechwood xylan into IGP-free CDA acetone solution shown in Figure S7, floating residues were clearly observed after centrifugation. Also, a difference in carbohydrate composition between the collected residues and beechwood xylan was not statistically significant. Therefore, the contribution of intermolecular interactions between dissolved IGP-free CDA and beechwood xylan in acetic acid to the formation of Type B IGP can be considered negligible. The forced formation of aggregates via precipitation should be preceded by a strong establishment of intermolecular interactions between IGP-free CDA and beechwood xylan in order to produce Type B IGP during redissolution.

### 3.3.3. Drying

During the paper-making process, the strength of a paper sheet is improved by undergoing consecutive wet pressing and drying [37, 38]. The wet pressing enables the formation of dense cellulosic fiber structure and the strength is endowed by the formation of direct hydrogen bonding among cellulosic fibers during the drying process [39]. Analogous to the paper-making process, aggregates become a dense structure during vacuum drying as shown in Figure 4.4a and 4.4b. Thus, to reveal the influences of drying, samples were prepared with and without vacuum drying. Instead of vacuum drying, an extended hours of vacuum filtration was additionally performed to remove free water as much as possible. No floating residues were observed in the supernatant. In contrast, the carbohydrate composition of the insoluble residues showed significant differences from both beechwood xylan and Type B IGP. The amount of IGP-free CDA (glucose) in the insoluble residues increased compared to that of beechwood xylan, however, it was significantly lower than that of Type B IGP. This suggests that the drying process contributed to the formation of additional intermolecular interaction between IGP-free CDA and beechwood xylan in aggregates, resulting in a persistent interaction between the entrapped IGP-free CDA and beechwood xylan. The formation of IGP-free CDA-beechwood xylan aggregates during the precipitation process, followed by the development of intermolecular interactions between IGP-free CDA and beechwood xylan, are essential for the persistent formation of Type B IGP.

### 3.4. Influences of Impurities

#### 3.4.1. Roles of Beechwood Xylan

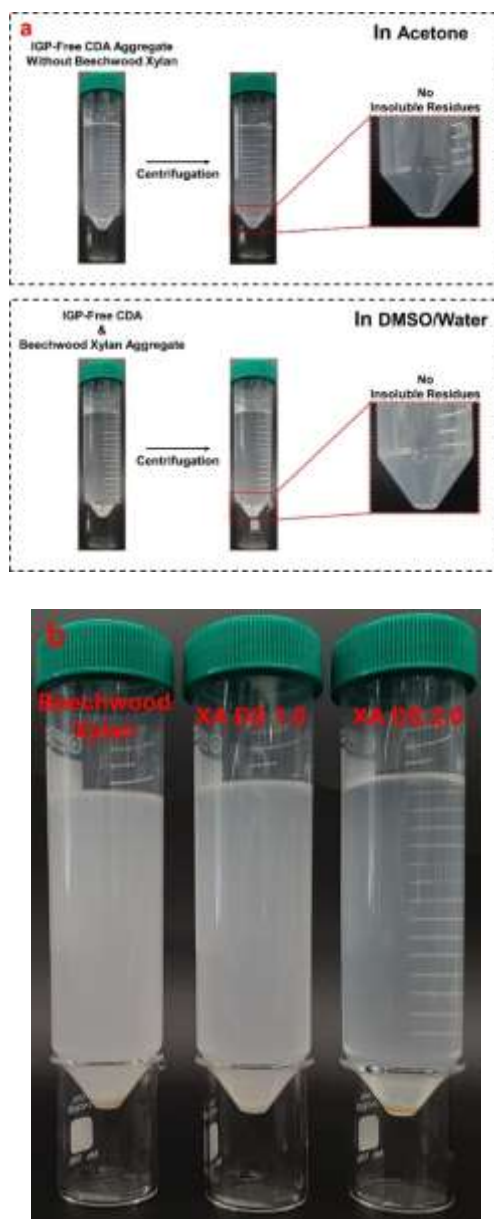


**Figure 4.7.** (a) The examination of roles of beechwood xylan, as well as its behavior in a solvent in the formation of Type B IGP and (b) Influences of DS of XA on the turbidity of IGP-free CDA/beechwood xylan or XA (DS = 1.0 and 2.0) aggregates acetone solution

**Table 4.3.** Carbohydrate composition of insoluble residues

		Glucose (%)	Xylose (%)	Floating Residues
Beechwood Xylan		5.9 ± 0.1 <sup>A</sup>	94.1 ± 0.1 <sup>A</sup>	N/A
Redissolution Solvent <sup>s</sup>	Acetone	21.3 ± 1.1 <sup>B</sup>	78.7 ± 1.1 <sup>B</sup>	X
	Acetic Acid	21.1 ± 0.7 <sup>B</sup>	78.9 ± 0.7 <sup>B</sup>	X
	DMSO/Water	N/A	N/A	N/A
XA DS <sup>b</sup>	Beechwood Xylan (DS = 0)	21.3 ± 1.1 <sup>B</sup>	78.7 ± 1.1 <sup>B</sup>	X
	XA (DS = 1.0)	12.4 ± 0.8 <sup>C</sup>	87.6 ± 0.8 <sup>C</sup>	X
	XA (DS = 2.0)	5.8 ± 0.3 <sup>A</sup>	94.2 ± 0.3 <sup>A</sup>	X
a: Aggregates made from IGP-free CDA and non-acetylated beechwood xylan was employed b: Aggregates were produced using IGP-free CDA and XA with varying DS and dissolved in acetone * Statistical analysis: ANOVA with Tukey's comparisons test; mean values with different superscript letters (A-C) in the same column indicate that there are significant differences (p <0.05)				

Precipitation experiments without beechwood xylan were conducted to examine the roles of beechwood xylan. As described in Figure 4.7a, IGP-free CDA produce a clear solution in acetone, and no insoluble residues are recovered. This confirms the need for the poorly soluble beechwood xylan component to drive the formation of Type B IGP.

### **3.4.2. Behavior of Beechwood Xylan in Relevant Solvents**

The behavior of beechwood xylan in the relevant solvents can be categorized into two different groups. In acetone and acetic acid, beechwood xylan is insoluble and forms a suspension. In contrast, DMSO/water can dissolve beechwood xylan or produce a clear dispersion. Since the formation of Type B IGP did not occur without beechwood xylan, it was hypothesized that the behavior of beechwood xylan in a solvent is critical to the formation of Type B IGP. To maintain the persistence of Type B IGP through continuous intermolecular interactions, it is essential to prevent the solubilization of beechwood xylan during redissolution. To test this hypothesis, the redissolution of IGP-free CDA/beechwood xylan aggregates was conducted in solvents where beechwood xylan exhibited different behaviors. This was confirmed by observing that the isolated Type B IGP remained intact during the redissolution process in both acetone and acetic acid. The higher glucose content observed in Table 4.3 underscores the differences between the starting beechwood xylan and the Type B IGP with entrapped CDA. However, in the case of DMSO/water (9:1), where both xylan and CDA are highly soluble, the formation of Type B IGP did not occur (Figure 4.7a). Based on the results, it could be inferred that the behavior of beechwood xylan in solvents matters in the formation of Type B IGP.

### **3.4.3. Influence of DS of XA**

The solubility and intermolecular interactions of carbohydrate esters are known to be influenced by differences in their DS [40, 41]. To investigate the impact of XA's DS on the formation of Type B IGP, acetylation was performed on beechwood xylan, and XA with varying DS values (DS = 0, 1.0, and 2.0) were used to create aggregates with IGP-free CDA. The

redissolution of the aggregates, formed with XA of differing DS, in acetone, revealed clear differences in the turbidity of the resulting solutions (Figure 4.7b). There was a significant decrease in turbidity for the solution made with IGP-free CDA/XA with DS of 2.0. Additionally, the carbohydrate composition of the insoluble residues collected from this solution did not differ significantly from that of beechwood xylan. These results confirmed that fully acetylated beechwood xylan cannot provide a sufficient intermolecular interactions to deter redissolution of adjacent IGP-free CDA fraction, resulting in the failure in the formation of Type B IGP. In contrast, beechwood xylan and XA with DS of 1.0 can participate in the formation of Type B IGP. Turbid solutions were produced and the carbohydrate compositions were significantly different from that of beechwood xylan. It was observed that as the DS of XA increased, there was a decrease in the glucose content of the insoluble residues. Therefore, it could be inferred that the amount of hydroxyl groups in XA plays a key role in the formation of Type B IGP.

### **3.5. Insoluble Residue Analysis with FTIR and Multivariate Analysis**

To further analyze the influences of hydroxyl groups on the formation of Type B IGP, CA/XA aggregates with varying DS were prepared. The carbohydrate compositions of insoluble residues are shown in Table 4.4. It was revealed that the XA with a DS of 2.0 cannot produce Type B IGP, regardless of DS of CA. The carbohydrate compositions of insoluble residues made with XA with DS of 2.0 did not exhibit significant differences from that of beechwood xylan, indicating that the strength of additional fiber bondings provided by the XA with DS of 2.0 was not sufficient enough to deter the redissolution of adjacent CA. With the carbohydrate compositions of 9 different insoluble residues, a direct relationship was established

between the glucose content and the total number of hydroxyl groups (CA and XA). Regardless of DS of CA, in the same group of CA, the glucose content of insoluble residues increased with a decrease in DS of XA.

**Table 4.4.** Carbohydrate composition of insoluble residues precipitated from acetic acid, and dried.

CA	XA	Glucose content (%)	Xylose content (%)	Ratio (%Glucose/%Xylose)
Beechwood xylan		5.9 ± 0.1 <sup>A</sup>	94.0 ± 0.1 <sup>A</sup>	-
1.85	0	34.0 ± 1.3 <sup>B</sup>	66.0 ± 1.3 <sup>B</sup>	0.52
	1.0	27.4 ± 1.4 <sup>C</sup>	72.6 ± 1.4 <sup>C</sup>	0.38
	2.0	6.7 ± 0.7 <sup>A</sup>	93.3 ± 0.7 <sup>A</sup>	0.07
2.45	0	20.1 ± 0.6 <sup>D</sup>	79.9 ± 0.6 <sup>D</sup>	0.25
	1.0	12.7 ± 0.8 <sup>E</sup>	87.3 ± 0.8 <sup>E</sup>	0.15
	2.0	5.8 ± 0.2 <sup>A</sup>	94.2 ± 0.2 <sup>A</sup>	0.06
2.85	0	12.9 ± 0.6 <sup>F</sup>	87.1 ± 0.6 <sup>F</sup>	0.15
	1.0	7.5 ± 0.4 <sup>G</sup>	92.5 ± 0.4 <sup>G</sup>	0.08
	2.0	6.0 ± 0.4 <sup>A</sup>	94.0 ± 0.4 <sup>A</sup>	0.06
* Mean values with different superscript letters (A-G) in the same column indicate that there are significant differences (p <0.05)				

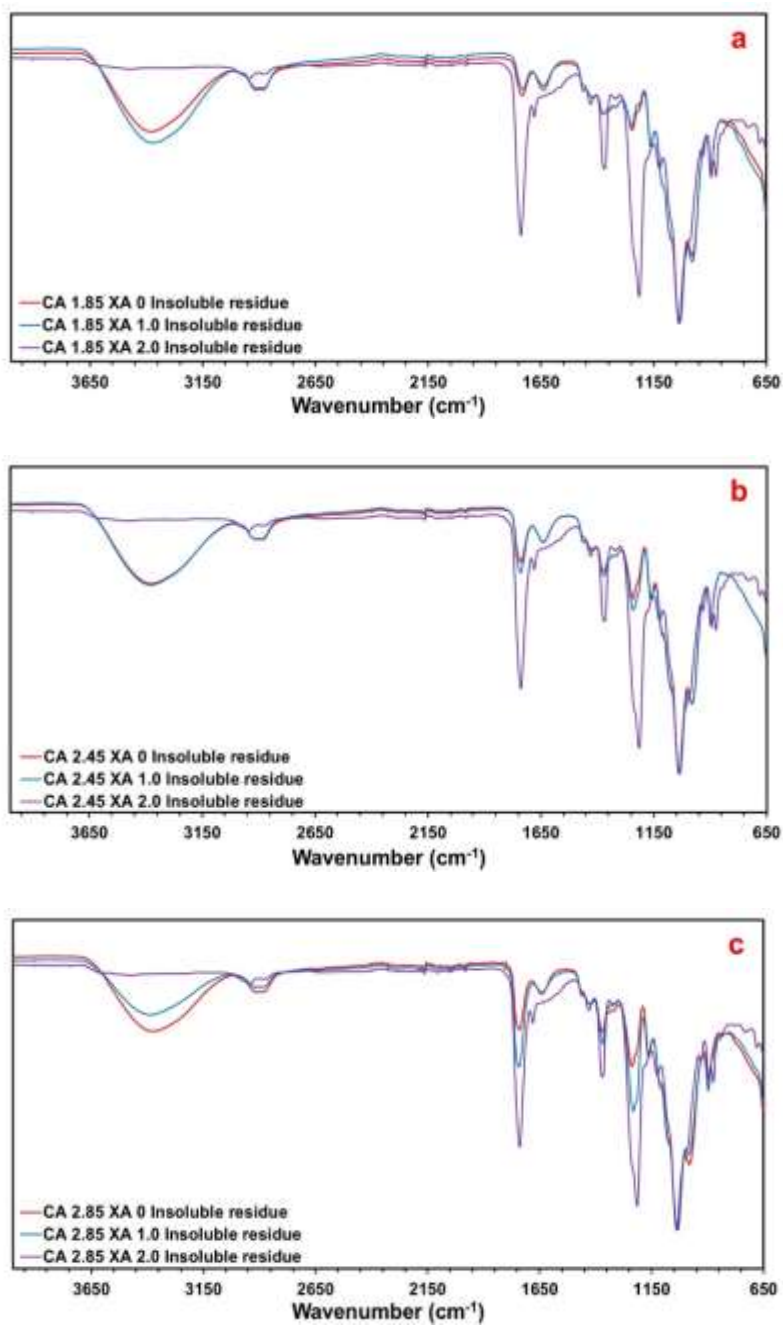


**Figure 4.8.** FTIR spectra collected from insoluble residues produced from (a) CA with DS of 1.85/XA with varying DS (0, 1.0, and 2.0), (b) CA with DS of 2.45/XA with varying DS (0, 1.0, and 2.0), and (c) CA with DS of 2.85/XA with varying DS (0, 1.0, and 2.0)

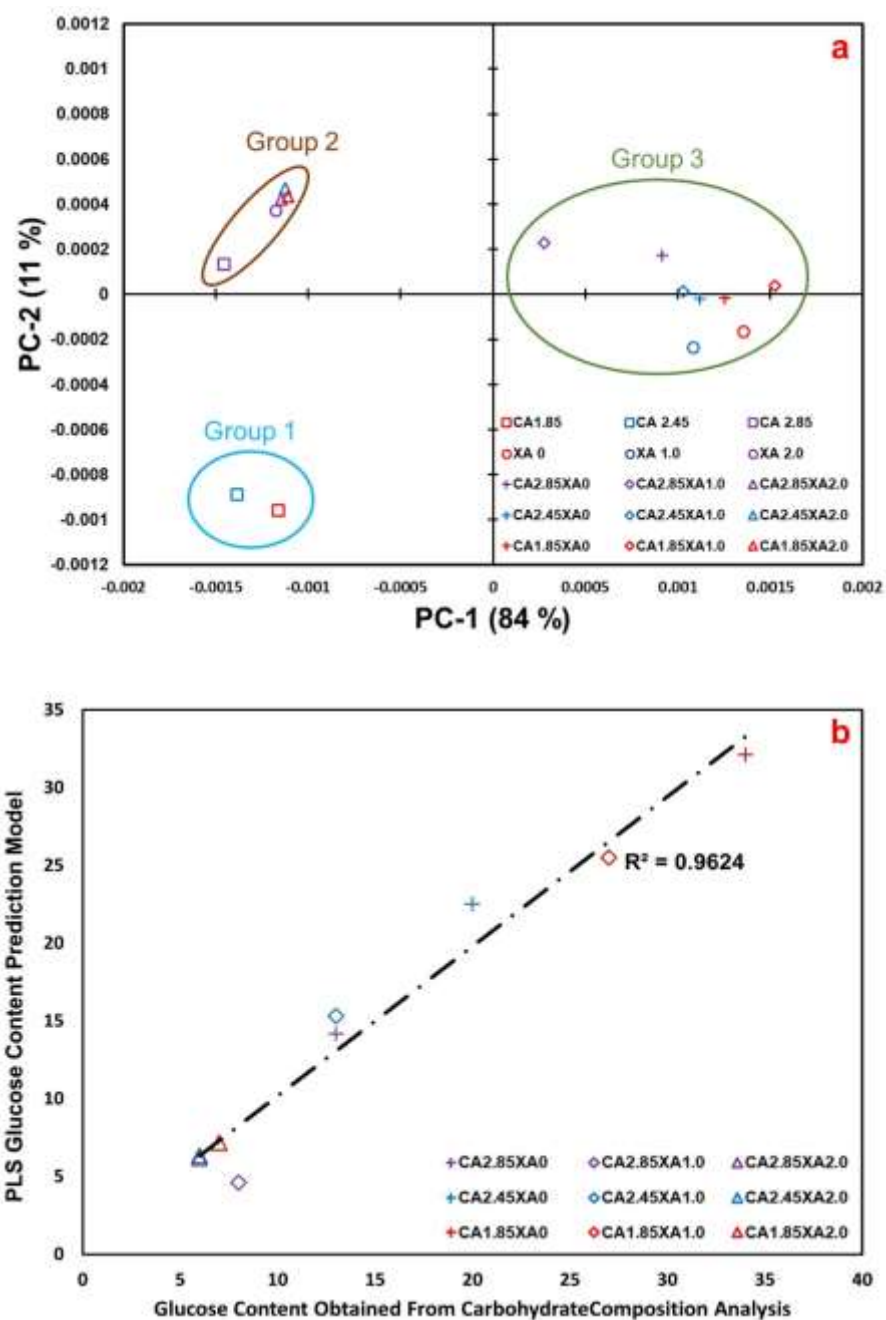


**Figure 4.9.** (a) PCA loading plot and showing the FTIR vibrations that differentiate the CA, XA, and insoluble residues and (b) Results of PLS analysis of the IR spectra predicting the glucose content of all the insoluble residues

It was revealed that IR spectral features obtained through PCA can differentiate the prepared insoluble residues. With PCA, the samples can be categorized into clearly defined three groups (Figure 4.8b). CA with two intermediate DS (DS of 1.85 and 2.45) are in Group 1. Group 2 consists of samples with relatively high DS of acetyl (e.g., CA with DS of 2.85, XA with DS of 2.0, and all insoluble residues produced from CAs/XA with a DS of 2.0 aggregates). Other samples fall into group 3. The PCA loading in Figure S8 provide insights into these groupings. The first principal component (PC), which contains 84 % of the spectral information is dominated by an inverse relationship between a series of hydroxyl vibrations ( $3,000 \sim 3,700 \text{ cm}^{-1}$ ) and vibrations originating from acetyl groups (centered at  $1,210 \text{ cm}^{-1}$  and  $1,740 \text{ cm}^{-1}$ ). The second PC, containing 11% of spectral information, differentiates samples in Group 1 from those in Group 2 and 3. Group 1, the CA with DS 1.85 and 2.45, both contain no xylan and have a relatively high hydroxyl content. Given the unique spectral features of the insoluble residue processed through PCA, it is possible to extract further information about the residues from their IR spectra using PLS analysis [42, 43]. The results of the PLS analysis predicting the glucose content are shown in Figure 4.8b. The PLS model required only two regression coefficients to achieve a high correlation coefficient ( $r^2=0.96$ ) for predicting the glucose content.. The regression coefficients for the PLS model predicting the glucose content of the insoluble residues are shown in Figure S9.

#### **4. Conclusion**

Through simulating industrial CA production at a lab scale, the influences of individual CA production steps, as well as the presence or absence of XA, on the formation of Type B IGP

were investigated. It was found that the contribution of acetylation and hydrolysis to the formation of Type B IGP was negligible. Contrary to previous reports, this study demonstrated that uniformly acetylated CA, in the presence of xylan or XA, could participate in the formation of Type B IGP. The precipitation process triggered the formation of these aggregates, where CA macromolecules became entangled with poorly soluble XA and formed aggregates. These aggregates allowed for formation of strong intermolecular interactions between the two components, which were further enhanced during the drying process. The inherent poor solubility of XA, in combination with persistent intermolecular interactions, deterred the redissolution of IGP-free CA adjacent to XA, resulting in the formation of Type B IGP.

XA contributed additional intermolecular interactions to adjacent CA in the aggregates. The DS of XA was identified as a crucial factor in controlling the formation of Type B IGP. Fully acetylated xylan (DS=2.0) did not significantly hinder the redissolution of the CA adjacent to XA. The turbidity of the solution that dissolved aggregates made from XA with a DS of 2.0 was significantly different. Additionally, the carbohydrate composition of the insoluble residues obtained after redissolving aggregates made from XA with a DS of 2.0 was similar to that of the initial beechwood xylan. In the case of beechwood xylan and XA with a DS of 1.0, they were found to contribute to the formation of Type B IGP. However, there was a difference observed in the glucose content in the carbohydrate composition of Type B IGP.

In combination FTIR and MVA could be used to identify trends in the six starting materials and nine Type B IGP. The FTIR spectral features of the insoluble residues identified with PCA were effective in distinguishing different types of starting materials and insoluble residues. Further information about the carbohydrate content of insoluble residues, regardless of the overall DS, could be extracted using PLS analysis. These findings could have important implications for the

industrial production of CA and contribute to the development of more efficient production processes.

## REFERENCES

- [1] S. Park, J.O. Baker, M.E. Himmel, P.A. Parilla, D.K. Johnson, Cellulose crystallinity index: measurement techniques and their impact on interpreting cellulase performance, *Biotechnology for biofuels* 3(1) (2010) 1-10.
- [2] I. Cumpstey, Chemical modification of polysaccharides, *International scholarly research notices* 2013 (2013).
- [3] P. Rustemeyer, 1. History of CA and evolution of the markets, *Macromolecular Symposia*, Wiley Online Library, 2004, pp. 1-6.
- [4] M. Granström, *Cellulose derivatives: synthesis, properties and applications*, (2009).
- [5] M. Kostag, M. Gericke, T. Heinze, O.A. El Seoud, Twenty-five years of cellulose chemistry: Innovations in the dissolution of the biopolymer and its transformation into esters and ethers, *Cellulose* 26(1) (2019) 139-184.
- [6] H. Steinmeier, 3. Acetate manufacturing, process and technology 3.1 Chemistry of cellulose acetylation, *Macromolecular Symposia*, Wiley Online Library, 2004, pp. 49-60.
- [7] B. Caballero, L. Trugo, P. Finglas, *Encyclopedia of food sciences and nutrition: Volumes 1-10*, Elsevier Science BV2003.
- [8] C.M. Kuo, R.T. Bogan, Process for the manufacture of cellulose acetate, *Google Patents*, 1997.
- [9] T. Heinze, O.A. El Seoud, A. Koschella, *Cellulose derivatives: synthesis, structure, and properties*, Springer2018.
- [10] H. Nakayama, N. Fukakagawa, Y. Nishiura, T. Yasuda, T. Ito, K. Miyahashi, Development of low-retardation TAC film for protection films of LCD's polarizer, *Journal of photopolymer science and technology* 19(2) (2006) 169-173.

- [11] R. Candido, G. Godoy, A.R. Goncalves, Characterization and application of cellulose acetate synthesized from sugarcane bagasse, *Carbohydrate polymers* 167 (2017) 280-289.
- [12] M.M.L. Loo, R. Hashim, C.P. Leh, Recycling of valueless paper dust to a low grade cellulose acetate: effect of pretreatments on acetylation, *BioResources* 7(1) (2012).
- [13] S. Saka, K. Takanashi, Cellulose triacetate prepared from low-grade hardwood dissolving pulp and its insoluble residues in acetylation mediums, *Journal of applied polymer science* 67(2) (1998) 289-297.
- [14] Z. Yang, S. Xu, X. Ma, S. Wang, Characterization and acetylation behavior of bamboo pulp, *Wood Science and Technology* 42(8) (2008) 621-632.
- [15] E. Fleury, J. Dubois, C. Léonard, J. Joseleau, H. Chanzy, Microgels and ionic associations in solutions of cellulose diacetate, *Cellulose* 1(2) (1994) 131-144.
- [16] X. Chen, S. Xu, W. Peng, J. Zhang, Y. Jiang, ISOLATION AND CHARACTERIZATION OF ACETONE-INSOLUBLE SUBSTANCES IN CELLULOSE ACETATE PREPARED BY AN ACETIC ACID ACETYLATION PROCESS, *CELLULOSE CHEMISTRY AND TECHNOLOGY* 48(5-6) (2014) 477-483.
- [17] A.M. Stepan, A.W. King, T. Kakko, G. Toriz, I. Kilpeläinen, P. Gatenholm, Fast and highly efficient acetylation of xylans in ionic liquid systems, *Cellulose* 20(6) (2013) 2813-2824.
- [18] Scienomics, MAPS Platform, Version 3.4.2, France. 2015. Available online: <http://www.scienomics.com/> (accessed on 30 September 2016).
- [19] J. Wang, R.M. Wolf, J.W. Caldwell, P.A. Kollman, D.A. Case, Development and testing of a general amber force field, *Journal of computational chemistry* 25(9) (2004) 1157-1174.
- [20] Y. Shen, Z. Chen, H. Qi, Z. Ma, Y. Dai, Q. Zhao, Z. Zhu, Y. Ma, Y. Wang, Mechanism analysis of extractive distillation for separation of acetic acid and water based on quantum

- chemical calculation and molecular dynamics simulation, *Journal of Molecular Liquids* 332 (2021) 115866.
- [21] N.E. de Jesús-González, A. Pérez de la Luz, J. López-Lemus, J. Alejandro, Effect of the Dielectric Constant on the Solubility of Acetone in Water, *Journal of Chemical & Engineering Data* 63(5) (2018) 1170-1179.
- [22] S.S. Stachura, C.J. Malajczuk, R.L. Mancera, Molecular dynamics simulations of a DMSO/water mixture using the AMBER force field, *Journal of molecular modeling* 24(7) (2018) 1-8.
- [23] H. Berendsen, J. Grigera, T. Straatsma, The missing term in effective pair potentials, *Journal of Physical Chemistry* 91(24) (1987) 6269-6271.
- [24] S. Plimpton, Fast parallel algorithms for short-range molecular dynamics, *Journal of computational physics* 117(1) (1995) 1-19.
- [25] M.C. Payne, M.P. Teter, D.C. Allan, T. Arias, a.J. Joannopoulos, Iterative minimization techniques for ab initio total-energy calculations: molecular dynamics and conjugate gradients, *Reviews of modern physics* 64(4) (1992) 1045.
- [26] R.W. Hockney, J.W. Eastwood, *Computer simulation using particles*, crc Press 2021.
- [27] G.J. Martyna, D.J. Tobias, M.L. Klein, Constant pressure molecular dynamics algorithms, *The Journal of chemical physics* 101(5) (1994) 4177-4189.
- [28] M. Parrinello, A. Rahman, Polymorphic transitions in single crystals: A new molecular dynamics method, *Journal of Applied physics* 52(12) (1981) 7182-7190.
- [29] S.S. Jawalkar, K.V. Raju, S.B. Halligudi, M. Sairam, T.M. Aminabhavi, Molecular modeling simulations to predict compatibility of poly (vinyl alcohol) and chitosan blends: a comparison with experiments, *The Journal of Physical Chemistry B* 111(10) (2007) 2431-2439.

- [30] A. Sluiter, B. Hames, R. Ruiz, C. Scarlata, J. Sluiter, D. Templeton, D. Crocker, Determination of structural carbohydrates and lignin in biomass, *Laboratory analytical procedure* 1617(1) (2008) 1-16.
- [31] S. Vahur, L. Eero, J. Lehtaru, K. Virro, I. Leito, Quantitative non-destructive analysis of paper fillers using ATR-FT-IR spectroscopy with PLS method, *Analytical and bioanalytical chemistry* 411(20) (2019) 5127-5138.
- [32] L.F. Leopold, N. Leopold, H.-A. Diehl, C. Socaciu, Quantification of carbohydrates in fruit juices using FTIR spectroscopy and multivariate analysis, *Spectroscopy* 26(2) (2011) 93-104.
- [33] C.K. Pezzei, S.A. Schönbichler, C.G. Kirchler, J. Schmelzer, S. Hussain, V.A. Huck-Pezzei, M. Popp, J. Krolitzek, G.K. Bonn, C.W. Huck, Application of benchtop and portable near-infrared spectrometers for predicting the optimum harvest time of *Verbena officinalis*, *Talanta* 169 (2017) 70-76.
- [34] S.M. Clegg, E. Sklute, M.D. Dyar, J.E. Barefield, R.C. Wiens, Multivariate analysis of remote laser-induced breakdown spectroscopy spectra using partial least squares, principal component analysis, and related techniques, *Spectrochimica Acta Part B: Atomic Spectroscopy* 64(1) (2009) 79-88.
- [35] S. Kishani, A. Escalante, G. Toriz, F. Vilaplana, P. Gatenholm, P. Hansson, L. Wagberg, Experimental and theoretical evaluation of the solubility/insolubility of spruce xylan (Arabino glucuronoxylan), *Biomacromolecules* 20(3) (2019) 1263-1270.
- [36] K. Ueda, S. Saka, Y. Funaki, S. Soejima, Characterization of acetone-insoluble substances in cellulose acetate as prepared by an acetylation; ripening process from wood pulps, *Journal of the Japan Wood Research Society* (1988).

- [37] A. Koubaa, Z. Koran, Effect of press-drying parameters on paper properties, *Pulp and Paper Processing*, IntechOpen2018, pp. 87-107.
- [38] T. Hansson, C. Fellers, M. Htun, Drying strategies and a new restraint technique to improve cross-directional properties of paper, *Fundamentals of Papermaking. Trans. 9 th Fund. Res. Symp*, 1989, pp. 743-781.
- [39] P. Przybysz, M. Dubowik, M.A. Kucner, K. Przybysz, K. Przybysz Buzala, Contribution of hydrogen bonds to paper strength properties, *PloS one* 11(5) (2016) e0155809.
- [40] M.A. Hamdan, N.A. Ramli, N.A. Othman, K.N.M. Amin, F. Adam, Characterization and property investigation of microcrystalline cellulose (MCC) and carboxymethyl cellulose (CMC) filler on the carrageenan-based biocomposite film, *Materials Today: Proceedings* 42 (2021) 56-62.
- [41] C.A. Hunter, Quantifying intermolecular interactions: guidelines for the molecular recognition toolbox, *Angewandte Chemie International Edition* 43(40) (2004) 5310-5324.
- [42] M.R. Plata, C. Koch, P. Wechselberger, C. Herwig, B. Lendl, Determination of carbohydrates present in *Saccharomyces cerevisiae* using mid-infrared spectroscopy and partial least squares regression, *Analytical and bioanalytical chemistry* 405(25) (2013) 8241-8250.
- [43] M. Kurzyna-Szklarek, J. Cybulska, A. Zdunek, Analysis of the chemical composition of natural carbohydrates—an overview of methods, *Food Chemistry* (2022) 133466.

## CHAPTER 5

### Predicting the Quality of Cellulose Acetate for Impurity Analysis of the Cotton Linter Pulp

#### Abstract

It is generally accepted that residual impurities in a dissolving pulp causes issues with both the quality of cellulose acetate and the overall processability of commercial cellulose acetates (CAs). Thus, understanding the chemical characteristics of a feedstock is necessary to enhance both the quality and processability. To fully understand the features of cotton linter pulps that impact the quality of cellulose derivatives, especially CAs, fiber fractionation was performed using the Bauer-McNett fiber classifier with three different cotton linter feedstocks. After fractionation, Fiber Quality Analyzer (FQA) and carbohydrate composition analyses were used to evaluate the effects of fractionation, and differences between the cotton linter pulps. The three cotton linter pulps were then used to prepare CAs, and the quality of the CA was determined by measuring the weight fraction of acetone insoluble substances in the CA. The quality of the CA was related to the xylan content of the starting cotton linter pulps. However, differences in xylan content, which varied between 0.80 and 0.9 wt. % did not provide a complete explanation for the amount of acetone insoluble substances. Consequently, a secondary test to measure the amount of sulfuric acid insoluble substances (SIS) was developed to evaluate the discrepancy. The combination of residual xylan and SIS were correlated with the acetone insoluble substances in the resulting CAs. Based on these results, we proposed a simple method to estimate the quality a cotton linter pulps used to produce CA.

## 1. Introduction

Cellulose is a valued feedstock for production of a wide array of derivative that are then used for production of films, fibers, thermoplastics and water-soluble applications. As the demand by high-tech industries for cellulose-based materials has increased, high-quality feedstocks have become more important [1-3]. High quality products, in particular optical films, can be negatively impacted by a small amount of impurities such as residual hemicelluloses and lignin. For example, residual hemicelluloses can form insoluble gel particles (IGP) which have adverse impacts on the complete solubility of cellulose acetates (CA) [4-8]. Residual hemicelluloses interfere with process control protocols during cellulose acetylation by causing false viscosity [7, 9]. Moreover, xylan acetates cause changes in the color of CAs, leading to problems in the performance of CA in optical films [7, 10]. For these reasons there have been extensive efforts to find suitable candidates for producing high-quality cellulose. Among potential candidates, cotton linters, which are by-product of cotton ginning process, have drawn attention because cotton linter cellulose is known to have very high purity directly from the plant [11]. Due to this high purity, cotton linter cellulose is used for producing many value-added cellulose based products [11, 12].

To properly control the production of cellulose derivatives, there is a need for quantifying the quality cellulose feedstocks with the performance of the resulting cellulose esters, especially CAs. Many researchers have attributed non-cellulosic impurities such as hemicelluloses and lignin found in all wood pulps to the quality problems in cellulose esters [13-16]. While the standard pulping processes that are effective for removing hemicelluloses and lignin, it is economically and technically impractical to completely remove the hemicelluloses

and lignin [17]. Therefore, small amounts of hemicelluloses and lignin remain in the dissolving pulps. However, a pulp made from cotton linters has a negligible amount of lignin in the native fiber, so these quality issues must be derived from other impurities [11, 18]. The residual xylan has been identified as the root cause of IGP [6, 19]. However, industrial experience suggests that the xylan content alone does not correlate with the quality of the resulting CA. Therefore, it is necessary to identify other cotton linter pulps' properties to better predict the relationship between cotton linter pulps' quality and the quality of the resulting CA. One notable fact is that the removal of SIS and the resulting improvement in the quality of a cotton linter dissolving pulp has been reported [20]. In this work, the presence of residual hemicelluloses and SIS, individually or in combination, was tested to explain the relationship between cotton linters pulp quality and the quality of the resulting CA.

## **2. Materials and Methods**

### **2.1. Materials**

Three different commercial samples of cotton linter pulps were obtained (named A, B, and C). Reference CA (CA398-30) with a degree of substitution (DS) of 2.45 was provided by Eastman. The CA were produced using the commercial heterogeneous process that produces a fully acetylated intermediate with a degree of substitution (DS) of 3.0, which is then hydrolyzed back to a final DS of 2.45. The CA dope is then precipitated and dried [19, 21]. Sulfuric acid, acetic acid, acetic anhydride, sodium bisulfate, and acetone were purchased from Fisher Scientific and utilized as received (Pittsburgh, PA).

## 2.2. Fiber Fractionation of Cotton Linter Pulps

9 g of oven-dried cotton linter pulps were soaked in DI water for 4 hours and fully disintegrated before introducing them into the Bauer-McNett fiber classifier. The Bauer-McNett fiber classifier comprises five compartments equipped with screens that have different sized holes (1.41, 0.64, 0.32, 0.16, and 0.074 mm) as illustrated in Figure 1. The cotton linter pulps were fractionated into six fractions based on the length of fibers, including a residual fines fraction, which can pass the last screen (0.074 mm). Fibers whose diameter were greater than a screen hole opening cannot pass through holes and were retained in a compartment. Screened fibers were collected from the compartment by vacuum filtration, then, oven-dried at 105 °C for 24 hours. A fiber quality analyzer (FQA) was used to confirm the average fiber length and the length distribution of fractionated fibers. To make the FQA measurement, 1 g of each oven-dried fractionated fibers was introduced into 1 L of DI water and disintegrated. The disintegrated samples were diluted enough to set fiber frequency value under 15.

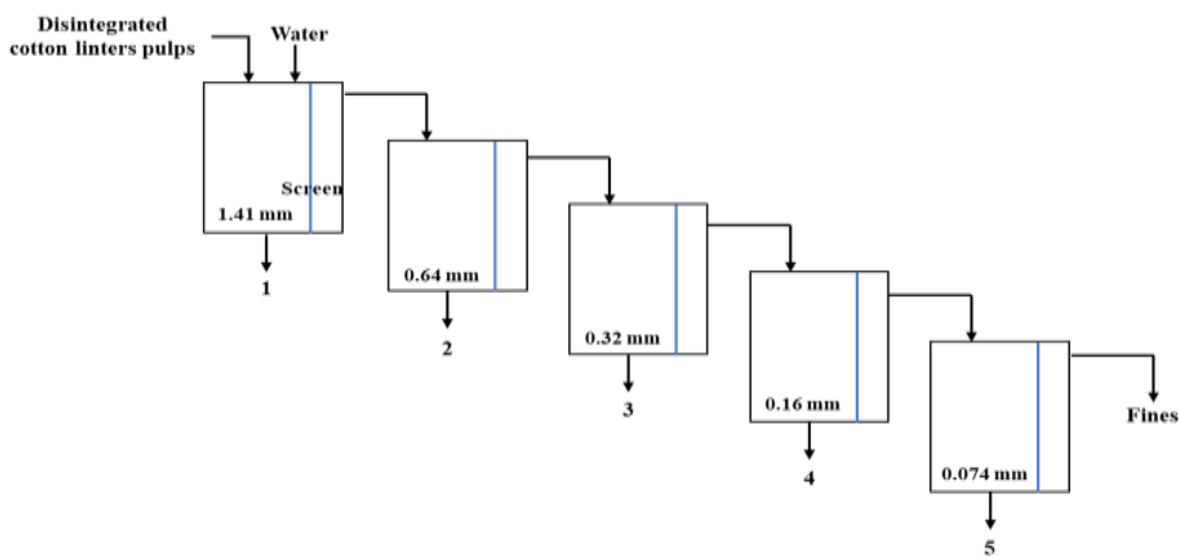


**Figure 5.1.** Schematic drawing of Bauer-McNett fiber classifier

### **2.3. Carbohydrate Composition Analysis of Fractionated Fibers**

Samples for carbohydrate composition analysis were prepared following a protocol suggested by National Renewable Energy Laboratory [22]. Briefly, each fractionated fiber (collected from the compartment 1 ~ 5, and fine) was hydrolyzed by introducing 3 ml of 72 % H<sub>2</sub>SO<sub>4</sub> at 30 °C for 1 hour. Then, the concentration of H<sub>2</sub>SO<sub>4</sub> in the solutions was adjusted to 4 % by adding DI water. Secondary hydrolysis was conducted at 121 °C for 1 hour using an autoclave. The pH of the hydrolysates was neutralized with CaCO<sub>3</sub>, and the concentration of monomeric sugars was quantified by Agilent 1200 HPLC equipped with Shodex sugar SP0810 column.

### **2.4. Turbidity of Hydrolysates and Sulfuric Acid Insoluble Substances**

The turbidity of the solutions was determined by the LaMotte 1970-ISO 2020WI ISO compliant portable turbidity meter. Calibration of the turbidity meter was done with 0 FNU and 10 FNU standards. Aqueous sulfuric acid solutions (4 wt. %) were filtered through a 0.2 μm syringe filter and used as a blank. To obtain the weight fraction, SIS in the solutions were collected by vacuum filtration with a fine-grade crucible filter. The recovered SIS was rinsed with DI water several times to remove sulfuric acid thoroughly, then oven-dried at 105 °C for 24 hours and weighed.

### **2.5. Cellulose Acetates Preparation and Quality Measurement**

Three cotton linter pulps and also the long fiber fraction from Sample C were used to prepare CA. To increase the efficiency of activation of samples, each sample was initially

pulverized with a IKA MF 10.2 impact grinding head lab mill. The CA synthesis was conducted following published methods [19, 21]. Briefly, a cotton linter pulp (1 part) was activated with DI water at room temperature for 1 hour, and the water was exchanged with acetic acid. Then, 12 parts of acetic acid with 0.15 parts of sulfuric acid and 0.02 parts of sodium bisulfate that acted as a catalyst and co-catalyst respectively were thoroughly mixed and added to activated cotton linter pulps. The actual acetylation was accomplished with five parts of acetic anhydride. The mixture was heated up to 50 °C to initiate the reaction. After 1 hour, sulfuric acid was neutralized, and four parts of 88% of aqueous acetic acid solution (88 wt. % of acetic acid and 12 wt. % of water) was slowly added to convert any remaining acetic anhydride to acetic acid. The solution was reacted approximately 2~3 hours at 55 °C until reaching desired DS (2.4~2.5). The CA was recovered by adding DI water and repeatedly washing to remove residual salts and acid. The final CA was oven-dried at 60 °C for 24 hours.

The quality of the CAs was determined by the weight fraction of acetone insoluble substances, which is often referred to as insoluble gel particle (IGP). These were determined by dissolving 900 mg of each synthesized CA in 29.1 g of acetone. After placing the samples on a shaker for 6 hours, IGP was collected by using a centrifuge at 4,400 rpm for 6 hours. IGP was washed with acetone 3 times and oven-dried at 60 °C for 24 hours.

## **2.6. Degree of Substitution of CAs**

The DS of the CAs was calculated by a method proposed elsewhere [23]. Before measuring DS, CAs were vacuum-dried at 50 °C overnight. A vacuum-dried CA sample (0.5 g) was introduced in 50 ml of 75 % aqueous ethanol solution. Then, 50 ml of 0.5 M sodium

hydroxide solution was added to the mixture. The mixture was kept at room temperature (23 °C) for 24 h. The titration was conducted with 0.5 M hydrochloric acid solution containing a trace amount of phenolphthalein as an indicator until the color of the indicator disappeared. The same experiment was conducted without the CA sample and set as a controlled experiment. The weight of acetic acid and DS were determined by the following equations.

$$\text{Weight of acetic acid} = [(D - C) \times C_{HCl} + (A - B) \times C_{NaOH}] \times 6.005/W$$

$$\text{Weight of acetic acid} = 6000 \times DS / (162 + 42 \times DS)$$

Where, *A* and *B* are the required volumes (mL) of NaOH for a CA sample and a controlled experiment (without CA), respectively; *C* and *D* are the volumes (mL) of HCl employed for the titration of a CA sample and a controlled experiment;  $C_{HCl}$  and  $C_{NaOH}$  is the molar concentration of HCl and NaOH solution, respectively; *W* is the weight of vacuum-dried CA sample.

## 2.7. Formation of IGP with SIS

IGP-free commercial DS 2.45 cellulose acetate was designated as a reference material to eliminate any influences of the IGP. To obtain IGP-free CA, one gram of the commercial CA was dissolved in 29.1 g of acetone. Pre-existing IGP fraction was removed by centrifugation at 4,400 rpm for 6 hours. Then, IGP-free CA was obtained by pouring the supernatant into DI water and oven-dried at 60 °C for 24 hours.

SIS was produced from cotton linter dissolving pulps. Briefly, one g of a cotton linter dissolving pulp were treated with nine ml of 72 % sulfuric acid at 30 °C for one hour. Then, the solution was transferred to a flask and diluted to 4 % by introducing a predetermined amount of water. Secondary hydrolysis was conducted using an autoclave at 121°C for one hour. SIS in the hydrolysate was collected by centrifugation at 4,400 rpm for 10 min. Then, the SIS was rinsed with DI water 3 times.

One gram of IGP-free CA was re-dissolved in 29 g of acetic acid. After the CA was fully dissolved, 100 mg of SIS was introduced to the solution. The mixture was placed on a shaker for 6 hours to disperse SIS properly. To precipitate dissolved CA, an excess amount of DI water was added to the mixture, which was then oven-dried at 60 °C for 24 hours. To examine the formation of SIS nucleated IGP, the oven-dried CA was re-dissolved in acetone. The insoluble substances were recovered by centrifugation at 4,400 rpm for 6 hours. Collected insoluble substances were rinsed with acetone three times and oven-dried at 60 °C for 24 hours.

## **2.8. SIS and SIS-based IGP Characterization**

The recovered SIS were oven-dried at 60 °C for 24 hours and manually ground for the next step. Solubility of SIS in acetic acid and acetone were measured by adding 20 mg of SIS to two ml of pure acetic acid or acetone. The mixtures were placed on a shaker for 6 hours. After that, the undissolved fraction was recovered by centrifugation, rinsed with ethanol three times, and oven-dried at 105 °C overnight and the weight loss measured.

PerkinElmer Spectrum 3 spectrometer equipped with attenuated total reflectance (FTIR-ATR) was used to verify the functional groups present in the SIS and SIS-based IGP. Samples were

scanned 16 times range from  $650\text{ cm}^{-1}$  to  $4000\text{ cm}^{-1}$  at a resolution of  $2\text{ cm}^{-1}$ . Malvern Zetasizer Nano ZS equipped with a back-scattering detector (DLS) was utilized to compare the particle size of two different IGP. One IGP was isolated from the commercial CA 398-30, and the second was IGP-free CA with the SIS added back to the sample.

### **3. Results and Discussions**

#### **3.1. Characterization of Fractionated Cotton Linter Pulp Fibers**

The three different cotton linter pulps labeled A, B, and C for the convenience. The FQA confirmed that the Bauer-McNett fiber classifier properly fractionated cotton linter pulps by the length of fibers (Table 1). As shown in Table 1, samples A and B exhibited no significant differences in terms of the wt. % of fractionated fibers. Also,  $L_w$  of both unfractionated (utilized as received without fractionation) A (1.73 mm) and B (1.70 mm) cotton linters pulp was equivalent as well. In contrast, the overall  $L_w$  of unfractionated C (1.52 mm) cotton linters pulp was shorter than those of A and B cotton linters pulps. Sample C contained 10 wt. % less long fibers recovered from compartment 1, however, it had more fibers collected in fractions 2, 3, and 4. There was a noticeable difference between samples A and B, and sample C in terms of the wt. % of short fibers. Combining the mass recovered from compartment 5 and the fines, sample C had roughly two times more short fiber (8.8 wt. %) than samples A and B.

It was reported that SIS was included in a cotton linter pulp [20]. However, their work did not specify which fraction of the cotton linter pulp contained the most SIS. After the fiber fractionations, two-step hydrolysis was carried out on each fraction. Based on the turbidity of two-step hydrolysate solutions (Figure 2), the SIS were primarily associated with the short fibers

(screened from 5 and fine). Hydrolysis of the long fibers (screened from compartment 1 ~ 4), produced relatively clear solutions, SIS free solutions, as shown in Figure 2 for cotton lint sample C (Images for the samples derived from cotton lint A and B are shown in the supplemental materials). Based on the turbidity of the hydrolyzed solutions, the presence of the SIS was dominated by the fraction screened from compartment 5 and fines. In this study, for the convenience of comparison, short fibers were newly defined as fibers that produced SIS during the two-step hydrolysis with sulfuric acid.

**Table 5.1.** Length weight mean length and weight fraction of each fractionated cotton linters pulp

FQA	A		B		C	
	$L_w$ (mm)	wt. % of fibers	$L_w$ (mm)	wt. % of fibers	$L_w$ (mm)	wt. % of fibers
<b>1</b>	$2.36 \pm 0.09$	$72.0 \pm 0.5$	$1.88 \pm 0.03$	$71.8 \pm 2.0$	$2.13 \pm 0.050$	$61.9 \pm 0.8$
<b>2</b>	$1.76 \pm 0.04$	$9.5 \pm 0.4$	$1.75 \pm 0.04$	$9.0 \pm 0.1$	$1.59 \pm 0.051$	$10.5 \pm 0.1$
<b>3</b>	$1.19 \pm 0.03$	$9.5 \pm 0.3$	$1.10 \pm 0.02$	$10.0 \pm 0.1$	$1.06 \pm 0.024$	$12.2 \pm 0.6$
<b>4</b>	$0.76 \pm 0.01$	$4.6 \pm 0.3$	$0.71 \pm 0.03$	$4.6 \pm 0.1$	$0.71 \pm 0.011$	$6.6 \pm 0.3$
<b>5</b>	$0.56 \pm 0.01$	$1.6 \pm 0.1$	$0.55 \pm 0.01$	$1.7 \pm 0.1$	$0.49 \pm 0.009$	$2.8 \pm 0.2$
<b>Fine</b>	$0.25 \pm 0.01$	$2.7 \pm 0.1$	$0.21 \pm 0.01$	$2.9 \pm 0.3$	$0.24 \pm 0.005$	$6.0 \pm 0.2$
<b>Whole</b>	$1.73 \pm 0.02$	-	$1.70 \pm 0.06$	-	$1.52 \pm 0.031$	-

Where,  $L_w$  = Length weight mean length of fiber i

Carbohydrate composition analyses were performed to measure differences in carbohydrate composition of the fractionated cotton linters pulps. Quantification of arabinan and mannan was computed as the sum of both monomeric sugars because they had a similar retention time in the IC system used for this work [24]. The impact of the lignin fraction was neglected because it was reported that the amount of lignin contained in a cotton linters pulp is insignificant [11, 18]. In contrast, the amount of hemicelluloses in cotton linters pulp is

important because the quality of CA is reported to be related to the amount of the residual hemicelluloses in a feedstock, in particular the xylan content [6, 8]. The weight percent of hemicelluloses in the fractionate fibers and fiber length show the opposite trends (Table 1 and 2). The mass of hemicelluloses increased as the length of the fibers decreased. However, when considering the relative mass of each fraction, most of the hemicelluloses were contained from the longest fibers (screened from 1).

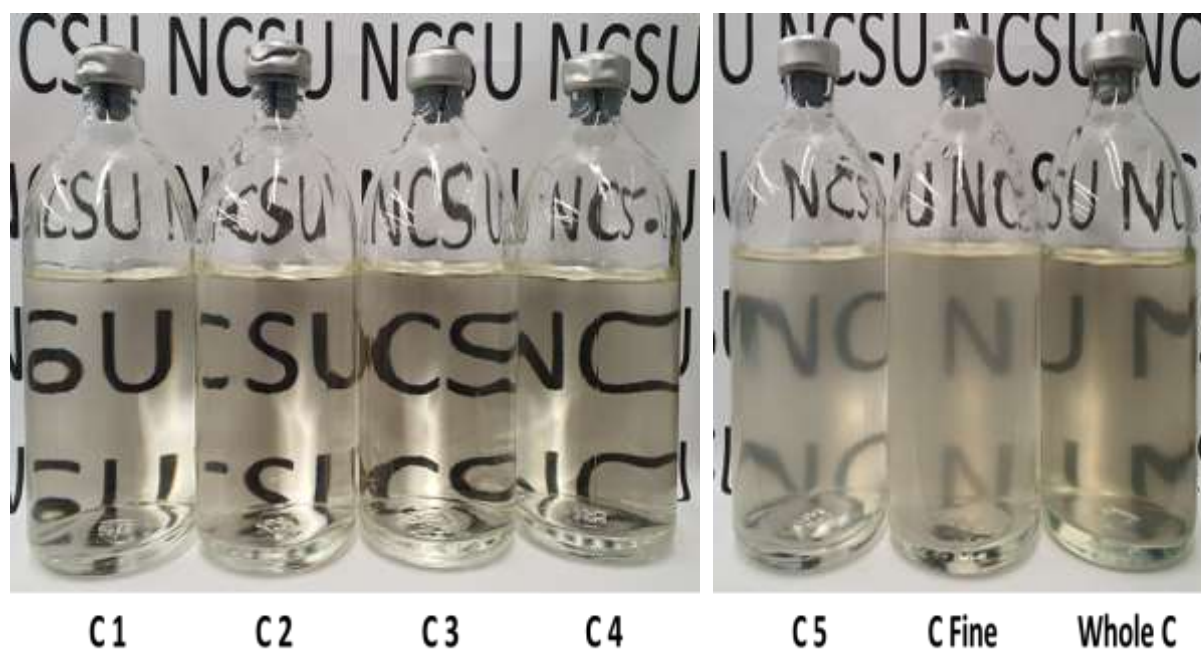


**Figure 5.2.** Two-step hydrolysate solutions produced from long fibers (left) and short fibers (right)

\* Whole C represents unfractionated cotton linter dissolving pulp C

From a quality control the perspective CAs, most researchers have focused on understanding the role of the xylan in the formation of IGP [6, 19, 25]. Based on the results in Table 2, the xylan content in the fractions isolated from all three cotton linter pulps increased as the fiber length decreased. However, when considering the total amount of xylan in the samples

the longer fibers with their lower xylan content dominate the total xylan content. This is due to the very large percentage of the total mass isolated in the long fiber fraction.

**Table 5.2.** Carbohydrate composition of fractionated cotton linter fibers

Carbohydrate composition	Hemicelluloses (wt. %)				Glucose (wt. %)
	Xylan	Galactan	Ara/Mannan	Sum of Hemi	
A_1	0.7	0.3	0.6	1.6	98.2
A_2	0.7	0.4	0.7	1.8	97.9
A_3	0.8	0.6	0.7	2.0	97.6
A_4	1.0	0.6	0.5	2.0	97.5
A_5	1.3	0.7	0.5	2.4	96.8
A_Fine	1.8	0.6	0.6	3.0	93.5
A_Whole	0.8	0.6	0.6	2.0	95.8
B_1	0.6	0.4	1.0	2.0	97.7
B_2	0.8	0.5	1.3	2.6	96.4
B_3	0.7	0.4	0.8	1.9	97.8
B_4	0.9	0.9	1.3	3.1	96.5
B_5	1.0	0.7	1.4	3.1	95.7
B_Fine	1.3	0.9	0.9	3.0	92.3
B_Whole	0.8	0.4	1.0	2.2	94.3
C_1	0.6	0.6	0.7	1.9	98.2
C_2	0.6	0.4	0.7	1.8	98.0
C_3	1.0	0.3	0.9	2.2	97.6
C_4	1.0	0.4	0.6	2.0	97.7
C_5	1.2	0.4	0.6	2.3	95.8
C_Fine	1.7	0.3	0.6	2.8	90.4
C_Whole	0.9	0.4	0.6	1.9	93.9

### 3.2. Quality of Cellulose Acetates

**Table 5.3.** Degree of substitution (DS) and the turbidity of synthesized cellulose acetates in acetone

	Cellulose Acetate			
	A	B	C	C_long
DS	2.47	2.43	2.49	2.46
IGP (wt. %)	1.8	2.9	5.0	2.1

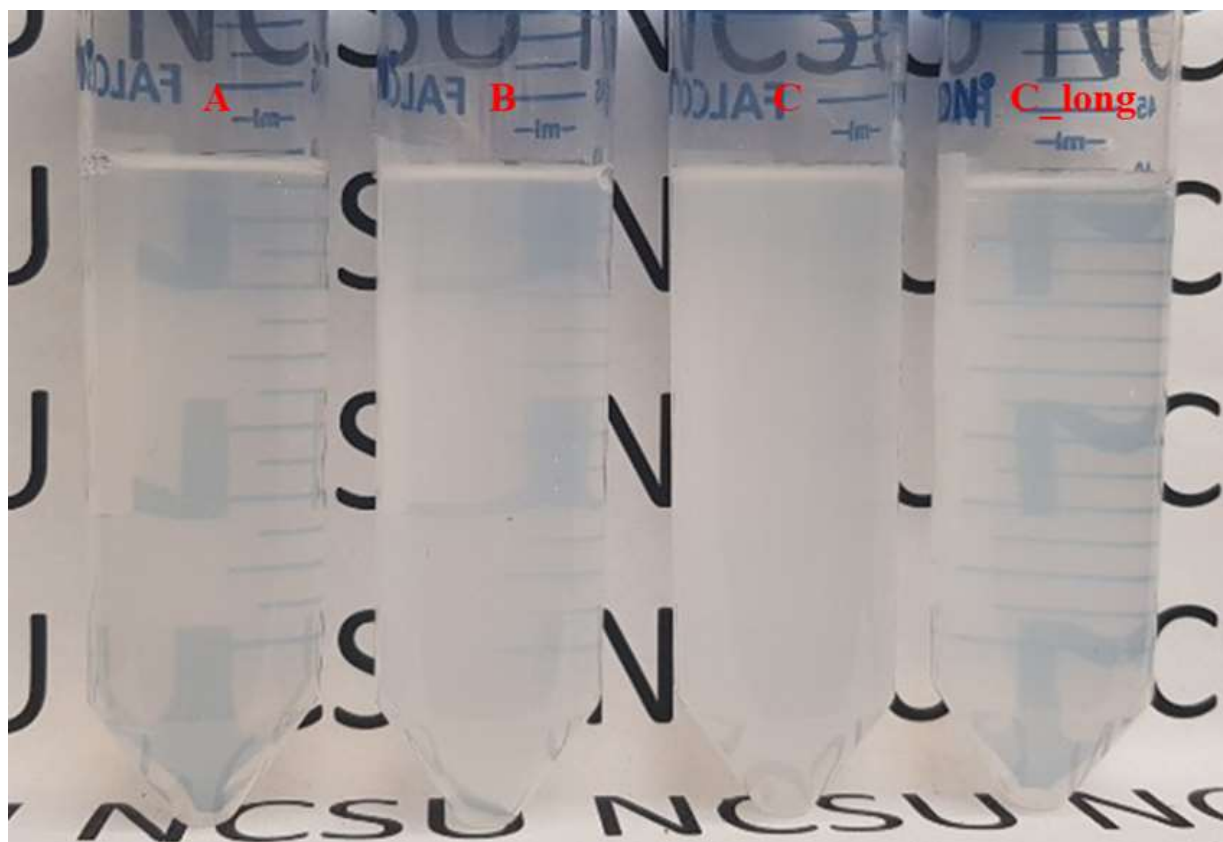


**Figure 5.3.** Cellulose acetate acetone solutions

Before carrying out acetylation, cotton linters pulps were pulverized to increase the overall efficiency of both activation and acetylation [26, 27]. Improper activation causes uneven acetylation which eventually hinders dissolution of CA in acetone [15] and the grinding step was used to minimize the influence of improper activation to the formation of IGP [28].

After the acetylation, the quality of the CA was measured by means by dissolution in acetone. Difference in the turbidity of the CA-acetone solutions are shown in Figure 3. The presence and the amount of IGP in a CA solution dominate the turbidity of the solution. The results in Figure 3, also suggest that sample C produces the worst quality CA. The quality of CA was quantified by measuring the mass of IGP in the CA-acetone solutions collected via centrifugation. The amount of IGP in each solution was listed in Table 3. As mentioned before, xylan plays an important role in the formation of IGP. However, even though a difference in the amount of the xylan in each unfractionated cotton linters pulp is insignificant (A: 0.8 %, B: 0.8%, C: 0.9%), samples B and C produce 1.6 times and 3 times more IGP than sample A, respectively. Considering the amount of the cotton linters pulps used for acetylation (15 g), 0.1 wt. % difference in xylan is not enough to explain a discrepancy in the amount of produced IGP among cotton linter pulps.

Based on the lack of differences in the total mass of xylan between the samples and the significant difference in the turbidity, we looked for other features of the cotton linter pulps that could help explain the turbidity. During CAs manufacturing, the lack of solubilities of xylan acetates in acetic acid is a root factor that has caused the formation of IGP. It was found that SIS had a similarity to the solubility of xylan acetates in acetic acid. Therefore, SIS was suspected as a possible contributing cause that could possibly act like hemicellulose acetates, especially xylan acetate, during the acetylation process. Since the SIS was mainly contained in short fibers (5 and fine) a CA was prepared from a combination of long fibers (1:2:3:4 = 1:1:1:1 based on oven-dried weight). The resulting CA was less turbid and had a significant decrease in the amount of isolated IGP (2.1 wt. %) compared to the one produced from unfractionated C cotton linters pulp (5.0 wt. %).

### **3.3. Proposing a Mechanism for Explaining the Formation of IGP with SIS**

Two different mechanisms for the formation of IGP have been proposed in the literature. One mechanism is related to the incomplete acetylation of cellulose and hemicelluloses, especially xylan acetate, and the resulting poor acetone solubility of these heterogeneously substituted polymers. Those collective substances are called IGP [19, 29]. The other mechanism is the fundamental poor solubility of xylan acetates in acetic acid and acetone results in the formation of IGP. After the hydrolysis process, homogeneously substituted CA dissolve in acetic acid. In contrast, xylan acetates are not soluble in acetic acid or acetone, regardless of DS. The precipitation process with water is employed in this experimental work to recover CA from the acetic acid reaction solution. This precipitation has the potential for the xylan acetates (XA) to entrain CA into aggregates. Even though uniformly acetylated CA which is highly soluble in acetone is utilized for the formation of CA/XA aggregates, once these CA/XA aggregates are subjected to re-dissolution in acetone, some fractions of the aggregates become undissolved and recovered as IGP. These IGPs show significant differences in the carbohydrate composition compared to that of XA, which represents that the IGPs consist of CA and XA. To elucidate a mechanism of formation of IGP with SIS, an experimental procedure proposed elsewhere was utilized.

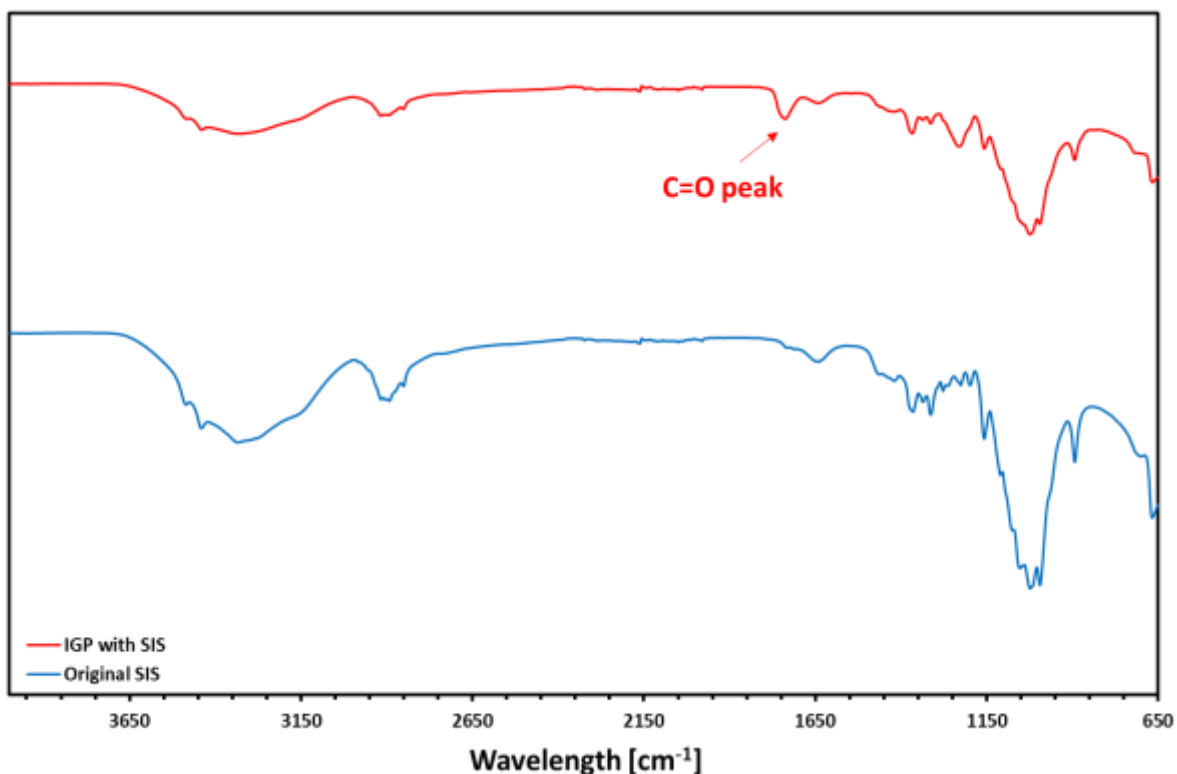


**Figure 5.4.** FT-IR spectra obtained from original SIS and IGP made from SIS

Based on the previous work, there are two prerequisites required for the formation of IGP: the inherent lack of XA solubility in both acetic acid and acetone, and the presence of functional groups that can act as both hydrogen bonding donors and acceptors. SIS and XA showed a similar lack of solubility in both acetic acid and acetone. Thus, SIS could act like XA and form aggregates during the precipitation process. These aggregates also have the potential for intermolecular hydrogen bonded interactions between SIS and CA. Based on the IR spectrum of SIS alone, broad peaks originating from hydroxyl groups were observed between  $3150\text{ cm}^{-1}$  and  $3650\text{ cm}^{-1}$  [30]. With these hydroxyl groups, SIS could interact with CA via hydrogen bonds within aggregates. Based on the IR spectrum and solubility data, CA aggregated with SIS could

be an additional source of the IGP, or the additional interactions between CA and SIS could increase the size of the aggregates.

To further investigate these interactions, a series of precipitation experiments were performed using the method proposed elsewhere. Commercial CA flakes (DS 2.45) were utilized as a reference material. The pre-existing IGP fractions in this commercial reference material were thoroughly removed via centrifugation to eliminate the influences of pre-existing IGP. SIS was completely dispersed in the IGP-free CA acetic acid solution, and then the mixture was precipitated. After precipitation, to examine the formation of IGP, the CA/SIS aggregates were subjected to re-dissolution in acetone. Then, residual acetone insoluble substances were collected with centrifugation. If the strength of interactions between CA and SIS is weaker than interactions between CA and acetone, then, the CA fraction would dissolve during re-dissolution and washing. Consequently, any remaining insoluble substances would be solely made of SIS. The FTIR spectrum of the insoluble substances confirmed the presence of both SIS and CA. A peak near  $1730 - 1740 \text{ cm}^{-1}$  which was assigned to carbonyl group was not observed from the IR spectrum of the original SIS [31]. Whereas IGP made with SIS showed a signature of C=O in carbonyl groups originating from captured CA. This is consistent with the presence of CA in the acetone insoluble residue [31].

The size of the IGP in acetone is of importance because the drying spinning method is commonly employed to produce CA fiber [32]. In this dry spinning process, the acetone solution of CA passes through holes in a fiber spinneret. Large IGP will plug the holes spinneret leading to a lower quality fiber product [33, 34]. If particle sizes of the IGP made from SIS-generated aggregates are significantly smaller than the one made from XA, SIS-based IGP could pass through holes of the spinneret. Smaller SIS-based IGP might not cause problems with the

spinning process. DLS was used to compare the sizes of IGP in commercial CA and IGP originated from SIS. As shown in Figure 5, the average size of SIS-based IGP is slightly larger than IGP in the commercial CA indicating that the SIS-based IGP also have the potential risk to block holes in a fiber spinneret.

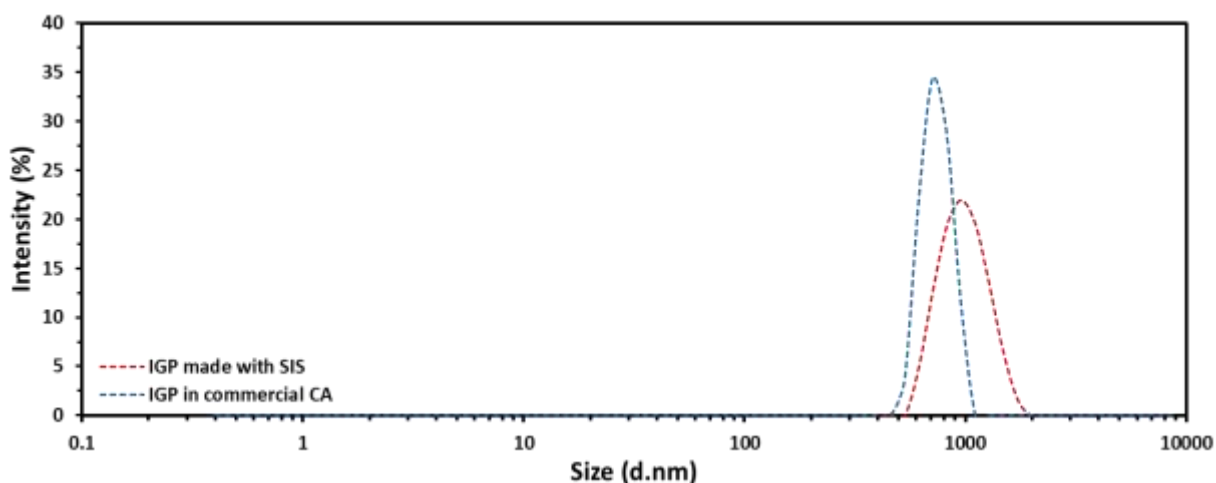


**Figure 5.5.** Size distribution of IGP measured by DLS

### **3.4. Proposing a Method to Predict the Quality of CA Synthesized from Cotton Linter**

#### **Dissolving Pulps**

This work shows that IGP can be attributed to both the presence of residual xylan, and SIS. Therefore, when establishing a correlation between potential of a feedstock and the quality of resulting CA, both these factors need to be taken into account. After two-step hydrolysis, the amount of SIS in the cotton linters showed noteworthy differences between feedstocks. Cotton linter pulp B and C contained 1.6 and 2.1 times more SIS compared to cotton linter pulp A, respectively. One of the disadvantages of the vacuum filtration method is the time required to collect and oven-dry SIS. To overcome the shortcoming of the time required to

isolate and recover the SIS fraction, an alternative method for measuring the SIS directly from a hydrolysate solution was evaluated. Given the strong positive correlation between the amount of IGP and turbidity of CA-acetone solutions (Table 3 and Figure 3), the turbidity of two-step hydrolysates was measured to test the correlation between the amount of SIS in each two-step hydrolysates. As shown in Figure 6a there was a strong ( $R^2 = 0.852$ ) positive correlation.

Based on the overall results, a simple method to predict the quality of CA from features of a feedstock can be proposed. For these cotton linter feedstocks, with relatively low amounts of residual xylan, instead of using a wt. % of xylan as the sole variable, the sum of wt. % of xylan and the turbidity of the SIS hydrolysate can be utilized together to improve the prediction. As shown in Figure 6b, strong ( $R^2 = 0.972$ ) correlation was observed between two variables. By using this method, the quality of a final product can be estimated directly from characteristics of a raw material without performing actual acetylation.

**Table 5.4.** The amount of SIS in two-step hydrolysate and turbidity of the solutions

	Two-step hydrolysate solution		
	A	B	C
SIS (wt. %)	1.8	2.9	3.8
Turbidity (FNU)	6.31	7.33	11.52
Xylan (wt. %)	0.8	0.8	0.9

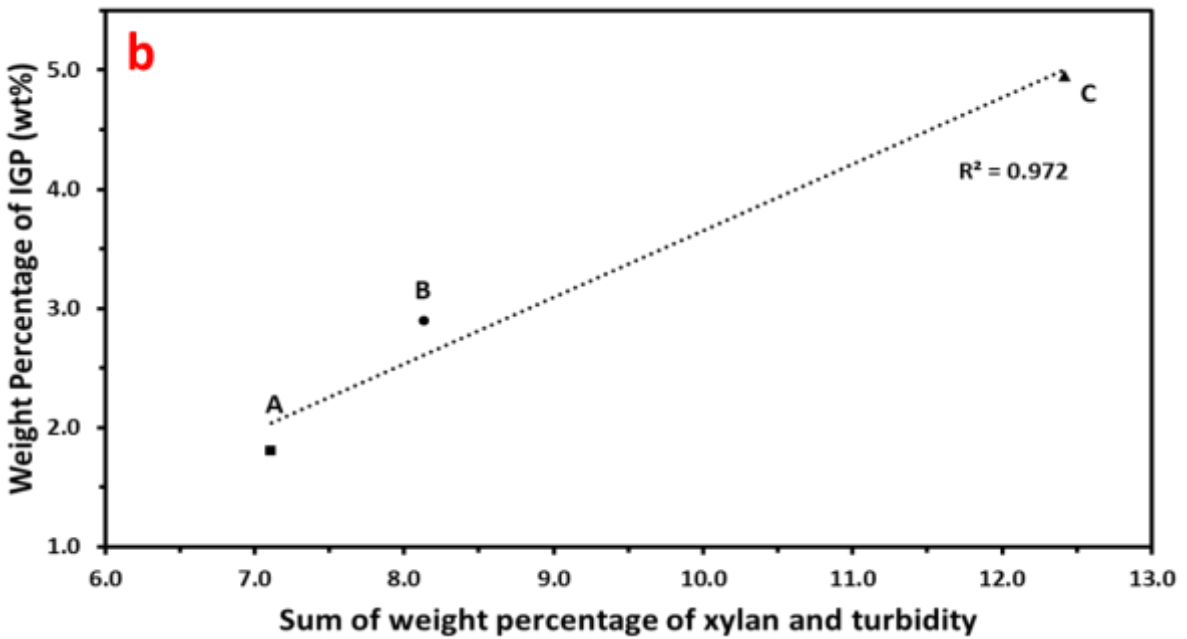
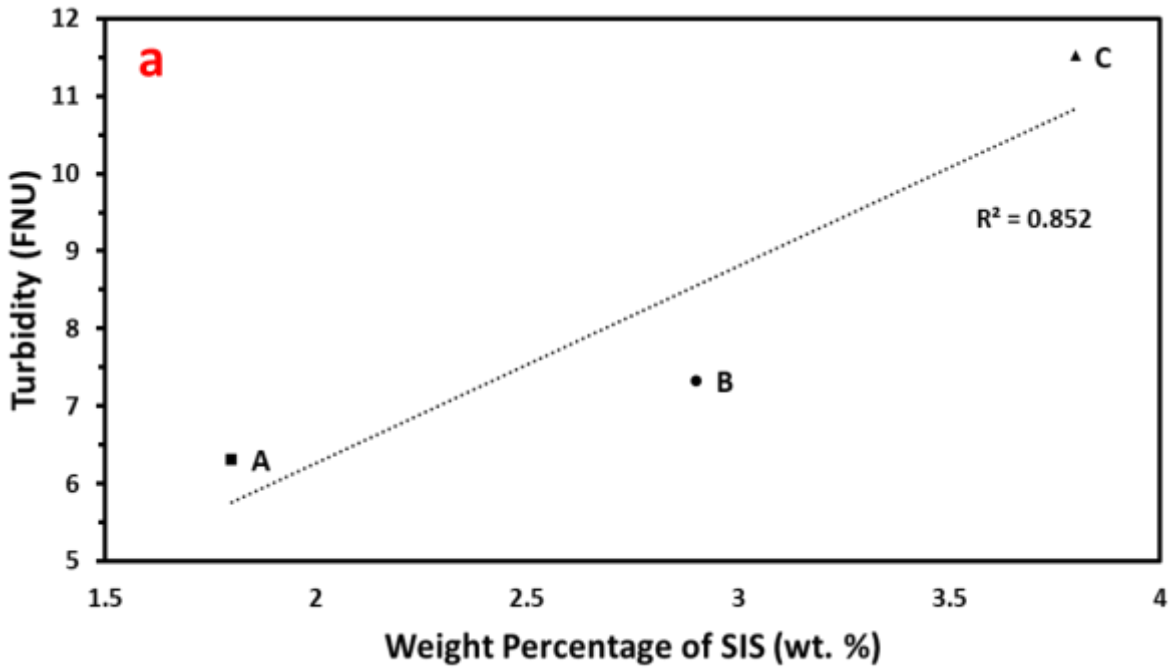


**Figure 5.6.** Correlation between (a) amount of SIS and turbidity and (b) Sum of wt. % of xylan and turbidity and amount of IGP

#### 4. Conclusion

Three different cotton linter dissolving pulps: A, B, and C were fractionated to understand the characteristics of the feedstocks. It was revealed that sample C had roughly 2 times more short fibers fraction relative to feedstocks A and B. In the past, researchers concerned with measuring the quality of a dissolving grade cellulose have mainly focused on the hemicelluloses, especially xylan, as a major source for formation of IGP. For all samples in this study, the contents of xylan increased with decreasing fiber length. However, considering the distribution of the total mass of xylan, the majority resided in longer fibers screened from compartment 1. The linters had very small differences in the total xylan content, contrasting to their relative significant differences in the turbidity of CA-acetone solutions suggested that there are other factors contributing to the IGP in CAs. The SIS were evaluated as a possible contributor to the differing turbidity results. To verify hypothesis the long fiber, low SIS fractions of Pulp C was acetylated. It was confirmed that the amount of IGP decreased if only long fiber, low SIS fraction is used for acetylation.

This work revealed that SIS could be a potential source that contributed to the formation of IGP. Even though IGP-free CA showed great solubility in acetone, if aggregates consisting of CA/SIS were formed during the precipitation, it was hard to achieve complete dissolution. The collected insoluble residues showed a signature peak assigned to C=O in acetyl groups that was not shown in the pristine SIS. This phenomenon represented that the SIS fraction in CA/SIS aggregates could capture adjacent CA via possibly hydrogen bonding, resulting in the formation of IGP during the re-dissolution in acetone. Lastly, we showed that the amount of IGP in the CA-acetone solutions was strongly correlated with the turbidity of SIS hydrolysis solutions. With this correlation, and also knowing the wt. % xylan, total amount of IGP recovered from a CA-acetone

solution could be predicted. This approach provides a simple, rapid method for estimating the quality of CA directly from the cotton linter feedstocks.

## REFERENCES

- [1] Y. Song, Z. Shi, G.-H. Hu, C. Xiong, A. Isogai, Q. Yang, Recent advances in cellulose-based piezoelectric and triboelectric nanogenerators for energy harvesting: a review, *Journal of Materials Chemistry A* 9(4) (2021) 1910-1937.
- [2] D. Zhao, Y. Zhu, W. Cheng, W. Chen, Y. Wu, H. Yu, Cellulose-based flexible functional materials for emerging intelligent electronics, *Advanced Materials* (2020) 2000619.
- [3] S. Kalia, A. Dufresne, B.M. Cherian, B.S. Kaith, L. Avérous, J. Njuguna, E. Nassiopoulos, Cellulose-based bio-and nanocomposites: a review, *International journal of polymer science* 2011 (2011).
- [4] G. Gübitz, T. Lischnig, D. Stebbing, J. Saddler, Enzymatic removal of hemicellulose from dissolving pulps, *Biotechnology Letters* 19(5) (1997) 491-495.
- [5] W. Russo, G. Serad, Characterization of insoluble cellulose acetate residues, *ACS Publications* 1977.
- [6] E. Fleury, J. Dubois, C. Léonard, J. Joseleau, H. Chanzy, Microgels and ionic associations in solutions of cellulose diacetate, *Cellulose* 1(2) (1994) 131-144.
- [7] H. Steinmeier, 3. Acetate manufacturing, process and technology 3.1 Chemistry of cellulose acetylation, *Macromolecular Symposia*, Wiley Online Library, 2004, pp. 49-60.
- [8] B. Saake, M. Zenker, A. Stein, J. Puls, Studies on pre-hump and main fractions of cellulose-2, 5-acetate in acetone, *Cellulose* 13(4) (2006) 449-458.
- [9] J. Nayeem, M. Sarkar, A.H. Quadery, M.S. Jahan, High purity dissolving pulp from jute, *Nordic Pulp & Paper Research Journal* 32(4) (2017) 620-626.
- [10] J. Wilson, T. RS, INFLUENCES OF HEMICELLULOSES ON ACETATE PROCESSING IN HIGH CATALYSTS SYSTEMS, (1974).

- [11] A. Sczostak, Cotton linters: an alternative cellulosic raw material, *Macromolecular Symposia*, Wiley Online Library, 2009, pp. 45-53.
- [12] S. Saka, H. Matsumura, 2.3 Wood pulp manufacturing and quality characteristics, *Macromolecular symposia*, Wiley Online Library, 2004, pp. 37-48.
- [13] D.G. Barkalow, R. Rowell, R. Young, A new approach for the production of cellulose acetate: Acetylation of mechanical pulp with subsequent isolation of cellulose acetate by differential solubility, *Journal of applied polymer science* 37(4) (1989) 1009-1018.
- [14] M. Ramsden, F. Blake, A kinetic study of the acetylation of cellulose, hemicellulose and lignin components in wood, *Wood Science and Technology* 31(1) (1997) 45-50.
- [15] T. Heinze, O.A. El Seoud, A. Koschella, *Cellulose derivatives: synthesis, structure, and properties*, Springer 2018.
- [16] R. Battisti, E. Hafemann, C.A. Claumann, R.A.F. Machado, C. Marangoni, Synthesis and characterization of cellulose acetate from royal palm tree agroindustrial waste, *Polymer Engineering & Science* 59(5) (2019) 891-898.
- [17] H. Sixta, Pulp properties and applications, *Handbook of pulp* (2006) 1009-1067.
- [18] F. Beltramino, M. Roncero, T. Vidal, C. Valls, Facilitating the selection of raw materials: Evaluation of the effects of TCF and ECF bleaching sequences on different wood and non-wood pulps, *Afinidad* 75(582) (2018).
- [19] X. Chen, S. Xu, W. Peng, J. Zhang, Y. Jiang, Isolation and characterization of acetone-insoluble substances in cellulose acetate prepared by an acetic acid acetylation process, *CELLULOSE CHEMISTRY AND TECHNOLOGY* 48(5-6) (2014) 477-483.
- [20] P.C. Gillette, C.E. Hall, Process for purification of cotton linters, Google Patents, 2009.

- [21] C.M. Kuo, R.T. Bogan, Process for the manufacture of cellulose acetate, Google Patents, 1997.
- [22] A. Sluiter, B. Hames, R. Ruiz, C. Scarlata, J. Sluiter, D. Templeton, D. Crocker, Determination of structural carbohydrates and lignin in biomass, Laboratory analytical procedure 1617(1) (2008) 1-16.
- [23] X. Fan, Z.-W. Liu, J. Lu, Z.-T. Liu, Cellulose triacetate optical film preparation from ramie fiber, Industrial & engineering chemistry research 48(13) (2009) 6212-6215.
- [24] X. Jiang, R.H. Narron, Q. Han, S. Park, H.m. Chang, H. Jameel, Tracing Sweetgum Lignin's Molecular Properties through Biorefinery Processing, ChemSusChem 13(17) (2020) 4613-4623.
- [25] P. Gardner, C. MY, The acetylation of native and modified hemicelluloses, (1974).
- [26] K. Igarashi, M. Wada, M. Samejima, Activation of crystalline cellulose to cellulose III results in efficient hydrolysis by cellobiohydrolase, The FEBS journal 274(7) (2007) 1785-1792.
- [27] Y. Hu, V.D. Thalangamaarachchige, S. Acharya, N. Abidi, Role of low-concentration acetic acid in promoting cellulose dissolution, Cellulose 25(8) (2018) 4389-4405.
- [28] T. Heinze, Cellulose: structure and properties, Cellulose chemistry and properties: fibers, nanocelluloses and advanced materials (2015) 1-52.
- [29] Y. Funaki, K. Ueda, S. Saka, S. Soejima, Characterization of cellulose acetate in acetone solution. Studies on prehum II in GPC pattern, Journal of applied polymer science 48(3) (1993) 419-424.
- [30] C. Chung, M. Lee, E.K. Choe, Characterization of cotton fabric scouring by FT-IR ATR spectroscopy, Carbohydrate Polymers 58(4) (2004) 417-420.
- [31] B.C. Smith, Fundamentals of Fourier transform infrared spectroscopy, CRC press 2011.

[32] P.R. Lord, Handbook of yarn production: Technology, science and economics, Elsevier2003.

[33] J.E. Kiefer, G.P. Touey, Cellulose acetate spinning solutions and process of spinning fine denier filaments, Google Patents, 1962.

[34] K. Oguni, Cellulose acetate band, and method for producing cellulose acetate band, Google Patents, 2020.

## **APPENDICES**

## Appendix A

### Supplementary Information for Chapter 1

#### DS<sub>acetyl</sub> Calculation

CAS powder samples (0.5 g) were subjected to air-drying and vacuum-drying sequentially to remove residual ethanol and moisture before measuring DS<sub>acetyl</sub>. The dried CAS powder samples were introduced into 50 ml of 75 % aqueous ethanol. The mixtures were heated to 50 °C and agitated for 1 h, then, 50 ml of NaOH solution (0.5 M) was added to initiate the cleavage of acetyl moieties. The mixtures were kept at room temperature (23 °C) for 24 h, then, slowly titrated with 0.5 M of HCl solution containing a trace amount of phenolphthalein as an indicator until the color of the indicator disappeared. The same experiments were conducted with commercial CAs having DS<sub>acetyl</sub> of 1.8, 2.5, and 2.8 as well as without CAS as control experiments. The mass of acetic acid generated during the titration was computed employing equation 1 [1, 2].

$$W_A = [(D - C)N_a + (A - B)N_b] \times 6.005/W$$

Equation 1

Where,  $W_A$  is the weight of acetic acid;  $A$  and  $B$  are the volume (ml) of NaOH solution employed for the titration of the CAS samples and controlled sample (without CAS), respectively;  $C$  and  $D$  are volume (ml) of HCl solution utilized for the titration of the CAS samples and controlled sample, respectively;  $N_a$  and  $N_b$  are molar concentrations (mol/L) of HCl and NaOH solution, respectively; and  $W$  is the weight of the CAS samples (g). Then, DS<sub>acetyl</sub> can be calculated by the following equation 2 [1, 2].

$$W_A = 6000DS_{acetyl}/(162 + 42DS_{acetyl})$$

Equation 2

#### DS<sub>sulfate</sub> Calculation

An ethanol solution containing 4 wt. % of NaOH and 8 wt. % of deionized water was prepared to cleave acetyl moieties. Dried CAS samples were introduced to 300 ml of the solution and agitated for 24 h at room temperature (23 °C). Then, pH of the mixture was adjusted to pH around 7 to stop the cleavage. The resulting cellulose sulfate (CS) was recovered via vacuum filtration and washed with pure ethanol several times, and air-dried overnight. Before measuring

$DS_{sulfate}$ , CS samples were subjected to additional vacuum drying for 24 h at 50 °C to remove moisture. Afterward, the sulfur content (%S) of CS was measured as followed. Dried CS samples (1.0 g) was refluxed in 250 ml of a 10 wt. % HCl solution for 24 hours, and the sulfate was precipitated by adding 50 ml of barium chloride solution (10 wt. %). The precipitates were collected on a pre-weighed Gooch crucible filter via vacuum filtration and rinsed with deionized water several times. The Gooch crucible filter with precipitates was treated 1 h at 300 °C and ignited 1 h at 600 °C using a Thermolyne small benchtop muffle furnace (Thermo Fisher Scientific, Waltham, MA). %S and  $DS_{sulfate}$  were calculated sequentially by the following equations 3 and 4 [3].

$$\%S = \frac{0.13737 \times \text{Weight of barium sulfate}}{\text{Weight of CS}}$$

Equation 3

$$DS_{sulfate} = \frac{162 \times \%S}{[3200 - (102 * \%S)]}$$

Equation 4

### **Gel Permeation Chromatography**

The molecular weight ( $M_w$ ) and polydispersity index (PDI) of the reference CA and synthesized CAS were measured using 1260 Infinity GPC/SEC equipped with a PLgel MIXED-B column (Agilent, Santa Clara, CA) as described previously with minor modifications [4]. The eluent used was LiBr/N-methylpyrrolidone (0.1 mol/L) at a flow rate of 0.25 mL/min, and the column oven temperature was set to 60 °C. Polystyrene was used as an internal standard. CA and CAS samples were prepared at a concentration of 0.5 wt.%, and the injection volume was set to 50  $\mu$ L.

### **Behavior of CAS hydrogels under the influences of drug release media**

To compare the behavior of CAS hydrogels under the influences of drug release media, CAS hydrogels with varying  $DS_{sulfate}/DS_{acetyl}$  ratios were molded into disks (solid content: 4 wt. %). Then, CAS hydrogel disks were immersed into deionized water and aqueous NaCl (0.5 wt. %) solution. The solid contents of CAS hydrogel disks were measured at predetermined time (0 h, 12 h, 24 h, 36 h, and 48 h). Before measuring the solid contents, moisture on the surface of CAS

hydrogels was removed with filter papers. The following equation 5 was employed to calculate solid contents of CAS hydrogels.

$$\text{Solid Content (wt. \%)} = \left[ 1 - \frac{(W_i - W_o)}{W_i} \right] \times 100$$

Equation 5

Where,  $W_i$  and  $W_o$  are the initial weight of a CAS hydrogel after removing moisture and the weight of a CAS hydrogel after oven drying at 105 °C overnight, respectively. Then, swelling ratio was computed by Equation 6[5].

$$\text{Swelling Ratio (\%)} = \frac{(W_s - W_d)}{W_d} \times 100$$

Equation 6

Where,  $W_s$  and  $W_d$  represent the weight of CAS hydrogels and the weight of oven-dried CAS hydrogels, respectively.

**Table S1.1.** DS<sub>acetyl</sub>, DS<sub>sulfate</sub>, and molecular weight of CAS samples

Starting Materials	Samples	DS <sub>acetyl</sub>	DS <sub>sulfate</sub>	M <sub>w</sub> (g/mol)	PDI (M <sub>w</sub> /M <sub>n</sub> )
DS 2.8 CA	Reference	2.80	0	323,000	2.9
	2.8_1	2.81	0.11	328,000	2.3
DS 2.5 CA	Reference	2.43	0	205,000	2.6
	2.5_1	2.42	0.31	176,000	2.2
	2.5_2	2.39	0.47	155,000	2.3
DS 1.8 CA	Reference	1.82	0	111,000	2.2
	1.8_1	1.81	0.20	97,000	2.0
	1.8_2	1.79	0.43	102,000	2.1
	1.8_3	1.83	0.62	100,000	1.9
	1.8_4	1.77	0.77	100,000	2.0
	1.8_5	1.82	0.87	94,000	1.9
	1.8_6	1.80	1.03	100,000	2.0
	1.8_7	1.81	1.08	93,000	1.9

Molecular weight (M<sub>w</sub>) and polydispersity index (PDI) were measured by GPC employing polystyrene as a standard.

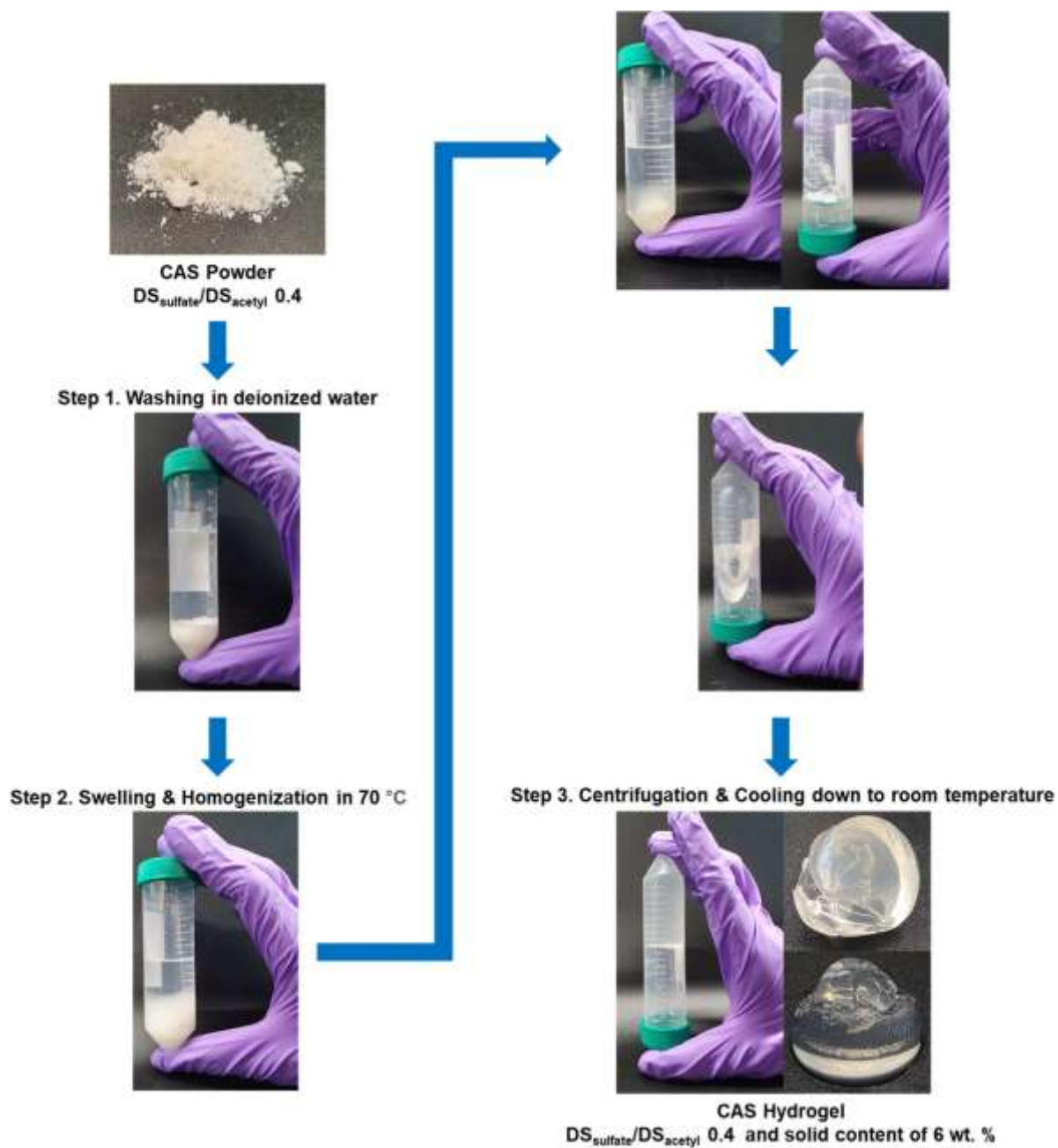


**Figure S1.1.** The formation procedure of CAS hydrogels (DS<sub>sulfate</sub>/DS<sub>acetyl</sub> 0.4 and 6 wt. %). Step 1, Washing CAS powder with deionized water 3 times; Step 2, introducing predetermined amount of deionized water to washed CAS and treating it in a water bath at 70 °C; Step 3, removing bubbles by centrifugation and cooling down to room temperature.

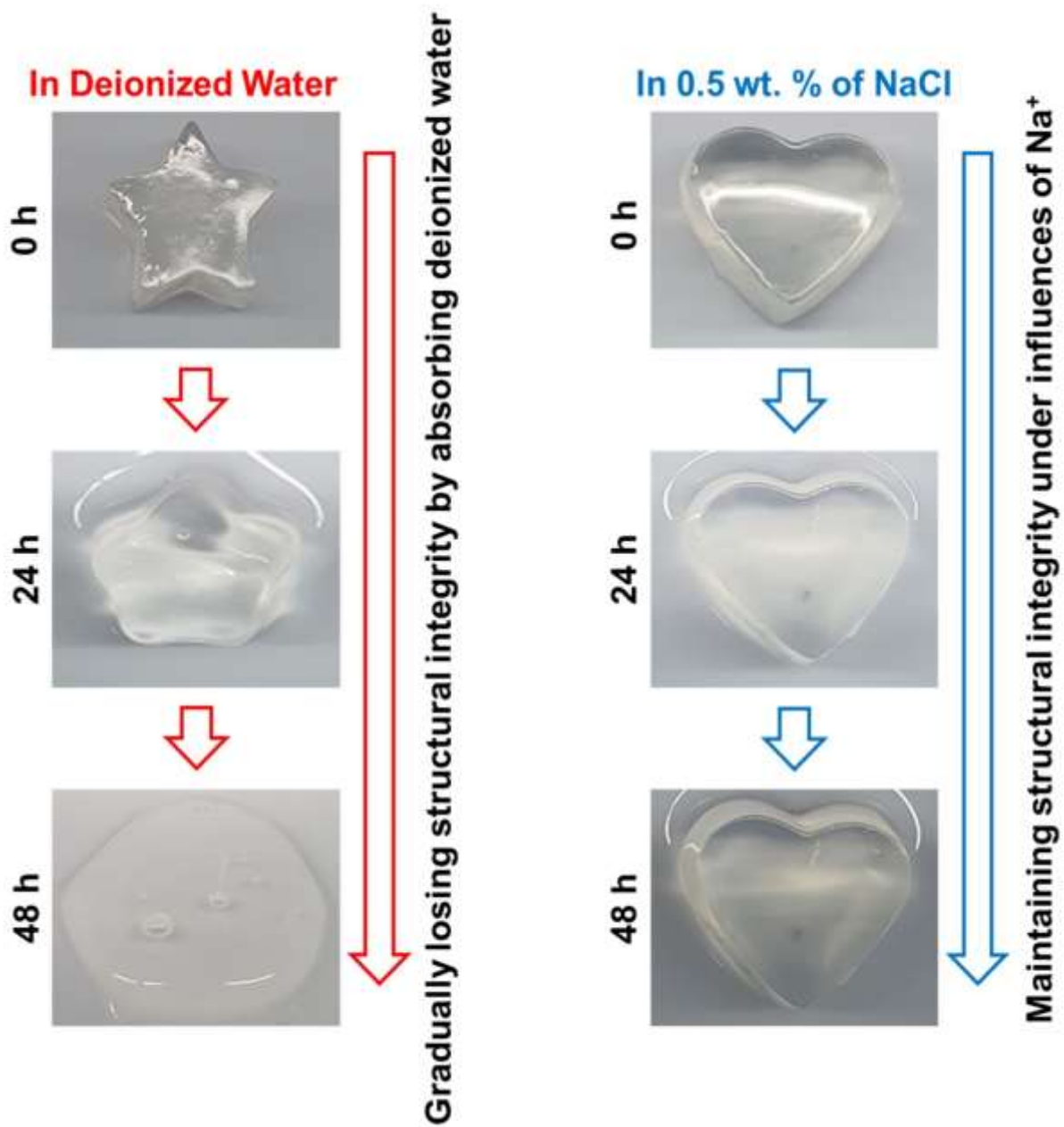


**Figure S1.2.** Behaviors of  $DS_{\text{sulfate}}/DS_{\text{acetyl}}$  ratio of 0.4 molded CAS hydrogels in deionized water and NaCl (0.5 wt. %) aqueous solution.

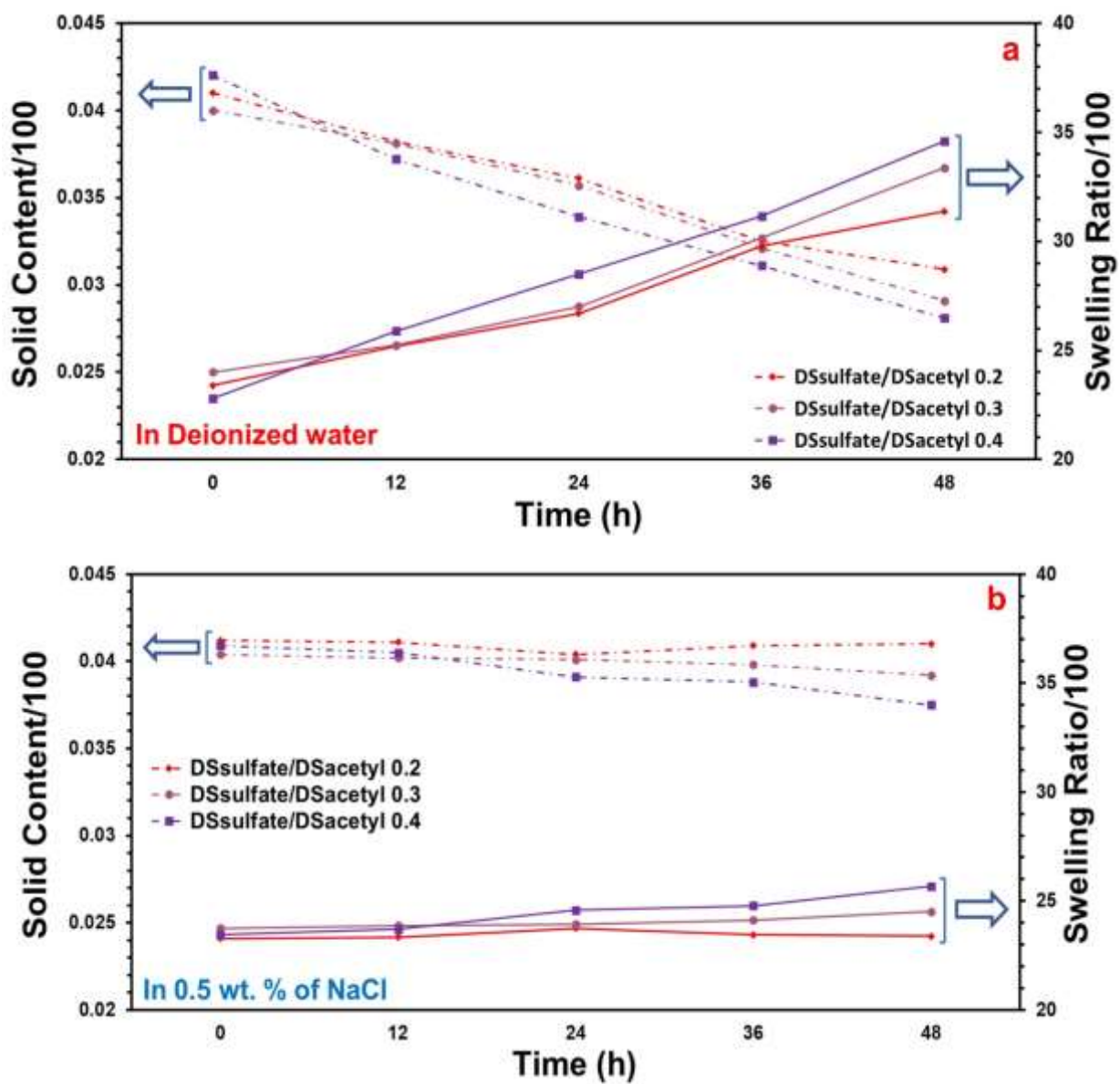


**Figure S1.3.** a-b) Changes in the solid contents and swelling ratios of CAS hydrogels with varying DS<sub>sulfate</sub>/DS<sub>acetyl</sub> ratios (0.2, 0.3, and 0.4) in (a) deionized water; and (b) NaCl (0.5 wt. %) aqueous solution.

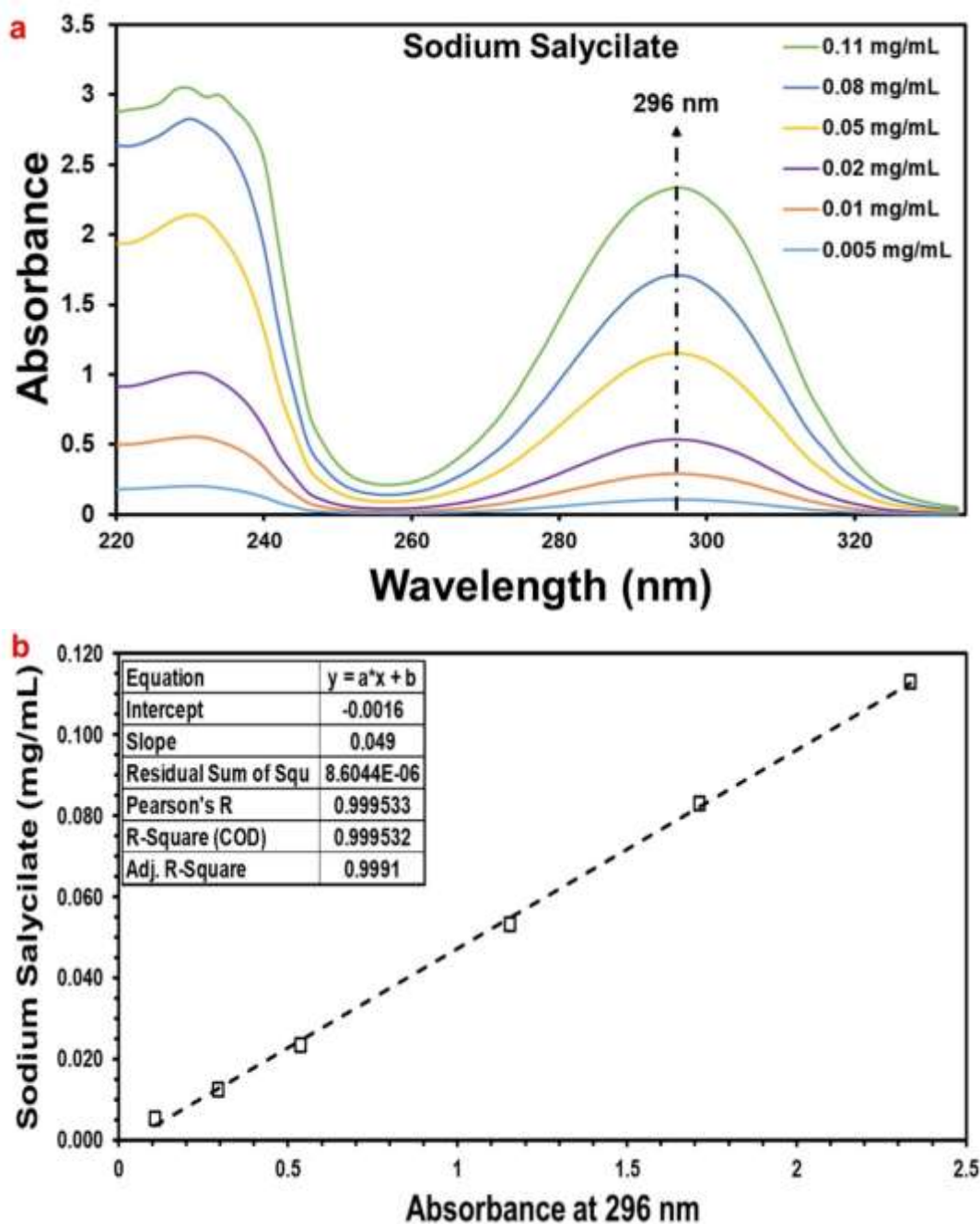


**Figure S1.4.** (a) UV spectra of sodium salicylate solution with varying concentrations in the drug release media (NaCl (0.5 wt. %) aqueous solution); and (b) the calibration curve plotted based on the absorbance at 296 nm for the drug release.

**Table S1.2.** Coefficient of determination and release rate coefficients of kinetics models employed to describe the drug release from CAS hydrogel matrices

Model		DS <sub>sulfate</sub> /DS <sub>acetyl</sub> 0.2	DS <sub>sulfate</sub> /DS <sub>acetyl</sub> 0.3	DS <sub>sulfate</sub> /DS <sub>acetyl</sub> 0.4
Zero $Q_t = k_0 * t$	R <sup>2</sup>	0.74	0.75	0.83
	k <sub>0</sub>	0.065 ± 0.003	0.064 ± 0.001	0.058 ± 0.001
First $\ln Q_t = k_1 * t$	R <sup>2</sup>	0.95	0.96	0.96
	k <sub>1</sub>	0.23 ± 0.04	0.21 ± 0.03	0.13 ± 0.01
Elovich $Q_t = k_E * \ln t$	R <sup>2</sup>	0.98	0.97	0.96
	k <sub>E</sub>	0.18 ± 0.012	0.16 ± 0.013	0.16 ± 0.009
Higuchi* $Q_t = k_H * t^{0.5}$	R <sup>2</sup>	0.96	0.95	0.98
	k <sub>H</sub>	0.40 ± 0.05	0.37 ± 0.04	0.28 ± 0.02
Korsmeyer-Peppas* $Q_t = k_{KP} * t^n$	R <sup>2</sup>	0.97	0.93	0.98
	k <sub>KP</sub>	0.46 ± 0.08	0.43 ± 0.05	0.31 ± 0.006
	n	0.41 ± 0.06	0.36 ± 0.07	0.45 ± 0.04
* Kinetics models marked with superscript * were plotted up to $Q_t < 0.6$				
Note: R <sup>2</sup> = coefficient of determination; t = time (h); Q <sub>t</sub> = fraction of drug released at the time t; n = release exponent of the Korsmeyer-Peppas model; k <sub>0</sub> , k <sub>1</sub> , k <sub>E</sub> , k <sub>H</sub> , k <sub>KP</sub> = release rate coefficients of zero, first, Elovich, Higuchi, and Korsmeyer-Peppas kinetic model, respectively.				

## REFERENCES

- [1] X. Fan, Z.-W. Liu, J. Lu, Z.-T. Liu, Cellulose triacetate optical film preparation from ramie fiber, *Industrial & engineering chemistry research* 48(13) (2009) 6212-6215.
- [2] D.-Y. Kim, Y. Nishiyama, S. Kuga, Surface acetylation of bacterial cellulose, *Cellulose* 9(3) (2002) 361-367.
- [3] N. Bhatt, P. Gupta, S. Naithani, Preparation of cellulose sulfate from  $\alpha$ -cellulose isolated from *Lantana camara* by the direct esterification method, *Journal of applied polymer science* 108(5) (2008) 2895-2901.
- [4] T. Hashizume, Y. Okamoto, K. Nagai, S. Shimamoto, Mechanism of sodium-hypochlorite-induced degradation of cellulose acetate and the enhancement of its degradation resistance by chemical modification, *Textile Research Journal* 92(13-14) (2022) 2487-2500.
- [5] H. Park, X. Guo, J.S. Temenoff, Y. Tabata, A.I. Caplan, F.K. Kasper, A.G. Mikos, Effect of swelling ratio of injectable hydrogel composites on chondrogenic differentiation of encapsulated rabbit marrow mesenchymal stem cells in vitro, *Biomacromolecules* 10(3) (2009) 541-546.

## Appendix B

### Supplementary Information for Chapter 2

**Table S2.1.** DS<sub>acetyl</sub> and DS<sub>sulfate</sub> of CA and CAS

Samples	DS <sub>acetyl</sub>	DS <sub>sulfate</sub>
CA DS <sub>acetyl</sub> 1.8	1.83	-
CAS DS <sub>sulfate</sub> /DS <sub>acetyl</sub> ratio of 0.2	1.79	0.43
CAS DS <sub>sulfate</sub> /DS <sub>acetyl</sub> ratio of 0.3	1.81	0.54
CAS DS <sub>sulfate</sub> /DS <sub>acetyl</sub> ratio of 0.4	1.82	0.69

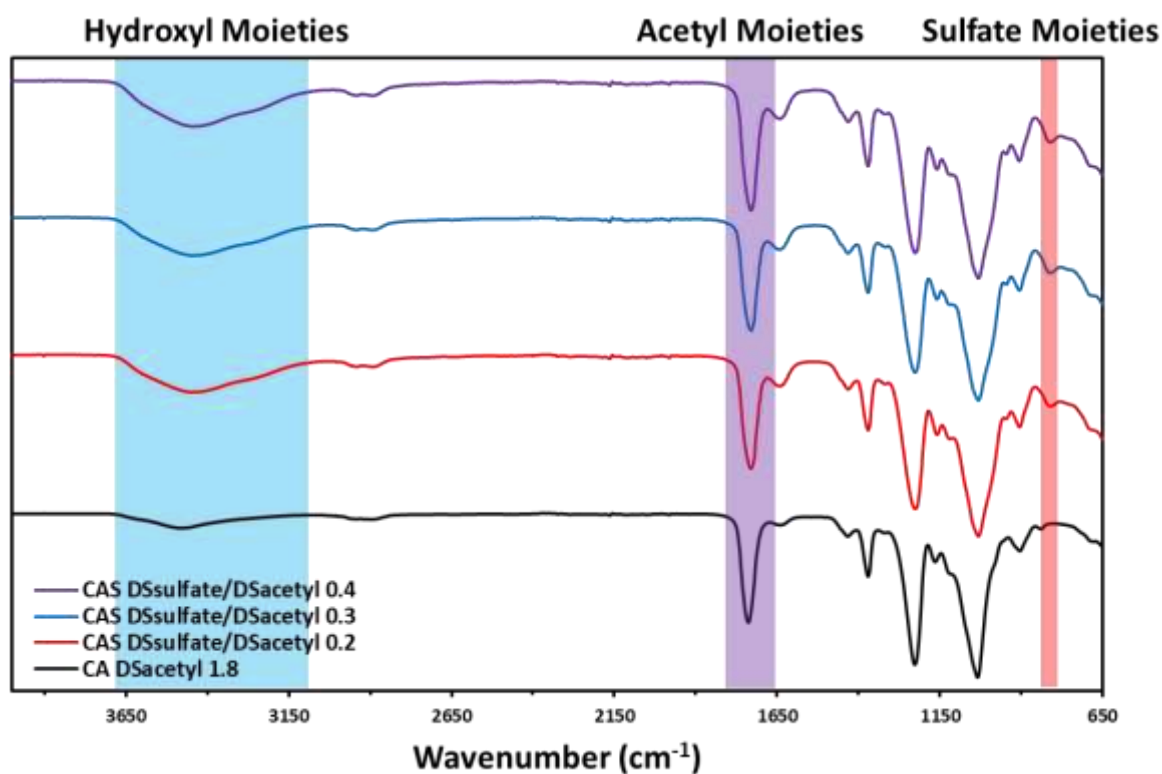


**Figure S2.1.** ATR-FTIR spectra of CA DS<sub>acetyl</sub> 1.8, CAS DS<sub>sulfate</sub>/DS<sub>acetyl</sub> ratio of 0.2, 0.3, and 0.4.

## Appendix C

### Supplementary Information for Chapter 3

**Table S3.1.** Equilibrium moisture content of CAS films

Sample	Equilibrium Moisture Content
DS <sub>sulfate</sub> /DS <sub>acetyl</sub> 0.4/1.8	15.3 ± 0.5 <sup>a</sup>
DS <sub>sulfate</sub> /DS <sub>acetyl</sub> 0.7/1.8	15.7 ± 0.4 <sup>a</sup>
DS <sub>sulfate</sub> /DS <sub>acetyl</sub> 1.0/1.8	16.8 ± 0.9 <sup>a</sup>
Mean values with different letter within a column indicate that there are significant differences (p < 0.05)	

## Appendix D

### Supplementary Information for Chapter 4

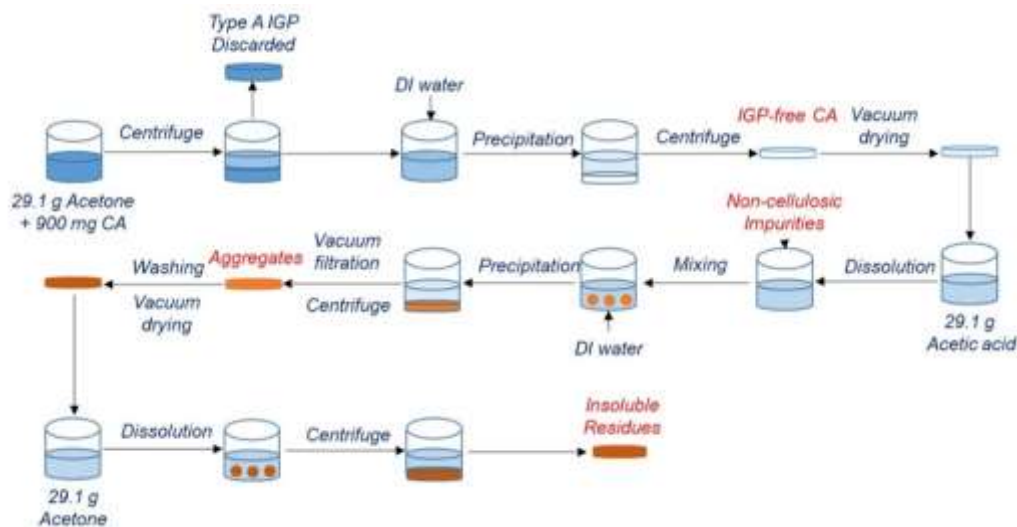


**Figure S4.1.** Experimental procedure of the Formation of Type B IGP

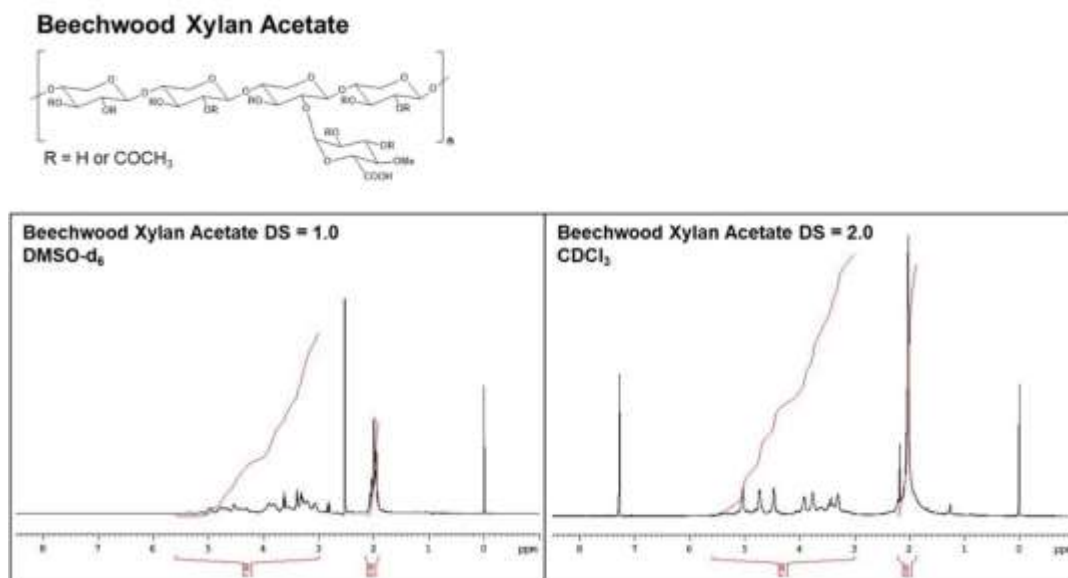


**Figure S4.2.** <sup>1</sup>H NMR spectra of DS 1.0 (left) and DS 2.0 (right) beechwood XA.

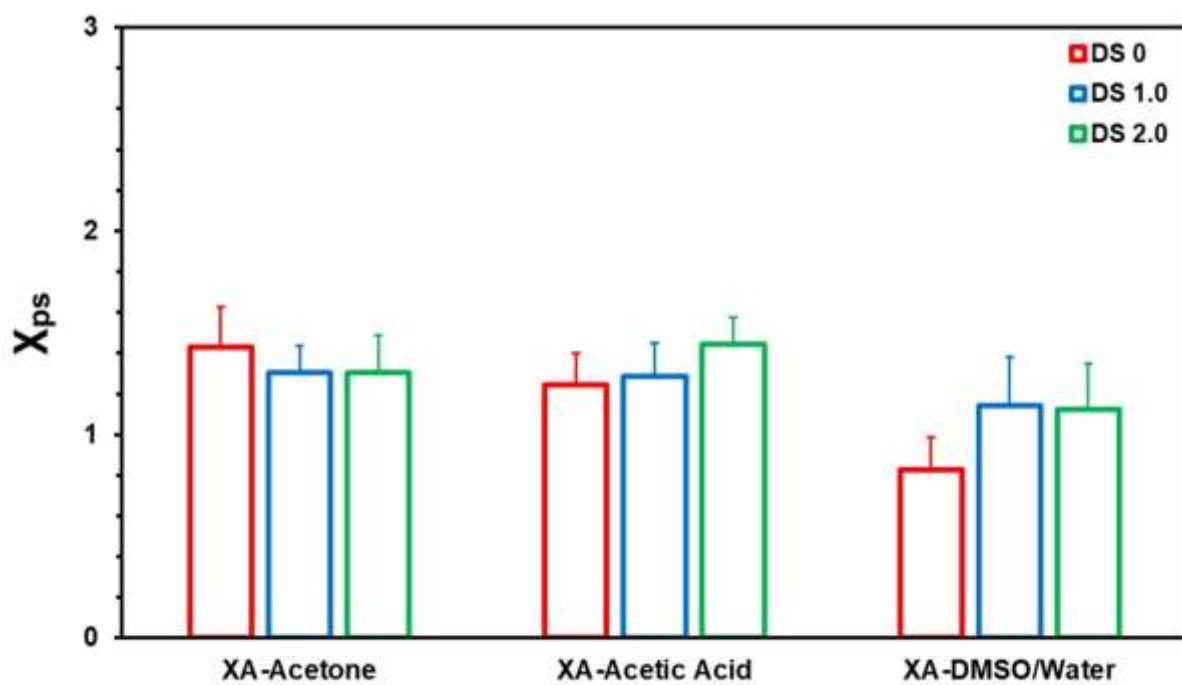


**Figure S4.3.** Flory-Huggins interaction parameter of XA in the relevant solvents

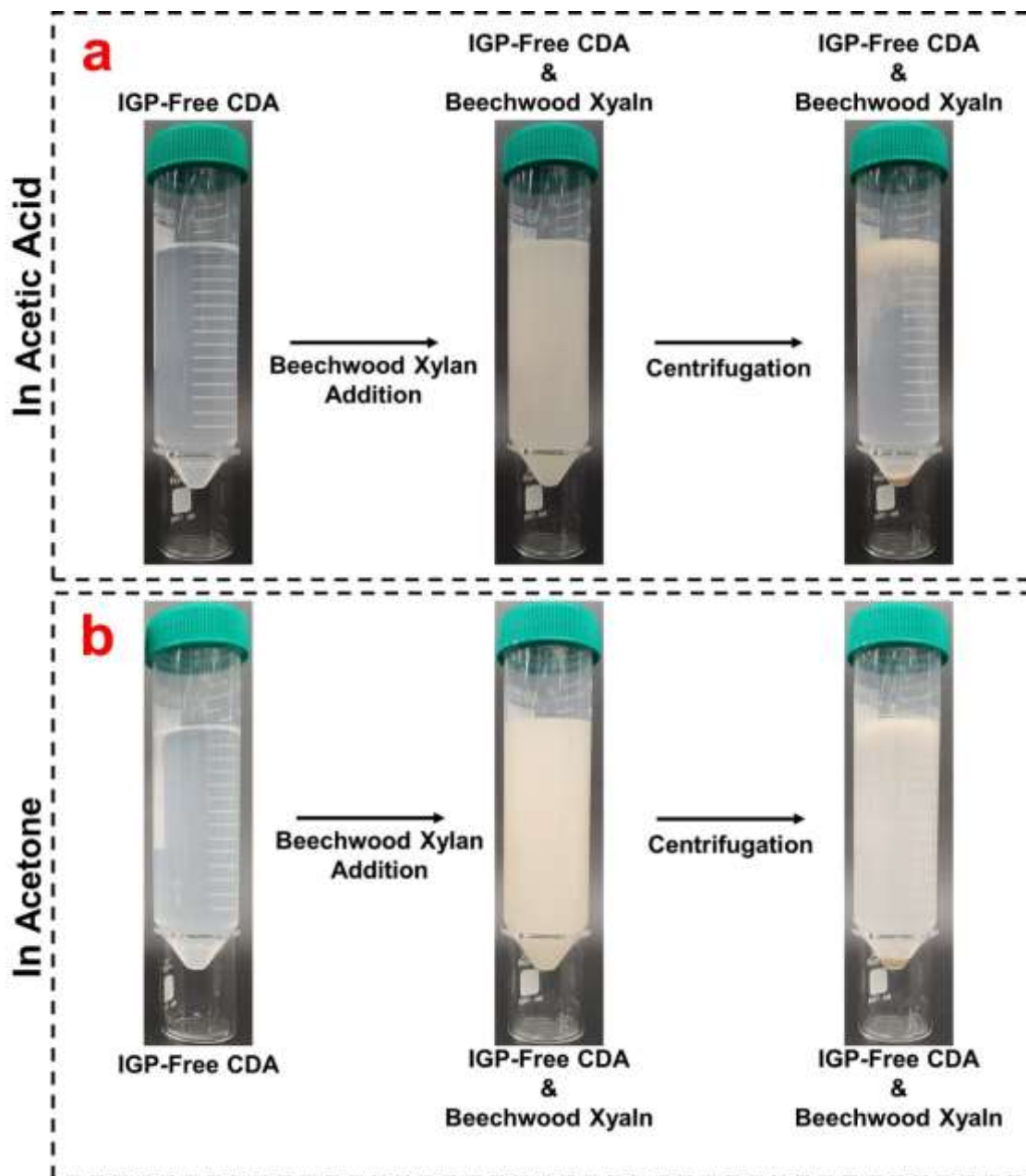


**Figure S4.4.** The behaviors of beechwood xylan in (a) IGP-free CDA acetone solution, and (b) IGP-free CDA acetic acid solution, which makes an incomplete recovery of beechwood xylan via centrifugation.

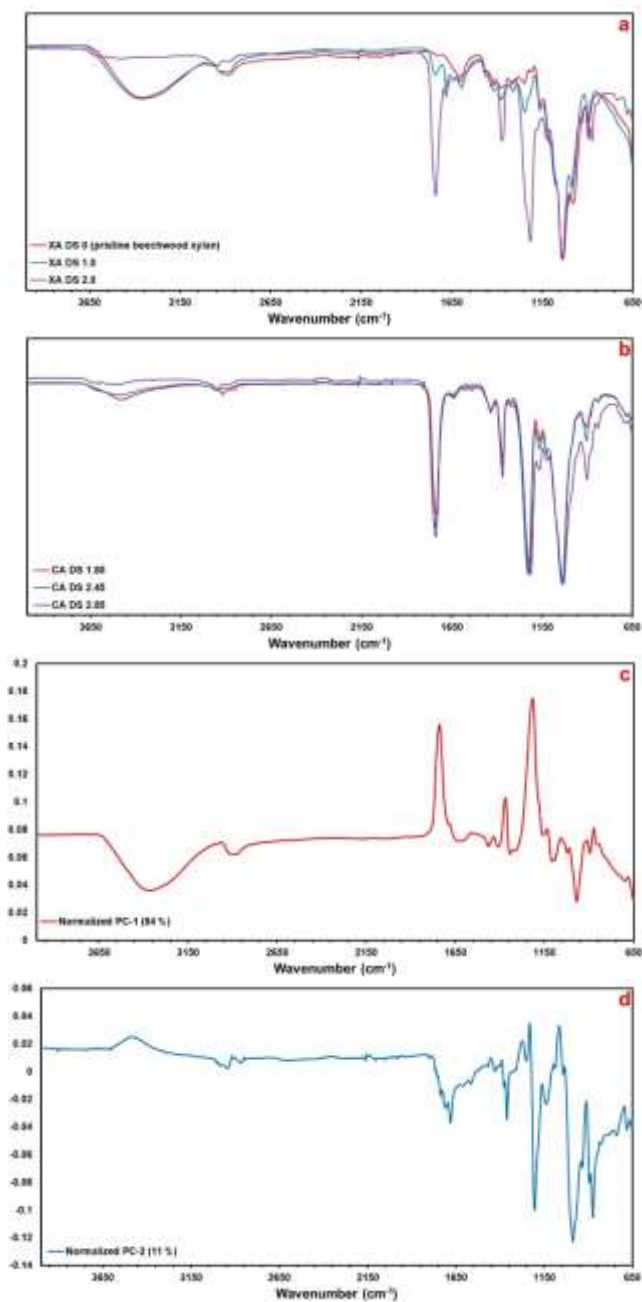


**Figure S4.5.** Averaged ATR-FTIR Spectra of (a) XA, (b) CA, (c) PCA loading plot of the first principle component, and (d) PCA loading plot of the second principle component showing that the vibrations obtained by ATR-FTIR are able to differentiate CA, XA, and insoluble residues.

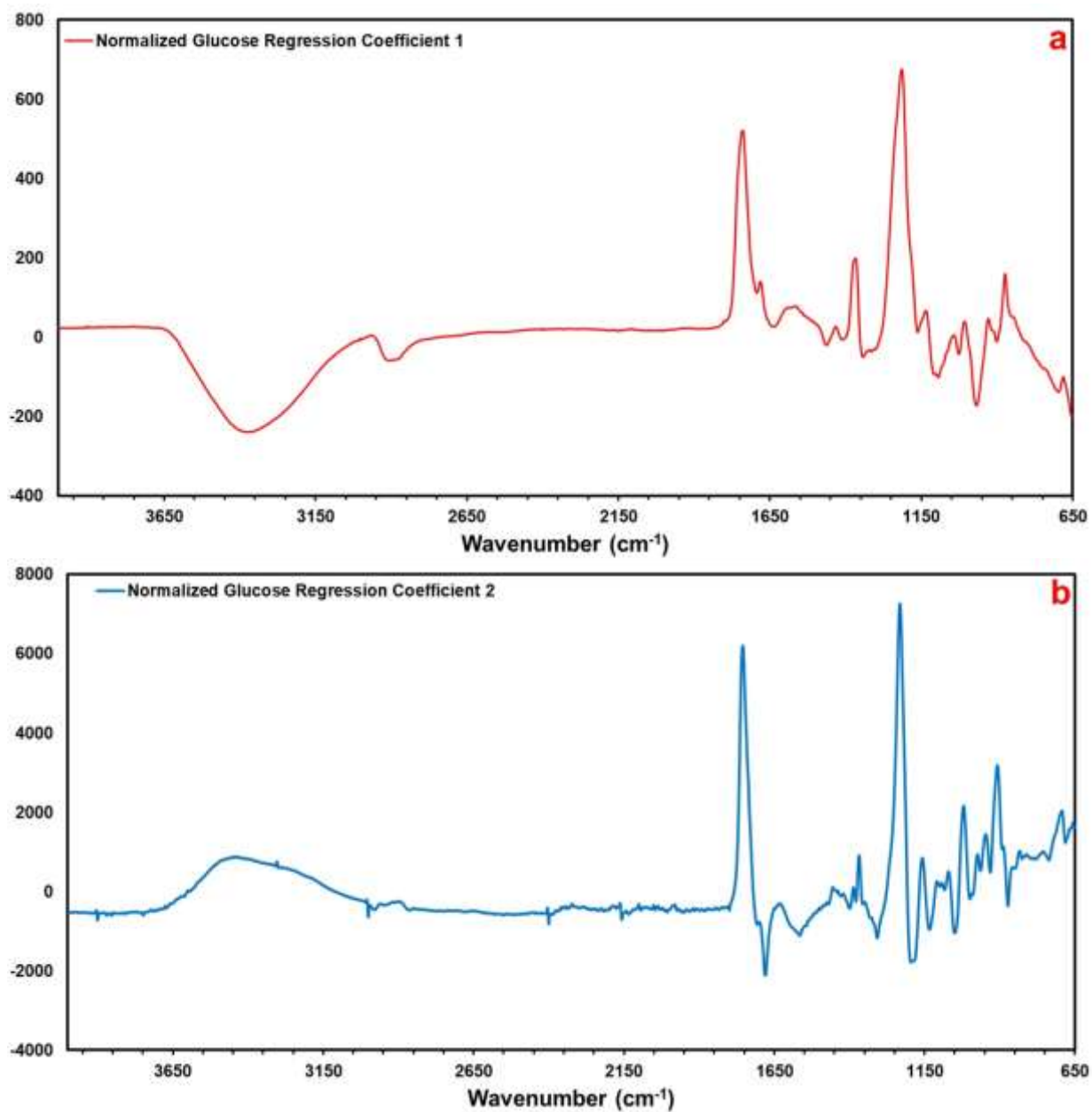


**Figure S4.6.** (a-b) Normalized regression coefficient 1 and 2 for the glucose content prediction model of the insoluble residues

## Appendix E

### Supplementary Information for Chapter 5



**Figure S5.1.** Two-step hydrolysate solutions produced from long fibers (left) and short fibers (right) of **a and b** cotton linter dissolving pulps A; **c and d** cotton linter dissolving pulp B, respectively

\* Whole A and B represent unfractionated cotton linter dissolving pulp A and B

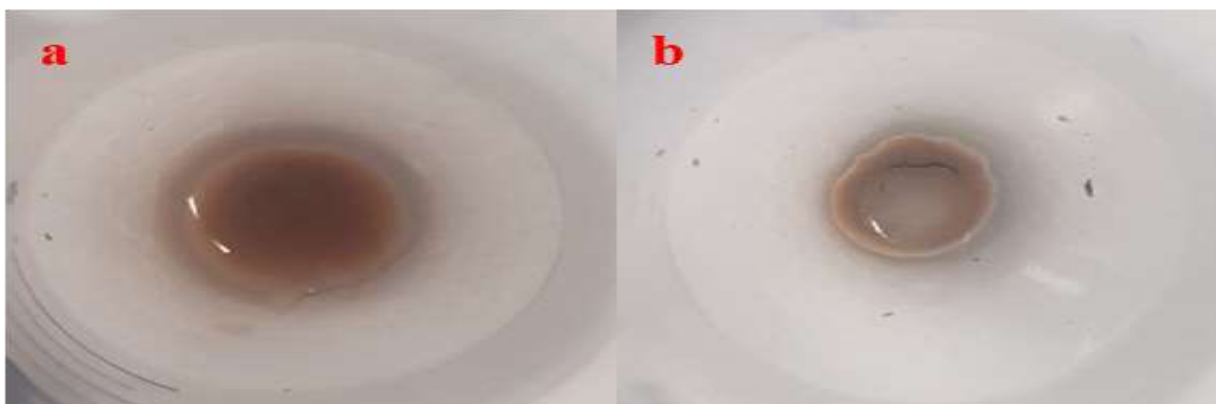


**Figure S2.** Photos of **a.** collected SIS; **b.** IGP obtained after the re-dissolution of CA/SIS aggregates in acetone.